UNIVERSITÀ DEGLI STUDI DI PADOVA

Dipartimento di Ingegneria Civile, Edile e Ambientale – ICEA

MASTER THESIS IN ENVIRONMENTAL ENGINEERING
-SOIL PROTECTION PROGRAMME-

THERMO-PHYSICAL PROPERTIES OF EUGANEAN HILLS LITHOLOGIES (PADUA, NORTH-EASTERN ITALY) RELATED TO UNDERGROUND THERMAL STORAGE FEASIBILITY.

Relatore: Prof. Raffaele Sassi
Correlatori: Prof. Antonio Galgaro
Dott.ssa Eloisa Di Sipio

Controrelatore:Prof. Michele De Carli

Laureando: Stefano Buggiarin

ANNO ACCADEMICO 2013/2014

Alla mia famiglia

Index

Abstract

The rapid growth of the world population has put a big problem on conventional energy resources such as fuel, coal and oil, which are estimated to be depleted in a few decades. These conventional resources are also accused by the excessive production of CO_2 and other harmful gases that lead to climate change issues, such as global warming and the deterioration of the ozone layer (Xu et al., 2013).

These serious consequences require people to start considering new models of sustainable development.

In particular solar energy is as a pollution-free, inexhaustible and affordable energy resource, has received extensive study and numerous applications throughout the world.

Luckily in recent years a considerable progress in renewable energy development has made new energy resources quite competitive with conventional energy in terms of both efficiency and reliability.

The term TES indicates all energy storage technologies (which can be used in combination with other energy sources) to economically buffer variable rates of energy supply and demand (Dincer, 2001). The heat which is stored usually come from solar thermal panel or from other renewable resources (for example a biomass power plant). Also the waste heat from an conventional industrial plant can be used for this purpose.

Energy storage can be classified into short term storage and long term storage according to different storage durations.

By means of energy storage, intermittentsolar energy is able to not only meet the demands of space heating and domestic water supply but also to offer a high grade heat source all year round regardless of timing or seasonal constraints: in this case it's possible use the excess heat collected in the summer for heat supply during the wintertime (Xu et al., 2013).

In this work are considered the preliminary studies voted to support the planning of Underground Thermal energy storage (UTES) systems.

In order to properly design this type of systems the knowledge of the main underground thermo-physical parameters is fundamental (Clauser, 2011).

In this study, the thermal properties of Euganean Hills principal lithologies (Eastern Po Plain) (South West of Padua) have been measured, such as thermal conductivity, volumetric heat capacity, thermal diffusivity, density and porosity.

A literature research has accompanied the study allowing to compare the experimental results.

Introduction

The rapid growth of the world population has put a big problem on conventional energy resources such as fuel, coal and oil, which are estimated to be depleted in a few decades. These conventional resources are also accused by the excessive production of CO_2 and other harmful gases that lead to climate change issues, such as global warming and the deterioration of the ozone layer (Xu et al., 2013). Another consequence of global warming is the melting of ice in Greenland and the South Pole, and with the thermal expansion of water, a subsequent increase in sea level could take place, which could submerge coastal areas which are often densely populated.

All of these serious consequences require people to start considering new models of sustainable development.

Due to these consequences, the United Nations Framework Convention on Climate Change (UNFCCC) has established the Kyoto Protocol and the Copenhagen Accord as measures of combating climate change due to the emission of greenhouse gases (Lau et al., 2012).

The Kyoto protocol has assigned to Europe the task of reducing (between 2008 and 2012) its CO_2 emissions by 7% compared to 1990 value (Orò et al., 2014). This objective has been achieved, but thanks to the less developed countries of the Union which have suffered most the economic crisis with relative decrease in energy use (Lau et al., 2012).

The Copenhagen Accord was held on 7-18 December 2009 with the aim of providing new targets after 2012.

It was concluded with a general objective of containing by 2100 warming below 2 degrees with respect to the pre-industrial era (Rubino, 2011).

To achieve this goal (or even improve it) is necessary both to design systems with low energy consumption, and use renewable energy in a massive way.

Luckily in recent years a considerable progress in renewable energy development has made new energy resources quite competitive with conventional energy in terms of both efficiency and reliability (Xu et al, 2013).

In particular solar energy as a pollution-free, inexhaustible and affordable energy resource, has received extensive study and numerous applications throughout the world. However, one of the long standing barriers to solar energy technology lies in the noticeable misalignment between energy supply and consumption. Therefore, the energy storage concept is proposed as an essential way to address the mismatch.

The idea of thermal energy storage (TES) was first mentioned and investigated to address the energy shortage crisis in the 1970s. By means of energy storage, intermittent

solar energy is able not only to meet the demands of space heating and domestic water supply but also to offer a high grade heat source all year round regardless of timing or seasonal constraints: in this case it is possible use the excess heat collected in the summer for heat supply during the wintertime (Xu et al., 2013).
Following the same logic it is possible to "accumulate" cold during the winter seasons and then use it when it is warm.
It is also possible have different source of heat (not only sun): for example, waste heat from conventional thermal power plants or from biomass plants.
Anyhow a TES system reduces energy consumption and emission of harmful gases.

The heat storage can take place in different ways depending on the TES system used.
Three TES categories exist (Cabeza et al., 2012):

- sensible heat: the energy is stored by changing the temperature of a storage medium such as water, air, oil, rock beds, bricks, concrete, or sand;
- latent: a material stores heat while at phase transition;
- thermochemical: uses chemical (reversible) reaction with high heat of reaction.

In this work the applications for the first type of TES are considered: to properly design this type of systems you should know the main thermophysical parameters of the materials on which the facility will be built.
This project was intended to determine the thermal conductivity, volumetric heat capacity, thermal diffusivity, density and porosity of principal lithologies present in the Euganean Hills (South West of Padua).
Thermal conductivity determines where and how much heat flows in response to temperature differences in the reservoir; the volumetric heat capacity specifies the amount of heat required to raise the temperature of unit volume of rock and thermal diffusivity determines the speed at which temperature front moves through the reservoir (Chekhonin et al., 2012).
Density and porosity are common physical parameters which are determined because they are related with the previous.
A literature search has accompanied the study so the laboratory results are compared with those obtained by other authors.
Relations between the different properties are made and it is presented a statistical study for verify the precision and accuracy of the instrumentation used for thermal analysis.
The data which are obtained from literature and laboratory are implemented in a Geografical Information System (GIS) in order to compare them and identify the areas in which there are outcrops with better thermal properties.

The applications that may result from this type of study can be linked to TES systems for domestic use, lodgings, bed and breakfasts, hostels and also for applications as the culture in the greenhouse.
A TES system can also be useful in those buildings not reached by conventional power network (electricity, gas).

1. Geothermal Energy and Thermal Energy Storage (TES)

This chapter provides an introduction to geothermal energy with particular attention to "low enthalpy" applications.
In this field the Ground Source Heat Pump (GSHP) is used for extract heat or cold from the ground and often is used coupled with system for heat energy storage. In particular three different mechanisms for energy storage exist, as sensible heat storage, latent heat storage and thermochemical heat storage.

1.1 Geothermal Energy

Geothermal energy is generally defined as the heat stored in the Earth. Heat that can be extracted from the subsoil and exploited by man.
Geothermal resources are usually subdivided into "high, medium and low enthalpy": this classification is based on the temperature of the heat transfer fluids that transfer the heat from the deep hot masses to the surface.
Clauser (2006) reported the classification presented in Table 1.1 but other authors give different range of temperature, sometimes with the only distinction between "low" and "high" enthalpy (De Carli et al., 2007).

Table 1.1 *Classification of geothermal reservoirs (Clauser, 2006)*

Type	Temperature range (°C)	Energy content
Water dominant	<100	Low enthalphy
Water dominant	100-150	Medium enthalpy
Vapor dominant	>150	High enthaply

Generally the geothermal resource at high enthalpy is classified into:

- Hydrothermal: hot water at moderate depth (i.e. 1-4 km) with temperature up to 350°C;
- Geopressured: hot, high-pressure reservoir brines contain dissolved natural gas (methane). Their energy content is about 58 % thermal, 32 % hydrocarbon chemical, and 10 % hydraulic, at best;
- Hot dry rock (HDR): systems where fluids are not produced spontaneously;
- Magma: molten rock at temperatures of 700°C−1200°C at accessible depth (about < 7 km).

This kind of resource can be used for the production of vapor which is required to drive turbines for generating electric power. This is called “indirect use” of geothermal resource and the first conversion occurred in Lardarello, Italy, in the year 1904, when the engineer Count Piero Ginori Conti succeeded in producing sufficient electricity from geothermal steam to power five electric light bulbs (Clauser, 2006).
In the low enthalpy systems the use of the subsoil does not necessarily imply that the temperature of this source is higher than ambient temperature (understood both as the annual average is as instantaneous); this is the case of ground source heat pump (GSHP) (De Carli et al., 2007) which represent a "direct use" of geothermal resource because heat is not transformed into other types of energy.
These systems use the ground as either a heat source, when operating in heating mode, or a heat sink, when operating in cooling mode. For exchange thermal energy the GSHP is connected to the ground with a loop. The most common connection is a closed loop, consisting of U-tubes of high density polyethylene inserted into boreholes of 50 to 200 meters deep (Hendriks et al., 2008).
In other cases the subsoil is used as "thermal tank" in which the heat is injected. These systems are called underground thermal energy storage (UTES) which are a subset of thermal energy storage (TES). For best results TES and GSHP can be used in combination.

1.2 TES systems

The term TES indicates all energy storage technologies (which can be used in combination with other energy sources) to economically buffer variable rates of energy supply and demand (Dincer, 2001).
The heat which is usually stored comes from solar thermal panel or from other renewable resources (for example a biomass power plant). Also the waste heat from a conventional industrial plant can be used for this purpose.
In the same manner also the “cold” can be stored. Usually in this case the cold come from a conventional cooling system but sometimes came from snow storage.
In both cases the process is made by three steps: the charge, the store and discharge phase (Figure 1.1).
Energy storage can be classified into short term storage and long term storage according to different storage durations. The latter has a greater potential in practical applications but requires large storage volumes and has a greater risk of heat losses (Xu et al.,2013).

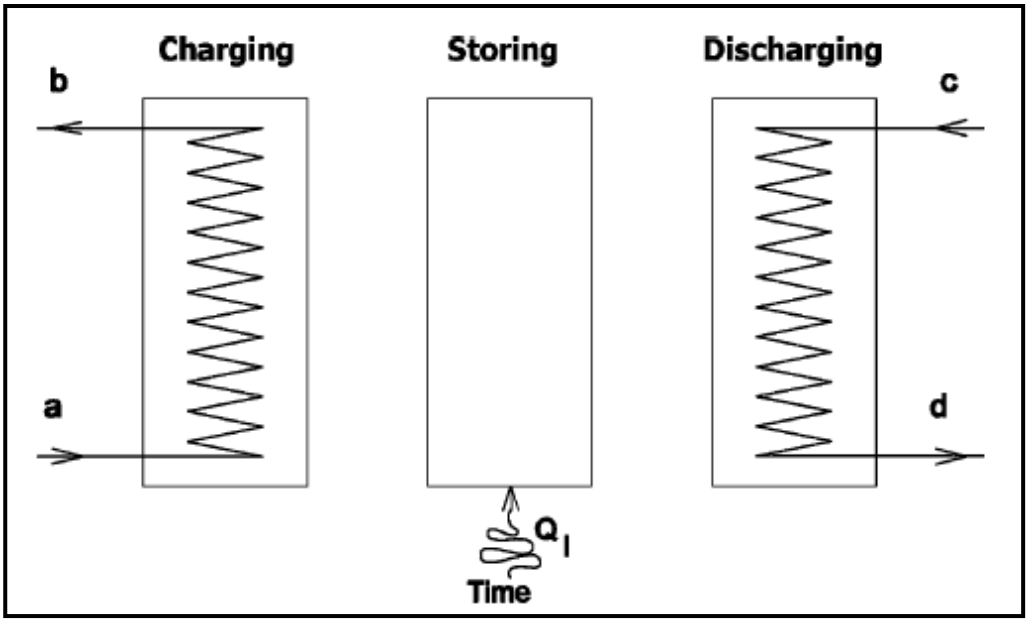

Figure 1.1 *The three processes in a general TES system for cooling capacity: charging (left), storing (middle) and discharging (right). The heat leakage into the system Ql is illustrated for the storing process but can occur in all three processes (Dincer, 2002)*

There are mainly three kinds of TES:

1) Sensible: involves a material as liquid medium (water, oil) or solid (rock, brick, sand, soil) subjected to a change of temperature with no phase change. What varies is then the internal energy of the accumulator. The amount of stored energy is proportional to (i) the difference between the final and the initial temperature, (ii) the mass and volumetric heat capacity of the medium:

$Q = \rho c_p V \Delta T \quad (J)$	1.1

Where Q is the amount of heat stored, ρ the density of material, c_p is the specific heat of the material, V the total volume of the material and ΔT the temperature difference (Dincer, 2002).

The ability to accumulate energy into the considered material depends definitively by the thermal capacity ρc_p.

A good material must have high thermal capacity and be economical and available in large quantities. That is why the water looks like the best candidate for the TES heat sensitive, responding extremely well to the previously mentioned requirements . However, over 100°C, the system has to be pressurized, which adds tremendously the cost (Dincer, 2002). There are a number of heat resistant oils in the market which can be readily used without pressurization at temperatures in a broad range from 10 to 320°C.

Rock is another good TES material from the standpoint of cost, but its thermal capacity is only half that of water: an amount of heat stored in rocks occupies more space respect the same amount stored in water. This disadvantage is quickly overcome if it is made an

analysis of the costs because it is very expensive built a proper water containment (Dincer, 2002).
In general TES technology is considered mature, simple and cheaper respects other alternative for energy storage. Therefore it has been implemented in many projects for the heating of buildings such as homes, hospitals or schools. For example, the hospital Balcali (Turkey), the school of Crailsheim (Germany) and some offices in Neuchatel (Switzerland) have heating systems based on this technology (Xu et al., 2013).

2) Latent: it is based on the absorption or release of heat in the moment in which the storage medium undergoes a phase change from solid to liquid or from liquid to gas (and vice versa) without significant changes in temperature, which is almost isothermally. Such materials are commonly referred to as phase change materials (PCM).
The total energy accumulated in a system based on latent TES (with phase change solid-liquid) is given by (Rubin, 2013):

$Q = m\lambda_m \quad (J)$	1.2

Where Q is the thermal energy stored, λ_m latent heat of fusion (J/kg), m mass of the storage medium (kg).
The high density of accumulation of PCM (also 100 kW/m^3) and the reduced variation of temperature make this type of storage very promising. Latent TES systems have much lower dimensions than a system based on sensible TES, but present fewer difficulties of design as regards the transmission of heat and the choice of materials.
The applications range from construction (active or passive systems that store energy during the day and release it at night for cooling or vice versa) by the integration of PCM in building materials, food preservation, to medical or aerospace applications.
Potentially this technology could be adapted to any application that requires the accumulation of thermal energy, provided that the convenience from the economic point of view must be assessed case by case.
The latent TES are usually classified considering the phase change of the material used for the accumulation (Figure 1.2). The transformations of the solid-gas and liquid-gas are not normally used, despite the high latent heat, due to the significant changes volume which makes the system too much complex.

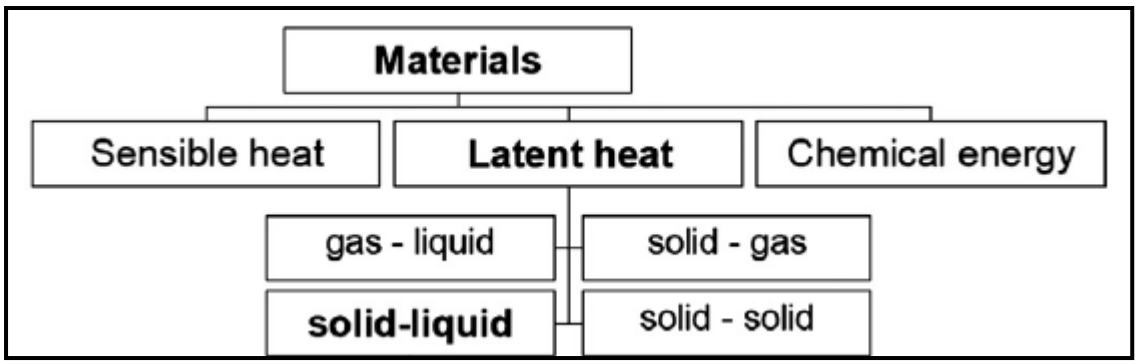

Figure 1.2 *Classification of different energy storage systems (modified from Xu et al., 2013)*

Attention therefore focuses on transitions solid-liquid or solid-solid (transition from a crystalline phase to another), as have the highest density of storage with low volumetric changes.
Finally, considering that the amount of heat associated with the transformation from solid to liquid is the highest, the main attentions are directed to this type of application (Rubin, 2013).

3) Thermochemical: this TES technology is based on energy absorbed and released during the break and formation of molecular bonds within a completely reversible chemical reaction (reversible thermochemical reactions, RTR).
For example, given two substances A and B, there is a phase with endothermic decomposition (which is the charge phase) and a second phase with exothermic synthesis process.
These systems are usually coupled to a solar receiver that provides heat necessary to trigger the endothermic chemical reaction.
In this case, the accumulated heat depends on the amount of material (mass), the heat of reaction and the degree of reaction (fraction of converted reactants) (Rubin, 2013):

$Q = a_r m \Delta h_r \quad (J)$	1.3

Where Q is the thermal energy stored, a_r the fraction of converted reactans, Δh_r (J/kg) the endothermic heat of reaction and m the mass of the medium (kg).
Chemical storage has distinctive advantages of high energy storage and low heat losses over other storage technologies and is regarded as the most promising alternative. The storage volume for 34 m^3 of water equivalent (70°C temperature increase) is only 1 m^3 by means of chemical storage.
Another attractive feature of chemical storage lies in its capability to conserve energy at ambient temperature as long as desired without heat losses given that sensible heat effect is negligible when compared with reaction heat. To optimize performance, the

two reactants A and B prior nominated can be stored separately by sealing the connection between them during the storage period (Xu et al., 2013). The materials used in this field must have high energy storage density, corrosiveness during storage and reaction phases, low price and low environmental impacts (Xu et al., 2013).

1.3 Applications for sensible TES systems

In general the Sensible TES is the application commonly adopted for the heating of homes (which do not require the high temperatures that can be achived in thermochemical TES) and respect the different types of heat storage are the most economical.

Sensible heat storage comprises water tank storage and underground thermal energy storage (UTES) (Xu et al., 2013). The UTES includes ATES, BTES (field in which finds application the study of thermal properties of rocks conducted in this work) and CTES i.e. thermal energy storage in aquifers, boreholes, and caverns (Nordell et al., 2007).

1.3.1 Water tank storage

Water tanks are artificial structures that are made of stainless steel or reinforced concrete surrounded by thick insulation. They are usually buried underground (also called water pits) or placed on the roof or outside of a building (Xu et al., 2013).

If this solution is adopted, is very important choose an appropriate type of insulator: glass wool polyurethane and high density concrete (HDC) are usually good for this purpose. Figure 1.3 shows a water tank storage: the reduction of heat losses are obtained with insulations in the top and in the lateral wall of the structure.

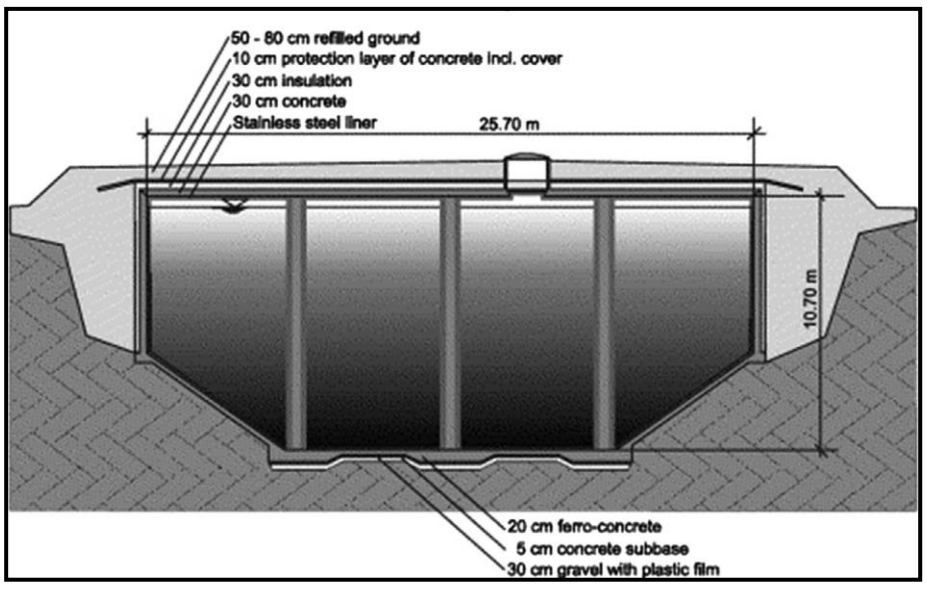

Figure 1.3 *Hot water storage tank in Hamburg-Bramfeld; 4.500 m^3(Xu et al., 2013)*

1.3.2 Underground thermal energy store (UTES)

As mentioned earlier the most common technologies are aquifer storage (ATES), borehole storage (BTES) and rock cavern storage (CTES).

ATES

Aquifer storage use groundwater (and the porous matrix through which the groundwater flows) as material for energy storage.

Generally ATES is used for seasonal heat storage (but it can be used also for daily or weekly purpose) and at least two thermal wells should be drilled: one is called the hot well and the other the cold well.

During the charging phase the groundwater is extracted from the cold well and heated by solar energy and then injected into the warm well (Xu et al., 2013).

During the discharge phase (winter) the flow is inverted. Figure 3.2 shows the operation of ATES system. This technology is effectively used for temperature ranges from 7 to 40°C.

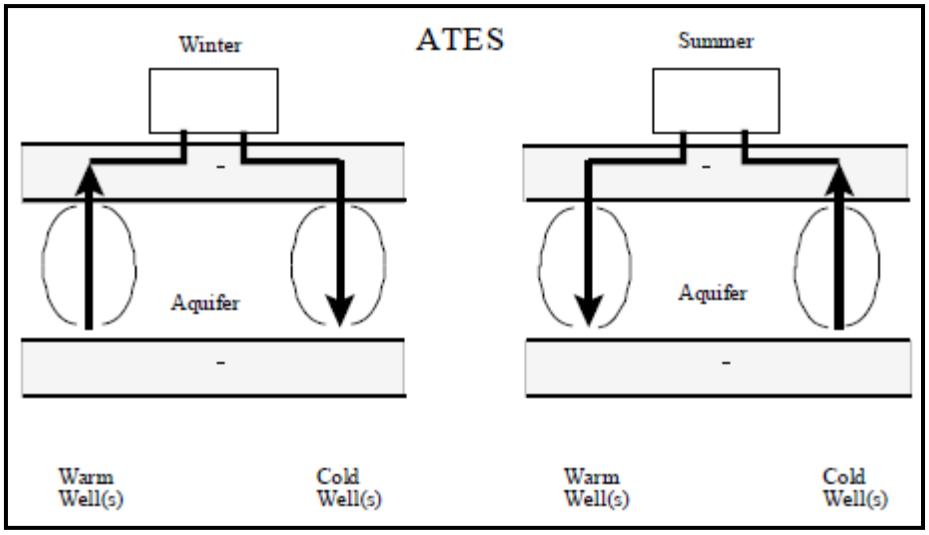

Figure 1.4 *ATES System: the arrows indicate the movement of water in the two different seasons*

In ATES is very important to know very well the groundwater system and make a correct assessment of the geological conditions of the site. Problems related at this systems are related to heat losses (Xu et al., 2013), water chemistry alteration and conflicts of interest in ground water use (Nordell et al., 2000).

BTES

Ground or rocks storage is another application of UTES. The underground structure can store a large amount of (for example) solar heat collected in the summer for later use in

winter. In this storage approach, the ground is excavated and drilled to insert horizontal or vertical tubes, for this why it is called borehole thermal energy storage (BTES). The inserted tubes serve as heat exchangers; the soil is the storage medium. In this case water is the heat carrier fluid which flows within the tubes and heat the rocks during the charge phase. Due to the lower heat capacity of rocks and soils, this application need more space than ATES (Xu et al., 2013).

In the horizontal configuration (Figure 1.5) a pipes system buried in the ground below the freezing depth is present. It can be used wherever there is sufficient surface area available for this kind of installation.

Nowadays they are more rarely installed for space heating and cooling of buildings than vertical borehole (Clauser, 2006).

Figure 1.5 *Horizontal configuration for a BTES System (Clauser, 2006)*

The vertical solution is based on shallow borehole heat exchanger, deep borehole heat exchanger and heat exchanger piles.

In the first solution heat exchangers are installed in boreholes with depth varying between 50-250 meters. For heat exchanges two common pipes arrangements are used, the “U” shape pipe or the coaxial pipe.

In Figure 1.6 is shown their functioning: in summer warm water is injected within the tubes and with its passage the surrounding rocks are heated. The heat is then recovered during the winter season: in this case, the injected water is cold and returns to the surface heated by the rocks.

The operating temperature of this plant is in the range of 40-70°C: if it is not sufficient a heat pump can be integrated to provide the desired temperature.

An example is given by the plant of Okotoks in Canada where a BTES system occupies about 50.000 m^3 with 144 holes drilled to a depth of 35m in a circular configuration with a mutual distance of about 2.25 m. Two long U-tubes of plastic material are installed in each well and interconnected to the surface, where they are connected to the central building that manages the flow of water by use of pumps; this plant supplies heat to about 52 houses of 140 m^2 (Rubin, 2013).
In the second solution the borehole heat exchangers reach 1500-3000 meters depth. This system use only coaxial pipes and the operating temperatures are about 60-110 °C: for this why these systems often do not require a heat pump (Clauser, 2006).

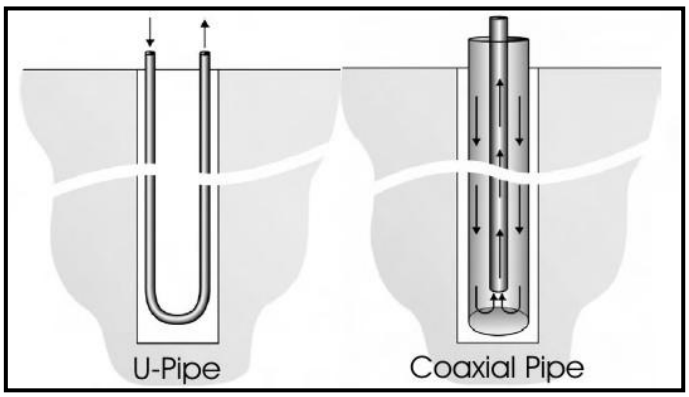

Figure 1.6 *U-pipe and coaxial pipe solution for shallow boreholes BTSE (Clauser, 2006)*

The last solution which is adopted in this field is the use of an exchanger piles integrated into the concrete foundations of buildings (Figure 1.7). This is a quite recent application and as with shallow borehole heat exchangers a heat pump is needed in order to increase the performances of the systems (Figure 1.7).

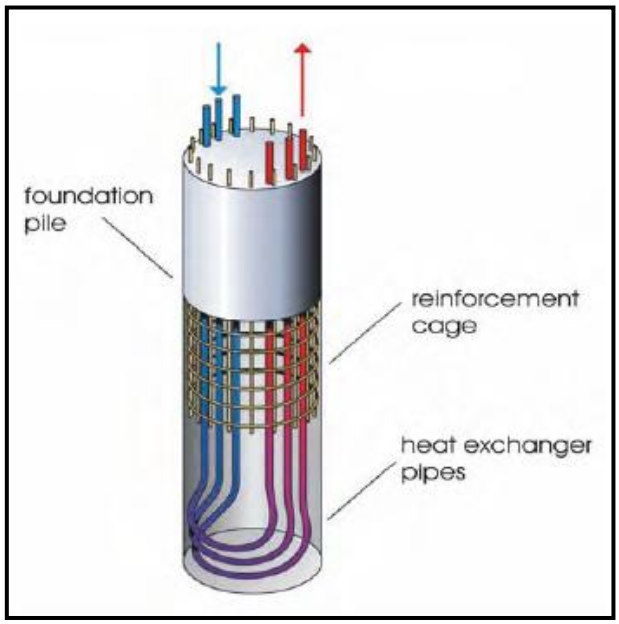

Figure 1.7 *Heat exchanger pipe systems integrated in building foundation piles (Clauser, 2006)*

CTES

In the Rock Cavern Thermal Energy Store (CTES) energy is stored as hot water in an underground cavern (Figure 1.8). In such a system with a large volume of water it is of great importance to maintain a stratified temperature profile in the cavern. During injection hot water is injected at the top of the store while colder water is extracted from the bottom (Nordell, 2000).

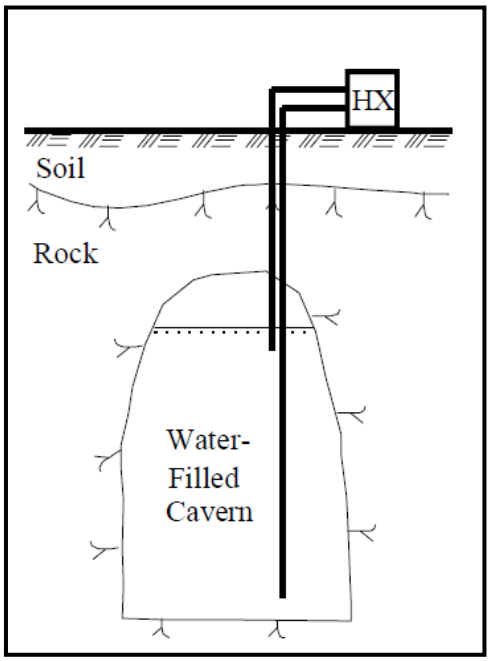

Figure 1.8 *Rock cavern for hot water storage (from Nordell, 2000)*

This kind of solution has very high construction cost so there are some examples of old rock caverns previously used for oil storage converted into high temperature water storage (Nordell, 2007).

Caverns can be also used for cold storage; since ancient time for cooling during summer snow and ice were thermally insulated with sawdust (Nordell, 2012).

This system delivers good results with considerable lower cost respect a conventional cooling system (Nordell, 2007).

1.4 Considerations about TES

TES is considered a mature technology with a variety of thermal applications, ranging from heating to cooling. Some benefits attributed to this technology are (Dincer, 2001; 2002):

- Increase generation capacity: excess generation available during low-demand periods can be used to charge a TES in order to increase the effective generation

capacity during high-demand periods. This process allows a smaller production unit to be installed;

- Shift energy purchase to low periods: energy consumers subject to time-of-day pricing can shift energy purchases from high- to low-cost periods (in particular for cold TES applications);
- Increased system reliability: the stored energy delivers a constant power supply;
- Reduced energy costs: decreases the purchase of raw materials;
- Reduce energy consumption;
- Improved air quality;
- Conservation of fossil fuels;
- Reduce pollutant emissions (in particular CO_2 and CFCs).

Dincer (2002) presents some TES systems applications and introduce the concept of energy and exergy analysis in order to have a better knowledge of the performance of the system.

The installation of TES plants must also have an economical justification. In order to keep low the initial costs is important to do a feasibility study which comprises the definition of the financial parameters of the project and an environmental impact analysis.

Very important (especially for UTES systems) is the knowledge of the thermal properties of the rocks. In contrast, if thermal properties are unknown or can only be estimated from literature data, this uncertainty is usually accommodated by the use of safety margins. A common result of this is an over-sizing of the system, (in the case of BTES, for example, the borehole is drilled to an unnecessarily great depth) and as a consequence, the system will be unnecessarily expensive (Clauser, 2006).

As mentioned a few lines ago also the environmental aspect should be considered. Some problems can be (Galgaro, 2008):

- Impairment of hydraulic barriers during the implementation phase of the underground excavations with the consequent mixing of waters of different quality;
- Chemical contamination due to leaks in the hydraulic circuit;
- Modifications of the chemical species dissolved in water induced by thermal variations;
- For ATES systems may be harmful alteration in the dynamics of groundwater due to the withdrawals and discharges of large quantities or in large numbers.

2. Geological outline

The Euganean Hills form an isolated body within the Venetian alluvial plain and represent the southernmost component of Southern Alps. They are located approximately 10 Km South-West of Padua, and cover an area of over 100 km^2 (Capedri et al., 2000).
The exposed rocks are sedimentary and volcanic, ranging in age from Lower Cretaceous to Lower Oligocene (Piccoli et al., 1981).

2.1 The stratigraphic sequence of Euganean Hills

The sequence includes rocks ranging from the Lower Jurassic to the Upper Oligocene (Figure 2.1).
Lower Jurassic rocks are represented by "Rosso Ammonitico" which outcrops only near Fontanafredda. It is gray or red nodular limestone characterized by the presence of fossils.
These limestones are followed by “Biancone” which is a white limestone, compact and fine-grained with conchoidal fracture (Upper Cretaceous - Lower Cretaceous).
The most diffuse sedimentary rock is “Scaglia Rossa” (Lower Cretaceous – Paleocene). It is reddish-pinkish limestone more or less rich in clays, thin bedded, with grey or red chert lenses (ISPRA, 2011).
The last rock of the stratigraphic series is “Marna Euganea” which refers to the period of the Eocene. This calcareous-clay rock is thickly layered, color from gray to yellowish or bluish, containing a rich fauna foraminifera (Astolfi et al., 2003).

2.2 The Euganean Hills District

The geology of the Euganean Hills is dominated by two rock series: an Upper Jurassic to Lower Oligocene marine sedimentary sequence, mainly composed of limestone and marl (as illustrated in §2.1), and a series of volcanic and subvolcanic products, diversified in both space and time (Schiavinato, 1950; Piccoli, 1966; Conedera et al., 1969; Sedea et al., 1973; Piccoli et al., 1981) (Fig. 2.2). The latter represents the most recent magmatic manifestation within the Palaeocene-Upper Oligocene Venetian Volcanic Province (VVP) (De Vecchi et al., 1974; Sassi et al., 2004; Bartoli et al., 2013). This activity covered a 30-Ma time-span, from Late Palaeocene to Late Oligocene, and developed during the Alpine orogenesis in the Southern Alps (Borsi et al., 1969; De Vecchi et al., 1976; and references quoted therein).

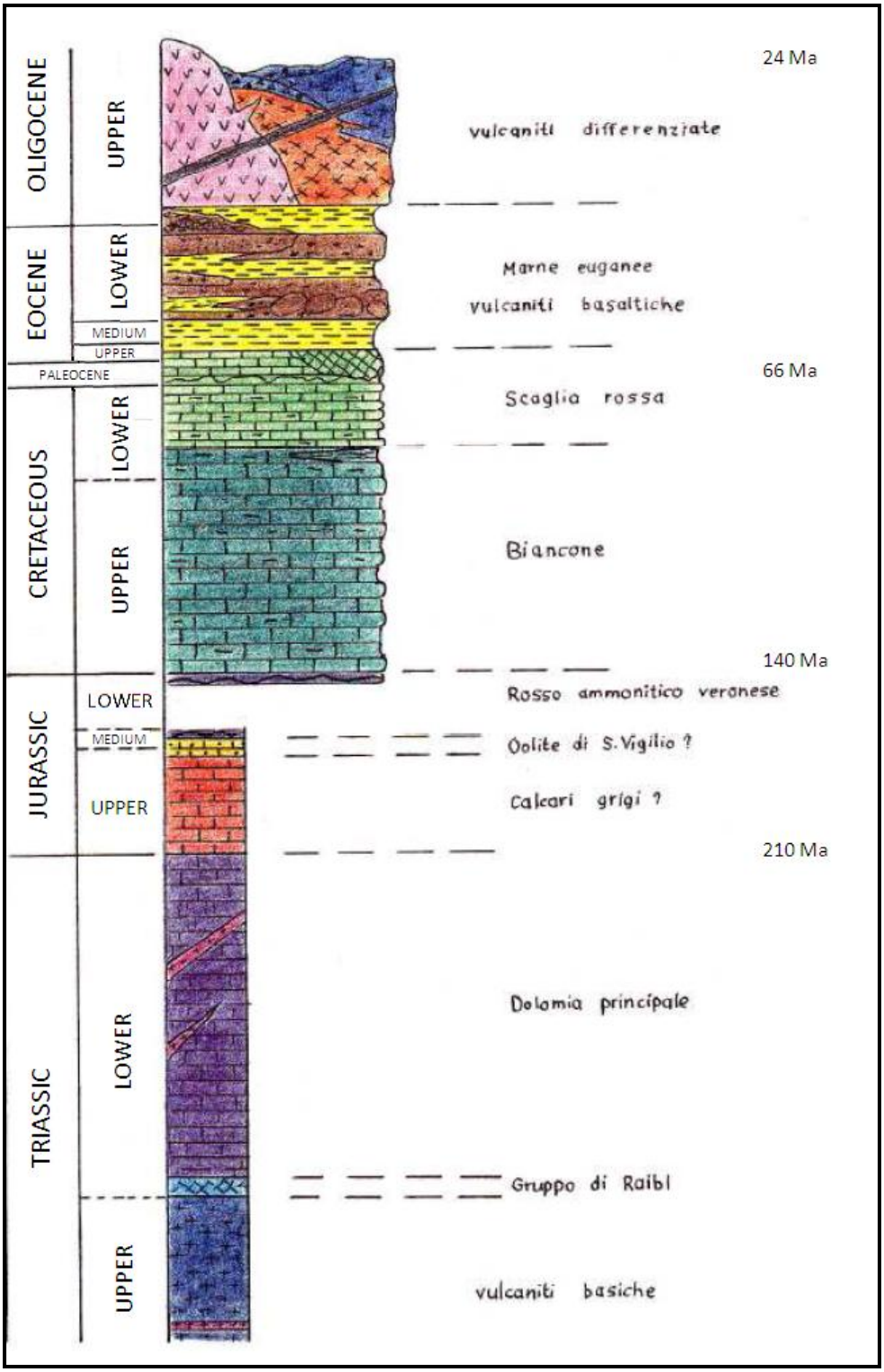

Figure 2.1 *Stratigraphic sequence of the Euganean Hill (modified from Piccoli et al., 1981)*

The Euganean Hills District is the most recent within the VVP. It developed over a relatively short time-span of 10 Ma (Eocene-Oligocene), during which two main volcanic events are recognised (Piccoli, 1966; Conedera et al., 1969; Sedea et al., 1973; Piccoli et al., 1981): the older event is Late Eocene in age (42 ± 1.5 Ma, Borsi et al.,

1969) and displays the typical features of submarine basic volcanism (pillow lava, breccias, hyaloclastites); the younger event is Oligocene in age (33 ± 1 Ma, Borsi et al., 1969; 32 + 3,5 Ma and 34 + 2 Ma according to Rb-Sr radiometric ages on biotite from trachyte and rhyolite, respectively); and is characterised by the emplacement of acidic and intermediate volcanic and sub-volcanic bodies (domes, plugs, laccolites and dykes). From the chemical and petrographic viewpoints, the most representative rock types of the Euganean Hills District are rhyolite and trachyte; latite and basalt occur in minor amounts. Rhyolite, generally slightly alkaline and only rarely peralkaline, is the most abundant volcanic rock. It covers the whole range from persilicic rhyolite to quartz-trachyte. As regards the origin of these acidic melts, petrologic and isotopic studies indicate that both trachyte and rhyolite crystallised from a trachytic parent magma, which formed through partial melting of the upper mantle in the presence of volatile components derived from crustal contamination. During their ascent towards the surface, these melts resided at depth, where fractionation processes developed and produced differentiated rocks, from trachyte to rhyolite (Schiavinato, 1950; Bailey, 1964; 1974; Marinelli, 1975; Barbieri et al., 1978).

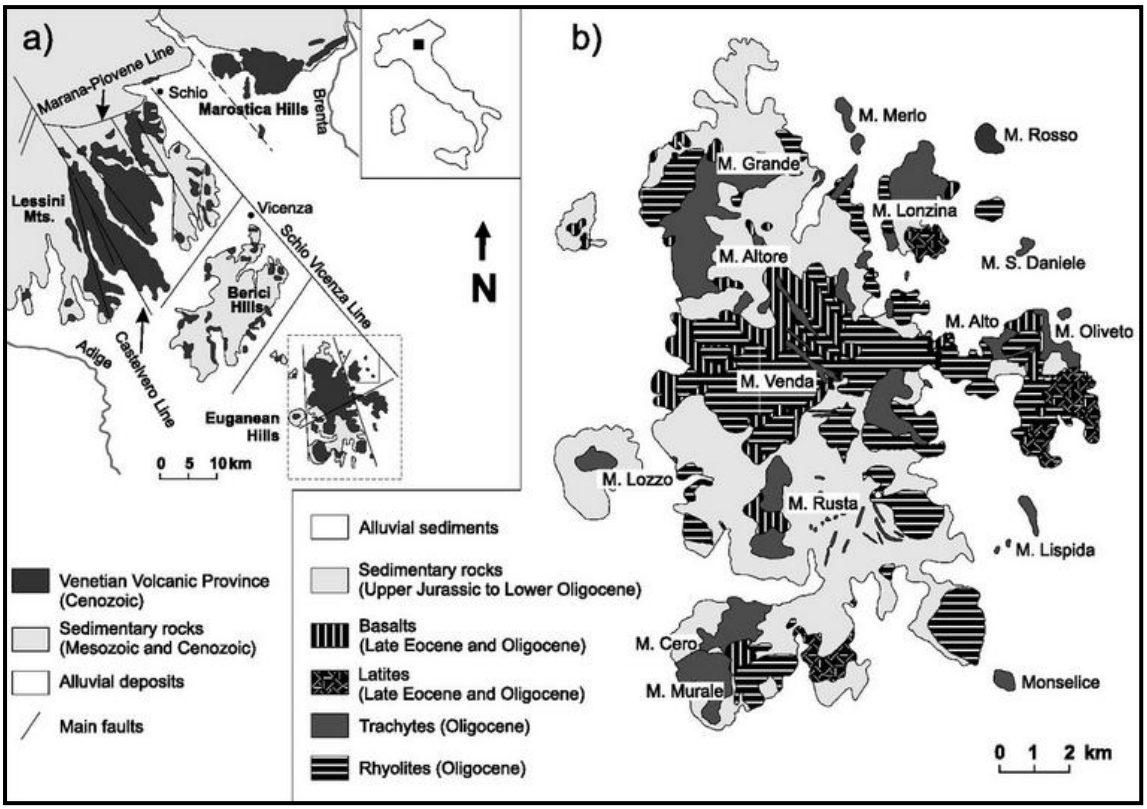

Figure 2.2 *Geological sketch of Venetian Volcanic Province (a) and zoom-in (dashed area) of Euganean Hills (b) (Maritan et al., 2013)*

3. The samples

In this chapter the samples used to characterize the thermal properties of the considered rocks are described. 47 samples of different lithologies have been collected in the Euganean Hills area. Among these samples, 21 samples have been selected, on the basis of petrographic and structural considerations, for the laboratory tests and analyses (Table 3.1). Localization of the selected samples is showed in Figure. 3.1.

Table 3.1 *List of the 21 samples used for laboratory tests. Note: The terms "S.R.", "B.", "R.A.", in parentheses are referred to the formations of "Scaglia Rossa", "Biancone" and "Rosso Ammonitico"; respectively*

Sample number	Day of sampling	Place	Lithology
1	11/07/2013	Cava di Montemerlo	Trachyte
22B	16/07/2013	Rocca Pendice	Trachyte
44	22/07/2013	Monte Cero	Trachyte
16	13/07/2013	Torreglia	Rhyolite
36	20/07/2013	Monte Rua	Rhyolite
39	20/07/2013	Monte Rua	Rhyolite
18	13/07/2013	Monte Sengiaro	Latite
42	22/07/2013	Monte Cecilia	Latite
43	22/07/2013	Baone	Latite
11	13/07/2013	Faedo	Marl
24	16/07/2013	Teolo	Marl
46	19/07/2013	Cinto Euganeo	Marl
3	11/07/2013	Teolo	Limestone (S.R.)
25	17/07/2013	Villa di Teolo	Limestone (S.R.)
47	22/07/2013	Monte Cecilia	Limestone (S.R.)
6A	11/07/2013	Bastia	Limestone (B.)
8	12/07/2013	Fontanafredda	Limestone (B.)
27A	17/07/2013	Villa di Teolo	Limestone (B.)
10A	12/07/2013	Fontanafredda	Limestone (R.A.)
34	19/07/2013	Fontanafredda	Limestone (R.A.)
35	19/07/2013	Fontanafredda	Limestone (R.A.)

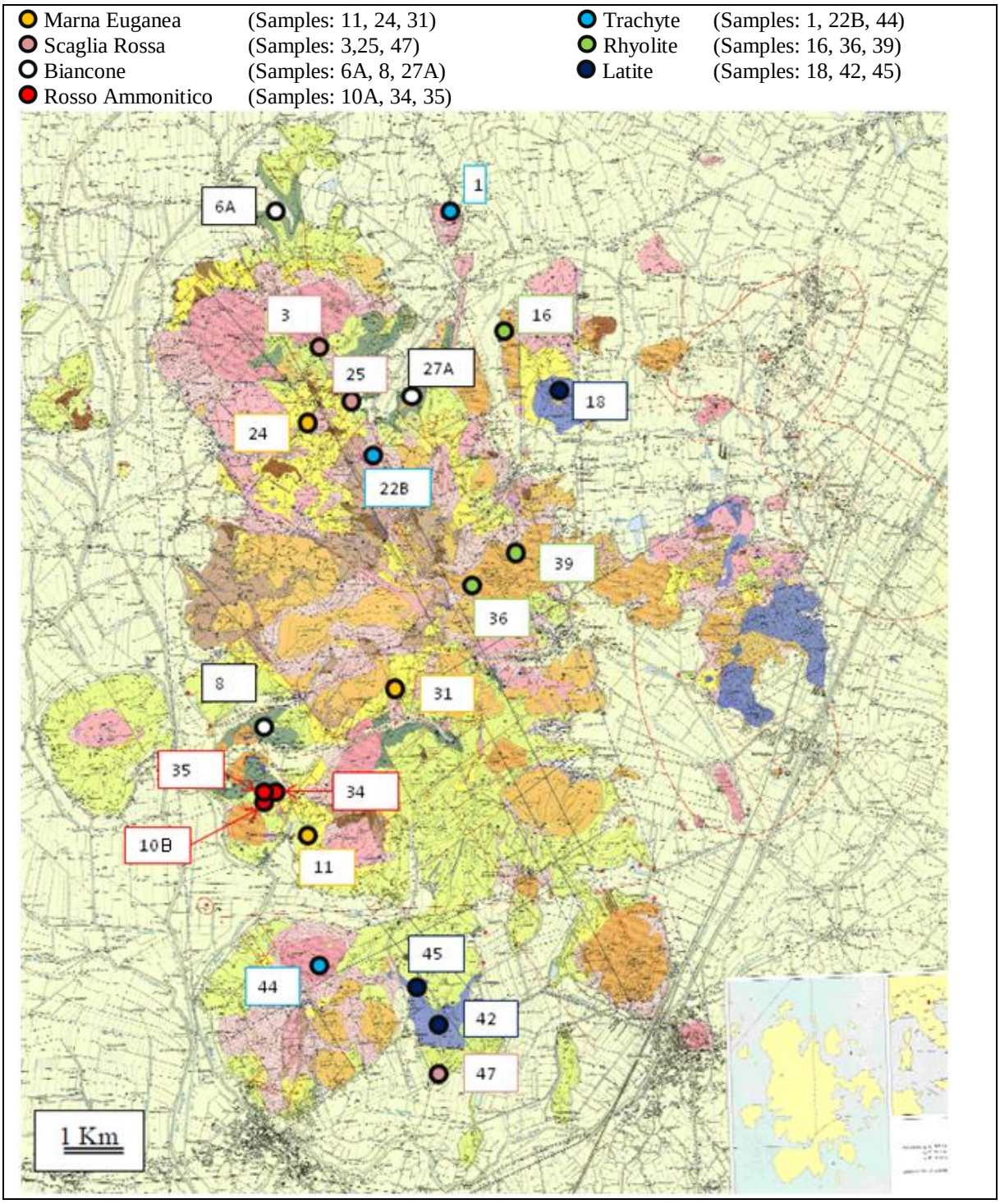

Figure 3.1 *Localization of the samples in the geological map of Euganean Hills (Source: Carta Geologica dei Colli Euganei, 1981)*

3.1 Geological data sheet of the samples

In this section the data sheet of the collected samples are given. They are made in order to provide specific information for every sample used on laboratory test. Every sheet shows the localization of the sample and gives a brief description of the outcrop and the sample.

Sample 1

Date of collection:
11/07/2013

Location of sampling:
Cava di Montemerlo

Coordinates (WGS84):
N 45°22'37.3",
E 11°42'19.7"

Lithology:
Trachyte

Geological formation:
Lave trachitiche alcaline

Age:
Upper Oligocene

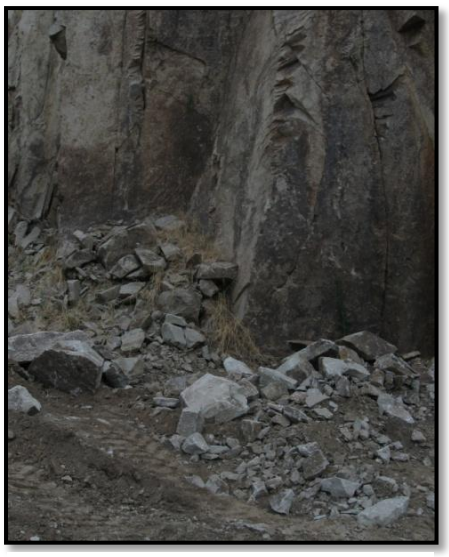

Figure 3.3 *The outcrop*

Figure 3.2 *Localization of Sample 1*

Outcrop description: The trachyte of Montemerlo is a laccolith; the contacts between the trachyte and sedimentary rock located on its roof appear concordant. As all shallow intrusion, this trachyte body shows an evident columnar jointing (Figure 3.3). It is also an excellent cut stone.

Lithological description: Grey – coloured, massive and rough to the touch, showing locally yellowish color as a result of secondary hydrothermal processes (Figure 3.4 and

3.5). It has porphyritic structure with light coloured sanidine and feldspars phenocrysts and dark amphibole and biotite phenocrysts.

Figure 3.4 *Photo of sample number 1*

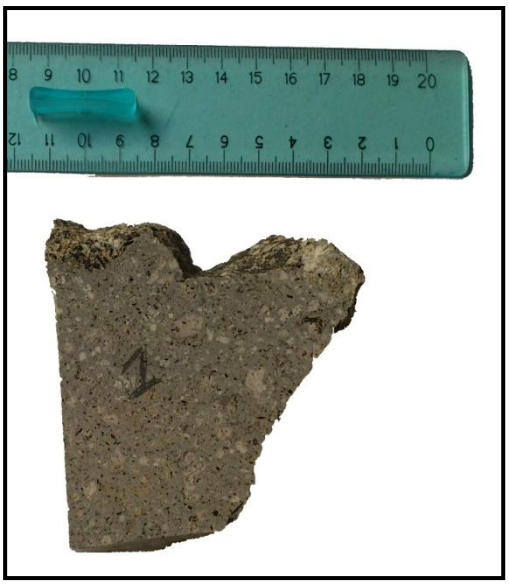

Figure 3.5 *Section of the sample*

Sample 22B

Date of collection:
16/07/2013
Location of sampling:
Rocca Pendice, Teolo (Fig. 3.6)
Coordinates (WGS84):
N 45°20'15.8", E 11°40'58.0"

Lithology:
Trachyte
Geological formation:
Quarzotrachiti alcaline
Age: Upper Oligocene

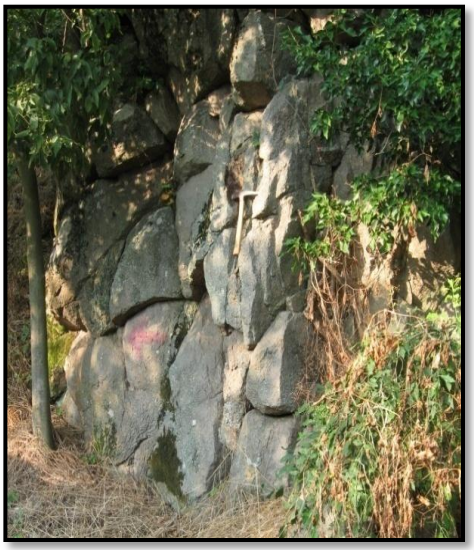

Figure 3.7 *The outcrop*

Figure 3.6 *Localization of Sample 22B*

Figure 3.8 *Photo of sample 22B*

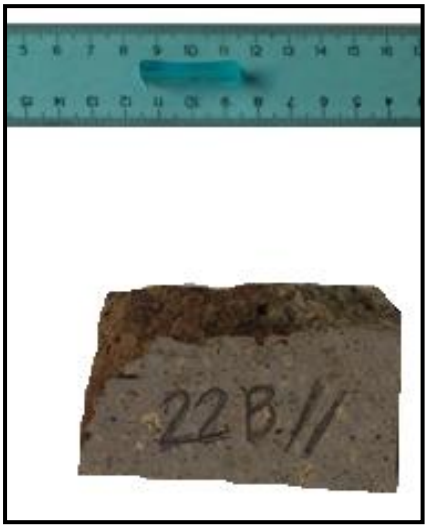

Figure 3.9 *Section of the sample*

Outcrop description: It is a large massive trachytic which is near at less resistant rocks created during Eocene and nowadays largely removed by erosion (Figure 3.7) (Piccoli et al., 1981).

Lithological description: Grey – coloured, massive and rough to the touch, showing locally yellowish color as a result of secondary hydrothermal processes. It has porphyritic structure with light coloured sanidine and feldspars phenocrysts and dark amphibole and biotite phenocrysts (Figure 3.8 and 3.9).

Sample 44

Date of collection:
22/07/2013

Location of sampling:
ex Cava Monte Cero, Baone (Fig. 3.10)

Coordinates (WGS84):
N 45° 15'12.2", E 11°39'59.9"

Lithology:
Trachyte

Geological formation:
Quarzotrachiti alcaline

Age:
Upper Oligocene

Figure 3.11 *The outcrop*

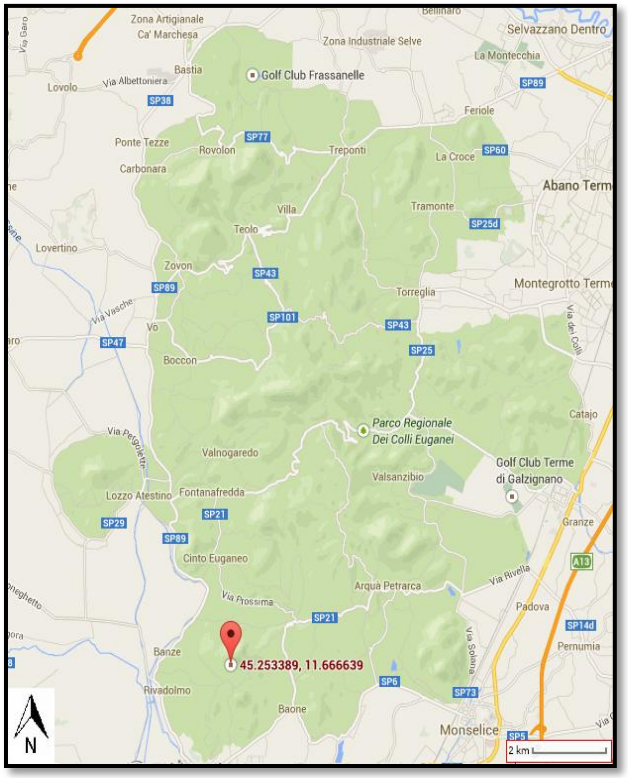

Figure 3.10 *Localization of Sample 22B*

Figure 3.12 *Photo of sample 44*

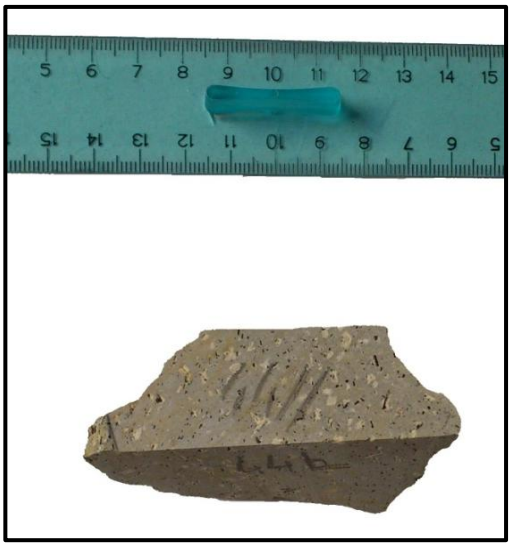

Figure 3.13 *Section of the sample*

Outcrop description: The Monte Cero outcrop is a eruption laccolith in which the alkaline trachyte seems to have come out fracturing the sedimentary cover. The sample comes from the former quarry located not far from the summit of the hill (Figure 3.11) (Piccoli et al., 1981).

Lithological description: Grey – coloured, massive and rough to the touch, showing locally yellowish color as a result of secondary hydrothermal processes. It has porphyritic structure with light coloured sanidine and feldspars phenocrysts and dark amphibole and biotite phenocrysts (Figure 3.11 and 3.12).

Sample 16

Date of collection:
13/07/2013
Location of sampling:
Torreglia (Fig. 3.14)
Coordinates (WGS84):
N 45°21'25.1", E 11°43'00.9"

Lithology:
Rhyolite
Geological formation:
Rioliti alcaline
Age:
Upper Oligocene

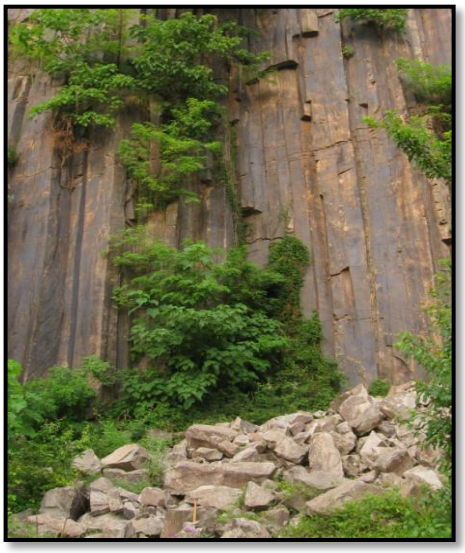

Figure 3.15 *The outcrop*

Figure 3.14*Localization of Sample 16*

Figure 3.16 *Photo of sample 16*

Figure 3.17 *Section of the sample*

Outcrop description: The outcrop is localized in the former quarry on the western flank of Monte Brusà. It appears as a remarkable example of columnar rhyolite (Figure 3.15) (Piccoli et al., 1981).

Lithological description: Fine grained effusive rock, featuring a porphyritic structure and a microcrystalline groundmass in which phenocrysts of quartz and feldspar (more rarely) are present. (Figure 3.16 and 3.17).

Sample 36

Date of collection:
20/07/2013

Location of sampling:
Monte Rua (Fig. 3.18)

Coordinates (WGS84):
N 45°19'03.1", E 11°42'54.0"

Lithology:
Rhyolite

Geological formation:
Rioliti alcaline

Age:
Upper Oligocene

Figure 3.19 *The outcrop*

Figure 3.18 *Localization of Sample 36*

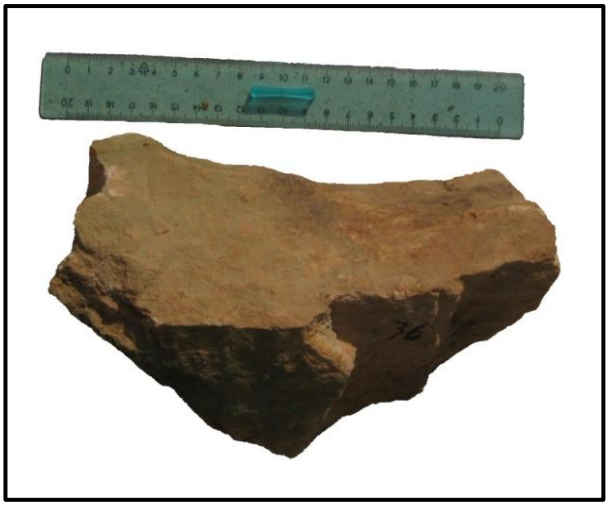

Figure 3.20 *Photo of sample 36*

Figure 3.21 *Section of the sample*

Outcrop description: The outcrop is near at "Eremo camaldolese" of the Monte Rua. The rhyolitic eruption apparatus of this hill corresponds to a lava dome (Figure 3.19) (Piccoli et al., 1981).

Lithological description: Fine grained effusive rock, featuring a porphyritic structure and a microcrystalline groundmass in which phenocrysts of quartz and feldspar (more rarely) are present. (Figure 3.20 and 3.21).

Sample 39

Date of collection:
20/07/2013
Location of sampling:
Monte Rua (Fig. 3.22)
Coordinates (WGS84):
N 45°19'10.4", E 11°42'56.1"

Lithology:
Rhyolite
Geological formation:
Rioliti alcaline
Age: Upper Oligocene

Figure 3.22 *Localization of Sample 39*

Figure 3.23 *The outcrop*

Figure 3.24 *Photo of sample 39*

Figure 3.25 *Section of the sample*

Outcrop description: The outcrop is near at "Eremo camaldolese" of the Monte Rua. The rhyolitic eruption apparatus of this hill corresponds to a lava dome (Figure 3.23) (Piccoli et al., 1981).

Lithological description: Fine grained effusive rock, featuring a porphyritic structure and a microcrystalline groundmass in which phenocrysts of quartz and feldspar (more rarely) are present (Figure 3.24 and 3.25).

Sample 18

Date of collection:
13/07/2013
Location of sampling:
Monte Sengiari (Fig. 3.26)
Coordinates (WGS84):
N 45°20’53.7", E 11°43’38.8"

Lithology:
Latite
Geological formation:
Lava latitica
Age:
Upper Oligocene

Figure 3.27 *The outcrop*

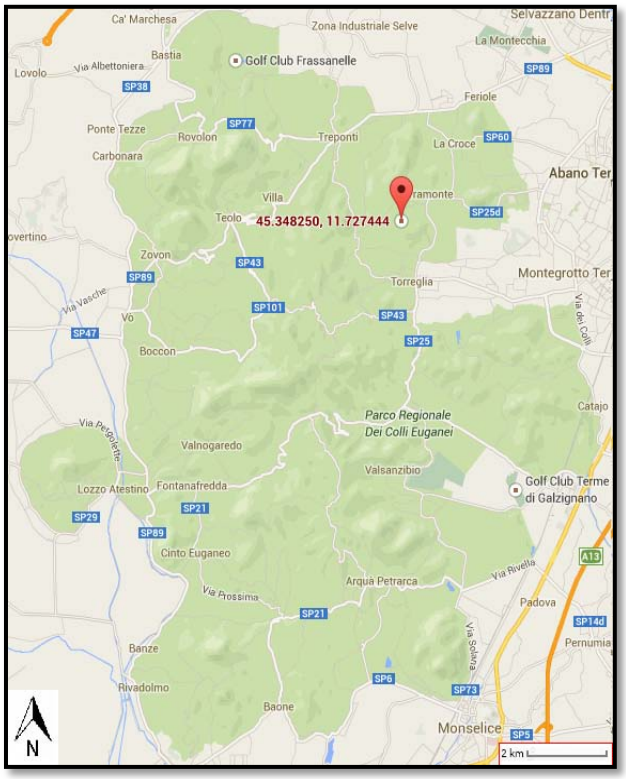

Figure 3.26 *Localization of Sample 18*

Figure 3.28 *Photo of sample 18*

Figure 3.29 *Section of the sample*

Outcrop description: Monte Sengiari is a eruptive body of latite and on the top of the hill is presents “Marna Euganea” that was raised during the eruptions . The sample is localized along the road that leads to the summit of Monte Sengiari (Figure 3.27) (Piccoli et al., 1981; Astolfi et al., 2003).

Lithological description: Effusive dark gray rock with porphyritic structure. Phenocrysts are: pyroxene, amphibole, plagioclase. (Figure 3.28 and 3.29).

Sample 42

Date of collection:
22/07/2013
Location of sampling:
Monte Cecilia (Fig. 3.30)
Coordinates (WGS84):
N 45°14’33.1", E 11°41’46.8"

Lithology:
Latite
Geological formation:
Lava latitica
Age:
Upper Oligocene

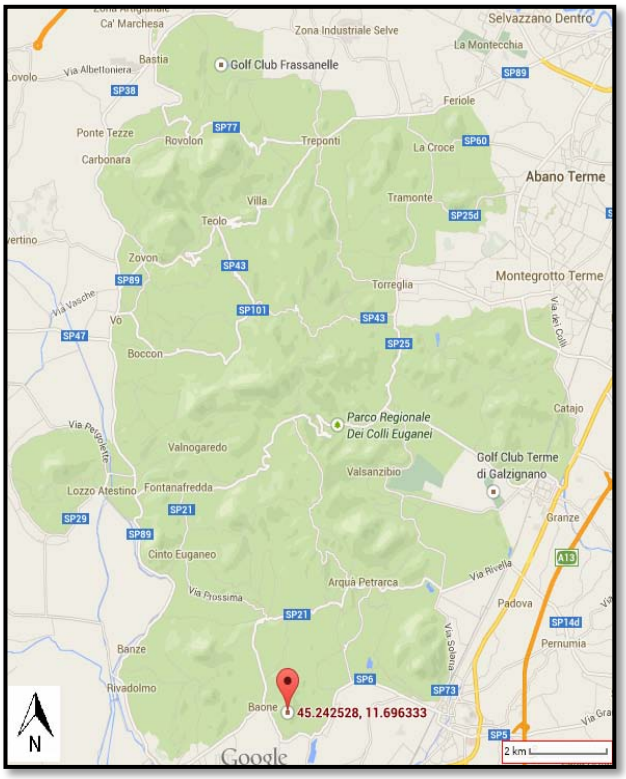

Figure 3.30 *Localization of Sample 42*

Figure 3.31 *The outcrop*

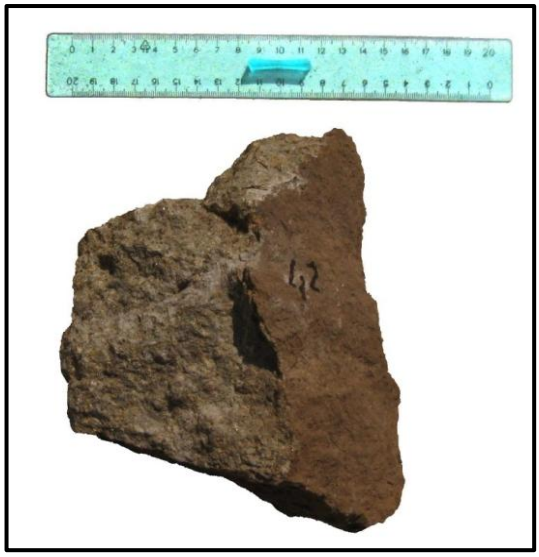

Figure 3.32 *Photo of sample 42*

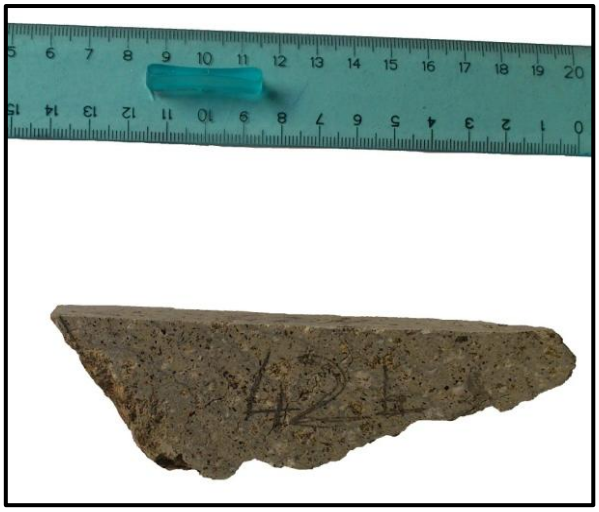

Figure 3.33 *Section of the sample*

Outcrop description: The outcrop is near the top of Monte Cecilia, who is the best example of laccolith of all the Euganean Hills. The eruptive mass is concordant with the stratifications of the sedimentary rock (Figure 3.31) (Piccoli et al., 1981).

Lithological description: Effusive dark gray rock with porphyritic structure. Phenocrysts are: pyroxene, amphibole, plagioclase. (Figure 3.32 and 3.33).

Sample 43

Date of collection:
22/07/2013

Location of sampling:
Monte Cecilia (Fig. 3.34)

Coordinates (WGS84):
N 45°14’52.9", E 11°41’33.2"

Lithology:
Latite

Geological formation:
Lava latitica

Age:
Upper Oligocene

Figure 3.35 *The outcrop*

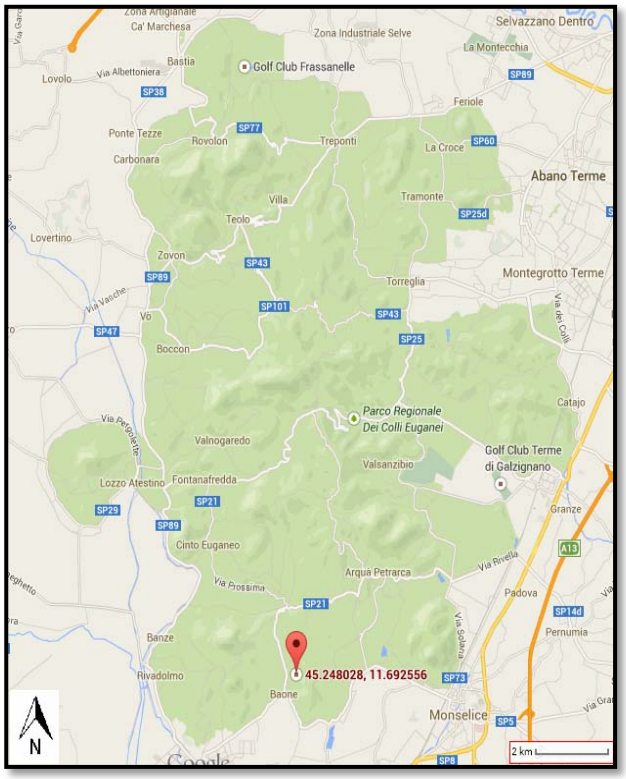

Figure 3.34 *Localization of Sample 43*

Figure 3.36 *Photo of sample 43*

Figure 3.37 *Section of the sample*

Outcrop description: The outcrop is near the top of Monte Cecilia, who is the best example of laccolith of all the Euganean Hills. The eruptive mass is concordant with the stratifications of the sedimentary rock (Figure 3.35) (Piccoli et al., 1981)

Lithological description: Effusive dark gray rock with porphyritic structure. Phenocrysts are: pyroxene, amphibole, plagioclase. (Figure 3.36 and 3.37).

Sample 11

Date of collection:
12/07/2013
Location of sampling:
Cinto Euganeo (Fig. 3.38)
Coordinates (WGS84):
N 45°18’20.7", E 11°41’36.1"

Lithology:
Marl
Geological formation:
Marna Silicizzata
Age:
Eocene

Figure 3.39 *The outcrop*

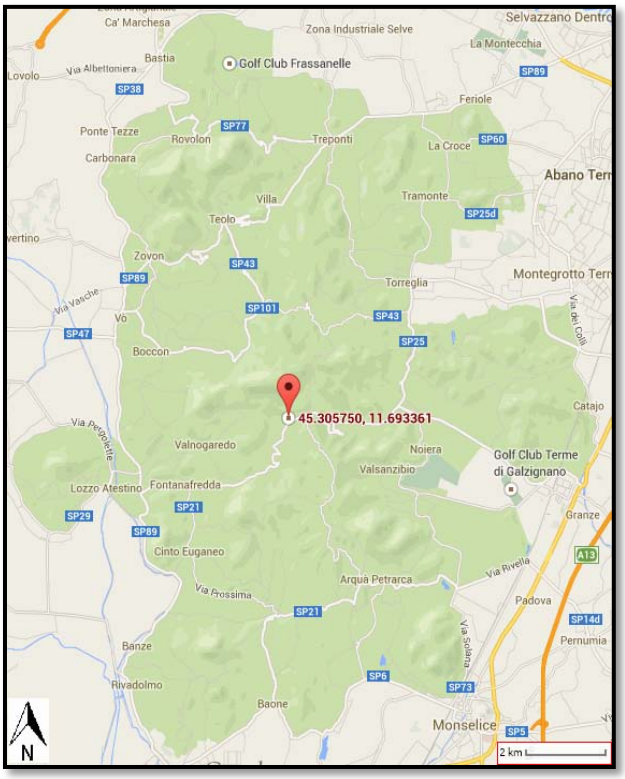

Figure 3.38 *Localization of Sample 11*

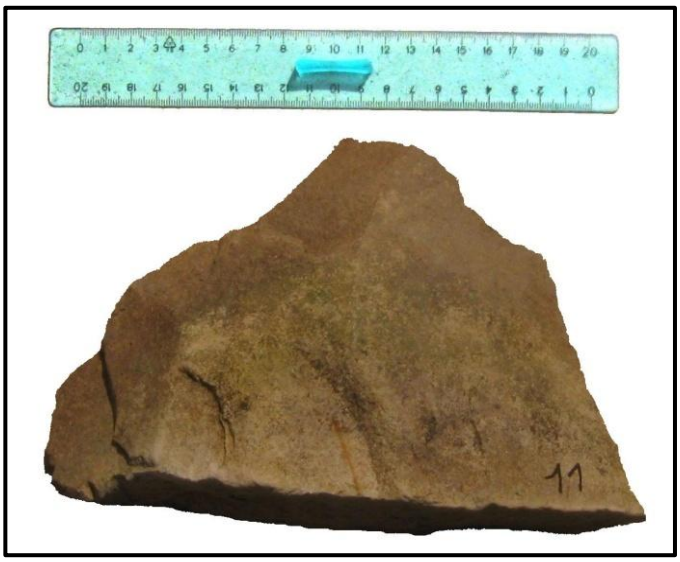

Figure 3.40 *Photo of sample 11*

Figure 3.41 *Section of the sample*

Outcrop description: The outcrop is located near Faedo fraction of Cinto Euganeo. It is small because this type of rock erodes easily (Figure 3.39) (Piccoli et al., 1981).

Lithological description: This calcareous-clay rock is thickly bedded. The ranges colors from gray to yellowish or bluish (Figure 3.40 and 3.41) (Astolfi et al., 2003).

Sample 24

Date of collection:
16/07/2013

Location of sampling:
Teolo (Fig. 3.42)

Coordinates (WGS84):
N 45°20’28.9", E 11°40’41.0"

Lithology:
Marl

Geological formation:
Marna Euganea

Age:
Eocene

Figure 3.43 *The outcrop*

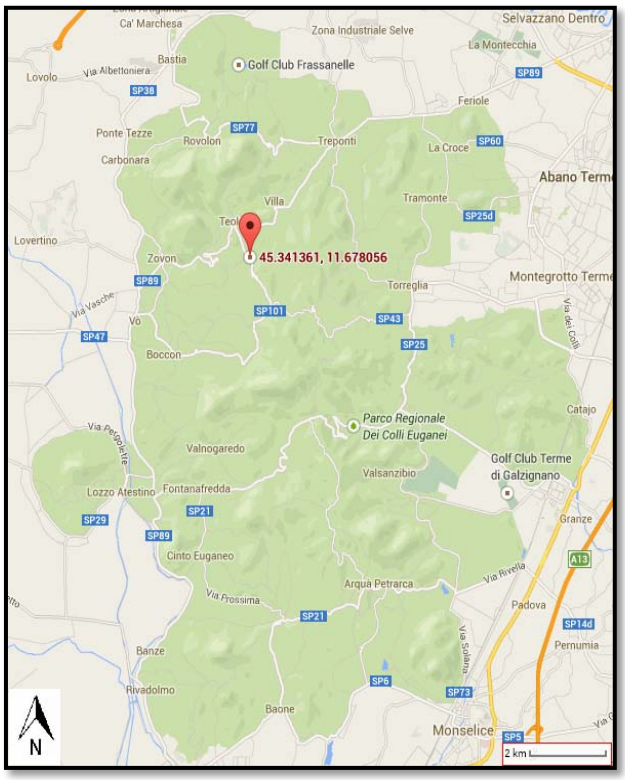

Figure 3.42 *Localization of Sample 24*

Figure 3.44 *Photo of sample 24*

Figure 3.45 *Section of the sample*

Outcrop description: The outcrop is located along the street which from Teolo goes to “Rocca Pendice”. As in the previous case, the outcrop is small because this type of rock erodes easily (Figure 3.43) (Piccoli et al., 1981).

Lithological description: This calcareous-clay rock is thickly bedded. The ranges colors from gray to yellowish or bluish (Figure 3.44 and 3.45) (Astolfi et al., 2003).

Sample 46

Date of collection:
17/07/2013
Location of sampling:
Cinto Euganeo (Fig. 3.46)
Coordinates (WGS84):
N 45°17'08.4", E 11°39'59.8"

Lithology:
Marl
Geological formation:
Marna Euganea
Age:
Eocene

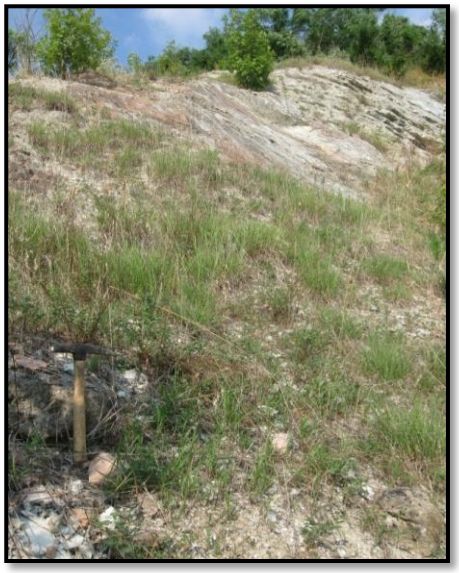

Figure 3.47 *The outcrop*

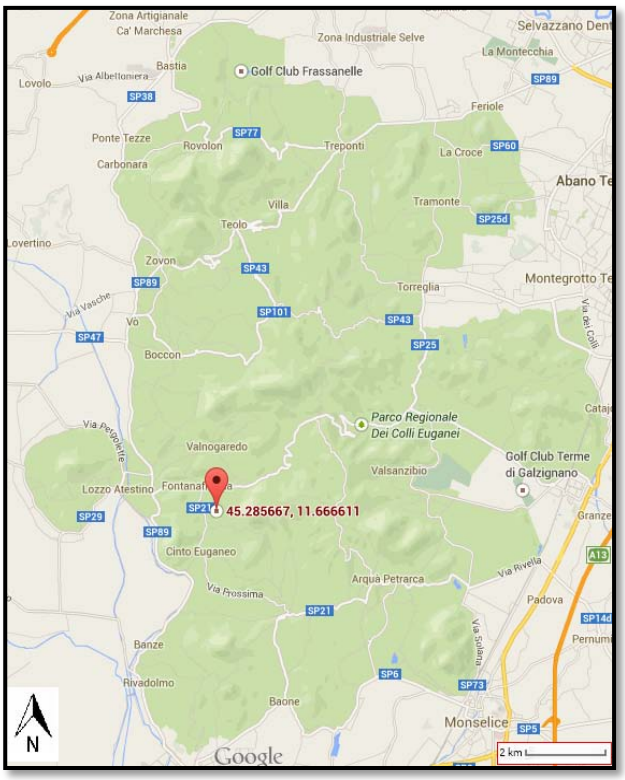

Figure 3.46 *Localization of Sample 46*

Figure 3.48 *Photo of sample 46*

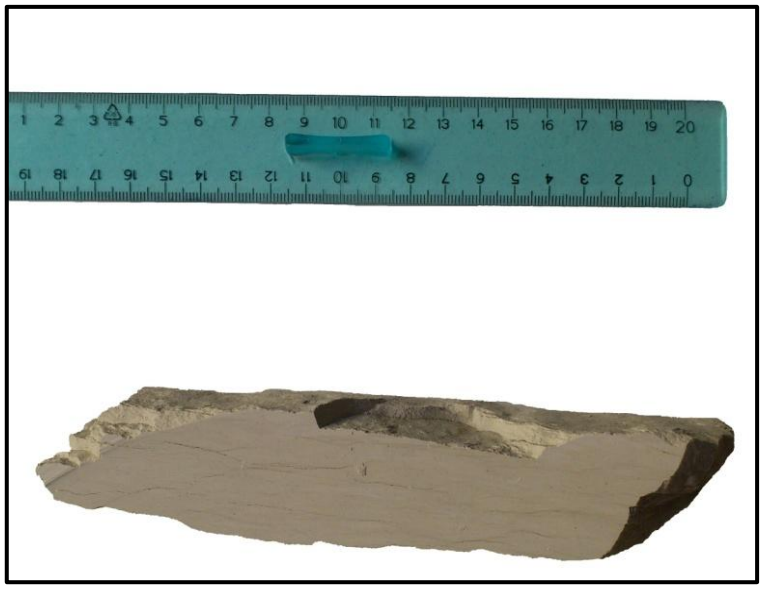

Figure 3.49 *Section of the sample*

Outcrop description: The outcrop is located in the former quarry of Monte Cucuzzola, closed since 1992. Mining activities has considerably altered the morphology of the territory: the front of the outcrop is unstable.(Aurighi, 1999).

Lithological description: This calcareous-clay rock is thickly bedded. The ranges colors from gray to yellowish or bluish. (Astolfi et al., 2003). (Figure 3.47 and 3.48).

Sample 3

Date of collection:
11/07/2013
Location of sampling:
Teolo (Fig. 3.50)
Coordinates (WGS84):
N 45°21'28.6", E 11°40'15.3"

Lithology:
Limestone
Geological formation:
Scaglia Rossa
Age:
Lower Cretaceous – Upper Eocene

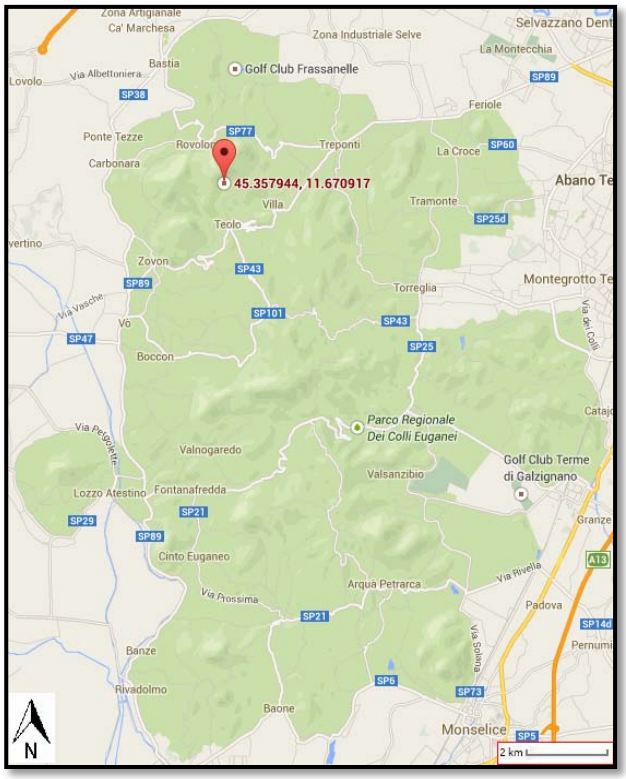

Figure 3.50 *Localization of Sample 3*

Figure 3.51 *The outcrop*

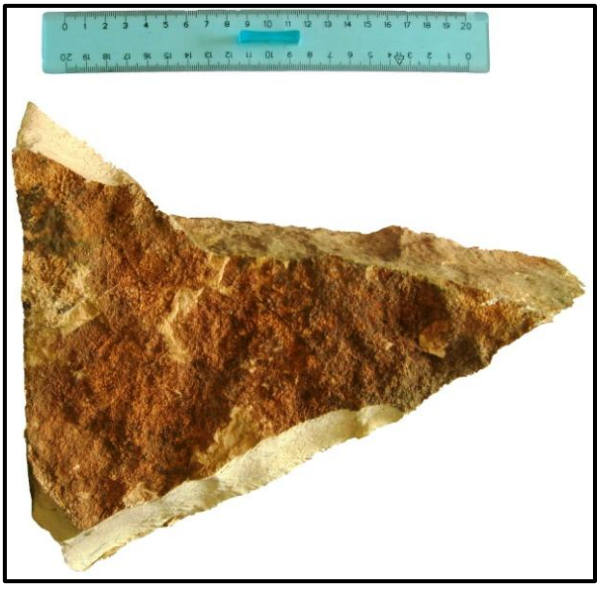

Figure 3.52 *Photo of sample 3*

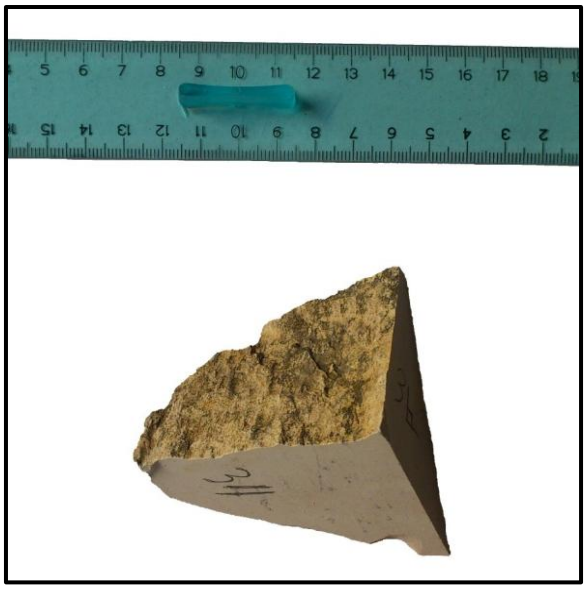

Figure 3.53 *Section of the sample*

Outcrop description: The outcrop is located in Via Monte Madonna, a road which link Teolo with Rovolon. It present a stratification which is more dense in the upper part (Figure 3.51).

Lithological description: The sedimentary rock "Scaglia Rossa" is a fine-grained marlstone, more or less rich in clays, predominantly reddish in color but can switch to white to yellow to deep red. The red colouration resulting from the dispersion in the limestone mass of iron oxide (hematite and limonites) (Astolfi et al.,2003) (Figure 3.52 and 3.53).

Sample 25

Date of collection:
17/07/2013
Location of sampling:
Villa di Teolo (Fig. 3.54)
Coordinates (WGS84):
N 45°20’54.5", E 11°40’51.0"

Lithology:
Limestone
Geological formation:
Scaglia Rossa
Age:
Lower Cretaceous – Upper Eocene

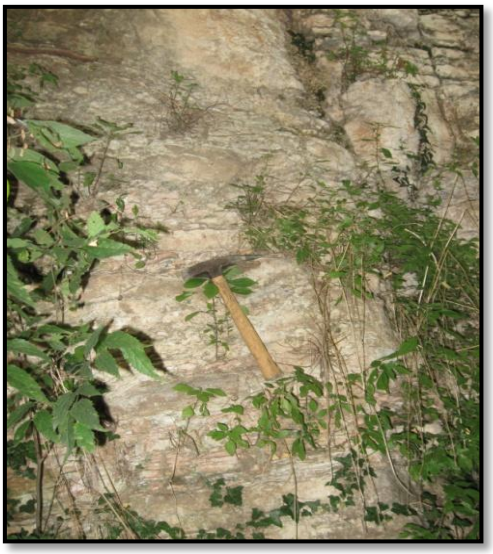

Figure 3.55*The outcrop*

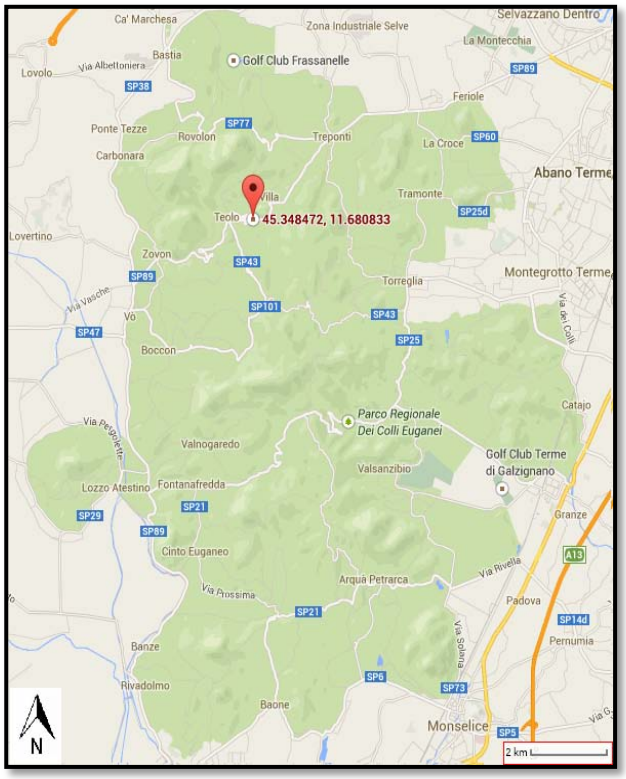

Figure 3.54 *Localization of Sample 25*

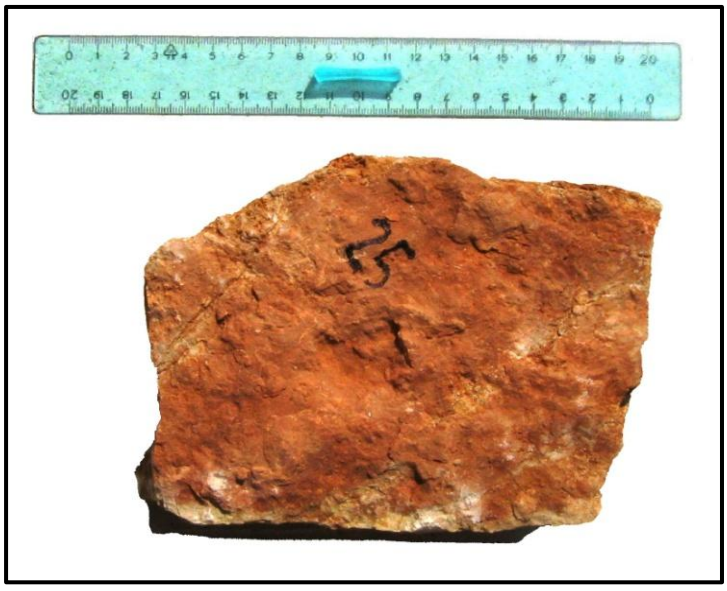

Figure 3.56 *Photo of sample 25*

Figure 3.57 *Section of the sample*

Outcrop description: The outcrop is located near the road which link Treponti with Teolo. It present a regular stratification; the dominant color is a light pink (Figure 3.55).

Lithological description: The sedimentary rock “Scaglia Rossa” is a fine-grained marl, more or less rich in clays, predominantly reddish in color but can switch to white to yellow to deep red. The red colouration resulting from the dispersion in the limestone mass of iron oxide (hematite and limonites) (Figure 3.56 and 3.57) (Astolfi et al.,2003) .

Sample 47

Date of collection:
17/07/2013
Location of sampling:
Villa di Teolo (Fig. 3.58)
Coordinates (WGS84):
N 45°14' 14.9", E 11° 41' 42.9"

Lithology:
Limestone
Geological formation:
Scaglia Rossa
Age:
Lower Cretaceous – Upper Eocene

Figure 3.59*The outcrop*

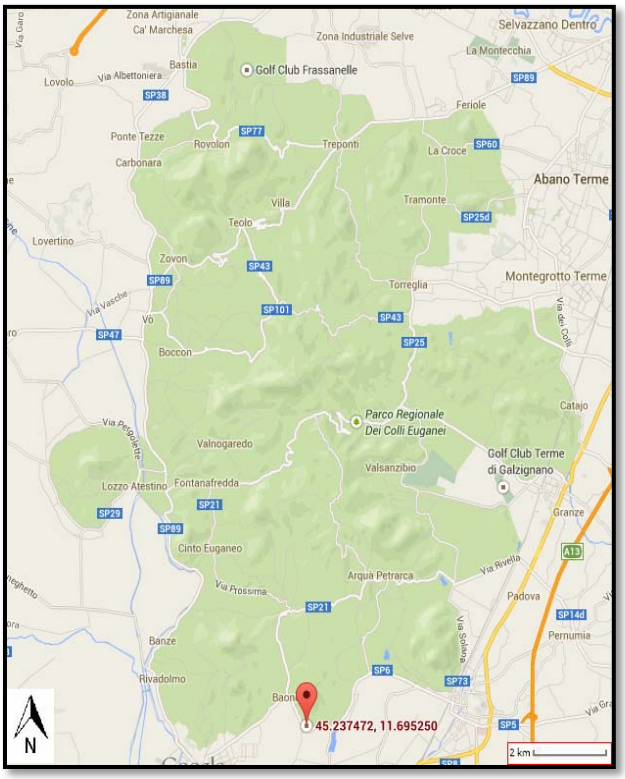

Figure 3.58 *Localization of Sample 47*

Figure 3.60 *Photo of sample 47*

Figure 3.61 *Section of the sample*

Outcrop description: The outcrop is at the base of Monte Cecilia. The stratification is regular and, as in other outcrops in the southern area of the Euganean Hills, the outcrop has very light colors (Figure 3.59) (Piccoli et al., 1981).

Lithological description: The sedimentary rock "Scaglia Rossa" is a fine-grained marl, more or less rich in clays, predominantly reddish in color but can switch to white to yellow to deep red. The red colouration resulting from the dispersion in the limestone mass of iron oxide (hematite and limonites) (Astolfi et al.,2003) (Figure 3.60 and 3.61).

Sample 6A

Date of collection:
11/07/2013

Location of sampling:
Bastia di Rovolon (Fig. 3.62)

Coordinates (WGS84):
N 45°22’38.8", E 11°40’09.2"

Lithology:
Limestone

Geological formation:
Biancone

Age:
Upper Creataceous–
Lower Creataceous

Figure 3.63*The outcrop*

Figure 3.62 *Localization of Sample 6A*

Figure 3.64 *Photo of sample 6A*

Figure 3.65 *Section of the sample*

Outcrop description: The outcrop is in “Via Monte Cereo” not far from “Golf Club Frassanelle”. It presents a clear stratification only at the upper part (Figure 3.63) (Piccoli et al., 1981).

Lithological description: Very fine-grained white limestone with conchoidal fracture. It presents lenses of flint which are often dark (Figure 3.64 and 3.65) (Astolfi et al., 2003).

Sample 8

Date of collection:
12/07/2013

Location of sampling:
Cinto Euganeo (Fig. 3.66)

Coordinates (WGS84):
N 45°17’36.8", E 11°39’20.3"

Lithology:
Limestone

Geological formation:
Biancone

Age:
Upper Creataceous–
Lower Creataceous

Figure 3.67*The outcrop*

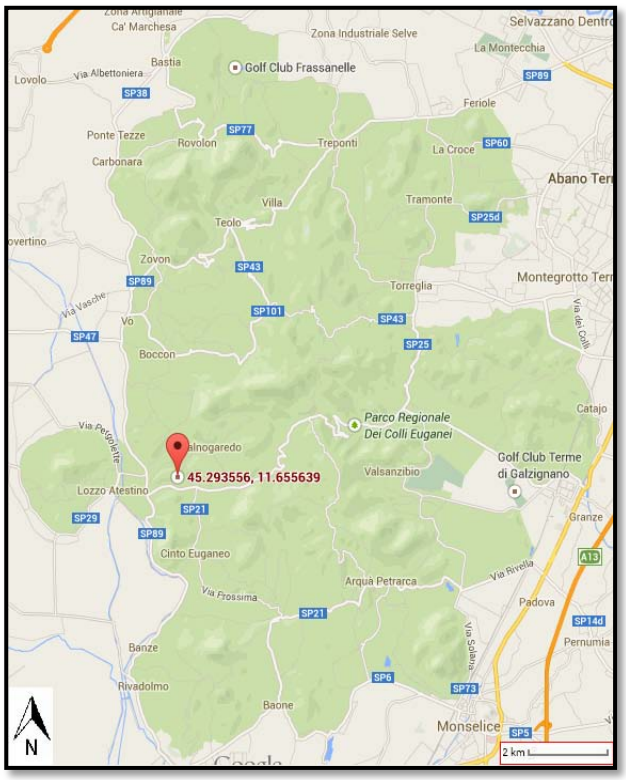

Figure 3.66 *Localization of Sample 8*

Figure 3.68 *Photo of sample 8*

Figure 3.69 *Section of the sample*

Outcrop description: The outcrop is located in Fontanafredda, a hamlet of “Cinto Euganeo” in “Via Chiesa”. It presents a regular stratification, the main colors are white and grey. (Figure 3.67) (Piccoli et al., 1981).

Lithological description: Very fine-grained white limestone with conchoidal fracture. It presents lenses of flint which are often dark. (Astolfi et al., 2003). (Figure 3.68 and 3.69).

Sample 27A

Date of collection:
17/07/2013
Location of sampling:
Teolo (Fig. 3.70)
Coordinates (WGS84):
N 45°21’24.7", E 11°41’16.3"

Lithology:
Limestone
Geological formation:
Biancone
Age:
Upper Creataceous–
Lower Creataceous

Figure 3.71*The outcrop*

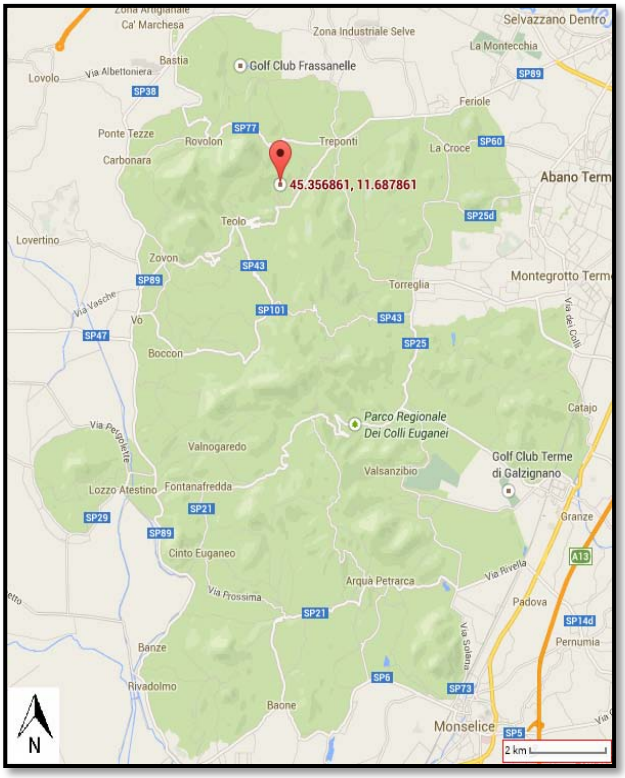

Figure 3.70 *Localization of Sample 27A*

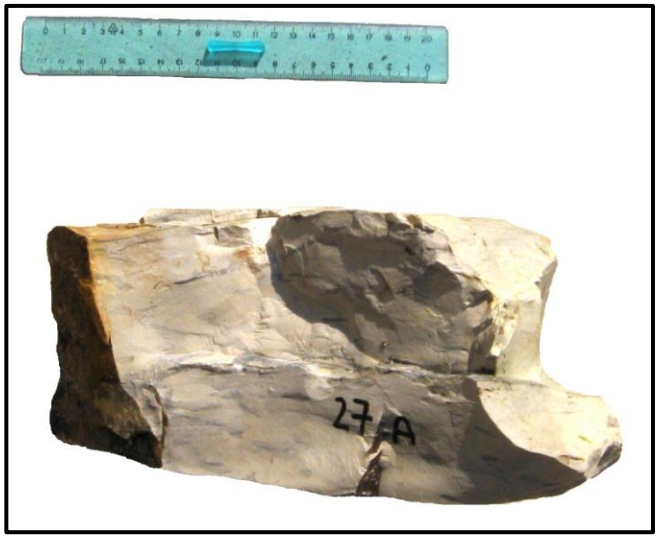

Figure 3.72 *Photo of sample 27A*

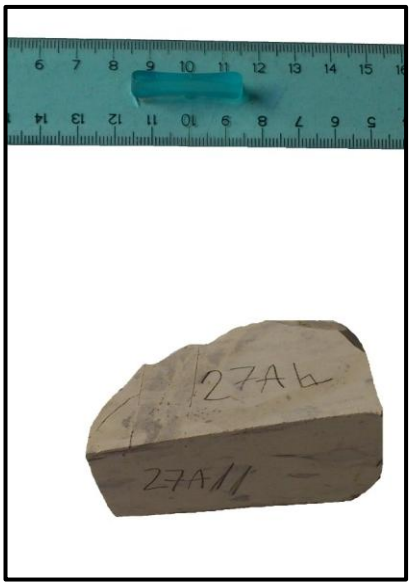

Figure 3.73 *Section of the sample*

Outcrop description: The outcrop is located in “Villa di Teolo” along the road that starts behind the church "Santa Maria Annunziata“. The outcrop is small and ruined by the surrounding vegetation (Figure 3.71).

Lithological description: Very fine-grained white limestone with conchoidal fracture. It presents lenses of flint (Figure 3.72 and 3.73) (Astolfi et al., 2003).

Sample 10B

Date of collection:
17/07/2013

Location of sampling:
Cinto Euganeo (Fig. 3.74)

Coordinates (WGS84):
N 45°17’16.9", E 11°39’25.3"

Lithology:
Limestone

Geological formation:
Rosso Ammonitico

Age:
Lower Jurassic

Figure 3.75*The outcrop*

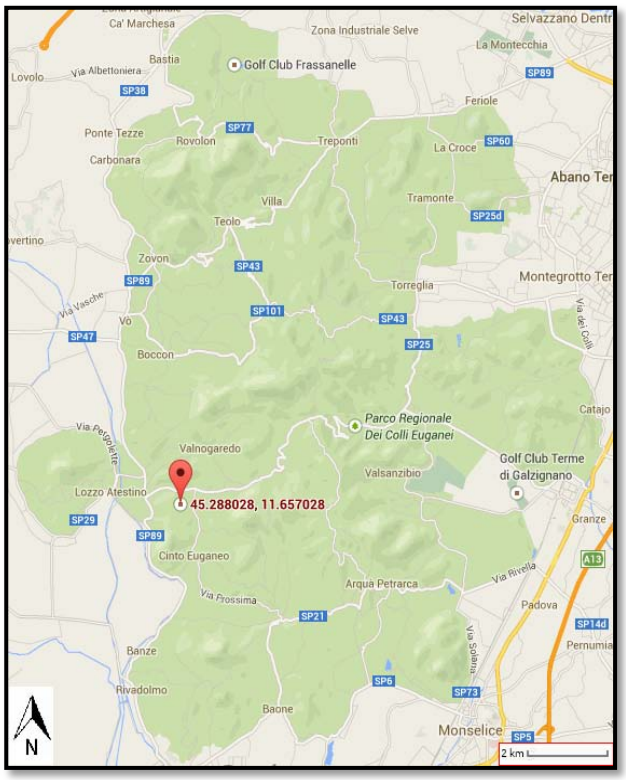

Figure 3.74 *Localization of Sample 10B*

Figure 3.76 *Photo of sample 10B*

Figure 3.77 *Section of the sample*

Outcrop description: The outcrop is located in Fontanafredda, a hamlet of Cinto Euganeo. It appear not big and quite ruined by the surrounding vegetation (Figure 3.75). Within Euganean Hills, this kind of rock is present only in this zone.

Lithological description: It has a characteristic nodular structure, the color is variable from purplish red to gray. It can be rich in ammonites, from which it takes its name. It also contains red and gray flint (Figure 3.76 and 3.77) (Astolfi et al., 2003).

Sample 34

Date of collection:
19/07/2013
Location of sampling:
Cinto Euganeo (Fig. 3.78)
Coordinates (WGS84):
N 45°17'16.5", E 11°39'25.2"

Lithology:
Limestone
Geological formation:
Rosso Ammonitico
Age:
Lower Jurassic

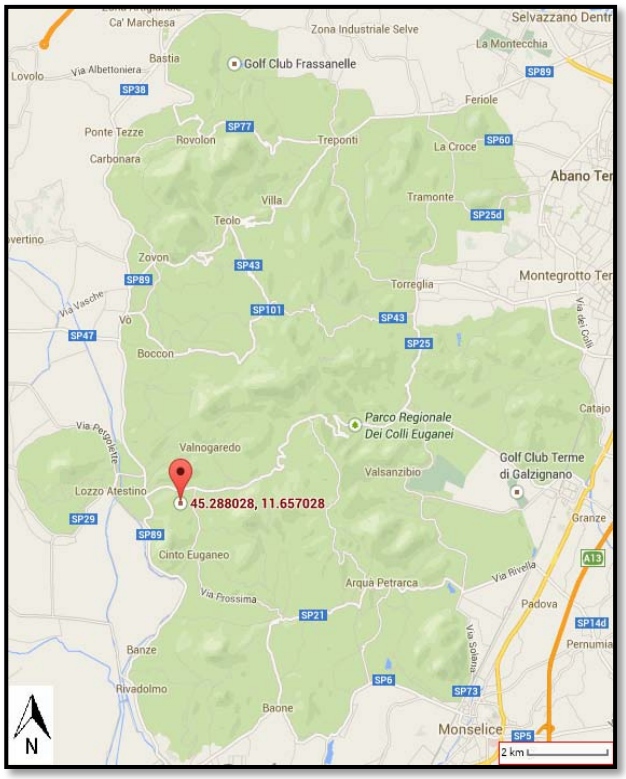

Figure 3.79*The outcrop*

Figure 3.78 *Localization of Sample 34*

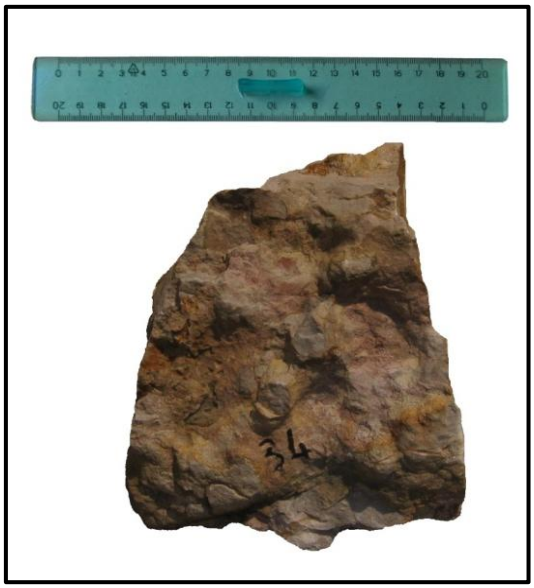

Figure 3.80 *Photo of sample 34*

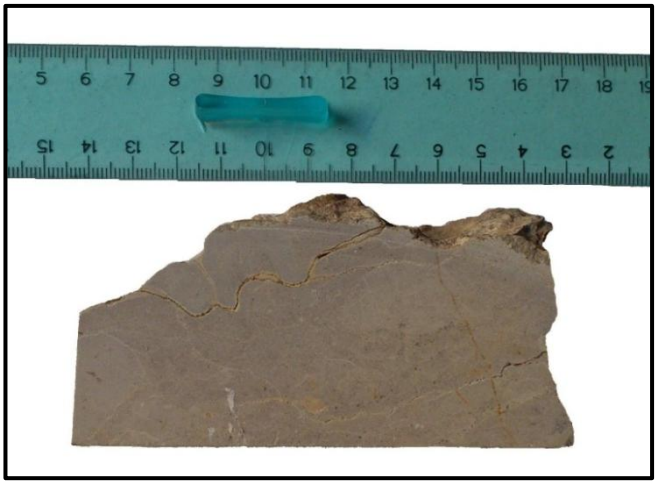

Figure 3.81 *Section of the sample*

Outcrop description: The outcrop is located in Fontanafredda, a hamlet of Cinto Euganeo. It appear not big and quite ruined by the surrounding vegetation (Figure 3.79). Within Euganean Hills, this kind of rock is present only in this zone.

Lithological description: It has a characteristic nodular structure, the color is variable from purplish red to gray. It can be rich in ammonites, from which it takes its name. It also contains red and gray flint (Figure 3.80 and 3.81) (Astolfi et al., 2003).

Sample 35

Date of collection:
19/07/2013

Location of sampling:
Cinto Euganeo (Fig. 3.82)

Coordinates (WGS84):
N 45°17’16.8", E 11°39’25.2"

Lithology:
Limestone

Geological formation:
Rosso Ammonitico

Age:
Lower Jurassic

Figure 3.83*The outcrop*

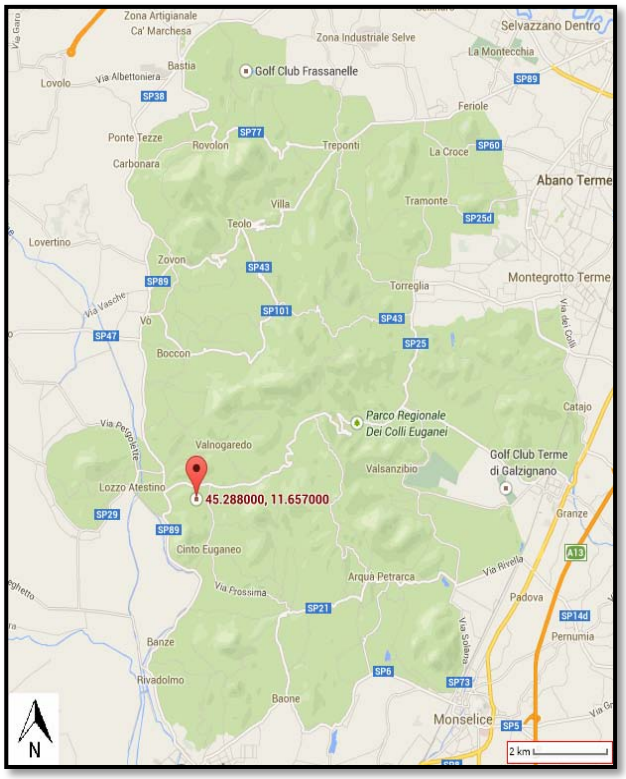

Figure 3.82 *Localization of Sample 35*

Figure 3.84 *Photo of sample 35*

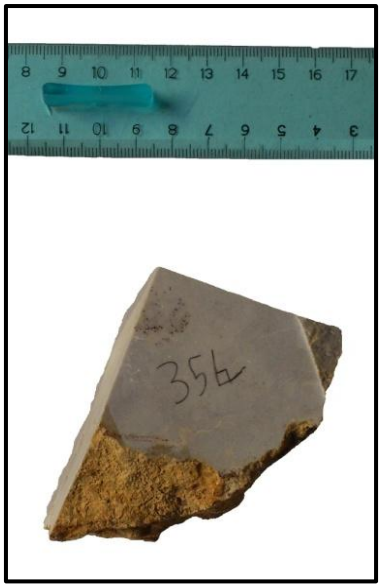

Figure 3.85 *Section of the sample*

Outcrop description: The outcrop is located in Fontanafredda, a hamlet of Cinto Euganeo (Figure 3.83). Within Euganean Hills, this kind of rock is present only in this zone.

Lithological description: It has a characteristic nodular structure, the color is variable from purplish red to gray. It can be rich in ammonites, from which it takes its name. It also contains red and gray flint (Figure 3.84 and 3.85) (Astolfi et al., 2003).

4. Thermophysical properties of rocks

In the design for Thermal Energy Storage (TES) is fundamental to know the lithologies present in the area devoted to build the system. Each lithology in fact has its own thermal characteristics and they will be analyzed in this chapter. Even some physical parameters such as density and porosity are important knowledge to be joined to the preceding.

A literature search has allowed us to determine the values of the thermo-physical parameters for the lithologies present in this work, then these values have been compared with the results of laboratory tests (Chapter 6).

4.1 Heat capacity, specific heat capacity and thermal capacity

Heat capacity *C* is defined as the ratio of heat ΔQ required to raise the temperature of a mass M of rock by ΔT (Clauser et al., 2011). Thus heat capacity can be expressed with Equation 4.1. Heat capacity can be expressed at constant volume (C_v) or constant pressure (C_p) (Waples et al., 2004).

$$C = \frac{\Delta Q}{\Delta T} \quad \left(\frac{J}{K}\right) \tag{4.1}$$

Where ΔQ is the energy required in order to have an increase of temperature of ΔT.

Specific heat capacity *c* of a substance is defined as heat capacity *C* related to unit mass:

$$c = \frac{\Delta Q}{M \Delta T} \quad \left(\frac{J}{kg\ K}\right) \tag{4.2}$$

Where M is the mass of the considered substance.

Also specific heat capacity can be expressed at constant volume (c_v) or constant pressure (c_p); in particular the latter is the first derivative of the entalphy with respect to the temperature (Clauser, 2006). For solid materials the term c_p-c_v is near to zero because this difference is a function of thermal expansion coefficients which, in these cases, has low values (Schön, 2004).

In general the great majority of the specific heat capacity of minerals at 20°C are between 600 and 900 (J $kg^{-1}K^{-1}$) (Waples, 2004). Specific heat capacities of minerals and nonporous rocks increase with temperature; for this why it is important to establish a standard reference temperature for comparing heat capacities of the various substances (Waples et al., 2004).

If we want to calculate the specific heat at different temperatures there are many formulas that provide corrected values: almost all of them, however, are based on

parameters which change in according with the rock or mineral considered. This problem was overcome by Waples et al. (2004), who presented a method that allows us to calculate the specific heat of rocks and minerals with a smaller number of data. First we calculate the parameter cpn_T at two different temperatures (for example T1, associated at the reference value of heat capacity, and T2) with this equation:

$$cpn_{Ti} = 8{,}95 * 10^{-10}T^3 - 2{,}13 * 10^{-6}T^2 + 0{,}00172T + 0{,}716 \qquad 4.3$$

Where cpn_T is unitless and it is used to calculate the specific heat capacity of any mineral or nonporous rock with Equation 4.4 in any units at any temperature T2, provided a measured value cp_{T1}.

$$cp_{T2} = cp_{T1} * \frac{cpn_{T2}}{cpn_{T1}} \qquad \left(\frac{J}{kgK}\right) \qquad 4.4$$

For example, if the measured value of cpT1 is 0,200 (cal $g^{-1}°C^{-1}$) at a temperature of 66°C, the sample's calculated specific heat capacity at our reference temperature of 20°C (T2) is obtained in two steps.

Equation 4.3 is applied at both temperatures. This calculation yields cpn_{T2} = 0.750 and cpn_{T1} = 0.820. Next applying the Equation 4.4, we obtain cp_{T2} = 0,183 (cal $g^{-1}°C^{-1}$) at 20°C, which is equivalent to 766 (J $kg^{-1}K^{-1}$) (Waples et al., 2004).

This method allows us to calculate high temperature values of specific heat capacity from knowledge of a single measured value at low temperature. In Figure 4.1 are reported the behaviors of specific heat capacities of six abundant metamorphic and igneous rocks. The plot is obtained using the method just showed.

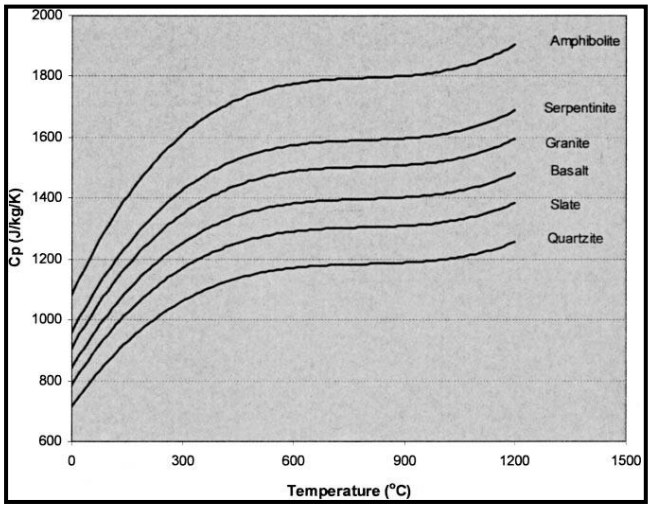

Figure 4.1 *Specific heat capacities of six abundant metamorphic and igneous rocks calculated as function of temperature (Waples et al., 2004)*

Thermal capacity (also called volumetric heat capacity) can be calculated as the product of specific heat capacity c and density ρ or as the ratio of thermal conductivity λ and thermal diffusivity *K* (which will be discussed in the following paragraphs) (Clauser et al., 2011):

$$\rho c = \frac{\lambda}{K} \quad \left(\frac{J}{cm^3 K}\right) \tag{4.5}$$

From a practical point of view it expresses the ability of a body to store heat. Among the most common materials, water has the highest value: 4.17 (J $cm^{-3}K^{-1}$) (Dincer, 2002).

In general rocks have values which are half that of water (which involves the creation of larger storage heat systems) and can be estimated with Kopp's law:

$$(\rho c)_b = (1-\varphi)(\rho c)_s + \varphi \sum_{i=1}^{N} S_i (\rho c)_i \quad \left(\frac{J}{cm^3 K}\right) \tag{4.6}$$

Where φ is porosity, $(\rho c)_s$ thermal capacity of the rock skeleton, S_i fractional saturation, and $(\rho c)_i$ thermal capacity of the i-th fluid phase in the pore space. The skeleton thermal capacity itself may be calculated again from Kopp's law for a given mineral assemblage and the corresponding volume fractions of the solid phase.

Because of the low density of air and gas the contribution of the gas phase to thermal capacity can often be ignored (Clauser et al., 2011).

Waples et al. (2004) present a relation between the thermal capacity and density of minerals. In particular for low density minerals (ρ < 4 g/cm^3) he extrapolated an exponential curve (Figure 4.2) governed by the equation:

$$\rho c = 1{,}0263 e^{(0{,}2697\rho)} \quad \left(\frac{J}{cm^3 K}\right) \tag{4.7}$$

For minerals with density greater than 4 (g/cm^3) he obtained polynomial regression curve (Figure 4.3) with the following equation:

$$\rho c = -0{,}0123\rho^4 + 0{,}399\rho^3 - 4{,}64\rho^2 + 22{,}62\rho - 36{,}42 \quad \left(\frac{J}{cm^3 K}\right) \tag{4.8}$$

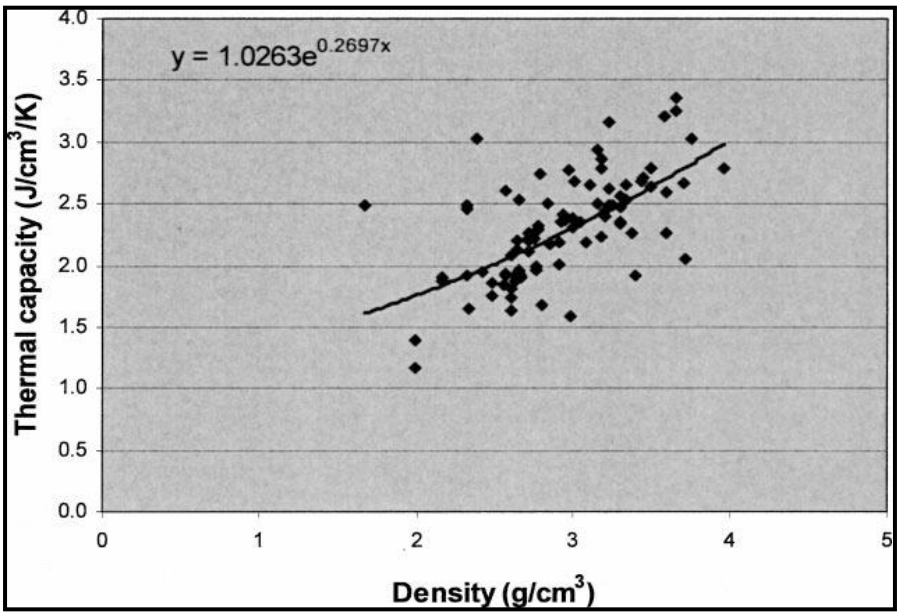

Figure 4.2 *Thermal capacity at 20°C plotted against mineral density for a set of low density minerals (Waples et al., 2004)*

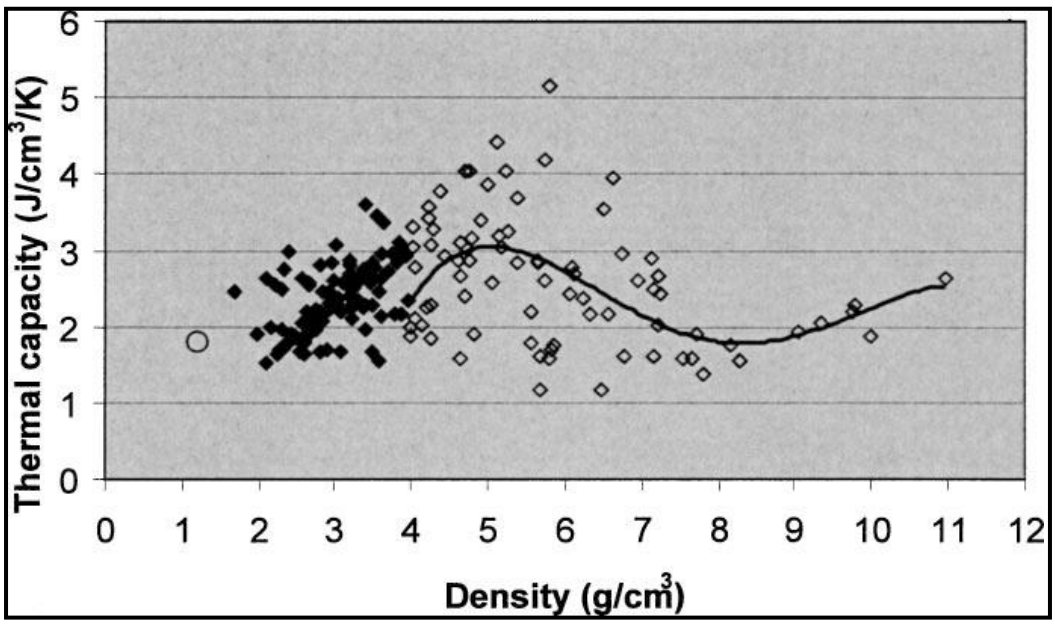

Figure 4.3 *Thermal capacity at 20°C plotted against mineral density for a set of about 190 minerals (Waples et al., 2004)*

4.2 Thermal conductivity

Thermal conductivity (or heat conductivity) λ (or k) is a physical property which governs heat diffusion in steady state. It defines how much heat flows across a unit cross section of rock along a unit distance per unit temperature decrease per unit time; dimension ($W\ m^{-1}K^{-1}$) (Clauser, 2011).

Thermal conductivity is an important parameter because it is connected with the dimension of the borehole heat exchanger: a 50 % increase in thermal conductivity in the range 2-3 (W $m^{-1}K^{-1}$) corresponds to an equal increase in mean thermal power which can be exchanged (Figure 4.4) (Clauser, 2006).

Thermal conductivity can be mainly divided into lattice conductivity (or phonon conductivity) (λ_p) and radiative conductivity (λ_r). Lattice conductivity is produced by the diffusion of thermal vibration in a crystalline lattice, while radiative conductivity is produced by infrared electromagnetic waves (Lee et al., 1998).

Radiative conductivity is negligible in comparison to lattice conductivity at temperatures less than 2500K for polycrystalline materials. In single crystals and glasses, however, radiation may become important at temperatures of 500-1000K (Clauser, 2011).

The value of thermal conductivity is obtained with laboratory measurements which may deviate significantly from in situ values even if the effects of temperature, pressure, and pore fluid are accounted for.

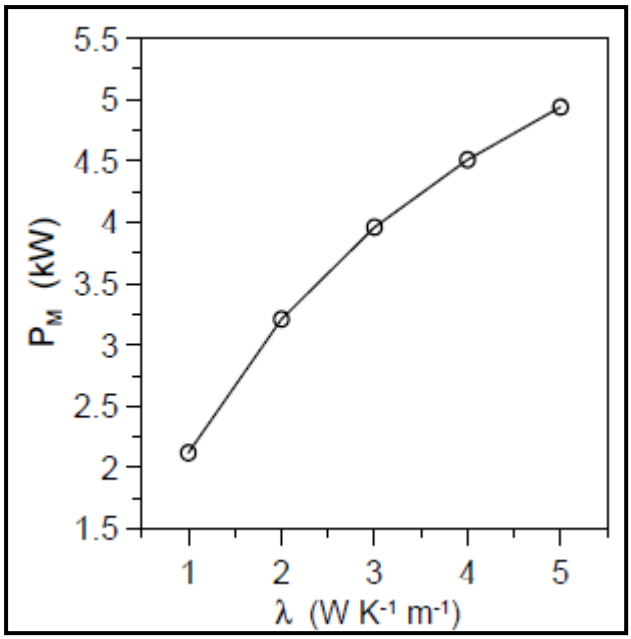

Figure 4.4 *Variation of the mean thermal power Pm of a coaxial borehole heat exchanger (at a given volume flow rate of 1.8 (m^3/ h) at a constant inflow temperature of 0 °C) with rock thermal conductivity λ (Clauser, 2006)*

This scale dependence involves different aspects: in situ measurements represent an average over a much larger rock volume than laboratory measurements (performed on small samples) but cannot resolve small-scale variations.

Which thermal conductivity is the "correct" one will depend on the specific question; for this why is difficult define *a priori* a "representative elementary volume" (REV) (Clauser et al., 1995; Clauser, 2011).

Generally thermal conductivity of minerals is much better constrained than that of rocks, due to the well-defined crystal structure and chemical formula for each mineral.

Factors as mineral content, density, porosity, pore fluid, saturation and anisotropy change the thermal conductivity of the rocks. The variation of rock thermal conductivity according to the four main diagenetic classes of rock (sedimentary, volcanic, plutonic, metamorphic) is presented by Clauser (2001) and results are synthesized in Table 4.1.

Table 4.1 *Main control factor of thermal conductivity for different classes of rock (Clauser, 2011)*

Classes	**Main control factors**
Sedimentary rocks	Porosity, sediment type
Volcanic rocks	Porosity
Plutonic rocks	Feldspar content
Metamorphic rocks	Quartz content

As previously mentioned, thermal conductivity changes also with some external factors; these factors are now discussed.

Temperature

Thermal conductivity changes with temperature (usually denoted by T). Thermal expansion increases with temperature (but with different magnitude for all minerals) and differential expansions may create contact resistances between mineral grains. This effect is less pronounced in water-saturated than in dry rocks. For single mineral aggregates the lattice (or phonon) thermal conductivity λ_p is related with the inverse of temperature (Clauser, 2011).

However, many rocks are composed of mixtures of highly disordered crystals of different compositions. For that reason, the thermal conductivity of rocks tends to decrease more slowly than T^{-1} relation and may tend to actually increasing, in some cases, with increasing temperature. For example, the thermal conductivities of feldspar aggregates increase with increasing temperature and the thermal conductivities of glasses and vitreous materials also increase with increasing temperature (Lee et al., 1998).

The radiative thermal conductivity λ_r, in contrast, follows a T^3 law. Thus measurements on thermal conductivity as a function of increasing temperature generally show a decrease with temperature but from around 1000-1200°C the radiative component balances and sometimes even inverts this decreasing trends (Clauser et al., 1995).

Many authors proposed relations of λ_p with temperature valid, in general, within the range 0-500°C which corresponds to conditions in the upper crust. In particular it was

found (Lee et al., 1998) which the correction introduced by Sekiguchi in 1984 (Equation 4.9) has the lowest "mean absolute value of relative error" (MARE) (Equation 4.11) for igneous and metamorphic rocks and the correction presented by Somerton in 1992 (Equation 4.10) has the lowest MARE for minerals and sedimentary rocks (Lee et al., 1998). This last correction is valid only for thermal conductivities lower than 9 (W $m^{-1}K^{-1}$) at 20°C.

$$\lambda(T) = \lambda_m + \left\{\frac{T_o T_m}{T_m - T_o} * (\lambda_o - \lambda_m) * (\frac{1}{T} - \frac{1}{T_m})\right\} \quad (4.9)$$

Where T is the estimated in situ temperature in Kelvins, λ(T) is the estimated thermal conductivity at the in situ temperature, λm and T_m are the thermal conductivity and absolute temperature (Kelvins) at what Sekiguchi refers to as "the assumed point", λ_o is the thermal conductivity at room temperature T_o, λ_m=1,8418 (W $m^{-1}K^{-1}$), T_m = 1473K.

$$\lambda(T) = \lambda_{20} - 10^{-3}(T - 293) * (\lambda_{20} - 1{,}38) * [\lambda_{20} * \left(1{,}8 * 10^{-3}T\right)^{-0{,}25\lambda_{20}} + 1{,}28] * \lambda_{20}^{-0{,}64} \quad (4.10)$$

Where T is the estimated in situ temperature in Kelvins, λ(T) is the estimated thermal conductivity at the in situ temperature (W $m^{-1}K^{-1}$), λ_{20} is the thermal conductivity in (W $m^{-1}K^{-1}$) at 20°C.

$$MARE\% = \frac{\sum 100 * \frac{|\lambda_T - \lambda_C|}{\lambda_T}}{N} \quad (4.11)$$

Where λ_T is the thermal conductivity measured at the temperature T, λ_C is the thermal conductivity inferred from a temperature correction at the same temperature, N is the total number of measurements.

The temperature dependence can be also expressed in function of the four diagenetic classes of rocks (Clauser et al.,1995).

For sedimentary rocks up to 300°C there is a reduction by nearly a factor of two, both for clastic and carbonaceous sediments. Above this temperature the decrease stops for clastic sediments and continues (but very slowly) for carbonaceous sediments.

Volcanics rocks have a different behaviour in function of their opacity that is related with the trasmission of energy by radiation. Due to the addition of radiative conductivity volcanic glasses and rocks with small iron content have an increase of thermal conductivity for temperatures above 800-1000°C.

In plutonic rocks the radiative contribute does not exist. For this class of rocks the decrease of thermal conductivity with increasing temperature change in function of feldspar content. Up to 300°C rocks rich in feldspar decrease by more than 40% and rocks poor in feldaspar decrease about of 10%. Over this temperature the decrease is gentle for both groups.

For metamorphic rocks, the decrease of termal conductivity is related to the amount of quartz present in the rocks. Quarzites show a decrease with a factor of three up to 500°C and for rocks poor in quartz the decrease in conductivity is in the order of one third of the room temperature value up to 200°C and remains constant up to 500°C. After this value the decrease is still about one third of the room-temperature value.

Pressure

The effect of pressure on phonon thermal conductivity λ_p depends on the value of applied pressure. For increasing pressure (up to 15 MPa) the micro cracks, developed during stress release after sampling, tend to close themselves: this reduces thermal contact resistence and thermal conductivity at 15 MPa has a value 20% higher respect atmospheric pressure.

In the interval between 15 MPa and 40 MPa there are not significant changes. Over 40 MPa a second process takes place, that is the reduction of the effective porosity. For the granite and metamorphic rocks the increase of the thermal conductivity is of a further 10% which occurs in the range of pressures between 50 MPa and 500 MPa (Clauser, 2011).

Other factors

Apart from temperature and pressure, thermal conductivity also varies with factors as large porosity, partial saturation and anisotropy (Clauser, 2011).

For large porosity ($\varphi >> 1\%$) thermal conductivity of the saturating fluid affects the bulk rock thermal conductivity. The influence depends on the thermal conductivity of the fluids involved, for example water, oil, natural gas or air.

The effect of partial saturation is different for porous (e.g. sandstone) or fractured rocks (e.g. granite). In the first case porosity comprises both bulk pore space and bottleneck formed by contact between individual grains. Dry bottlenecks act as thermal contact resistances between grains, while the bulk pore volume contributes proportionally to the effective rock thermal conductivity.

In fractured rocks, in contrast, there are no bottlenecks between grains as in porous rocks, and the small void volume in the fractures corresponds to the bulk pores space of porous rocks.

In Figure 4.5 is plotted the different behaviour of two rocks taken as example. When sandstone is totally dry the thermal conductivity is the 60% of the saturated value, but with a water saturation of 10% the bottlenecks are filled and the conductivity increases rapidly. In granite this phenomena does not exist and only the fractures contribute is present, responsible for a quasi linear increase of the value (Clauser, 2011).

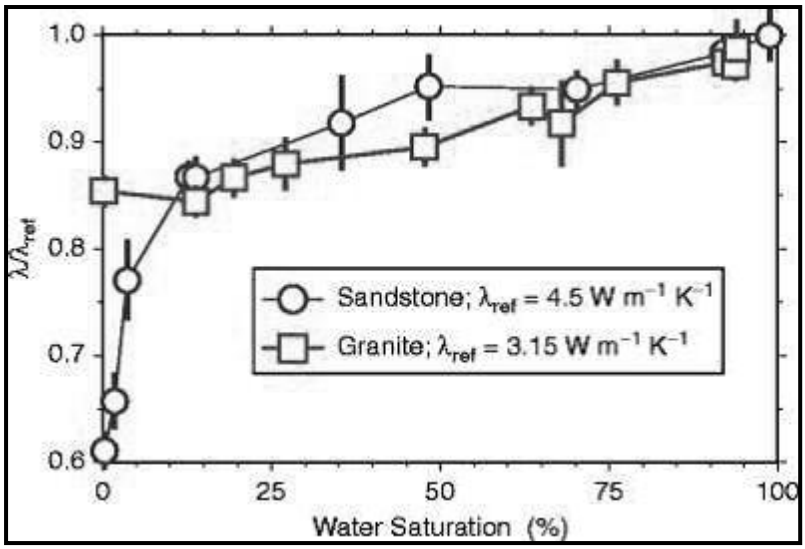

Figure 4.5 *Variation of thermal conductivity with partial saturation for a sandstone (circles; φ = 18 %) and granite (squares; φ = 1 %) saturated with water (Clauser, 2011)*

Anisotropy exists at different scale: microscopic scale, laboratory scale and outcrop scale. For sedimentary and metamorphic rocks this factor is due to the conditions of their formation and in order to account it almost two measures in the same sample are needed: one parallel to the direction of layering (λ//), one in the perpendicular direction (λ⊥).

The factor of anisotropy is defined as (λ//)/(λ⊥) and typical values falls into the range 0,9-3 (Clauser, 2011).

When no data are available or no direct measurements can be performed, thermal conductivity can be inferred indirectly. Thermal conductivity of a rock can be estimated from minerals and fluids content. Numerous models based on volume fraction of the individual mineral phases exist and everyone has specific advantages and disadvantages.

The simplest model is made for layered media: if the heat flow is parallel to the bedding, the global thermal conductivity is the weighted arithmetic means (Equation 4.12) of the all layers; if the flow is perpendicular the global thermal conductivity is the harmonic mean of the all layer (Equation 4.13).

$\lambda_{max} = \lambda_{ari} = \lambda_{//} = \sum_{i=1}^{N} n_i \lambda_i$	4.12

$\lambda_{min} = \lambda_{har} = \lambda_{\perp} = (\sum_{i=1}^{N} \frac{n_i}{\lambda_i})^{-1}$	4.13

Where n_i and λ_i are the volume fraction and the thermal conductivity of i-th layer, respectively. These two values are important because the results of all other models are within the boundary made by these two results; in particular the arithmetic mean gives the higher results and harmonic means gives the lower.
In "Thermal Storage and Transport Properties of Rocks, II: Thermal Conductivity and Diffusivity" (Clauser, 2011) are presented different models including those just presented.

4.3 Thermal diffusivity

Thermal diffusivity *K* (or α) is a physical property governing transient heat diffusion and is defined by the ratio of thermal conductivity and thermal capacity (Equation 4.14), i.e., by the ratio of heat flowing across the face of a unit volume and heat stored in the unit volume per unit time (Clauser, 2011). In other words it represents the rate at which heat can be released and extracted (Dincer, 2001). Thermal diffusivity is usually expressed in (m^2s^{-1}) (or mm^2s^{-1}) as all diffusion coefficients.

$$\alpha = \frac{\lambda}{\rho\, c} \quad \left(\frac{m^2}{s}\right) \tag{4.14}$$

As specific heat capacity and thermal conductivity, also thermal diffusivity changes with different external factor.

Temperature

Due to the opposite behaviour of thermal conductivity and thermal capacity with respect to temperature, thermal diffusivity is very sensible at temperature variation.
However, due to several self-compensating factor, thermal capacity generally varies within ±20% of 2.3(MJ $m^{-3}K^{-1}$) so thermal diffusivity can be expressed only in function of λ:

$$K = \frac{\lambda}{\rho c} = \frac{\lambda}{2{,}3} = 0{,}44\lambda \quad \left(\frac{mm^2}{s}\right) \tag{4.15}$$

So expression for K(T) based only on λ(T) exists; this is the case of Equation 4.16 (Clauser, 2011) .

$$K(T) = \frac{\lambda(T)}{2{,}134 + 0{,}0044T} \quad \left(\frac{mm^2}{s}\right) \tag{4.16}$$

where temperature T is expressed in °C.

In case thermal diffusivity at room temperature is known and the objective is to estimate its value at higher temperatures it is possible to use the equation introduced by Ray et al. in 2006:

$$K(T) = 0{,}7 + 144\frac{K_{rt}}{T - 150} \quad \left(\frac{mm^2}{s}\right) \qquad (4.17)$$

Where K_{rt} is the thermal diffusivity at room temperature and T is the temperature [K].

The field of application of Equation 4.17 is for temperature lower than 450°C: for higher value the radiative component is not negligible and there is the need to resort to more complicated models (Clauser, 2011).
Some authors, however, do not agree with this temperature boundary and (still neglecting the radioactive component) propose models valid for a temperature range greater than that described above.

For example Whittington et al., in 2009 proposed the following equation:

$$K(T) = \begin{cases} -0{,}062 + \frac{567{,}3}{T}; & T > 846\ K \\ 0{,}732 - 0{,}000135 * T; & T < 846\ K \end{cases} \quad \left(\frac{mm^2}{s}\right) \qquad (4.18)$$

Where T is the temperature [K].

Other effects

The effect of pressure in thermal diffusivity is about 0,03% every 10 MPa. Thus pressure effects are negligible compared to the temperature effects (Waples et al., 2004). Also the effects due to grain boundaries or the presence of micro-cracks are not very important (Clauser, 2011).

4.4 Density and porosity

The density and porosity of a rock are fundamental physical properties: the other properties as thermal conductivity and thermal capacity are directly or indirectly related to them.
Density ρ is defined as the quotient of the mass *m* and the volume *V* of a material as expressed by the Equation 4.19:

$$\rho = \frac{m}{V} \quad \left(\frac{kg}{m^3}\right) \qquad (4.19)$$

Considering that in varying degrees all the rocks are porous, two kinds of densities are generally used and are the bulk density and matrix density. The first is defined with the following equation (Gong, 2005):

$$\rho_b = \frac{m}{V_{total}} \quad \left(\frac{kg}{m^3}\right) \qquad (4.20)$$

where *m* is the sum of the mass of matrix and the mass of the substances present within the pores:

$$m = m_{matrix} + m_{pore} \qquad (4.21)$$

In the case of dry rock the mass of air in the pore can be neglected without significant errors. V_{total} is the volume of rock consisting of matrix and pore, then (Gong, 2005):

$$V_{total} = V_{matrix} + V_{pore} \qquad (4.22)$$

Matrix density considers that only the mass in the matrix volume; and that the void volume of the pores inside the rock is excluded. Therefore, matrix density is defined as the mass in the matrix volume (Gong, 2005):

$$\rho_m = \frac{m}{V_{matrix}} \quad \left(\frac{kg}{m^3}\right) \qquad (4.23)$$

Porosity φ is an adimensional parameter defined as the ratio of volume of pore space V_{pore} to the total volume V_{total} of the rock:

$$\varphi = \frac{V_{pore}}{V_{total}} = 1 - \frac{V_{matrix}}{V_{total}} \qquad (4.24)$$

From the bulk density ρ_b and matrix density ρ_m, one can obtain the porosity by using equation (4.20) and (4.23) in equation (4.24) (Gong, 2005):

$$\varphi = 1 - \frac{\rho_b}{\rho_m} \qquad (4.25)$$

The general relation between porosity and density can be written as below:

$$\rho_b = \rho_{pore}\varphi + \rho_m(1 - \varphi) \quad \left(\frac{kg}{m^3}\right) \qquad (4.26)$$

When $\rho_{pore} << \rho_b$ the Equation 4.26 become equal to the Equation (4.25).

The density of a rock ρb depends on the density of its rock forming minerals. The main rock forming minerals have the average density of 2.89 (g/cm^3). This value is obtained with data proposed by Gong (2005).
The value of ρ_{pore} depends on the substance which occupies the pores; Waples et al. (2004) indicate some values for the most common saturating fluid (Table 4.2).

Table 4.2 *Density values of principal saturating fluid at 20°C(Waples et al., 2004)*

Saturating fluid	Density (g/cm3)
Water	1,03
Oil	0,9
Air	0,12

Both density and porosity are functions of different factors. The first mainly depends from mineral composition, content of pores (or fracture) with respective filling material and degree of saturations. The latter mainly depends on geometric properties of grain (size, sorting and shape) (Schön, 2004).
For this reason, it is reasonable to think that the two parameters are inter-related: in Figure 4.6 is showed a linear relationship between these two quantities for a density lowers than 2.6 (g/cm^3) (Gong, 2005). In particular density and porosity show an opposite behaviour: decreasing porosity (due for example to an increase of pressure which compacts the rock) causes increasing density and vice versa (Schön, 2004).

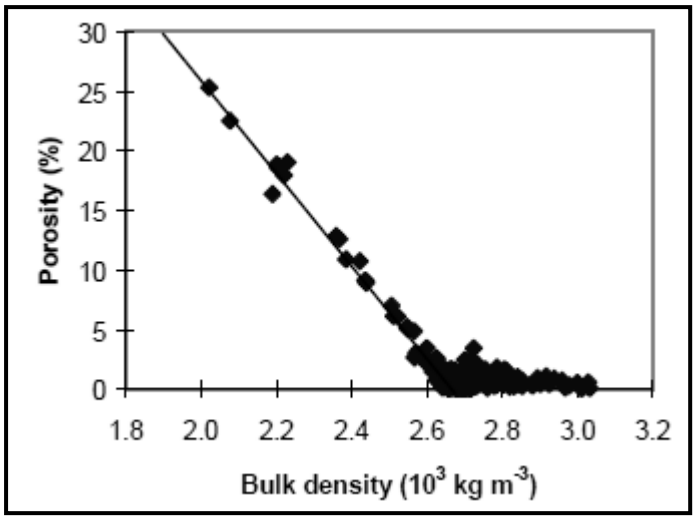

Figure 4.6 *Variation of porosity as a function of bulk density (Gong, 2005)*

5. Laboratory tests

In this chapter are reported the different steps of laboratory tests and operations. The objective is to measure the physical and thermal properties of the samples. In order to do this each rock has been subjected to cutting operations, obtaining from each of them:

a) Three cubes of side 3 cm if possible, or at least three parallelepipeds of similar size in order to develop the density and porosity measurements (as explained in section 5.2);
b) a section of about one centimeter thick, which will be used for the realization of thin sections in order to confirm the correct lithology of the sample and for the eventual observation of the mineralogical composition (which can affect the thermal properties);
c) a piece that has two smooth surfaces mutually orthogonal, in order to do the thermal analysis both in parallel and perpendicular faces respect the stratification so in this way it is possible determine the factor of anisotropy (which is discussed in Chapter 4). This operations are treated within the paragraph 5.4.

5.1 Rocks cutting

This operation was carried out with the miter saws "Unitom-2" (Figure 5.1) which has a power of 4.7 kW and the "Labotom-3" (Figure 5.2) which develop a power of 3.2 (kW). Both devices are manufactured by Struers.

Figure 5.1 *Miter saw "Unitom 2"(Source: struers.com)*

Figure 5.2 *Miter saw "Labotom-3"(Source: struers.com)*

In order to have an idea of the dimension of the sample which this device is able to cut, it is useful give a look at the "Cutting capacity curve" delivered by Struers (Figure 5.3 for Unitom 2 and Figure 5.4 for Labotom-3).
For example, related at Unitom 2, a sample with an height of 9 cm and a deep of 20 cm can be cut without problems. In general, Labotom-3 works well with little specimens.

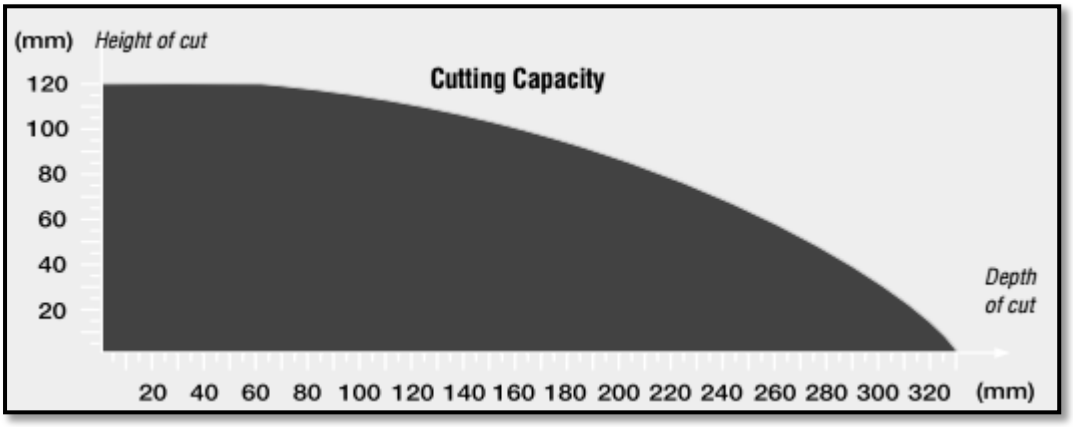

Figure 5.3 *Cutting capacity curve for "Unitom 2" (Source: struers.com)*

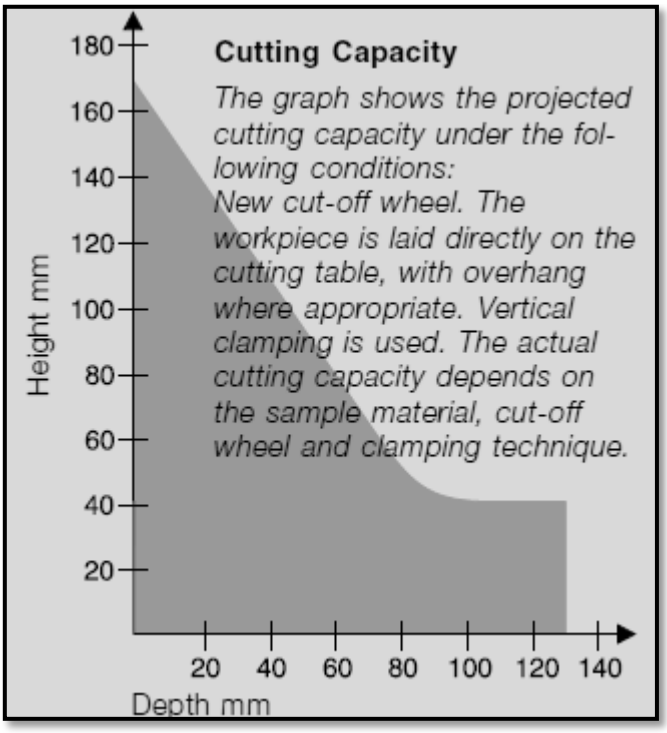

Figure 5.4 *Cutting capacity curve for "Labotom-3" (Source: struers.com)*

In Figure 5.5 is showed a cutting phase: the portion of the rock just cut will be used to realize the thin section while the bigger part of the rock will be used in order to measure the thermal properties

on one face of the rock. The second smooth face is than obtained with a second perpendicular cut respect those just made.

Figure 5.5 *Cutting operations for the sample number 43 with the miter saw"Unitom 2"*

The results of the cutting operations for the sample 43 are shown in Figure 5.6: on the left there is the piece which will be used for realize the thin section, on the right there are the three cubes which will be used for the determination of physical parameters and on the top is present the sample that will be used for the thermal analysis.

Figure 5.6 *Results of Cutting operations for the sample number 43 with the miter saw"Unitom 2"*

5.2 Physical properties of rocks

The next step was to determine the bulk density and open porosity of the rocks; these properties are strictly related with density and porosity. This operation are made following the steps specified by the UNI EN 1936.

The cubes of each sample were placed in a ventilated oven at a constant temperature (70 ±5°C) for the duration of 24 hours. Once removed from the oven cubes are marked with a permanent marker and placed inside the dryer (Figure 5.7).

Figure 5.7 *Dryer containing cubes removed from the oven*

The dryer should be placed in the thermal analysis laboratory at constant temperature of 21°C. When the cubes are in equilibrium with this temperature, one can measure the dry weight (called md) with the use of the electronic analytical balance METTLER PM400. This type of balance gives results with the precision of 10^{-3} (g). The balance is protected by two covers in order to avoid which external agents like air currents or dust could affect the measurement results. The next step is to put the cubes into new dryers. They are then connected to the vacuum pump with the purpose of removing the air present in the pores of the rocks; the pressure that must be reached is of 20±0.7 (kPa) = 150±5 (mmHg). This condition is maintained for 24 hours (Figure 5.8).

Subsequently, while maintaining the vacuum state, demineralized water is added up to a level sufficient to ensure that each cube is completely immersed in water. The filling time of each dryer must be at least 15 minutes (Figure 5.9).

After both dryers were filled with water, vacuum conditions are maintained for the next 24 hours.

After this time the two dryers are disconnected from the vacuum pumps and left to rest for the next day.

Figure 5.8 *Near-vacuum conditions are maintained for 24 hours for both dryers, both connected to the vacuum pump through the orange tubes.*

Figure 5.9 *The filling of the dryers with demineralized water: the dryer in the left is already filled while the right one is in the filling phase. The water is introduced into the opening through the transparent small tube and adjusted by the green and blue tap.*

After this time the dryers are removed from the old location and you can complete the measures which will be based on Archimedes' principle which states that "everybody partially or completely immersed in a fluid (liquid or gas) receives a vertical thrust from the bottom to the top, which intensity is equal to the weight of the fluid that occupies the volume displaced" (Mazzoldi et al., 2007).

So the balance is equipped with a special plate for weighing in water, which is placed above a spacer that will support a plastic container filled with demineralized water whose temperature is measured with a special thermometer. This is important because the water changes its density with temperature (Figure 5.10) and this influence the results of laboratory test.

The cube of rock is taken from the dryer and placed on the sample holder. The latter is attached to the bow of the special plate (Figure 5.11) and we register the weight. Before to do this is measured the weight of the sample holder in water without the cube: the difference of these two weights gives the weight of the saturated sample in water (mh).

This procedure is repeated for all blocks which once weighed are put back in the dryer full of water.

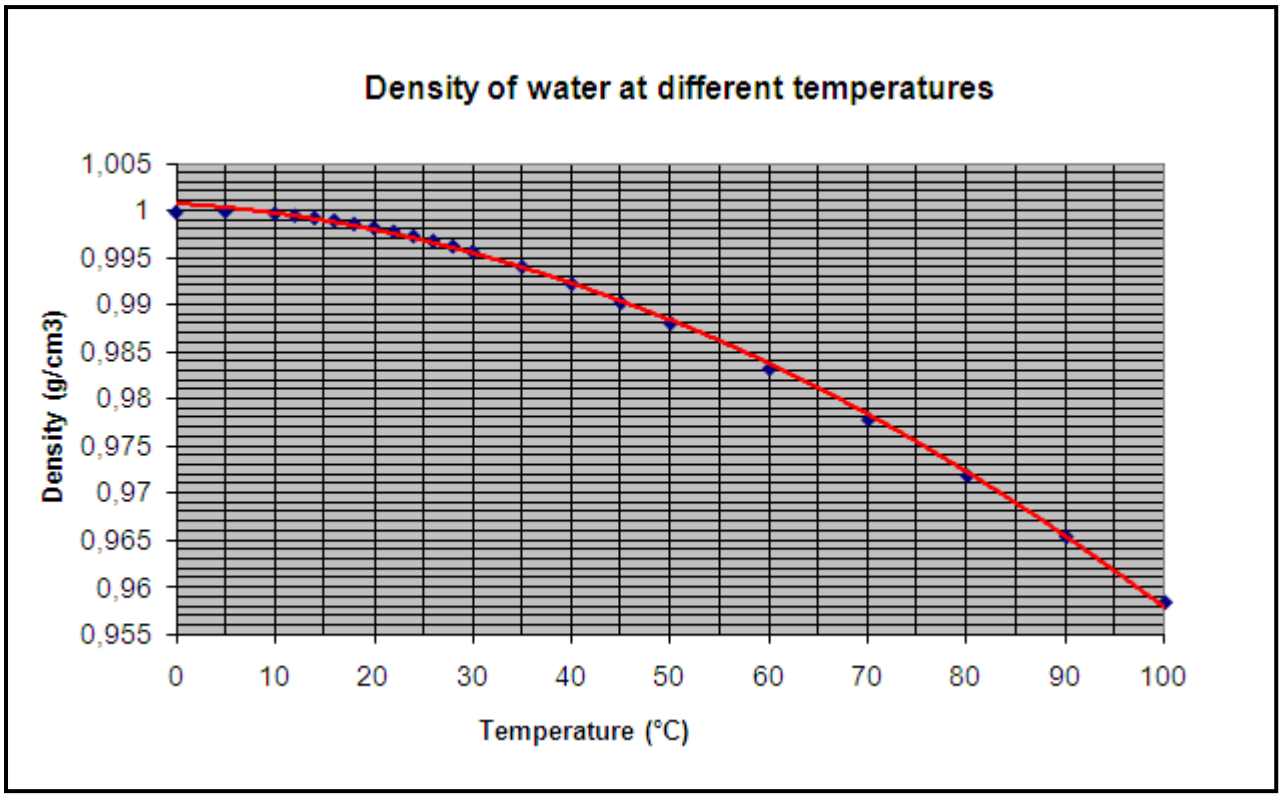

Figure 5.10 *Density of water at different temperatures*

The last measure needed is the weight of the cube saturated with water (ms). To measure this value the balance must be prepared in its original configuration (Figure 5.12). The sample is taken from the dryer and after a fast drying with a damp cloth it is weighted. After this operation, the cubes are placed in a package used for such storage. The dryers can contain about 15 cubes at a time: for this reason, to complete all the measurements you need to carry twice the steps in this section.

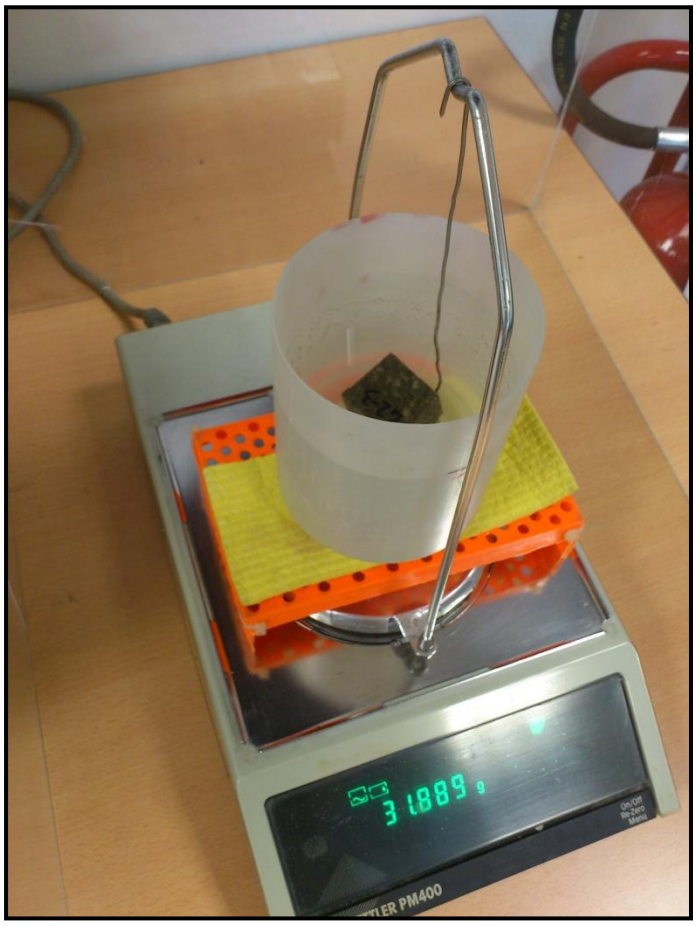

Figure 5.11 *Cube number 42-3 is positioned above the sample holder and then put within the plastic container filled with demineralized water.*

Figure 5.12 *Cube number 25-3 in positioned above the balance for the measure of saturated sample in air (ms)*

All measurements should be recorded in duplicate in a precompiled table identical to Table 5.1.

Table 5.1 *Table used for recording measurements*

Sample name			
Weight of dry sample "md" (g)			
Weight of saturated sample "ms" (g)			
Weight of the wire in the water "C" (g)			
Weight of saturated sample + weight of the wire in water "D" (g)			
Weight of saturated sample in water "mh =D-C" (g)			
Density of water at the temperature of measurement (g cm^{-3})			

From this data are calculated density and porosity using Equation 5.1 and 5.2.

$$\rho_b = \frac{md}{ms - mh} * \rho rh \quad \left[\frac{g}{cm^3}\right] \qquad 5.1$$

$$\rho_o = \frac{ms - md}{ms - mh} * 100 \quad [\%] \qquad 5.2$$

Where ρb is the bulk density in (g cm^{-3}), md is the weight of dried sample in air (g), ms is the weight of saturated sample in air (g), mh is the weight of saturated sample immersed in water (g) and ρo is the open porosity.

5.3 Thermal properties of rocks: how measure them

5.3.1 Different methods for their determination

The determination of thermal properties of rocks is the more important target of this work.
In general it is useful to classify the methods into two large categories: stationary and transient. Both groups of measurement provide a temperature gradient and verify the reaction of the material; steady-state techniques perform a measurement when the temperature of the material measured does not change with time and the transient techniques perform a measurement during the process of heating up or cooling down. The techniques differ also in areas such as sample size, testing time, and range (Mathis, 2000; Kuvandykova et al., 2013).

Stationary method

This method is based on the creation of a constant flux of heat which passes through the sample. In the simplest way it is made with the specimen (of fixed dimension) sandwiched by two plates: the first hot and the second cold (Mathis, 2000). In this way two faces of the sample are at controlled temperature (Figure 5.13).

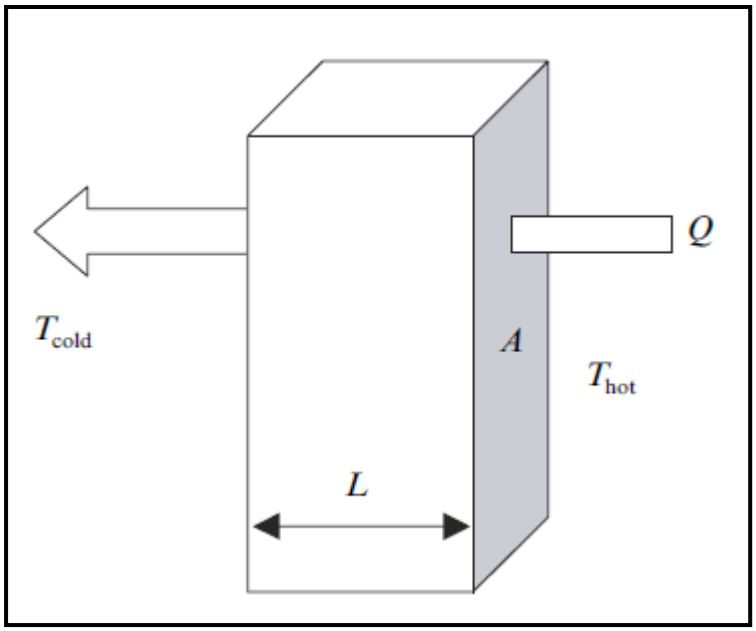

Figure 5.13 *Stationary method: functioning principle (Mathis, 2000)*

Assuming that the other four faces are thermally insulated, the phenomena can be described with Fourier's law (1D case):

$$Q = \frac{\lambda A}{L} \ (T_{hot} - T_{cold}) \ [W] \qquad 5.1$$

Where Q is the heat which flows through the specimen, λ is the thermal conductivity (W $m^{-1}K^{-1}$), A the cross-sectional area (m^2), L the distance of travel (m) and T_{hot}, T_{cold} (K) the controlled temperatures imposed by the two plates (Mathis, 2000).

A part λ all the other parameters are known, thus at this point it is possible to determine the thermal conductivity of the material.

This method gives good results especially for heterogeneous materials (Kuvandykova et al., 2013). However, it takes a long time (in particular for materials with low conductivity), and the samples used for the measurements must be of predetermined dimensions (Mathis, 2000; Kuvandykova et al., 2013; Milovanovic et al., 2011).

Many techniques belong to the stationary method: for example the guarded-hot plate, the comparative technique, the pipe test method and the cut bar technique (Mathis, 2000; Slifka, 2000; Kuvandykova et al., 2013; Cha et al., 2012)

Transient method

This method is quick respect to the stationary one and allows to measure the thermal properties using only one face of the specimen; for these reasons this method find a lot of applications (Mathis, 2000; Bateman et al., 2011; Milovanovic et al., 2011; Borinaga et al., 2012; Cha et al.,

2012; Kuvandykova et al., 2013). However, the mathematical analysis of data is, in this case, more difficult respect to the stationary method.
The more diffused techniques are hot wire, needle probe, laser flash, traditional transient plane source and modified transient plane source (Mathis, 2000; Kuvandykova et al., 2013). The instrument used for the laboratory measurements belongs to the latter category.

5.3.2 Mathis TCi Thermal Property Analyzer

The instrument used for the determination of thermal properties is "Mathis TCi Thermal Property Analyzer" manufactured by C-Therm Technologies which provides non-destructive thermal sensor technology solutions (www.ctherm.com). The system is comprised of a sensor (circular area of 17 mm of diameter), control electronics and computer software (Mikulic et al., 2010; Iqbal et al., 2012) (Figure 5.14).

Figure 5.14 *Mathis TCi Thermal Property Analyzer (Mikulic et al., 2010)*

The measure starts with a small amount of heat provided at sample by applying a known constant current to the sensor's heating element. This results in a rise in temperature (about 2°C) at the interface between the sensor and the sample and in a rapid voltage decrease at the heating source. The rate of voltage decrease is inversely proportional to the ability of the sample to transfer heat (Di Sipio et al., 2014).
The measured parameters are the thermal conductivity and also the thermal effusivity. The thermal effusivity is defined as the square root of the product of thermal conductivity and volumetric heat capacity. All other thermal quantities are indirectly determined with formulas reported within the operator manual; it is important to notice that the software uses a default value of density to perform these calculations.

Other characteristics of the instrument are:

- The sensor is capable of producing thermal conductivity results with precision of 1% and accuracy of 5% (Kuvandykova et al., 2013);
- the size or the shape of a specimen is not important (Kuvandykova et al., 2013), there is only a suggested thickness which is 4 (mm) for the materials which cover a range from 1.2 to 29 ($W\ m^{-1}K^{-1}$) (Bateman et al., 2011);
- the overall range for the equipment is 0 to 120 ($W\ m^{-1}K^{-1}$) (with different calibrations available for alternative ranges) (Bateman et al., 2011);
- a contact agent (silica gel or deionized water used in dry or wet conditions, respectively) is applied between the sample and the sensor to reduce the contact resistance to a negligible level (Di Sipio et al., 2014).

5.4 Thermal properties of rocks: employed procedure in laboratory tests

As seen in Chapter 4 the thermal properties of the rocks (such as conductivity) vary as a function of temperature. For this reason the measurements are carried out in air-conditioned environment with temperature fixed at 20-21 °C.

The measurements are conducted on the two smooth faces of the sample, which are prepared as illustrated in § 5.1.

An internal laboratory disposition for thermal measurements (which is born with the purpose to give more protection at the thermal sensor from scratches that can damage it) imposes which the sample must be subjected to a polishing process.

In order to perform the measurement it is necessary that both surfaces do not present any imperfections (also small): for this reason a pre-polishing operation was made with "Struers LaboPol 5". This machine is equipped with a circular plane that can perform from 50 to 500 revolutions per minute. Over this plane it is possible puts a disc of sandpaper with the desired granulometry (struers.com) (Figure 5.15).

As example, the results obtained with pre-polishing operations are showed for sample 6A (Biancone) in Figure 5.16.

Subsequently all samples were subjected to the polishing using the machine "Lapidello 400" produced by Gemmarum Lapidator (www.gemmarum.it) (Figure 5.17).

This device is equipped with a circular plate in cast iron with the diameter of 400 mm which can do up 300 revolutions per minute. For our purpose the cast iron disk is replaced by a felt grinding wheel and above it is sprinkled on the polishing agent (aluminums oxide).

The roughness of the abrasive is 18.2±1 (μm) which corresponds to a rating of 500 in the F-series presented by the Federation of the European Producers of Abrasives (FEPA).

The use of this machine is reserved for the processing of stone materials.

Figure 5.15 *Sample 47 after the operation of pre-polishing*

Figure 5.16 *Sample 6A before (on the left) and after (on the right) the operations of pre-polishing: the imperfection presents on the left is removed*

Figure 5.17 *The machine "Lapidello 400" produced by Gemmarum Lapidator*

At this point the samples are put in a ventilated oven at a constant temperature (70 ±5°C) for the duration of 24 hours and then kept at a constant temperature of 20-21°C for the subsequent 24 hours.

Finally the phase measurements begun. The measurements are made on the two smoothed faces of each sample: parallel and perpendicular with respect to the stratification. In this way it is possible determine the anisotropy which is another factor which influences some thermal properties (Chapter 4).

The methodology follows how suggests by Di Sipio et al. (2014). Each sample surface was subjected to 3 sets of measurements (in 3 different points), each consisting of the continuous detection of 8 acquisitions. The first two values were generally not considered due to possible contact problems between the probe and the analyzed surface, while the remaining six were averaged.

In Figure 5.18 is showed the phase of data acquisition of a set of measures for sample 6A (Biancone) on the perpendicular face with respect to the stratification.

In addition at the beginning of each working day was made the instrument calibration. Two materials with known thermal properties (provided by the manufacturer) are subjected to measurements verifying that the values provided by the instrument are within the expected ranges.

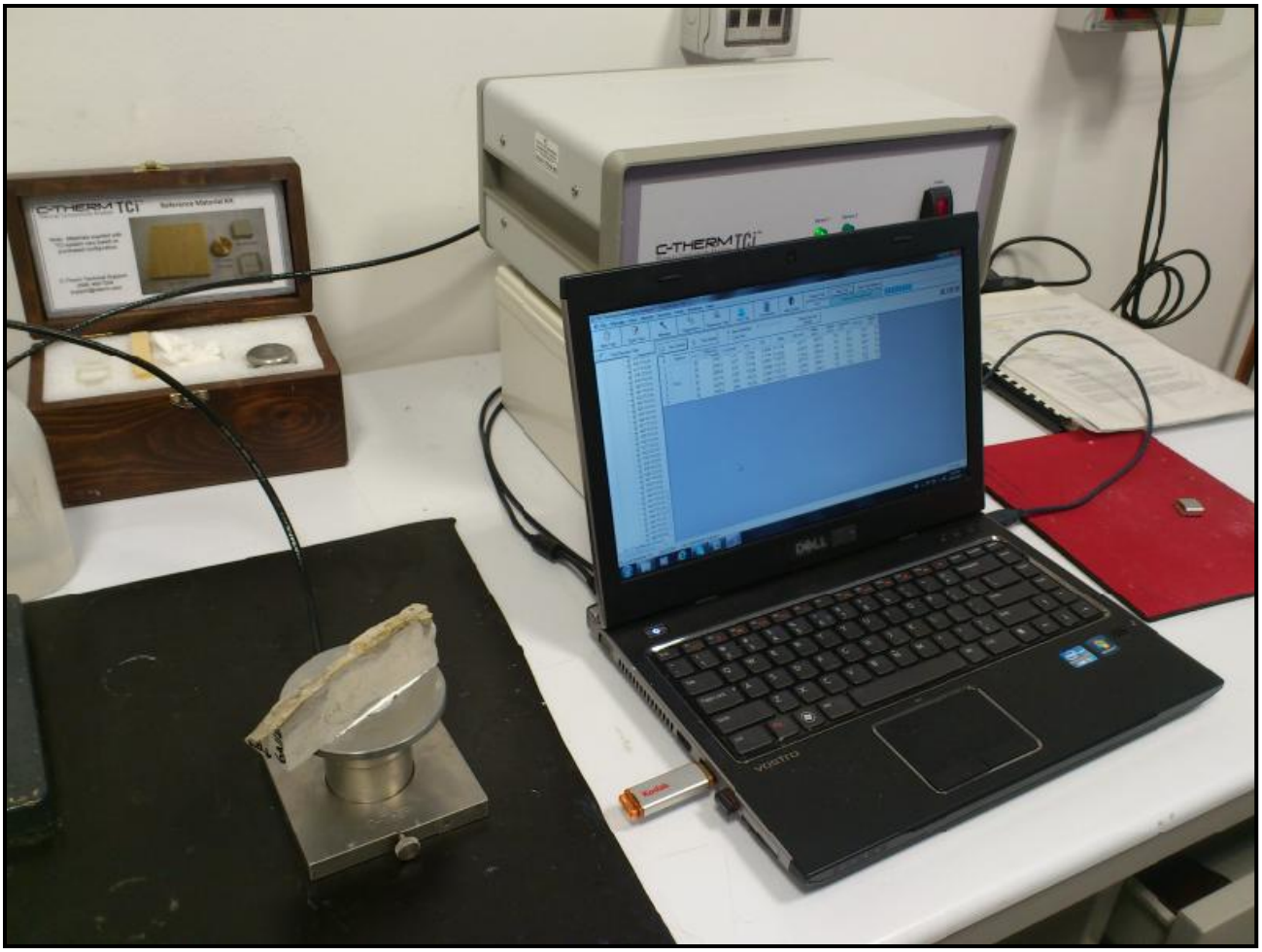

Figure 5.18 *Measurement of the thermal properties on the sample 6A*

To facilitate contact between the sample and the rock has been used a thermal joint compound. This material, made specifically for this purpose, does not alter the results of the measurements.
The weighted average of the 18 values obtained in the three series of measurements was considered to be representative of the analyzed surface.
Repeating this operation for all the 21 samples are obtained 756 validated acquisitions (from a total of 1,008 considering the first two discarded).

6. Results and their discussion

In this chapter are presented and discussed the results obtained from this work. In the first paragraph are reported the data obtained with a literature search: in particular for density, porosity, thermal conductivity and volumetric heat capacity the collected data are considered sufficient to be represented also by the box-plots.
The results of laboratory are reported in paragraph 6.2. Relations between the physical and thermal parameters are highlighted, in detail those between the thermal conductivity and thermal diffusivity, focused on leading to an estimation of the volumetric heat capacity.
Section 6.3 is devoted to the comparison between the bibliographical data and those obtained by laboratory tests while section 6.4 is dedicated to an analysis of the instrumentation with particular attention to its accuracy and precision.

6.1 Bibliographic results

Typical values of thermo physical properties for the rocks used in this work are reported in this paragraph: in this collection are present effusive rocks (trachyte, rhyolite and latite) and sedimentary rocks (marl and limestone) whose presence is linked to genesis of the Euganean Hills as indicated in Chapter 2 (Geological outline). Other lithologies (as basalt and ialoclastiti) are not considered due to low presence on the territory. The different formations of limestone present in the Euganean Hills (Biancone, Scaglia Rossa, Rosso Ammonitico) are not distinguished because in literature was not found specific values related to them.

6.1.1 Bibliographic results about density

Are here presented he bibliographic results about density (ρ). They are obtained consulting scientific paper, thesis, specialized books, geological reports and indications provided by standards.

Table 6.1 *Bibliographic values of bulk density for the rocks used in this work. Notes about the authors: (1) Cava di Montemerlo (cavepietra.it); (2) Seconda Università di Napoli; (3) Verein Deutscher Ingenieure; (4) Geologisches Landesamt Baden-Württemberg; (5) Ufficio Geologico Cantonale, Switzerland; (6) Year of the consultation of web resource*

Lithology	Author	Year	ρ (g/cm3)
Trachyte	CDM[(1)]	2014[(6)]	2.40-2.60
	Hegger	2009	2.50-2.80
	Klein (britannica.com)	2014[(6)]	2.57

Lithology	Author	Year	ρ (g/cm3)
	marbleandmore.it	2014[6]	2.45
	Primavari	2008	1.76
	Sarda Trachiti s.r.l.	2014[6]	2.20
	SUN[2]	2009	2.30
	VDI 4640[3]	2010	2.6
Rhyolite	Bagdassarov et al.	1992	2.33
	Gonzalez de Vallejo	2004	2.40-2.60
	Klein (britannica.com)	2014[6]	2.51
	Türkdönmez et al.	2012	2.14
	VDI 4640[3]	2010	2.60
Latite	Ross	1970	2.49
	Ross	1970	2.71
	Ross	1970	2.44
	VDI 4640[2]	2010	2.9-3
	Zharikov et al.	2009	2.66
Marl	Homand et al.	2000	2.30
	Pasquale et al.	2011	1.79-2.28
	Schön	2004	2.30-2.70
	VDI 4640[3]	2010	2.30-2.60
	Waples et al.	2004	2.72
Limestone	Alishaev et al.	2012	2.38
	GLA[4]	2014[6]	2.41-2.67
	Gong	2005	2.70
	Gong	2005	2.81
	Gong	2005	2.73
	Hegger	2009	2.60-2.90
	Homand et al.	2000	2.31
	Klein (britannica.com)	2014[6]	1.55-2.75
	Kodešová et al.	2013	2.76-2.77
	Pereira	2008	2.32
	Primavari	2008	2.67
	Sanna et al.	2009	2.64
	Sanna et al.	2009	2.30
	Sanna et al.	2009	2.51
	Sanna et al.	2009	2.52
	Sanna et al.	2009	2.84
	Sanna et al.	2009	2.10
	Sanna et al.	2009	2.63
	Sanna et al.	2009	2.61
	Sanna et al.	2009	2.60
	Schön	2004	2.30-2.90
	UGC[5]	1982	2.60
	VDI 4640[3]	2010	2.40-2.70
	Waples et al.	2004	2.77
	Waples et al.	2004	2.76

For the trachyte the higher value is 2.80 (g cm^{-3}) and the lower is 1.76 (g cm^{-3}). For rhyolite the range is between 2.14 and 2.60 (g cm^{-3}). and it is the lithology with the minor difference between the maximum and the minimum value registered (0.46 g cm^{-3}).

Latite shows a minimum and a maximum value of 2.44 and 3.00 (g cm^{-3}). respectively. This last value is the highest of the all bibliographic research.

The values of marl range between 1.79 and 2.72 (g cm^{-3}). The limestone is the lithology with the lower density (1.55 g cm^{-3}) and a very high difference with respect to the maximum value associated at this lithology (2.9 g cm^{-3}). Probably the high variability of the data is linked to the extreme variability of the limestone in the world, whose density depends on the different processes of generation, compaction and age of formation.

The box-plot in Figure 6.1 gives a graphical representation of the data collected, subdivided following the main lithologies typical of the Euganei Hills.

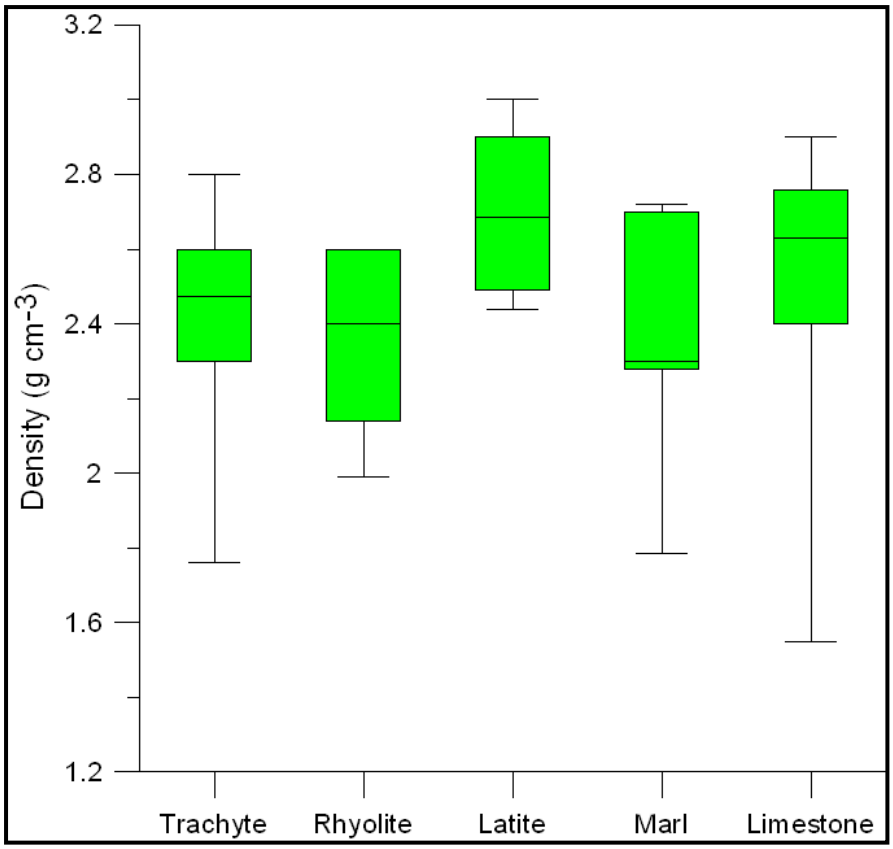

Figure 6.1 *Box-plot representation of bibliographic values of density for the rocks used in this work*

The figure highlights the large variability of values for the limestone. In addition this lithology has a median value equal to 2.63 (g cm^{-3}). This value in not the highest: latite has a median value of 2.69 (g cm^{-3}). The lowest value (2.30 g cm^{-3}) is related to marl

and rhyolite and trachyte have values very near each other: 2.46 and 2.48 g cm^{-3} respectively; in fact these two rocks have similar genesis processes.

6.1.2 Bibliographic results about porosity

The bibliographic results for porosity (η) are reported in Table 6.2.

Table 6.2 *Bibliographic values of porosity for the rocks used in this work. Notes about the authors: (1) Ufficio Geologico Cantonale. Notes about the data: (*) limestone mixed with shale*

Lithology	Author	Year	η (%)
Trachyte	marbleandmore.it	2014	6.60
	Sanna et al.	2009	10-40
	Sarda Trachiti s.r.l.	2014	17
Rhyolite	Bargar et al.	1985	15.70-45.80
	Cashman et al.	2003	22-85
	Gonzalez de Vallejo	2004	4-6
	Türkdönmez et al.	2012	13.72
	Türkdönmez et al.	2012	21.27
	Wood et al.	1988	3-15
Latite	Zharikov et al.	2009	0.82
Marl	Holston et al.	1989	31-35
	Holston et al.	1989	36-41
	Pasquale et al.	2011	6 -37
Limestone	Alishaev et al.	2012	5
	Gong	2005	0.48
	Gong	2005	0.29
	Gong	2005	1.55
	Gong	2005	0.91
	Lee	1999	2.30(*)
	Lee	1999	3.70(*)
	Lee	1999	3.60(*)
	Popov et al.	2004	1.70-36.60
	Sanna et al.	2009	15-40
	Sanna et al.	2009	3-10
	Schön	2004	0.10-1.40
	Schön	2004	2.20-14.90
	Schön	2004	1.20-36.50
	Schön	2004	1.20-5.70
	UGC(1)	1982	0.50-5

To enable a better understanding of the data, a box plot was obtained. In this way, it is easiest to determine the range of values and the most representative value to be assigned for each lithology

For example, the porosity of trachyte ranges between 6.60 and 40.00%, while that of rhyolite from 4.00% up to 85.00%, the highest difference of all the set of data collected. This high variability is due at the different conditions of the samples used for the experiments: in some cases fracturing or weathering phenomena can alter profoundly the rocks.

For latite only one value was found: 0.82%. Marl ranges between 6 and 41% and limestone has the lower values of all lithologies (0.29%) and a maximum value equal to 40%. As density, also porosity depends on the different processes of generation, compaction and age of formation: the oldest limestone have smaller porosity than the newer ones which are subjected at a minor burial pressures.

In Figure 6.2 is showed a box-plot representation of the data just presented. The median value of rhyolite and limestone (15.35 and 2.65%, respectively) is much lower compared to the maximum values given above: from a statistical point of view they are called outliers (an outlier is an observation which is distant from all other observations).

For other lithologies: 13.50% is related to trachyte and 35.5% for marl, which is the highest value.

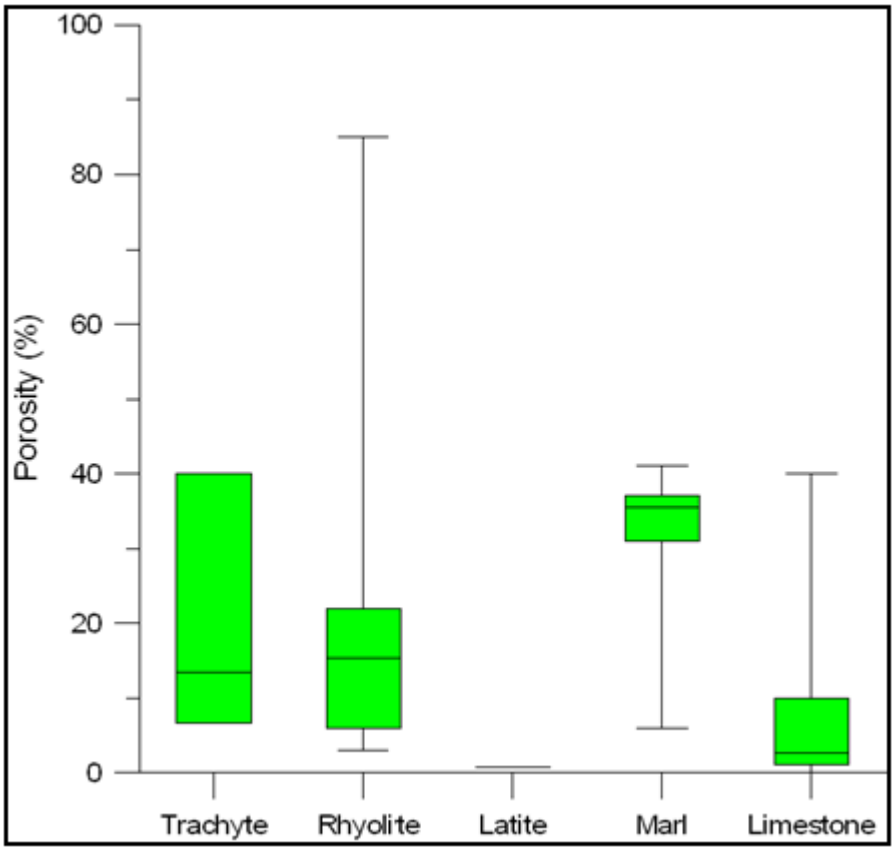

Figure 6.2 *Box-plot representation of bibliographic values of porosity for the rocks used in this work*

6.1.3 Bibliographic results about thermal conductivity

Thermal conductivity (λ) is a very important parameter, for this reason the bibliographic research has focused a lot on it. In table 6.3 are subdivided the values into dry and wet values. First are lower respect the latter because the thermal conductivity of air (which filled the pores in dry conditions) are lower respect the thermal conductivity of water, that is the saturating fluid generally used because in this way it is possible have indications about thermal conductivity values in areas where a groundwater is present. Another distinction is made between values measured parallel and perpendicular with respect to the stratification; this distinguished is made because (as illustrated in Chapter 4) this thermal properties can changes depending on the direction along which it is measured.

Table 6.3 *Bibliographic values of thermal conductivity for the rocks used in this work. Notes about the authors: (1) Personenkreises Oberflächennahe Geothermie; (2) Seconda Università di Napoli; (3) Verein Deutscher Ingenieure; (4) Geologisches Landesamt Baden-Württemberg; (5) Ufficio Geologico Cantonale, Switzerland; (6) Year of the consultation of web resource. Notes about the data: (*) in source test was not specified if the measure is parallel or perpendicular to the stratification so it is attributed to both. Convention for the acquisition: if in the source test there isn't any information, the measure is considered made in "dry" conditions and refers to the ambient temperature*

Lythology	Author	Year	$\lambda^{\perp}$ dry ($W\ m^{-1}K^{-1}$)	λ//dry ($W\ m^{-1}K^{-1}$)	$\lambda^{\perp}$wet ($W\ m^{-1}K^{-1}$)	λ// wet ($W\ m^{-1}K^{-1}$)
Trachyte	Hegger	2009	3.5*	3.5*		
	PK OG(1)	2008	3.55*	3.55*		
	Primavari	2008	1.15*	1.15*		
	SUN(2)	2014(6)	2.9*	2.9*		
	VDI 4640(3)	2010	3.1-3.4*	3.1-3.4*		
Rhyolite	Froldi	2013	3.1*	3.1*	3.3*	3.3*
	Herrera de Figueiredo	2006	3.79*	3.79*		
	PK OG(1)	2008	3.3*	3.3*		
	VDI 4640(3)	2010	3.1-3.4*	3.1-3.4*		
Latite	PK OG(1)	2008	1.7*	1.7*		
	VDI 4640(3)	2010	2.0-2.9*	2.0-2.9*		
Marl	Andolfsson	2013	0.59*	0.59*		
	Froldi	2013	1.5-1.8*	1.5-1.8*	2.3-2.9*	2.3-2.9*
	Froldi	2013	1.5*	1.5*	2.1*	2.1*
	Homand et al.	2000	1.04-1.4*	1.04-1.4		
	PK OG(1)	2008	1.5-3.9*	1.5-3.9*		
	Schön	2004	1.92*	1.92*		
	Schön	2004	2.21*	2.21*		
	VDI 4640(3)	2010	1.8-2.9*	1.8-2.9*		
	Pasquale et al.	2011			2.15-3.08*	2.15-3.08*
Limestone	Alishaev et al.	2012	1.94*	1.94*	2.6*	2.6*
	Andolfsson	2013	1.17*	1.17*		
	Andolfsson	2013	0.77*	0.77*		

Lythology	Author	Year	λ⊥ dry (W m^{-1}K^{-1})	λ//dry (W m^{-1}K^{-1})	λ⊥wet (W m^{-1}K^{-1})	λ// wet (W m^{-1}K^{-1})
	Andolfsson	2013	2.81*	2.81*		
	Buntebarth	1980	2.2-2.8*	2.2-2.8*		
	Froldi	2013	2.8-3.3*	2.8-3.3*	2.8-3.3*	2.8-3.3*
	Froldi	2013	2.5*	2.5*	2.8*	2.8*
	GLA[4]	2014[6]	2.5-3.5*	2.5-3.5*		
	Gong	2005	3.08	3.66	3.21	3.19
	Gong	2005	3.3	3.5	3.95	3.98
	Gong	2005	4.38	4.41	4.78	4.79
	Gong	2005	2.56	2.55	2.76	2.86
	Grunert et al.	2010	1.0777	0.85		
	Hartmann et al.	2008	2.6*-2.8*	2.6*-2.8*		
	Hegger	2009	2.3*	2.3*		
	Homand et al.	2000	3.5*	3.5*		
	Lee	1999	1.49*	1.49*		
	Lee	1999	1.94*	1.94*		
	Lee	1999	2.61*	2.61*		
	Lee et al.	1999	1.94*	1.94*		
	Lee et al.	1999	2.61*	2.61*		
	Liebethat	2012	3.037*	3.037*		
	Liebethat	2012	2.537*	2.537*		
	Liebethat	2012	2.504*	2.504*		
	Popov et al.	2004	0.65-2.69*	0.65-2.69*	1.57-2.73*	1.57-2.73*
	Sanna et al.	2009	1.5*	1.5*		
	Schön	2004	2.29*	2.29*		
	Schön	2004	3.44*	3.44*		
	Schön	2004	2.4*	2.4*		
	SUN[2]	2014[6]	2.9*	2.9*		
	UGC[5]	1982	1.8-3.3*	1.8-3.3*		
	VDI 4640[3]	2010	2.0-3.9*	2.0-3.9*		

For many data found was not specified if the value was on the face parallel or perpendicular to the stratification, it was decided to keep the distinction. Some authors provide results in wet conditions: although not directly comparable with the results obtained in this work, however, they may represent a starting point for future investigations.

Trachyte has value between 1.15 and 3.55 (W m^{-1}K^{-1}); despite the few data found, the range of variability is quite large because the minimum value is very low: it is associated at the trachyte of Fordongianus (Sardinia).

The second considered lithology (rhyolite) has values from 3.1 to 3.79 (W m^{-1}K^{-1}) while latite ranges from 1.7 to 2.9 (W m^{-1}K^{-1}).

As trachyte, also marl has a big variation from the lower value (0.59 W m^{-1}K^{-1}) and the highest (3.9 W m^{-1}K^{-1}).

Limestone ranges from 0.65 to 4.79 (W $m^{-1}K^{-1}$). This last value is also the higher value found in all bibliographic research.

In Figure 6.3 and 6.4 are reported the box-plot for the thermal conductivity measured parallel and perpendicular to stratification, respectively.

The values used to build the box-plot are referred to "dry" condition in order to make they comparable with whose that will be obtained using laboratory data

They appear similar because few source data are distinguished between parallel and perpendicular with respect to the stratification.

Trachyte and rhyolite show the highest median values which are 3.25 and 3.30 W $m^{-1}K^{-1}$ (same values are for perpendicular and parallel with respect to the stratification). Also latite (2.00 W $m^{-1}K^{-1}$), marl (1.65 W $m^{-1}K^{-1}$) and limestone (2.58 W $m^{-1}K^{-1}$) have the same median values for measures taken from parallel and perpendicular with respect the stratification.

These considerations jointed with the observation of Figure 6.3 and 6.4 which the minimum and maximum values are very similar it is possible conclude which, in general line, the considered lithologies are theoretically isotropic: this affirmation will be (or not) verify after the laboratory results.

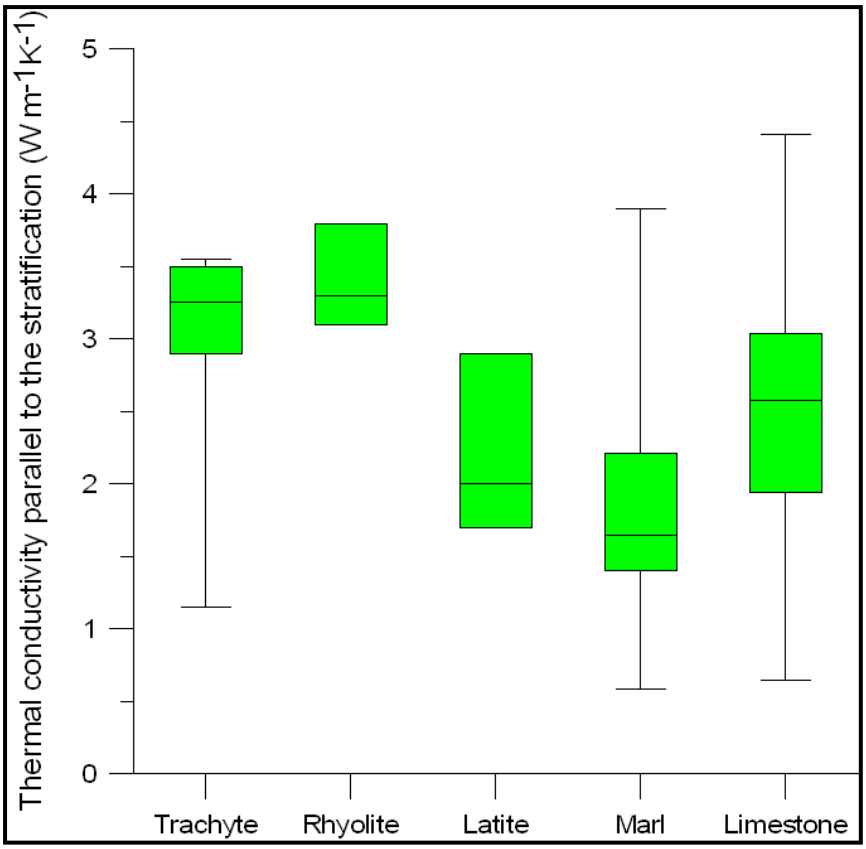

Figure 6.3 *Box-plot representation of bibliographic values of parallel thermal conductivity for the rocks used in this work*

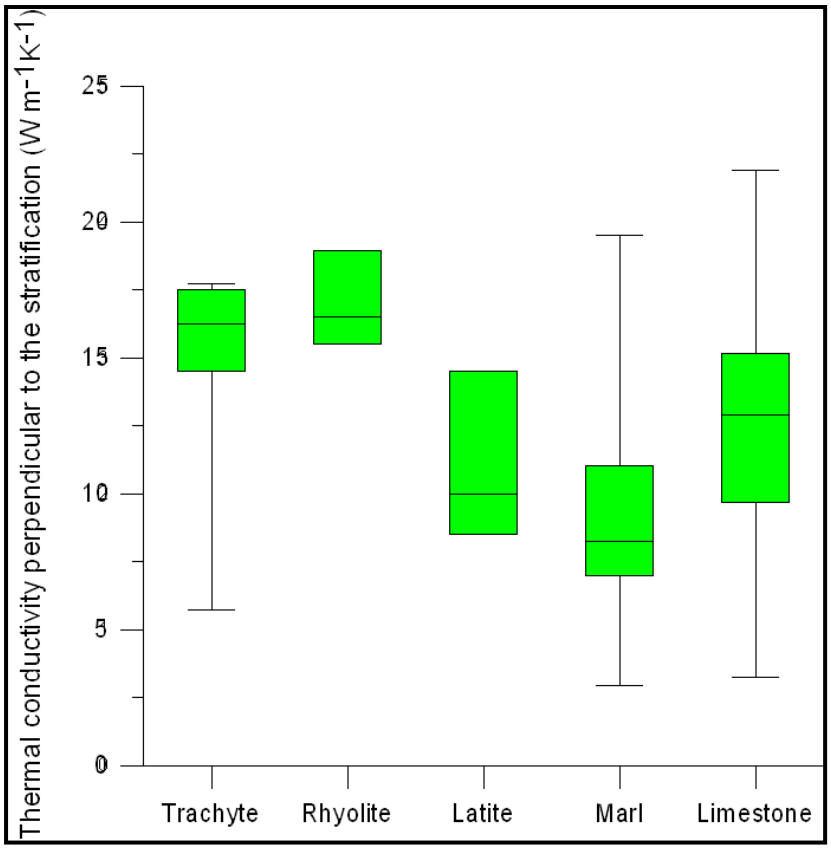

Figure 6.4 *Box-plot representation of bibliographic values of perpendicular thermal conductivity for the rocks used in this work*

6.1.4 Bibliographic results about volumetric heat capacity

The volumetric heat capacity (ρ cp) is defined as the product of density and specific heat capacity and represent the second thermal property considered in literature search. The results was found for dry conditions and are reported in Table 6.4. As seen in Chapter 4, this parameter is related with the quantity of heat which can be stored for unit of volume. In addition this parameter is a scalar property (Verrone, 2009) so no distinction between data parallel and perpendicular with respect to the stratification was made.

For trachyte and latite is found one value: 2.1 and 2.9 (J $cm^{-3}K^{-1}$) respectively. The value of latite is also the highest value of all considered lithologies. Rhyolite ranges from 2.1 to 2.23 (J $cm^{-3}K^{-1}$). Marl has the lowest value equal to 1.31 (J $cm^{-3}K^{-1}$) and a maximum value of 2.58 (J $cm^{-3}K^{-1}$). The lowest value of marl is also the lowest value of all lithologies. Limestone ranges from 1.88 to 2.4 (J $cm^{-3}K^{-1}$).

Generally all values fall within the boundary proposed by Clauser (2011): 2.3 (J $cm^{-3}K^{-1}$) ±20%; this is not true for marl because the value of 1.31 (J $cm^{-3}K^{-1}$) is out of this boundaries. Probably it is due at low value of density (1.71 g cm^{-3}) associated at the sample (Pasquale et al., 2011).

Also the value of latite is out of this range: in this case the data came from VDI 4640 is more difficult to comment because this value is an indicative value provided by the

"Association of German Engineers" (in German: Verein Deutscher Ingenieure) and no experimental data and comments are reported on the consulted sheet.

Table 6.4 *Bibliographic values of thermal capacity for the rocks used in this work. Notes: (1) Verein Deutscher Ingenieure; (2) Ufficio Geologico Cantonale, Switzerland*

Lithology	**Author**	**Year**	**ρ cp (J cm^{-3}K^{-1})**
Trachyte	VDI 4640	2010	2.10
Rhyolite	Froldi	2013	2.10
	Herrera de Figueiredo	2006	2.23
Latite	VDI 4640[(1)]	2010	2.90
Marl	Froldi	2013	2.20-2.30
	Pasquale et al.	2011	1.31-2.04
	Waples et al.	2004	2.58
Limestone	Clauser	2011	1.88-2.43
	Froldi	2013	2.10-2.40
	UGC[(2)]	1982	2.3
	Waples et al.	2004	1.88
	Waples et al.	2004	2.43

In Figure 6.5 is reported a box-plot representation for bibliographic values of thermal conductivity.

The graph reflects the consideration just made. In particular the median value for the lithologies (with more than one bibliographic value) are: for rhyolite 2.17 (g cm^{-3}), for marl 2.20 (g cm^{-3}), for limestone 2.30 (g cm^{-3}).

The three values are very close. This confirms the lack of variability of the volumetric heat capacity also between different rocks type (sedimentary and volcanic) reflecting what has been illustrated in Chapter 4.

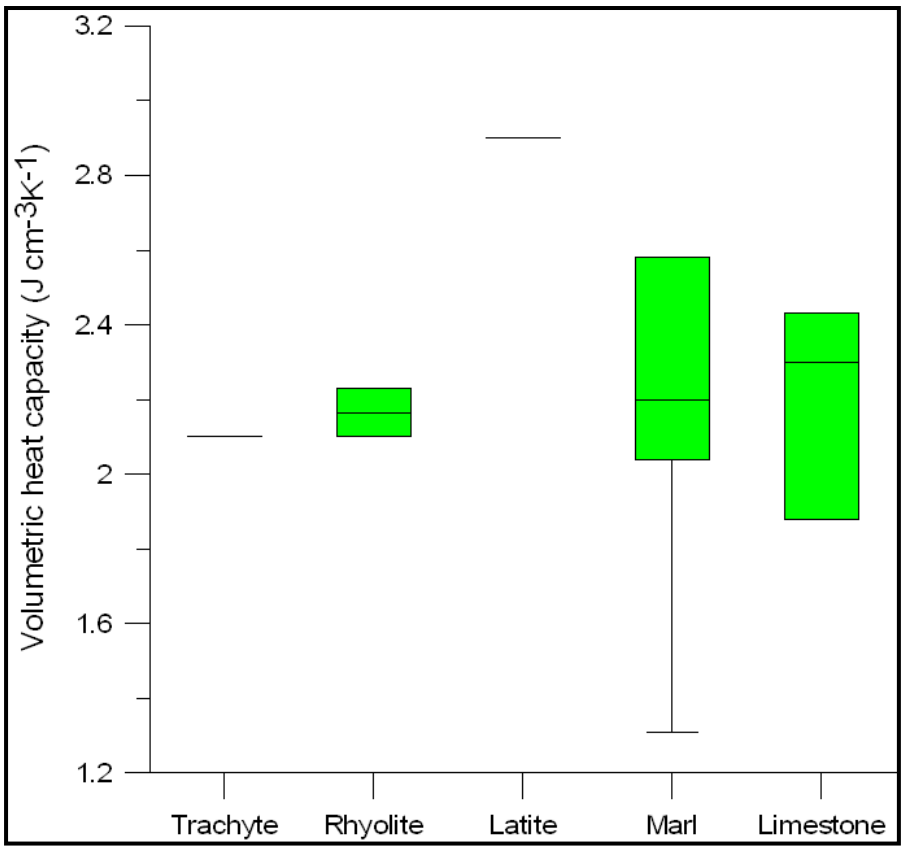

Figure 6.5 *Box-plot representation of bibliographic value of volumetric heat capacity for the rocks used in this work*

6.1.5 Bibliographic results about thermal diffusivity

The last bibliographic research is related to thermal diffusivity (indicated with α). Respect the other thermal properties there are a lower number of authors which have focused the attention on this parameter.

As thermal conductivity this parameter can changes if measured parallel or perpendicular with respect to the stratification. For this reason in Table 6.5 are reported this distinction. The data collected are referred to dry conditions.

It is possible have an idea about the magnitude of this parameter: it ranges from 0,39 (mm^2/s) (marl) to 1,56 (mm^2/s) (limestone).

Table 6.5 *Bibliographic values of thermal diffusivity for the rocks used in this work. Notes about the data: (*) in source test was not specified if the measure is parallel or perpendicular to the stratification so it is attributed to both. Convention for the acquisition: if in the source test there isn't any information, the measure is considered made in "dry" conditions and refers to the ambient temperature*

Lythology	Author	Year	$\alpha^{\perp}$ dry (mm^2/s)	α//dry (mm^2/s)
Trachyte	/	/	/	/
Rhyolite	Herrera de Figueiredo	2006	1.7*	1.7*
Latite	/	/	/	/
Marl	Andolfsson	2013	0.39*	0.39*
Limestone	Andolfsson	2013	0.83*	0.83*
	Andolfsson	2013	0.52*	0.52*
	Pereira	2008	1.1*	1.1*

6.2 Laboratory results

6.2.1 Laboratory results about density

In Table 6.1 are reported the density (ρ) results obtained for the 21 samples. As required by the standard density were determinate using three cubes for each sample.

Table 6.6 *Values of density for sampled lithologies. Note: The terms "S.R.", "B.", "R.A.", in parentheses are referred to the formations of "Scaglia Rossa", "Biancone" and "Rosso Ammonitico"; respectively. The column "S.D." refers to standard deviation of the single sample*

Lithology	Sample (3cubes)	ρ (g/cm3)	Average sample (g/cm3)	S.D. (g/cm3)	Average lithology (g/cm3)
Trachyte	1_1	2.454			
Trachyte	1_2	2.464	2.450	0.016	
Trachyte	1_3	2.433			
Trachyte	22B_1	2.263			
Trachyte	22B_2	2.428	2.326	0.089	2.380
Trachyte	22B_3	2.288			
Trachyte	44_1	2.366			
Trachyte	44_2	2.361	2.363	0.002	
Trachyte	44_3	2.363			
Rhyolite	16_1	2.374			
Rhyolite	16_2	2.374	2.377	0.005	
Rhyolite	16_3	2.382			
Rhyolite	36_1	2.215			
Rhyolite	36_2	2.172	2.199	0.024	2.229
Rhyolite	36_3	2.210			
Rhyolite	39_1	2.088			
Rhyolite	39_2	2.133	2.111	0.022	
Rhyolite	39_3	2.112			
Latite	18_1	2.573			
Latite	18_2	2.566	2.566	0.008	

Lithology	Sample (3cubes)	ρ (g/cm3)	Average sample (g/cm3)	S.D. (g/cm3)	Average lithology (g/cm3)
Latite	18_3	2.558			
Latite	42_1	2.417			
Latite	42_2	2.421	2.422	0.006	2.509
Latite	42_3	2.429			
Latite	43_1	2.543			
Latite	43_2	2.532	2.539	0.006	
Latite	43_3	2.541			
Marl	11_1	2.378			
Marl	11_2	2.386	2.380	0.006	
Marl	11_3	2.375			
Marl*	24_1	1.367			
Marl*	24_2	1.278	1.319	0.045	2.431
Marl*	24_3	1.313			
Marl	46_1	2.479			
Marl	46_2	2.482	2.481	0.002	
Marl	46_3	2.483			
Limestone (S.R.)	3_1	2.357			
Limestone (S.R.)	3_2	2.343	2.351	0.007	
Limestone (S.R.)	3_3	2.353			
Limestone (S.R.)	25_1	2.608			
Limestone (S.R.)	25_2	2.616	2.608	0.009	
Limestone (S.R.)	25_3	2.599			
Limestone (S.R.)	47_1	2.300			
Limestone (S.R.)	47_2	2.299	2.296	0.005	
Limestone (S.R.)	47_3	2.290			
Limestone (B.)	6A_1	2.233			
Limestone (B.)	6A_2	2.274	2.262	0.025	
Limestone (B.)	6A_2	2.279			
Limestone (B.)	8_1	2.614			
Limestone (B.)	8_2	2.613	2.619	0.009	2.516
Limestone (B.)	8_3	2.629			
Limestone (B.)	27A_1	2.533			
Limestone (B.)	27A_2	2.525	2.531	0.006	
Limestone (B.)	27A_3	2.536			
Limestone (R.A.)	10B_1	2.655			
Limestone (R.A.)	10B_2	2.650	2.659	0.012	
Limestone (R.A.)	10B_3	2.672			
Limestone (R.A.)	34_1	2.643			
Limestone (R.A.)	34_2	2.635	2.638	0.004	
Limestone (R.A.)	34_3	2.636			
Limestone (R.A.)	35_1	2.672			
Limestone (R.A.)	35_2	2.677	2.676	0.003	
Limestone (R.A.)	35_3	2.678			

Density in all lithologies has a small variation; in fact it ranges from the minimum of 2.229 (g cm^{-3}) of rhyolite to the maximum of 2.516 (g cm^{-3}) of limestone.
Even within the single rock the variability is very low, affecting only the second decimal.
The lowest value is referred to sample 24 (marl) with a density equal to 1.319 (g/cm^3). In this regard it should be underlined that the three cubes for sample 24 were damaged during the imbibition of water inside the dryer and so the measures were altered. For this reason this sample is marked with a "*" and its value is not used for any further elaboration.
Within the limestone, the different formations have the mean value reported in Table 6.7.

Table 6.7 *Values of density for different limestone formations*

Formation	Sample	Average sample (g/cm3)	Average formation (g/cm3)
Scaglia Rossa	3	2.351	
Scaglia Rossa	25	2.608	2.418
Scaglia Rossa	47	2.296	
Biancone	6A	2.262	
Biancone	8	2.619	2.471
Biancone	27A	2.531	
Rosso Ammonitico	10B	2.659	
Rosso Ammonitico	34	2.638	2.658
Rosso Ammonitico	35	2.676	

The higher density value is referred to sample 35 (2.676 g cm^{-3}) which belongs at "Rosso Ammonitico" formation. This formation has also the highest mean value (2.658 g cm^{-3}).
This result is not unexpected: This limestone formation is the oldest in the Euganean Hills (as shown in Chapter 2), and so the more recent formations are above it. This has created strong compressions that have increased the density of the deposited material.
In order to have an idea of the casual errors introduced by measurement uncertainties it was decided to calculate the standard deviation for all measurements. Standard deviation is useful to know how much (on average) the single measure deviates from the mean value.
In particular, the highest value (0.089 g cm^{-3}) belongs to sample 22B (trachyte), while the lowest (0.002 g cm^{-3}) to samples 44 (trachyte) and 46 (marl).
In Figure 6.6 is reported the box-plot representation for laboratory results about density.
The median value are all very close: 2.363 (g cm^{-3}) for trachyte, 2.199 (g cm^{-3}) for rhyolite, 2.539 (g cm^{-3}) for latite, 2.431 (g cm^{-3}) for marl, 2.608 (g cm^{-3}) for limestone.

Rhyolite and limestone have respect other lithologies a greater variability: for rhyolite this is due to some process of weathering related to samples 36 and 39 (collected in different points of Monte Rua); for limestone the variability is due to the different loading history related to the different formations.

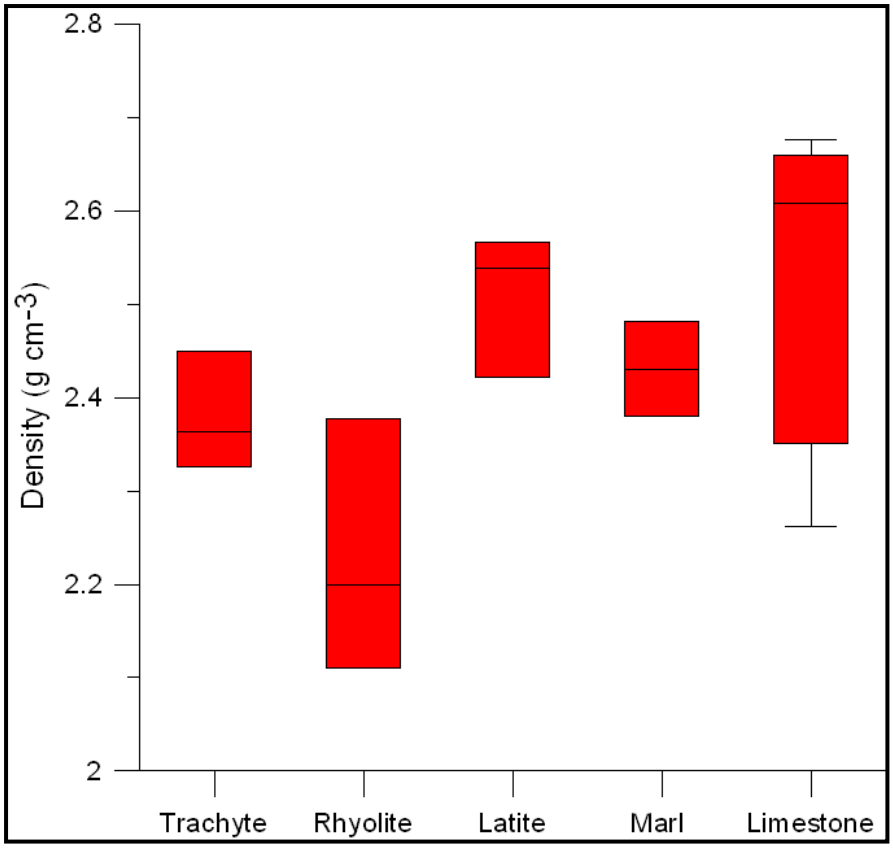

Figure 6.6 *Box-plot representation of laboratory values of density for the rocks used in this work*

6.2.2 Laboratory results about porosity

The results about porosity (η) are reported in Table 6.8. For this parameter the highest value is for rhyolite: 13.613% and the lower is for limestone: 6.616%.
The sample with the higher value is sample 39 (rhyolite) with a porosity of 18.84%; the sample with lower value is 10B (Rosso Ammonitico): 0.693%.
As for density (and for same reason) the values associated at sample 24 (marl) is marked with "*" and not considered for any applications.

Table 6.8 *Values of porosity for sampled lithologies. Note: The terms "S.R.", "B.", "R.A.", in parentheses are referred to the formations of "Scaglia Rossa", "Biancone" and "Rosso Ammonitico"; respectively. The column "S.D." refers to standard deviation of the single sample*

Lithology	Sample	η (%)	Average sample (%)	S.D. (%)	Average lithology (%)
Trachyte	1_1	6.102			
Trachyte	1_2	5.814	6.225	0.484	
Trachyte	1_3	6.758			
Trachyte	22B_1	12.559			
Trachyte	22B_2	12.393	12.109	0.640	8.953
Trachyte	22B_3	11.376			
Trachyte	44_1	8.431			
Trachyte	44_2	8.533	8.524	0.089	
Trachyte	44_3	8.608			
Rhyolite	16_1	7.468			
Rhyolite	16_2	7.616	7.547	0.074	
Rhyolite	16_3	7.557			
Rhyolite	36_1	14.028			
Rhyolite	36_2	15.148	14.451	0.608	13.613
Rhyolite	36_3	14.176			
Rhyolite	39_1	19.769			
Rhyolite	39_2	17.895	18.840	0.937	
Rhyolite	39_3	18.857			
Latite	18_1	4.029			
Latite	18_2	4.125	4.061	0.055	
Latite	18_3	4.030			
Latite	42_1	9.219			
Latite	42_2	8.568	8.872	0.328	6.170
Latite	42_3	8.829			
Latite	43_1	5.341			
Latite	43_2	5.605	5.576	0.222	
Latite	43_3	5.782			
Marl	11_1	7.872			
Marl	11_2	7.579	7.832	0.236	
Marl	11_3	8.046			
Marl*	24_1	32.416			
Marl*	24_2	27.199	31.253	3.615	7.887
Marl*	24_3	34.143			
Marl	46_1	8.039			
Marl	46_2	7.889	7.941	0.085	
Marl	46_3	7.894			
Limestone (S.R.)	3_1	12.911			
Limestone (S.R.)	3_2	13.379	13.128	0.236	
Limestone (S.R.)	3_3	13.094			
Limestone (S.R.)	25_1	3.513			
Limestone (S.R.)	25_2	3.188	3.518	0.333	

Lithology	Sample	η (%)	Average sample (%)	S.D. (%)	Average lithology (%)
Limestone (S.R.)	25_3	3.853			
Limestone (S.R.)	47_1	14.761			
Limestone (S.R.)	47_2	14.807	14.891	0.187	
Limestone (S.R.)	47_3	15.104			
Limestone (B.)	6A_1	15.809			
Limestone (B.)	6A_2	14.204	14.850	0.847	
Limestone (B.)	6A_2	14.537			
Limestone (B.)	8_1	3.435			
Limestone (B.)	8_2	3.393	3.245	0.293	6.616
Limestone (B.)	8_3	2.907			
Limestone (B.)	27A_1	5.689			
Limestone (B.)	27A_2	5.734	5.756	0.081	
Limestone (B.)	27A_3	5.846			
Limestone (R.A.)	10B_1	1.667			
Limestone (R.A.)	10B_2	1.857	1.492	0.477	
Limestone (R.A.)	10B_3	0.952			
Limestone (R.A.)	34_1	1.921			
Limestone (R.A.)	34_2	2.273	1.967	0.286	
Limestone (R.A.)	34_3	1.707			
Limestone (R.A.)	35_1	0.942			
Limestone (R.A.)	35_2	0.607	0.693	0.219	
Limestone (R.A.)	35_3	0.531			

Within the limestone, the different formations have the mean value reported in Table 6.9.

Table 6.9 *Values of porosity for different formations of limestone*

Formation	Sample	Average sample %	Average formation %
Scaglia Rossa	3	13.128	
Scaglia Rossa	25	3.518	10.512
Scaglia Rossa	47	14.891	
Biancone	6A	14.850	
Biancone	8	3.245	7.950
Biancone	27A	5.756	
Rosso Ammonitico	10B	1.492	
Rosso Ammonitico	34	1.967	1.384
Rosso Ammonitico	35	0.693	

The formation of Rosso Ammonitico has the lowest value (1.384%), the highest value in instead for Scaglia Rossa (10.512%).

In general the standard deviation ranges in 0.055% (sample 18, latite) and 3.615 (sample 24, marl). In Figure 6.7 is reported the box-plot representation for laboratory results about porosity.

The median value for trachyte is 8.524%, for rhyolite is 14.451%, for latite 5.576% for marl 7.787% and for limestone 3.518%. As for density rhyolite and limestone have the highest range. The reasons are the same explained for density: for the case of rhyolite the weathering processes has create some cracks and cavities within the sample, so the volume of pores increases.

The different loading history related to different formations of limestone conducted in a conspicuous variability of porosity.

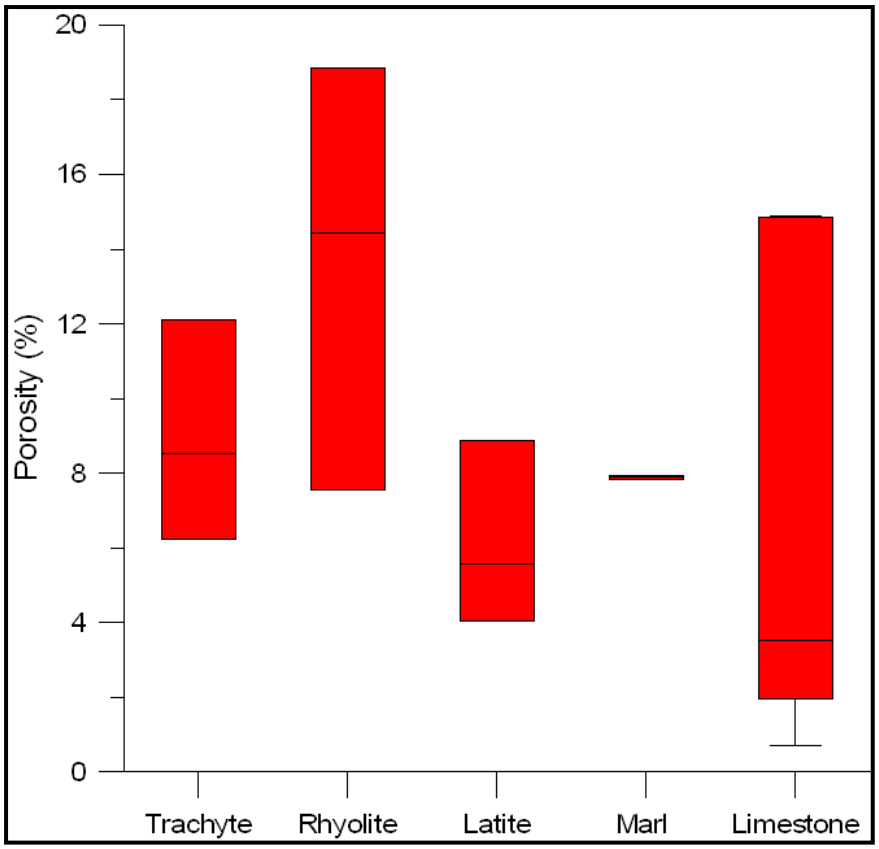

Figure 6.7 *Box-plot representation of laboratory values of porosity for the rocks used in this work*

Density and porosity are related to each other. In particular (Chapter 4) increasing density the porosity decreases (and vice versa). Such behavior is also confirmed for the samples considered in this work (Figure 6.8). In particular for density equal or higher than about 2.6 (g cm^{-3}) the values of porosity are low, as already stated by Gong (2005) for a collection of alpine rocks.

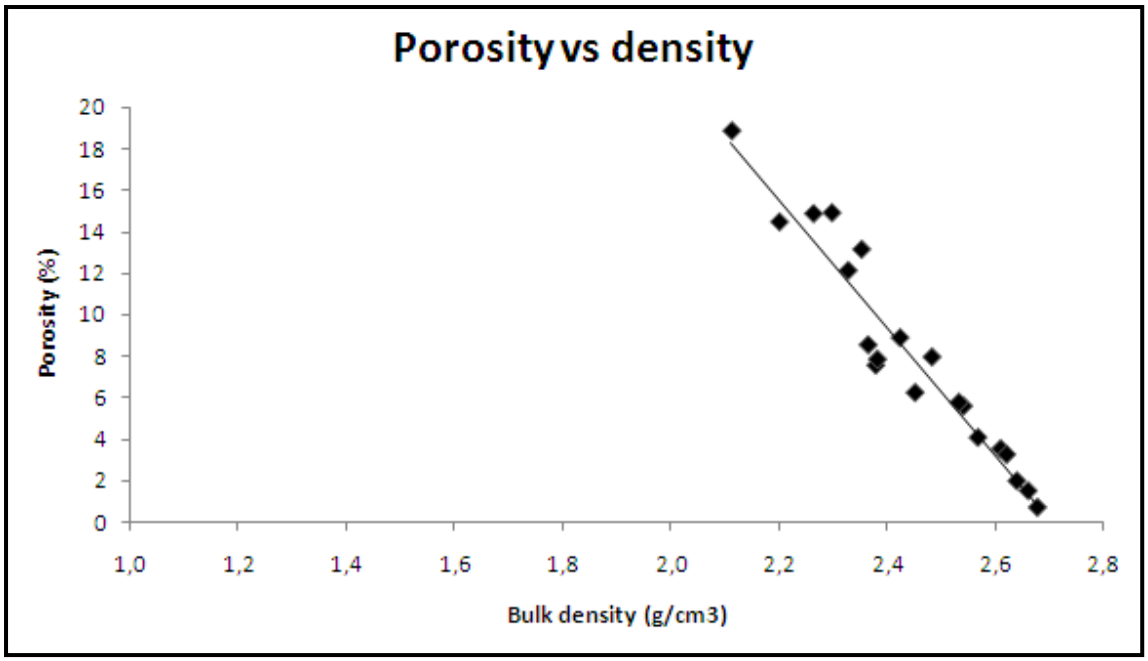

Figure 6.8 *Porosity versus bulk density*

6.2.3 Laboratory results about thermal conductivity

Thermal conductivity (λ) is (with thermal effusivity) the unique parameter which the Thermal analyzer measures directly. The method of acquisition is reported in Chapter 5.

The representative value calculated for a single face is reported in Table 6.10 (the detail of their calculations are reported in Annex I).

As indicated in Chapter 5, the measures are made on two mutually orthogonal faces of the sample, in order to get measures parallel and perpendicular with respect to the stratification.

For thermal conductivity the highest value is for sample 10B (limestone, Rosso Ammonitico formation): 3.26 (W $m^{-1}K^{-1}$, measured perpendicular with respect to the stratification) and the lower is for sample 22B (trachyte): 1.36 (W $m^{-1}K^{-1}$, measured both perpendicular and parallel with respect to the stratification).

This table is also intended to highlight that apart from the sample 47 (Scaglia Rossa, which has a value of 1.26, confirmed also by a second test) all other sample have an anisotropy factor (calculated as the ratio of λ// over λ⊥) comprises between 0.91 (sample 18, latite) and 1.09 (sample 16, rhyolite) confirming the range (0.9-3) proposed by Clauser (2011).

For this reason 20 of 21 rocks can be regarded as isotropic or lightly anisotropic and then assign to them a single representative value for the rock (λ mean).

Table 6.10 *Values of thermal conductivity for sampled lithologies. Note: The terms "S.R.", "B.", "R.A.", in parentheses are referred to the formations of "Scaglia Rossa", "Biancone" and "Rosso Ammonitico"; respectively*

Lithology	**Sample**	**λ⊥ ($Wm^{-1}K^{-1}$)**	**λ// ($Wm^{-1}K^{-1}$)**	**Anisotropy (/)**	**λ mean ($Wm^{-1}K^{-1}$)**
Trachyte	1	1.65	1.53	0.93	1.58
Trachyte	22B	1.36	1.36	1.00	1.36
Trachyte	44	1.45	1.43	0.99	1.44
Rhyolite	16	1.62	1.76	1.09	1.66
Rhyolite	36	1.44	1.44	1.00	1.44
Rhyolite	39	1.53	1.51	0.99	1.52
Latite	18	1.93	1.75	0.91	1.80
Latite	42	1.46	1.53	1.05	1.50
Latite	43	1.73	1.75	1.01	1.74
Marl	11	1.99	1.97	0.99	1.98
Marl	24	1.66	1.77	1.07	1.68
Marl	46	2.34	2.48	1.06	2.38
Limestone (S.R.)	3	2.83	2.60	0.92	2.79
Limestone (S.R.)	25	2.60	2.82	1.08	2.72
Limestone (S.R.)	47	1.88	2.36	1.26	/
Limestone (B.)	6A	2.55	2.52	0.99	2.53
Limestone (B.)	8	2.90	2.93	1.01	2.91
Limestone (B.)	27A	2.55	2.58	1.01	2.56
Limestone (R.A.)	10B	3.26	3.04	0.93	3.11
Limestone (R.A.)	34	2.98	2.86	0.96	2.93
Limestone (R.A.)	35	3.08	3.08	1.00	3.08

For the same reason at the sample 47 (which presents visible stratification at the scale of sample) cannot be assigned a unique representative value because the factor of anisotropy is too much high: in all next considerations will keep separate the value of λ// and λ⊥.

The mean value for each lithology is reported in Table 6.11(fourth and sixth column for thermal conductivity parallel and perpendicular to the stratification, respectively).

The lithology with the lowest value is associated at trachyte (1.44 W $m^{-1}K^{-1}$, measured parallel to the stratification).

The limestone presents the highest value (2.75 W $m^{-1}K^{-1}$) measured paralell to the stratification.

In Table 6.12 are reported the mean values for the different limestone formations.

Within the different limestone formations, Rosso Ammonitico has the highest value (3.11 W $m^{-1}K^{-1}$, measured perpendicular respect the stratification) and Scaglia Rossa has the lowest (2.44 W $m^{-1}K^{-1}$, measured perpendicular respect the stratification).

Table 6.11 *Values of thermal conductivity for sampled lithologies. Note: The terms "S.R.", "B.", "R.A.", in parentheses are referred to the formations of "Scaglia Rossa", "Biancone" and "Rosso Ammonitico"; respectively*

Lithology	Sample	λ// ($Wm^{-1}K^{-1}$)	Average lithology ($Wm^{-1}K^{-1}$)	λ⊥ ($Wm^{-1}K^{-1}$)	Average lithology ($Wm^{-1}K^{-1}$)
Trachyte	1	1.53		1.65	
Trachyte	22B	1.36	1.44	1.36	1.49
Trachyte	44	1.43		1.45	
Rhyolite	16	1.76		1.62	
Rhyolite	36	1.44	1.57	1.44	1.53
Rhyolite	39	1.51		1.53	
Latite	18	1.75		1.93	
Latite	42	1.53	1.68	1.46	1.71
Latite	43	1.75		1.73	
Marl	11	1.97		1.99	
Marl	24	1.77	2.43	1.66	2.00
Marl	46	2.48		2.34	
Limestone (S.R.)	3	2.60		2.83	
Limestone (S.R.)	25	2.82		2.60	
Limestone (S.R.)	47	2.36		1.88	
Limestone (B.)	6A	2.52		2.55	
Limestone (B.)	8	2.93	2.754	2.90	2.74
Limestone (B.)	27A	2.58		2.55	
Limestone (R.A.)	10B	3.04		3.26	
Limestone (R.A.)	34	2.86		2.98	
Limestone (R.A.)	35	3.08		3.08	

Table 6.12 *Values of thermal conductivity for different formations of limestone*

Formation	Sample	λ// ($Wm^{-1}K^{-1}$)	Average formation ($Wm^{-1}K^{-1}$)	λ⊥ ($Wm^{-1}K^{-1}$)	Average formation ($Wm^{-1}K^{-1}$)
Scaglia Rossa	3	2.60		2.83	
Scaglia Rossa	25	2.82	2.59	2.60	2.44
Scaglia Rossa	47	2.36		1.88	
Biancone	6A	2.52		2.55	
Biancone	8	2.93	2.68	2.90	2.67
Biancone	27A	2.58		2.55	
Rosso Ammonitico	10B	3.04		3.26	
Rosso Ammonitico	34	2.86	2.99	2.98	3.11
Rosso Ammonitico	35	3.08		3.08	

In Figure 6.9 and 6.10 are showed a box-plot representations of the data for thermal conductivity parallel and perpendicular to the stratification, respectively.

Limestone shows the highest median values (which are 2.82 and 2.83 W $m^{-1}K^{-1}$ for perpendicular and parallel with respect to the stratification, respectively). Marl has the

second highest median values (which are 1.97 and 1.99 W $m^{-1}K^{-1}$ for perpendicular and parallel with respect to the stratification, respectively).

Effusive rocks show lower values respect volcanic. Trachyte has a median values of 1.43 and 1.45 (W $m^{-1}K^{-1}$), rhyolite has a median values of 1.51 and 1.53 (W $m^{-1}K^{-1}$), latite has a median values of 1.75 and 1.73 (W $m^{-1}K^{-1}$) (parallel and perpendicular to the stratification, respectively).

The two graphs are similar: only limestone shows some differences. These differences are due to the presence of sample 47 (Scaglia Rossa formation) which presents an anisotropy equal to 1.26 (Table 6.10).

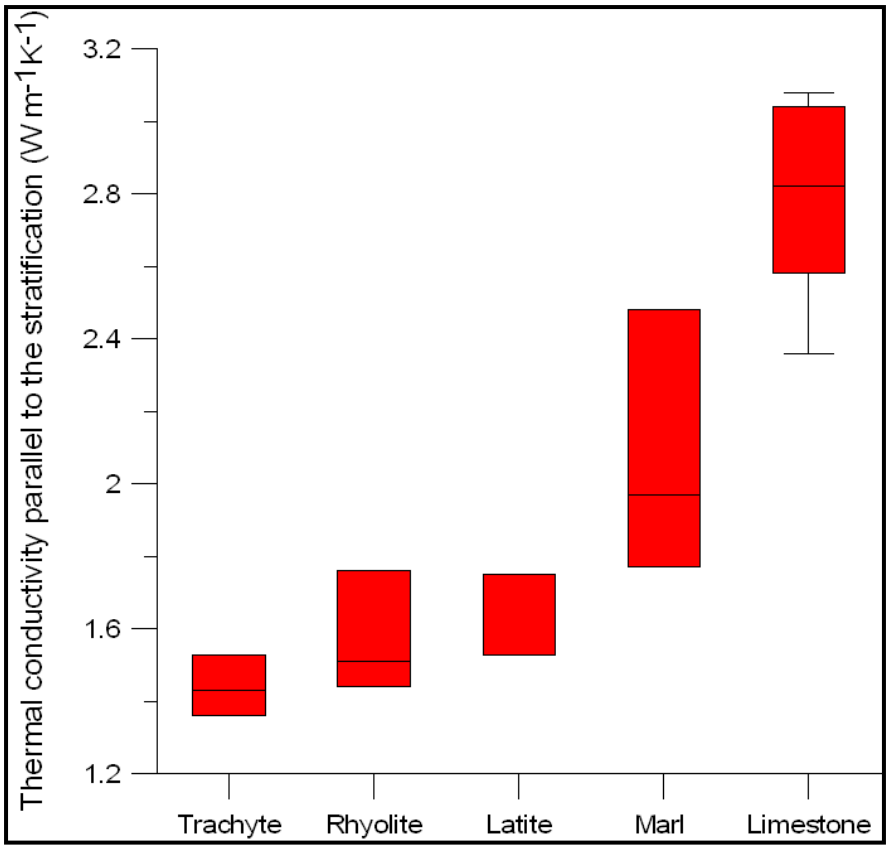

Figure 6.9 *Box-plot representation of laboratory values of parallel thermal conductivity for the rocks used in this work*

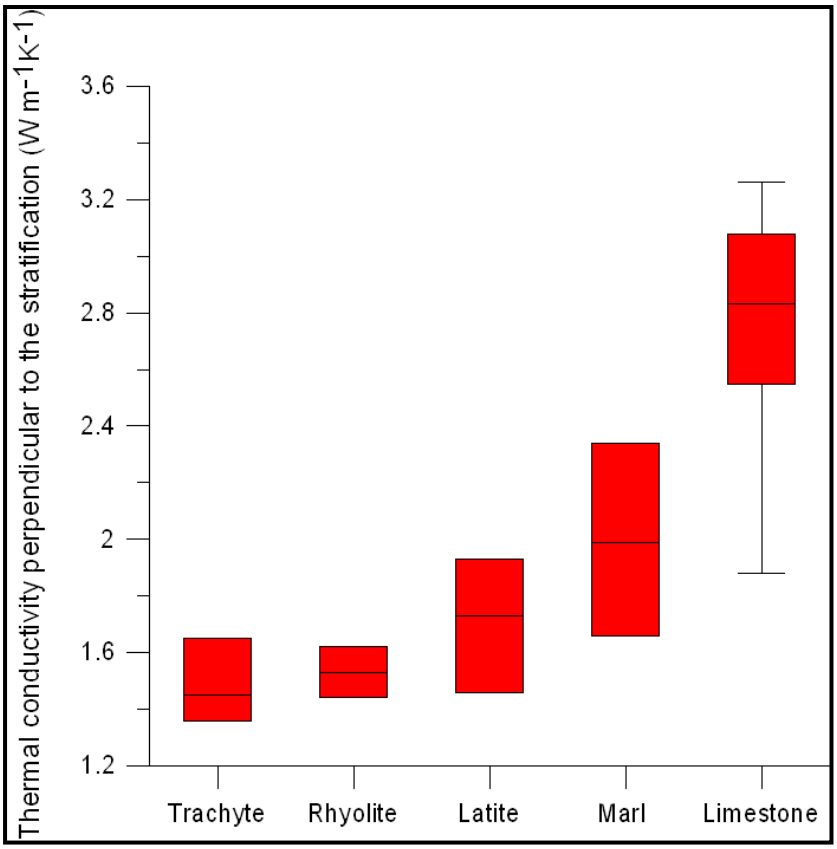

Figure 6.10 *Box-plot representation of laboratory values of perpendicular thermal conductivity for the rocks used in this work*

This thermal property was then put in relation to the density (Figure 6.11 and 6.12) and porosity (Figure 6.13 and 6.14).

In the first two graphs it is possible to see (in particular for parallel thermal conductivity case) an increasing of thermal conductivity value with an increasing of density. The results relative to the relation with porosity are clearer: in both cases (apart some outlier) an increasing thermal conductivity corresponds to a decreasing in porosity (and vice versa).

These results were predictable: as has been verified (Figure 6.8) to a density increases the porosity decreases. In these case there is less quantity of air within the rocks and this fact increase thermal conductivity because the thermal conductivity of air (0.026 W $m^{-1}K^{-1}$) is negligible respect thermal conductivity of the solid matrix.

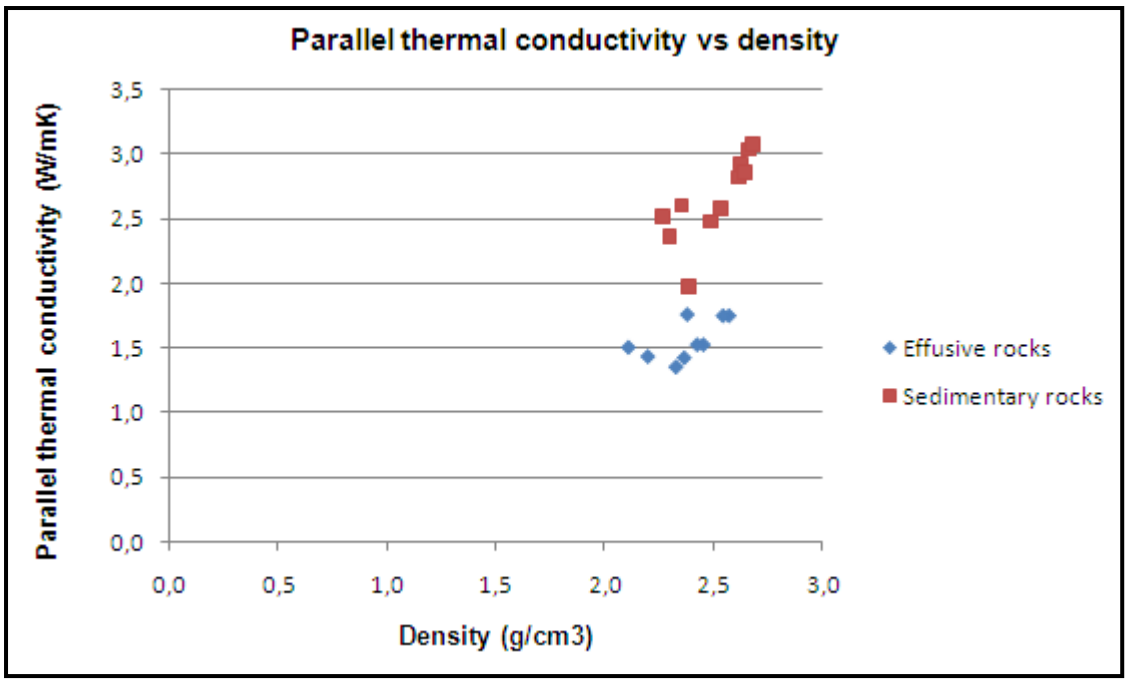

Figure 6.11 *Parallel thermal conductivity vs density for the rocks used in this work*

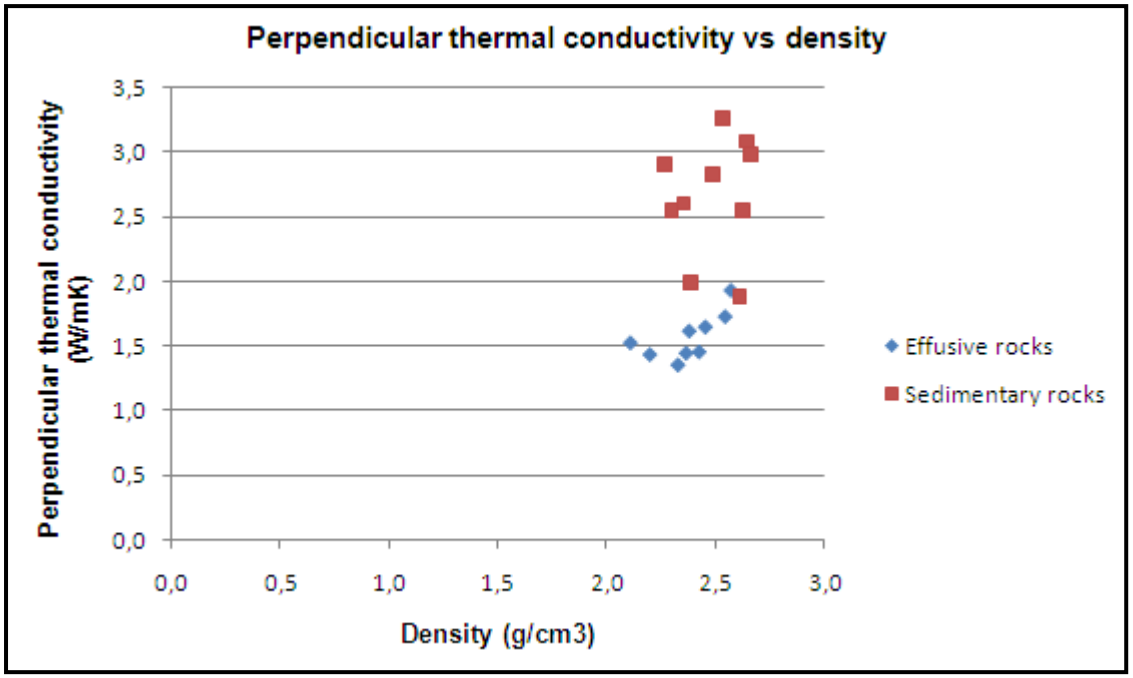

Figure 6.12 *Perpendicular thermal conductivity vs density for the rocks used in this work*

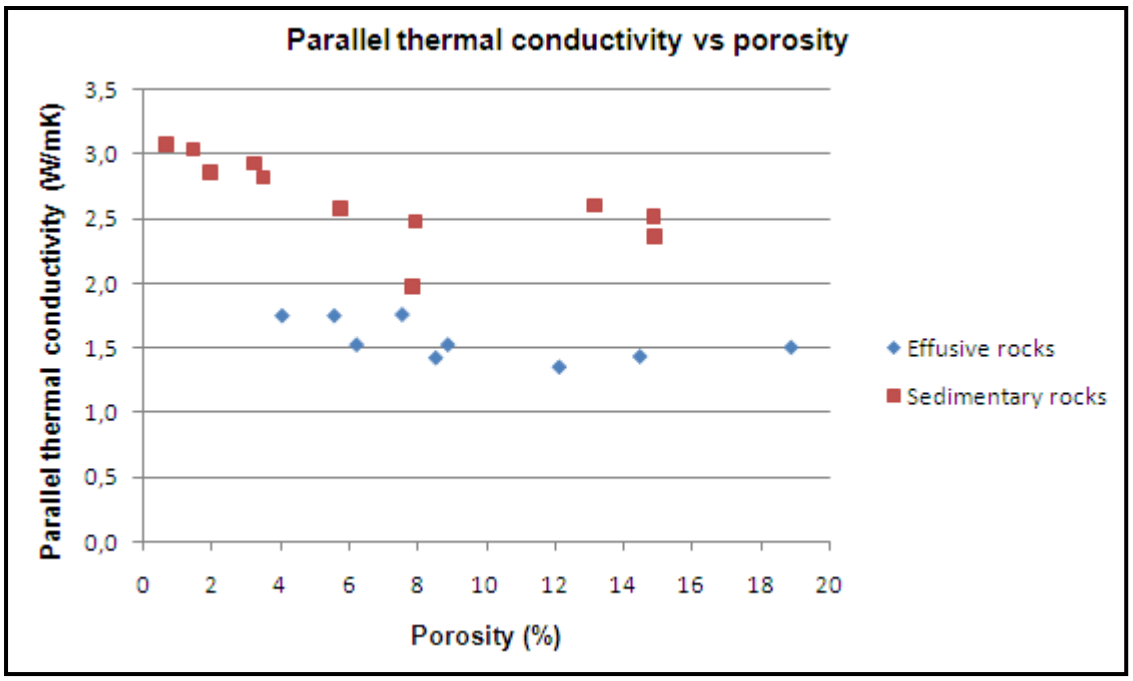

Figure 6.13 *Parallel thermal conductivity vs porosity for the rocks used in this work*

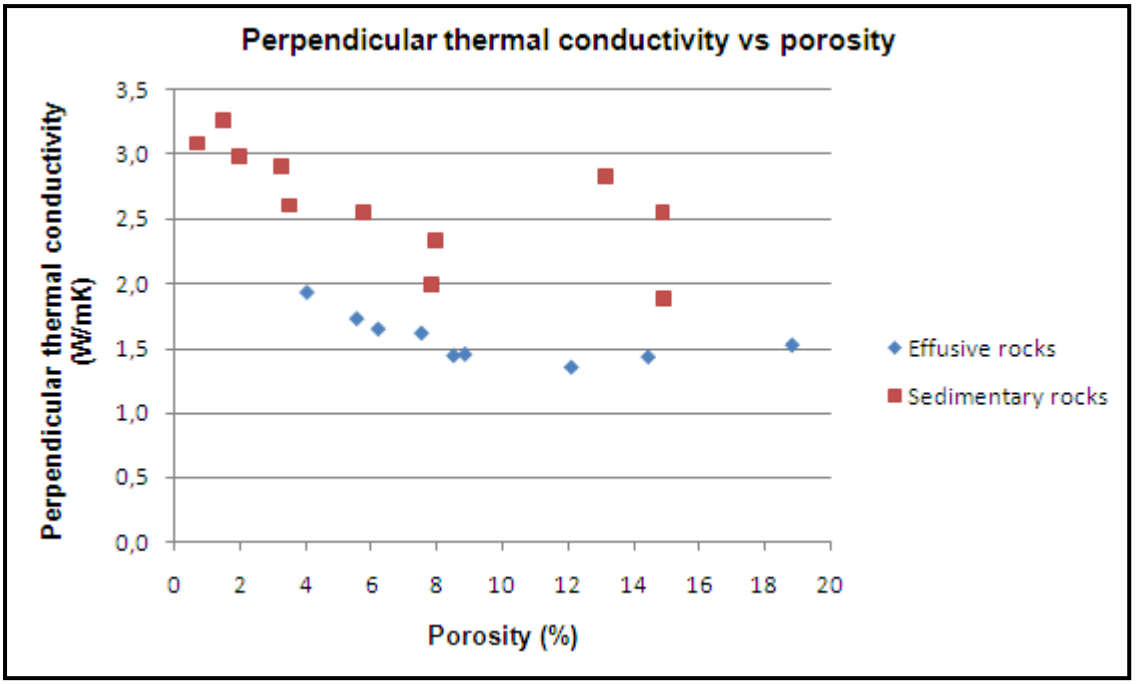

Figure 6.14 *Perpendicular thermal conductivity vs porosityfor the rocks used in this work*

6.2.4 Laboratory results about specific and volumetric heat capacity

The value of specific heat capacity is calculated for every sample using the formula provided by the manufacturer:

$$cp = \frac{e^2}{\lambda\,\rho} \quad \left(\frac{J}{kg\,K}\right) \qquad (6.1)$$

Where e is the effusivity (W $s^{1/2}$ $m^{-2}K^{-1}$), λ the thermal conductivity (W m^{-1} K^{-1}) and ρ the density (kg m^{-3}). The first two values are directly measured by the instrument while the value of the density was obtained by previous laboratory tests. The results are reported in Table 6.13.

It is important to underline that the specific (and also volumetric) heat capacity is a scalar property: for this reason in this section is not subdivided the values into "parallel" and "perpendicular" to the stratification.

Table 6.13 *Values of specific heat capacity for sampled lithologies. Note: The terms "S.R.", "B.", "R.A.", in parentheses are referred to the formations of "Scaglia Rossa", "Biancone" and "Rosso Ammonitico"; respectively*

Lithology	Sample	cp ($Jkg^{-1}K^{-1}$)	Average lithology ($Jkg^{-1}K^{-1}$)
Trachyte	1	820.68	
Trachyte	22B	819.72	820.05
Trachyte	44	819.75	
Rhyolite	16	822.82	
Rhyolite	36	819.75	851.85
Rhyolite	39	912.99	
Latite	18	826.83	
Latite	42	795.78	795.57
Latite	43	764.09	
Marl	11	834.65	
Marl	24	823.03	837.37
Marl	46	854.42	
Limestone (S.R.)	3	874.27	
Limestone (S.R.)	25	873.19	
Limestone (S.R.)	47	831.90	
Limestone (B.)	6A	862.60	
Limestone (B.)	8	883.79	873.60
Limestone (B.)	27A	863.91	
Limestone (R.A.)	10B	894.73	
Limestone (R.A.)	34	884.97	
Limestone (R.A.)	35	893.01	

The highest value is related to the limestone (873.60 $Jkg^{-1}K^{-1}$) and the lowest to the latite (795.57 $Jkg^{-1}K^{-1}$). It is now possible to determine the value of volumetric heat capacity: it is calculated simply multiplying the value of specific heat capacity with the density. The results are reported in Table 6.14.

Table 6.14 *Values of volumetric heat capacity for sampled lithologies. Note: The terms "S.R.", "B.", "R.A.", in parentheses are referred to the formations of "Scaglia Rossa", "Biancone" and "Rosso Ammonitico"; respectively*

Formation	**Lithology**	**Sample**	**ρ cp** ($Jcm^{-3}K^{-1}$)	**Average lithology** ($Jcm^{-3}K^{-1}$)
Lave trachitiche alcaline	Trachyte	1	1.93	
Lave trachitiche alcaline	Trachyte	22B	1.93	1.93
Lave trachitiche alcaline	Trachyte	44	1.93	
Rioliti alcaline	Rhyolite	16	1.93	
Rioliti alcaline	Rhyolite	36	1.93	1.93
Rioliti alcaline	Rhyolite	39	1.93	
Lava latitica	Latite	18	1.94	
Lava latitica	Latite	42	1.93	1.94
Lava latitica	Latite	43	1.94	
Marna silicizzata	Marl	11	1.93	
Marna euganea	Marl	24	1.96	1.97
Marna euganea	Marl	46	2.01	
Scaglia Rossa	Limestone (S.R.)	3	2.06	
Scaglia Rossa	Limestone (S.R.)	25	2.05	
Scaglia Rossa	Limestone (S.R.)	47	1.96	
Biancone	Limestone (B.)	6A	2.03	
Biancone	Limestone (B.)	8	2.08	2.05
Biancone	Limestone (B.)	27A	2.03	
Rosso Ammonitico	Limestone (R.A.)	10B	2.10	
Rosso Ammonitico	Limestone (R.A.)	34	2.08	
Rosso Ammonitico	Limestone (R.A.)	35	2.10	

As for specific heat capacity limestone has the highest value (2.05 $Jcm^{-3}K^{-1}$) but now the lowest value belongs both to rhyolite and trachyte (1.93 $Jcm^{-3}K^{-1}$).

In all lithologies this parameter has a small variation and all values are within the boundary proposed by Clauser (2011): 2.30 ($Jcm^{-3}K^{-1}$) ±20%.

The relative values for each limestone formations are reported in Table 6.15. They range between 2.09 ($Jcm^{-3}K^{-1}$) of Rosso Ammonitico and 2.02 ($J\ cm^{-3}K^{-1}$) of Scaglia Rossa.

Table 6.15 *Values of volumetric heat capacity for different formations of limestone*

Formation	Sample	ρ cp ($Jcm^{-3}K^{-1}$)	Average formation ($Jcm^{-3}K^{-1}$)
Scaglia Rossa	3	2.06	
Scaglia Rossa	25	2.05	2.02
Scaglia Rossa	47	1.96	
Biancone	6A	2.03	
Biancone	8	2.08	2.05
Biancone	27A	2.03	
Rosso Ammonitico	10B	2.10	
Rosso Ammonitico	34	2.08	2.09
Rosso Ammonitico	35	2.10	

In addition, a box-plot representation for the different lithologies is reported in Figure 6.15. Rhyolite and trachyte have same value (1.93 $Jcm^{-3}K^{-1}$), latite ranges from 1.93 to 1.94 ($Jcm^{-3}K^{-1}$). These value are very close because latite has respect trachyte and rhyolite a lower value of specific heat (795.57 $Jkg^{-1}K^{-1}$ compare to 820.05 and 851.85 $Jkg^{-1}K^{-1}$) but a higher value of density (1.71 g cm^{-3} is the mean value for latite, 1.49 g cm^{-3} for trachyte and 1.53 g cm^{-3} for rhyolite) so the product is approximately the same.

Sedimentary rocks have similar values of specific heat capacity respect the volcanic but they have higher values in density (Table 6.6 and 6.7) so the volumetric heat capacity is higher respect effusive rocks.

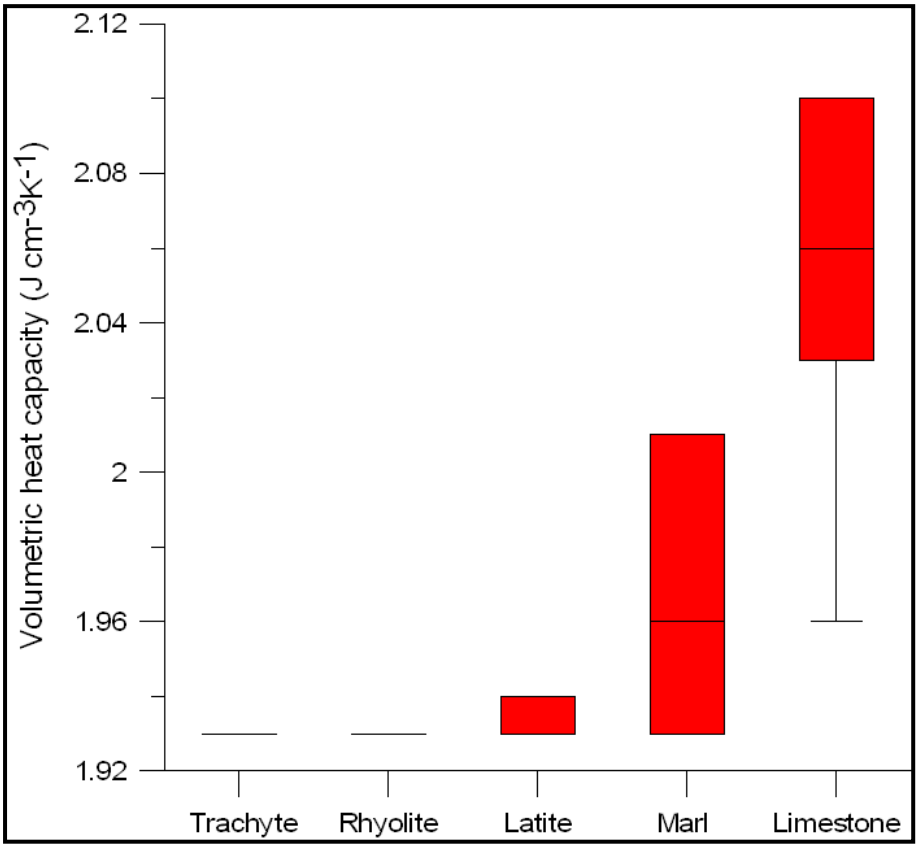

Figure 6.15 *Box-plot representation of laboratory values of volumetric heat capacity for the rocks used in this work*

Also volumetric heat capacity is related with density and porosity of rocks: the results are showed in Figure 6.16 and 6.17.

As for thermal conductivity this parameter increases when density increases and increases where porosity decreases (and vice versa).

The variation in more pronounced for sedimentary rocks: for effusive rocks it was demonstrated which volumetric heat capacity is constant among trachyte, rhyolite and latite (which have different densities and porosities.)

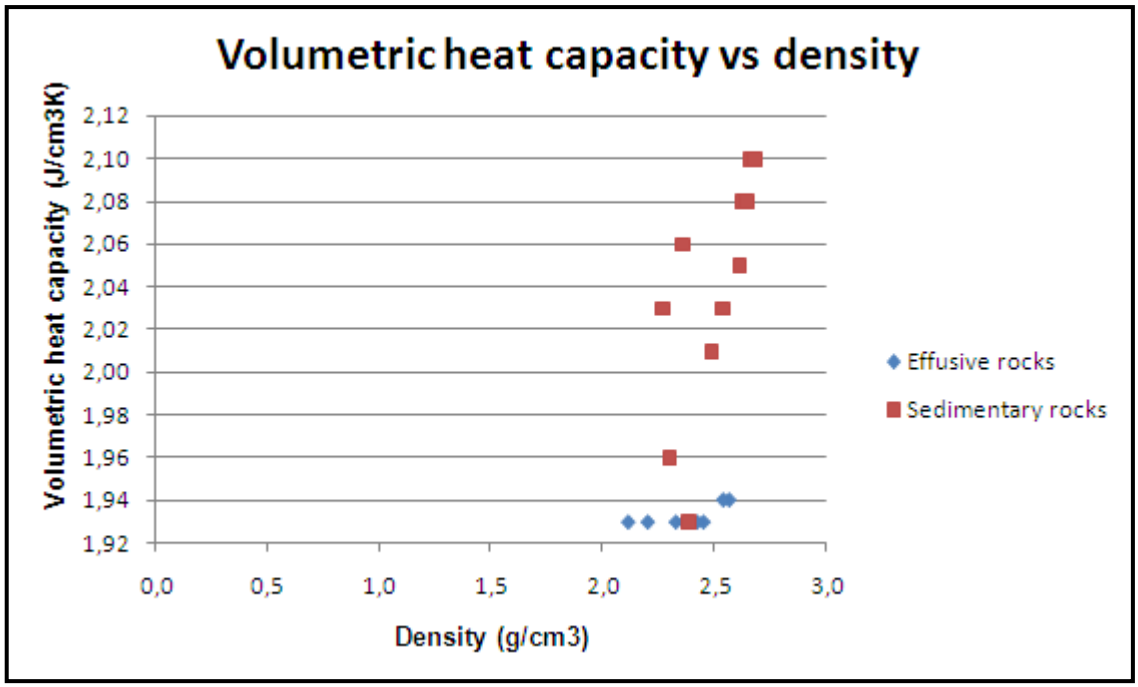

Figure 6.16 *Volumetric heat capacity vs density for the rocks used in this work*

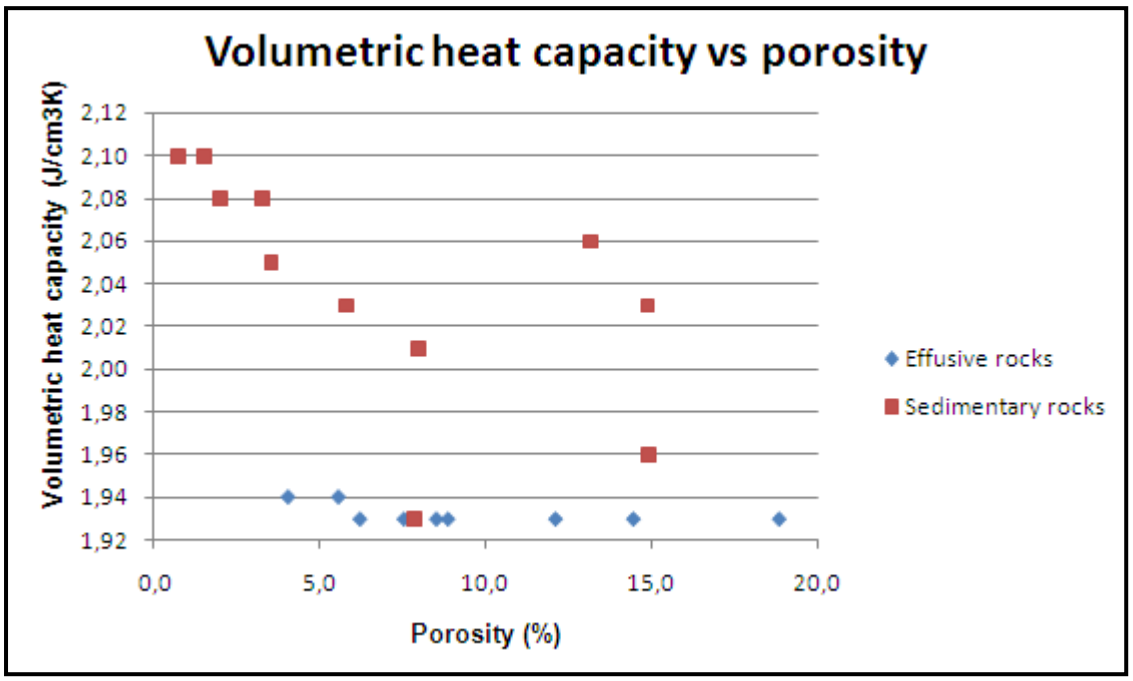

Figure 6.17 *Volumetric heat capacity vs porosity for the rocks used in this work*

6.2.5 Laboratory results about thermal diffusivity

Thermal diffusivity (α) is the last thermal parameters considered in this work. It is provided by the instrumentation (Table 6.16) (which uses internal values for density and specific heat capacity in order to determine it) and also recalculated with the Equation 4.14: all necessary data are now available. A comparison of the results given by instrumentation and those recalculated is given in Table 6.18.

Table 6.16 *Values of thermal diffusivity for sampled lithologies. Note: The terms "S.R.", "B.", "R.A.", in parentheses are referred to the formations of "Scaglia Rossa", "Biancone" and "Rosso Ammonitico"; respectively*

Lithology	Sample	α// (mm2/s)	Average lithology (mm2/s)	α⊥ (mm2/s)	Average lithology (mm2/s)
Trachyte	1	0.78		0.84	
Trachyte	22B	0.69	0.73	0.69	0.76
Trachyte	44	0.73		0.74	
Rhyolite	16	0.89		0.82	
Rhyolite	36	0.73	0.80	0.73	0.78
Rhyolite	39	0.77		0.78	
Latite	18	0.89		0.98	
Latite	42	0.78	0.85	0.74	0.87
Latite	43	0.89		0.88	
Marl	11	1.00		1.01	
Marl	24	0.90	1.05	0.84	1.01
Marl	46	1.26		1.19	
Limestone (S.R.)	3	1.25		1.44	
Limestone (S.R.)	25	1.43		1.32	
Limestone (S.R.)	47	1.11		0.90	
Limestone (B.)	6A	1.28		1.29	
Limestone (B.)	8	1.49	1.38	1.47	1.38
Limestone (B.)	27A	1.31		1.29	
Limestone (R.A.)	10B	1.54		1.65	
Limestone (R.A.)	34	1.45		1.51	
Limestone (R.A.)	35	1.56		1.56	

This parameters ranges from the minimum of 0.73 ($mm^2 s^{-1}$) (measured parallel respect to the stratification) of trachyte to the maximum of 1.38 ($mm^2 s^{-1}$) of limestone.
The differentiation for different limestone formations are presented in Table 6.17: the formation of Rosso Ammonitico has the highest value 1.57 ($mm^2 s^{-1}$) (measured perpendicular respect to the stratification) while the lowest 1.22 ($mm^2 s^{-1}$) is measured for Scaglia Rossa (perpendicular respect to the stratification).

Table 6.17 *Values of thermal diffusivity for different formations of limestone*

Lithology	**Sample**	**α//** **(mm2/s)**	**Average lithology** **(mm2/s)**	**α⊥** **(mm2/s)**	**Average lithology** **(mm2/s)**
Scaglia Rossa	3	1.25		1.44	
Scaglia Rossa	25	1.43	1.26	1.32	1.22
Scaglia Rossa	47	1.11		0.90	
Biancone	6A	1.28		1.29	
Biancone	8	1.49	1.36	1.47	1.35
Biancone	27A	1.31		1.29	
Rosso Ammonitico	10B	1.54		1.65	
Rosso Ammonitico	34	1.45	1.52	1.51	1.57
Rosso Ammonitico	35	1.56		1.56	

The results are also visible in a box-plot representation: the values parallel with respect to the stratification are visible in Figure 6.18, those perpendicular in Figure 6.19.
Limestone shows the highest median values (which are 1.43 and 1.44 $mm^2 s^{-1}$ for perpendicular and parallel with respect to the stratification, respectively). Marl has the second highest median values (which are 1.01 and 1.00 $mm^2 s^{-1}$ for perpendicular and parallel with respect to the stratification, respectively).
Effusive rocks show lower values respect volcanic. Trachyte has a median values of 0.74 and 0.73 ($mm^2 s^{-1}$), rhyolite has a median values of 0.78 and 0.77 ($mm^2 s^{-1}$), latite has a median values of 0.88 and 0.89 ($mm^2 s^{-1}$) (parallel and perpendicular to the stratification, respectively).
The two graphs are similar: only limestone shows some differences. These differences are due to the presence of sample 47 (Scaglia Rossa formation) which has anisotropic properties.

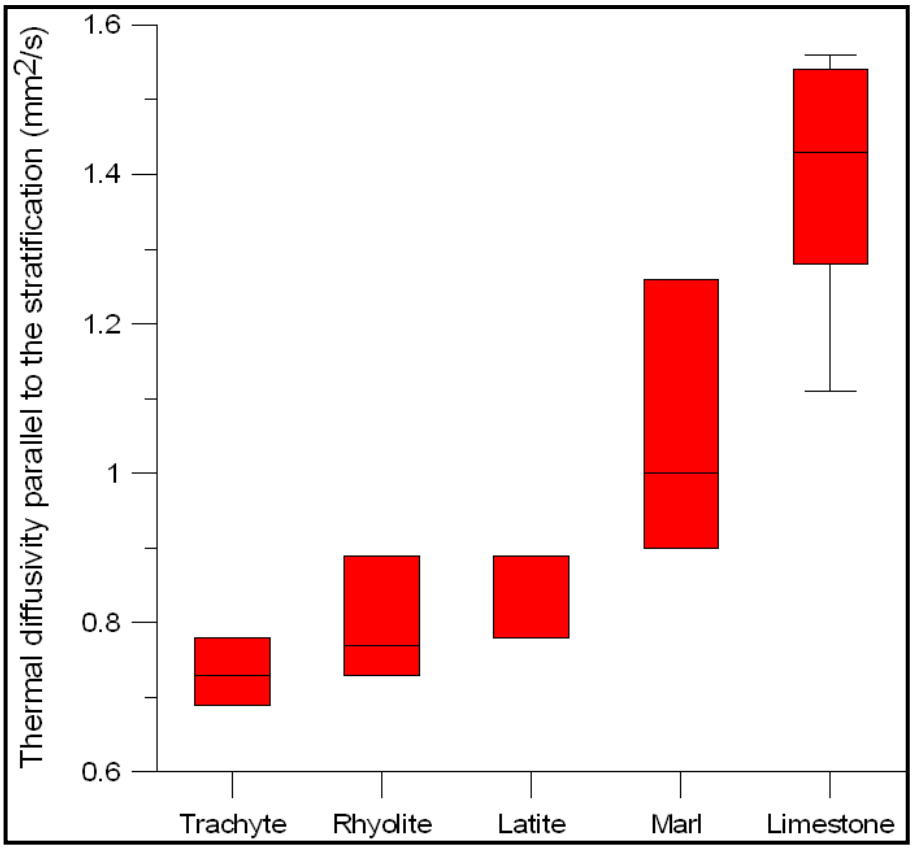

Figure 6.18 *Box-plot representation of laboratory values of parallel thermal diffusivity for the rocks used in this work*

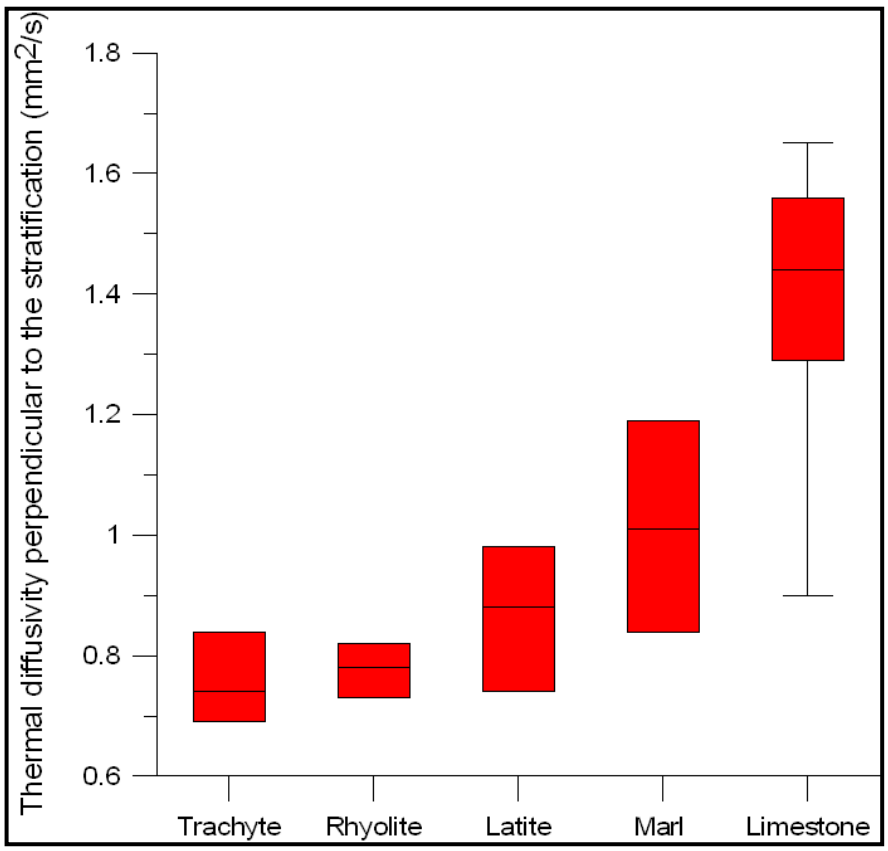

Figure 6.19 *Box-plot representation of laboratory values of perpendicular thermal diffusivity for the rocks used in this work*

Thermal diffusivity was then put in relation to the density (Figure 6.20 and 6.21) and porosity (Figure 6.22 and 6.23).
The behavior is very similar to that showed by thermal conductivity: in the first two graphs it is possible to see (in particular for parallel thermal conductivity case) an increasing value of thermal diffusivity with an increasing value of the density. The results relative to the relation with porosity are clearer: in both cases (apart some outlier) an increasing thermal diffusivity corresponds to a decreasing in porosity (and vice versa).
The behavior is governed by Equation 6.1:

$$\alpha = \frac{\lambda}{\rho cp} \quad \left(\frac{mm^2}{s}\right) \qquad 6.2$$

Where λ is the thermal conductivity, ρ density, cp the isobaric specific heat capacity and α diffusivity. This is an apparent in contrast with the results because it appear which when density increases the diffusivity decreases. This is not totally true because also cp is a function of density (Equation 6.1) and in particular it decreases when density increases as indicate from the operator manual of the instrument.
In addition, also thermal effusivity and conductivity changes with density (the latter as showed in Figure 6.11 and 6.12).
Ultimately, for this reasons, is difficult make a prevision *a priori* about the behavior of thermal diffusivity with density and is difficult comment the results: more investigations should be performed on all the properties that contribute to the calculation of the thermal diffusivity and the relationship which they have with respect to the density.
For this reason is difficult have a unique conclusion but probably when density increases, diffusivity increases.
As previously mentioned a comparison between the thermal diffusivity values provided by instrumentation and those calculated using the specific parameters of the examined rocks was made (Table 6.18).
The values differ, ranging from 2.90 % for sample 22B (trachyte) and -5.84% for sample 35 (limestone, Rosso Ammonitico formation) in the case perpendicular with respect to the stratification and for case parallel with respect to stratification values range between 2.90% and -7.27% for the same samples.
These results are also explained into the graphs of Figure 6.24 and 6.25. The line called 1:1 is the line which represents the "ideal" behavior which is verified when all recalculated values are equal to the measured ones. The points show a good agreement because tend to overlap at this line.

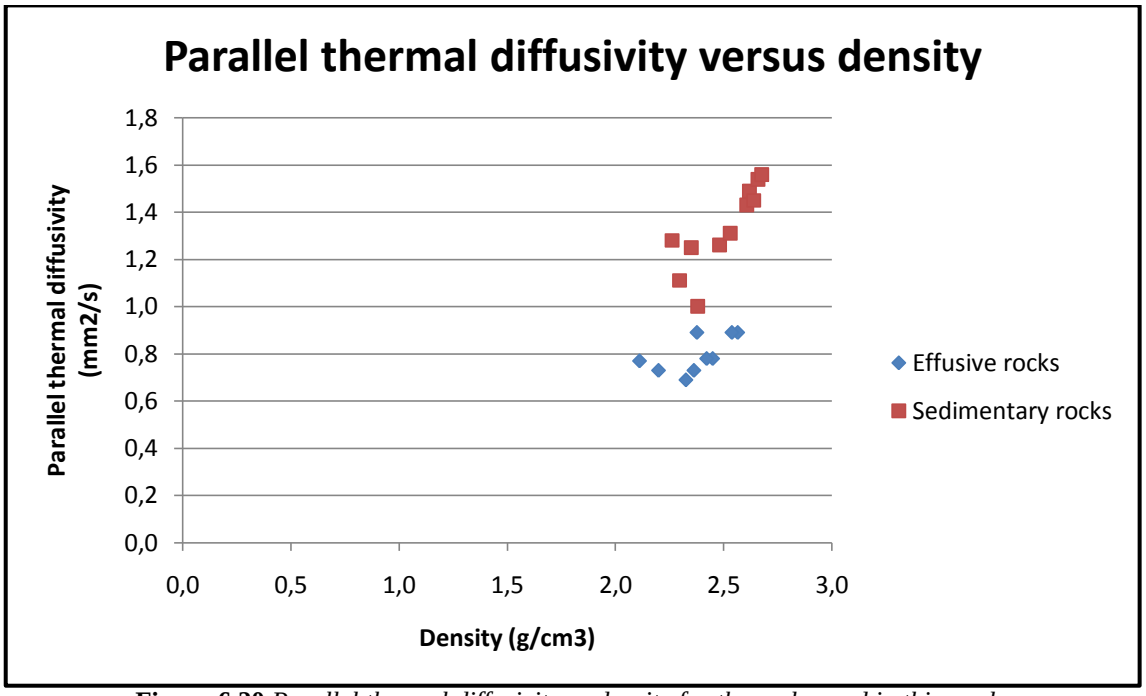

Figure 6.20 *Parallel thermal diffusivity vs density for the rocks used in this work*

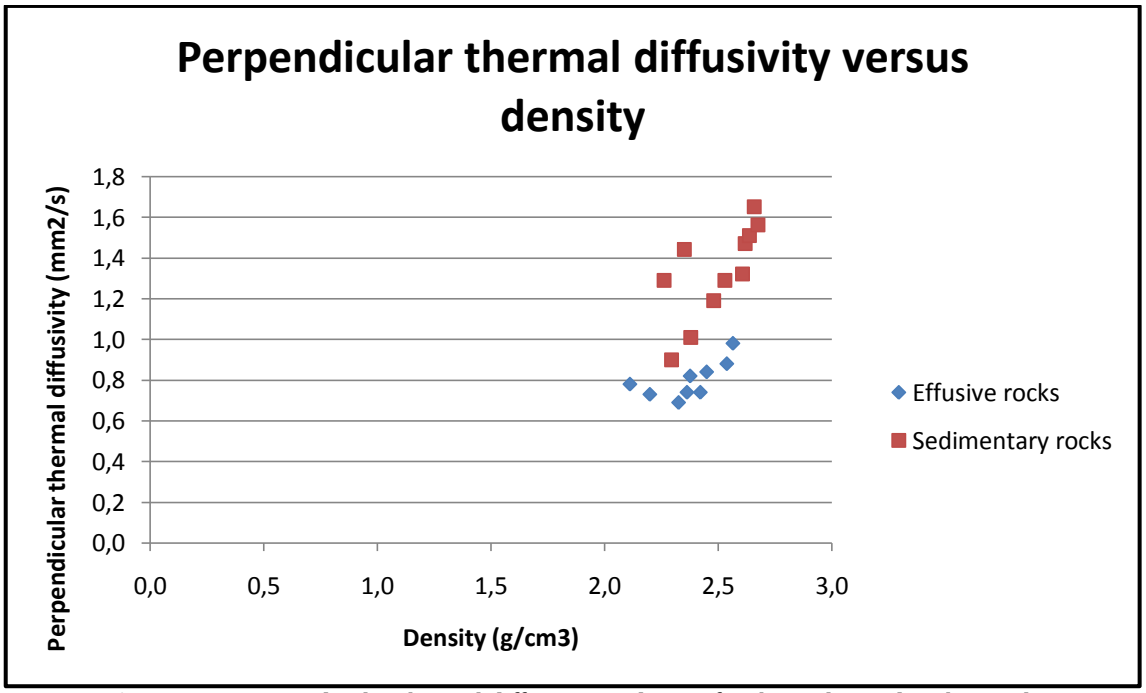

Figure 6.21 *Perpendicular thermal diffusivity vs density for the rocks used in this work*

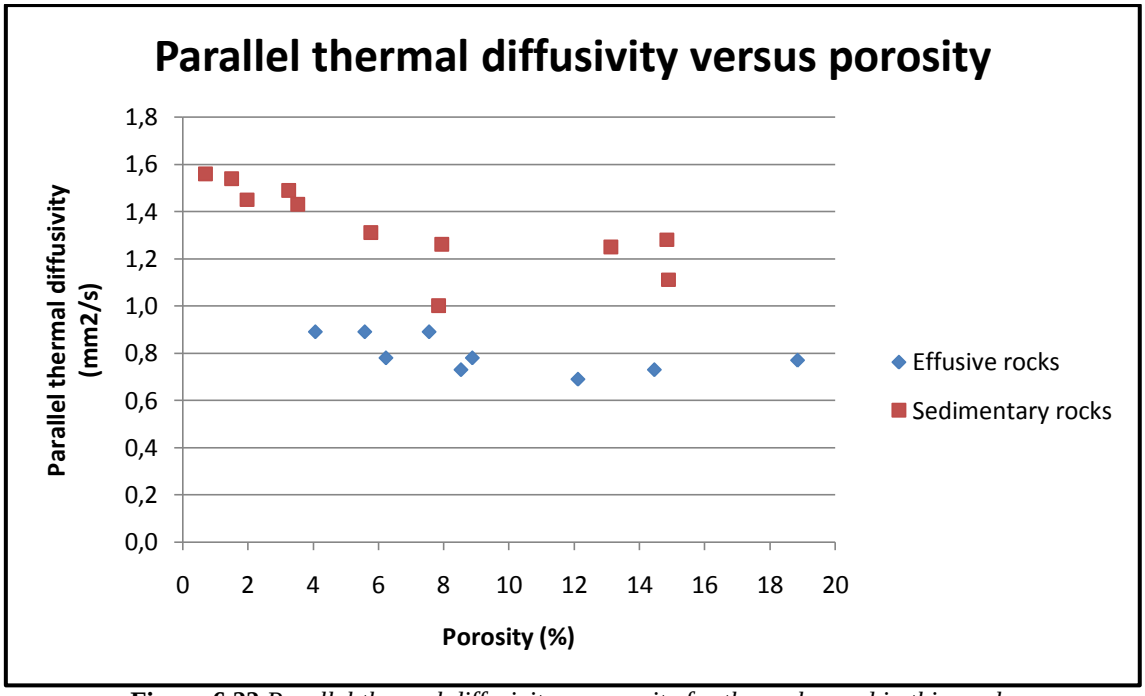

Figure 6.22 *Parallel thermal diffusivity vs porosity for the rocks used in this work*

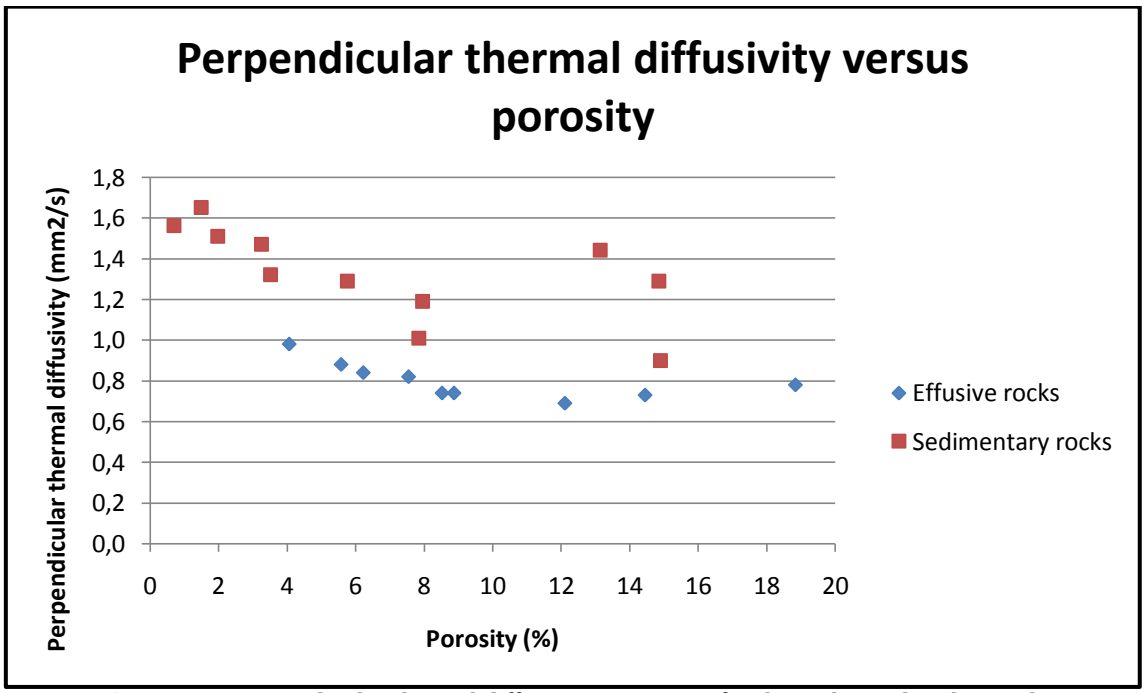

Figure 6.23 *Perpendicular thermal diffusivity vs porosity for the rocks used in this work*

Table 6.18 *Comparison between thermal diffusivity mesured and recalculated. Note: The terms "S.R.", "B.", "R.A.", in parentheses are referred to the formations of "Scaglia Rossa", "Biancone" and "Rosso Ammonitico"; respectively*

Lithology	Sample	α// (mm2/s)	α// (recalculated) (mm2/s)	Variation (%)	$\alpha^{\perp}$ (mm2/s)	$\alpha^{\perp}$ (recalculated) (mm2/s)	Variation (%)
Trachyte	1	0.78	0.79	1.28	0.84	0.85	1.19
Trachyte	22B	0.69	0.71	2.90	0.69	0.71	2.90
Trachyte	44	0.73	0.74	1.37	0.74	0.75	1.35
Rhyolite	16	0.89	0.90	1.12	0.82	0.84	2.44
Rhyolite	36	0.73	0.75	2.74	0.73	0.75	2.74
Rhyolite	39	0.77	0.79	2.60	0.78	0.79	1.28
Latite	18	0.89	0.90	1.12	0.98	0.99	1.02
Latite	42	0.78	0.79	1.28	0.74	0.76	2.70
Latite	43	0.89	0.90	1.12	0.88	0.89	1.14
Marl	11	1.00	1.00	0.00	1.01	1.01	0.00
Marl	24	0.90	0.91	1.11	0.84	0.86	2.38
Marl	46	1.26	1.23	-2.38	1.19	1.17	-1.68
Limestone (S.R.)	3	1.25	1.22	-2.40	1.44	1.37	-4.86
Limestone (S.R.)	25	1.43	1.37	-4.20	1.32	1.28	-3.03
Limestone (S.R.)	47	1.11	1.10	-0.90	0.90	0.91	1.11
Limestone (B.)	6A	1.28	1.24	-3.13	1.29	1.26	-2.33
Limestone (B.)	8	1.49	1.41	-5.37	1.47	1.40	-4.76
Limestone (B.)	27A	1.31	1.27	-3.05	1.29	1.26	-2.33
Limestone (R.A.)	10B	1.54	1.45	-5.84	1.65	1.53	-7.27
Limestone (R.A.)	34	1.45	1.38	-4.83	1.51	1.43	-5.30
Limestone (R.A.)	35	1.56	1.47	-5.77	1.56	1.46	-6.41

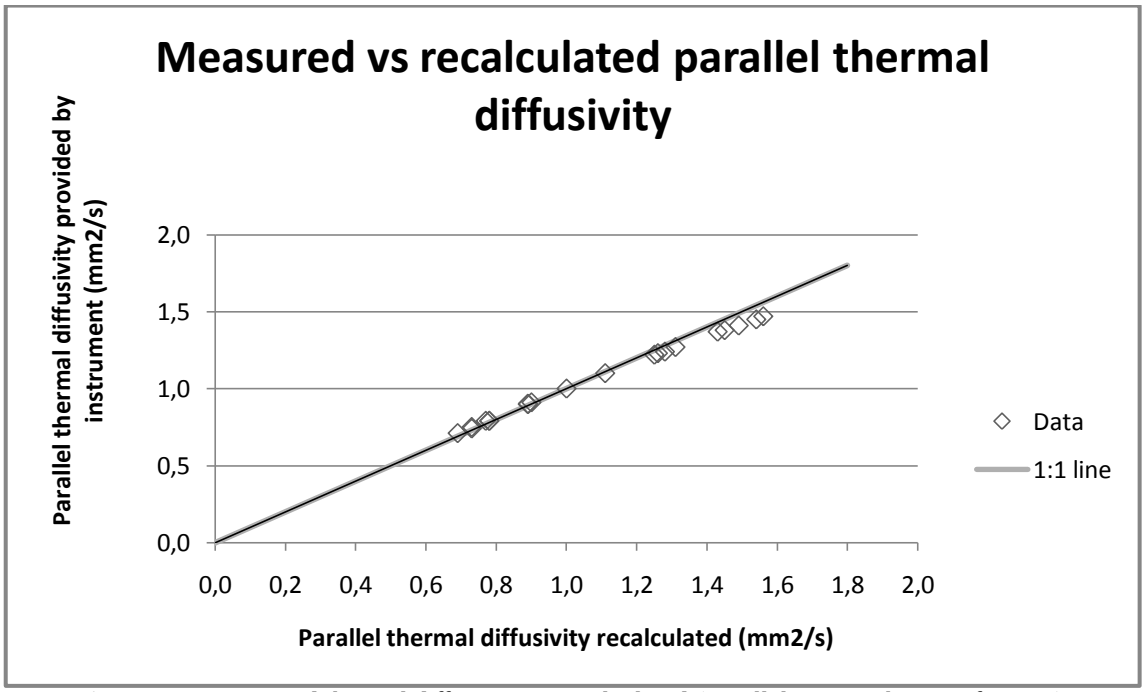

Figure 6.24 *Measured thermal diffusivity vs recalculated (parallel respect the stratification)*

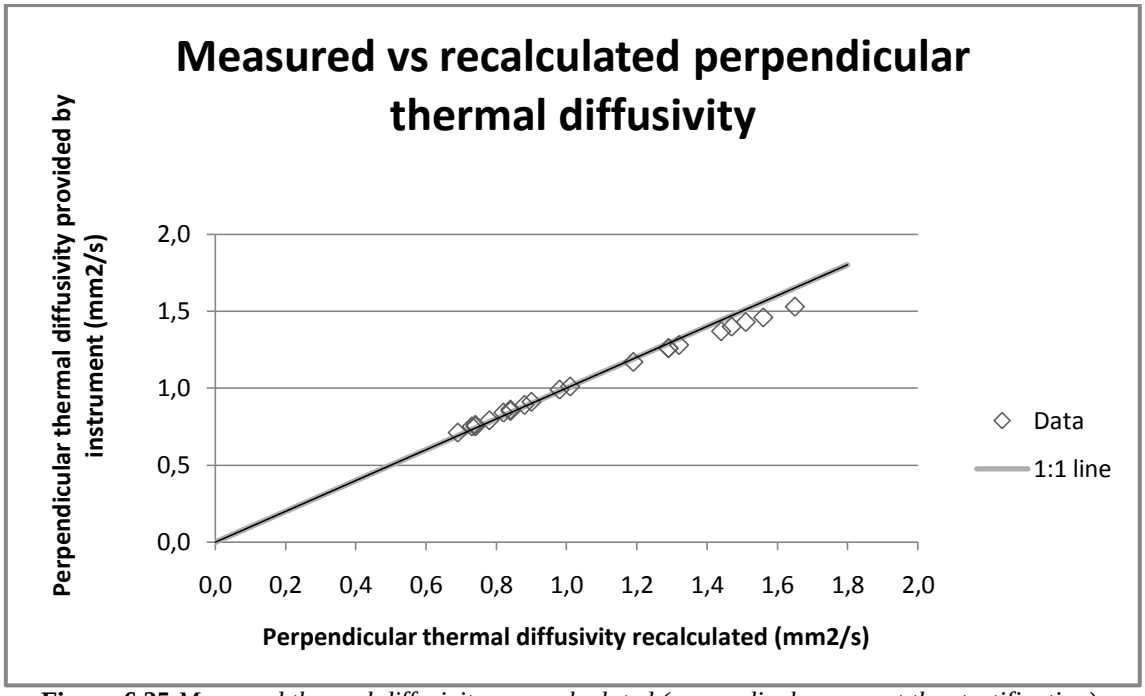

Figure 6.25 *Measured thermal diffusivity vs recalculated (perpendicular respect the stratification)*

Thermal diffusivity are also studied in relation with thermal conductivity: the experimental values of thermal diffusivity were plotted versus thermal conductivity. Following how stated from Equation 6.1 there is a linear relation between thermal diffusivity and thermal conductivity and the reciprocal of volumetric heat capacity is the coefficient of proportionality. So the slope of the interpolating line is traced and its angular coefficient is determinate. In according with just written, the reciprocal of angular coefficient is the volumetric heat capacity.

In this way for the effusive rocks was determined a value of 1.98 (J $cm^{-3}K^{-1}$) and 1.99 (J $cm^{-3}K^{-1}$) (parallel and perpendicular to the stratification, respectively), while for the sedimentary rocks was found a value of 1.97 (J $cm^{-3}K^{-1}$) in both cases (Figure 6.26, 6.27).

The values obtained separately by using the thermal conductivity and diffusivity in parts parallel and perpendicular to the stratification are virtually identical between them because the volumetric heat capacity is, in fact, a scalar quantity. In addition these values are similar to those reported in Table 6.14.

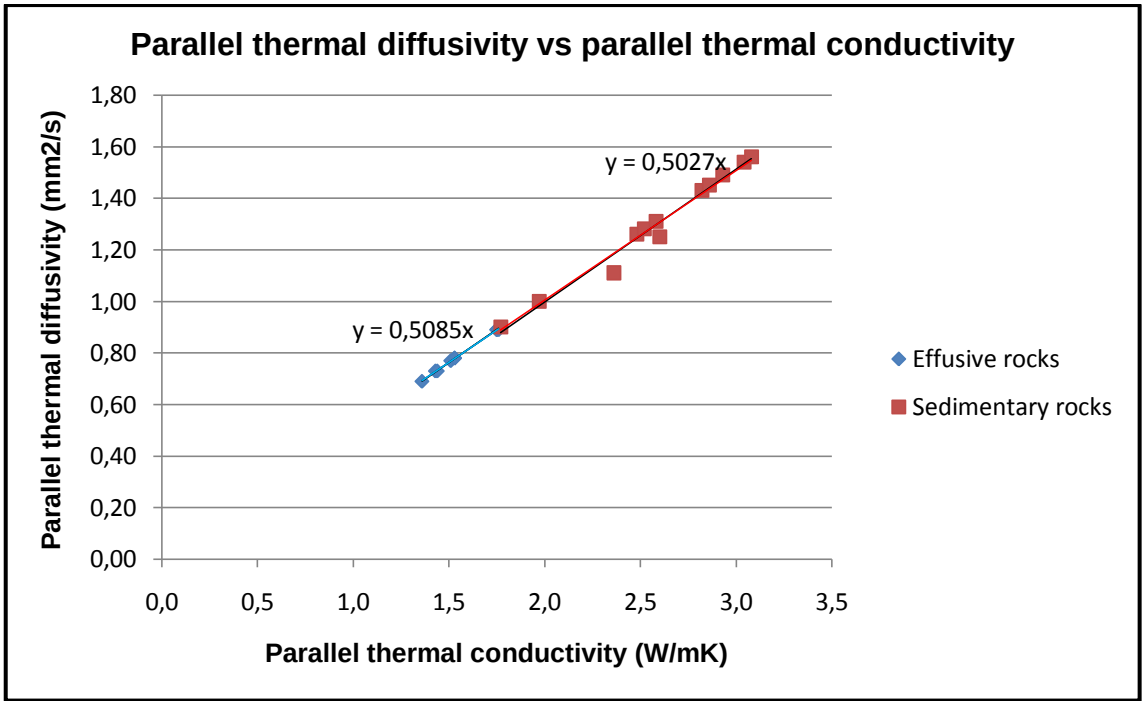

Figure 6.26 *Parallel thermal diffusivity vs parallel thermal conductivity*

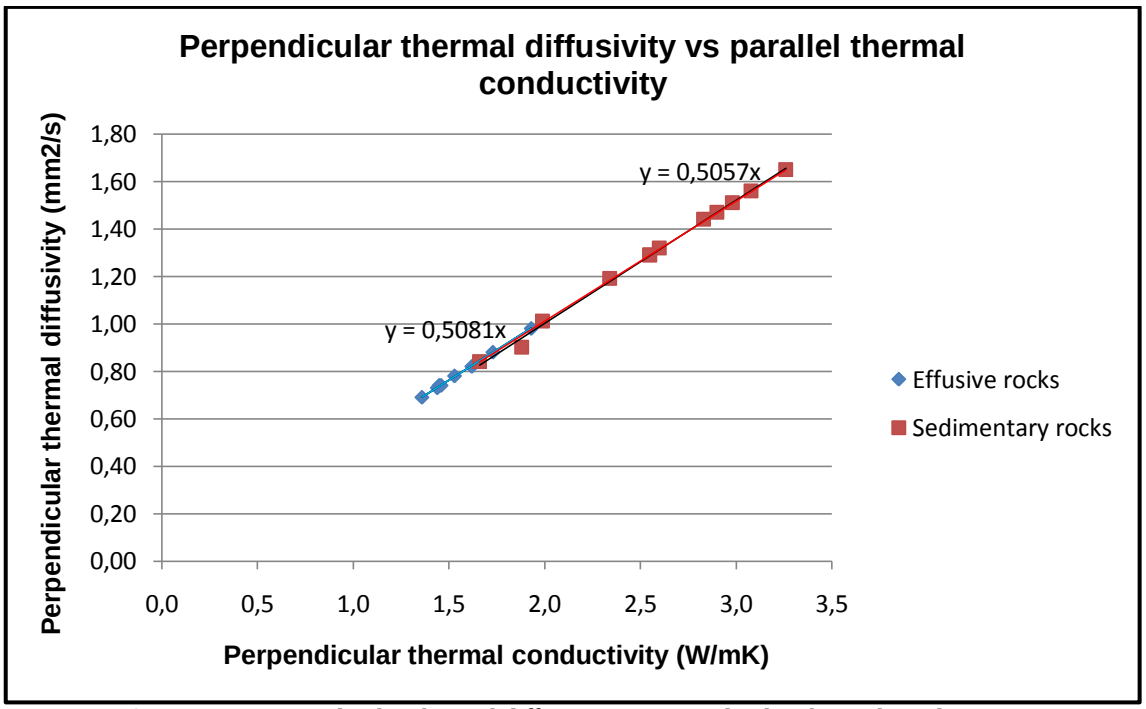

Figure 6.27 *Perpendicular thermal diffusivity vs perpendicular thermal conductivity*

6.3 Comparison between bibliographic and laboratory results

In this paragraph are compared the results between the values of density, porosity, thermal conductivity and volumetric heat capacity obtained by bibliographic search and by laboratory measurements. Thermal diffusivity is not considered due to the scarcity of the data obtained by literature review.

For each considered parameter the comparison was made with the help of a box-plot.

A general comment for all thermo-physical parameters can be made: the laboratory values defining a much narrower range because are analyzed samples from a specific zone and belong to a well-defined lithological distribution while the bibliographic reference come from to general contexts and different case studies located anywhere in the world. Bibliographic data are characterized by a greater range of values: the conditions of formation, alteration and mineralogical composition on a global scale show a greater variation than a single case study geographically well-defined.

6.3.1 Density

The results are showed in Figure 6.28. For this parameter all laboratory values fall within the values founded in bibliographic search (apart latite: the lowest bibliographic value is 2.44 g $cm^{-3}$and the lowest value obtained in laboratory is 2.422 g cm^{-3}).
Also the median values (bibliographic and experimental, respectively) are similar: 2.48 (g cm^{-3}) and 2.363(g cm^{-3}) for trachyte, 2.46 (g cm^{-3}) and 2.199 (g cm^{-3}) for rhyolite, 2.539 (g cm^{-3}) and 2.9 (g cm^{-3}) for latite, 2.30 (g cm^{-3}) and 2.431 (g cm^{-3}) for marl, 2.63(g cm^{-3}) and 2.608 (g cm^{-3}) for limestone.

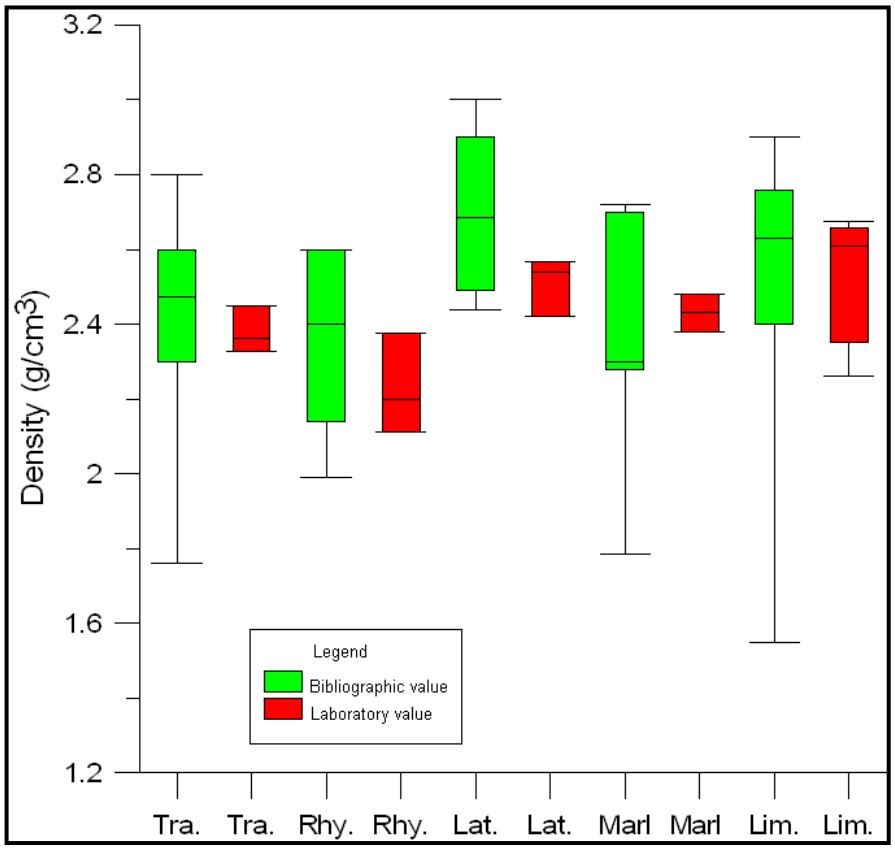

Figure 6.28 *Comparison between bibliographic values (green) and laboratory values (red) for density. Note: ""Tra." = Trachyte, "Rhy." = Rhyolite, "Lat." = Latite, Lim." = Limestone*

6.3.2 Porosity

For this parameter the comparison is reported in Figure 6.29. The considerations are similar respect to those made for density but in this case the values determinate in laboratory (3 values are obtained) for latite is different respect the value found in literature (one value was found).

Probaly this difference is related with the scarcity of bibliographic data. The values of all other lithologies fall within the boundary defined by literature search.

Also the median values (bibliographic and experimental, respectively) are similar: 13.50 (%) and 8.524 (%) for trachyte, 15.35 (%) and 14.451 (%) for rhyolite, 0.82 (%) and 5.576 (%) for latite, 35.50 (%) and 7.787 (%) for marl, 2.65 (%) and 3.518 (%) for limestone.

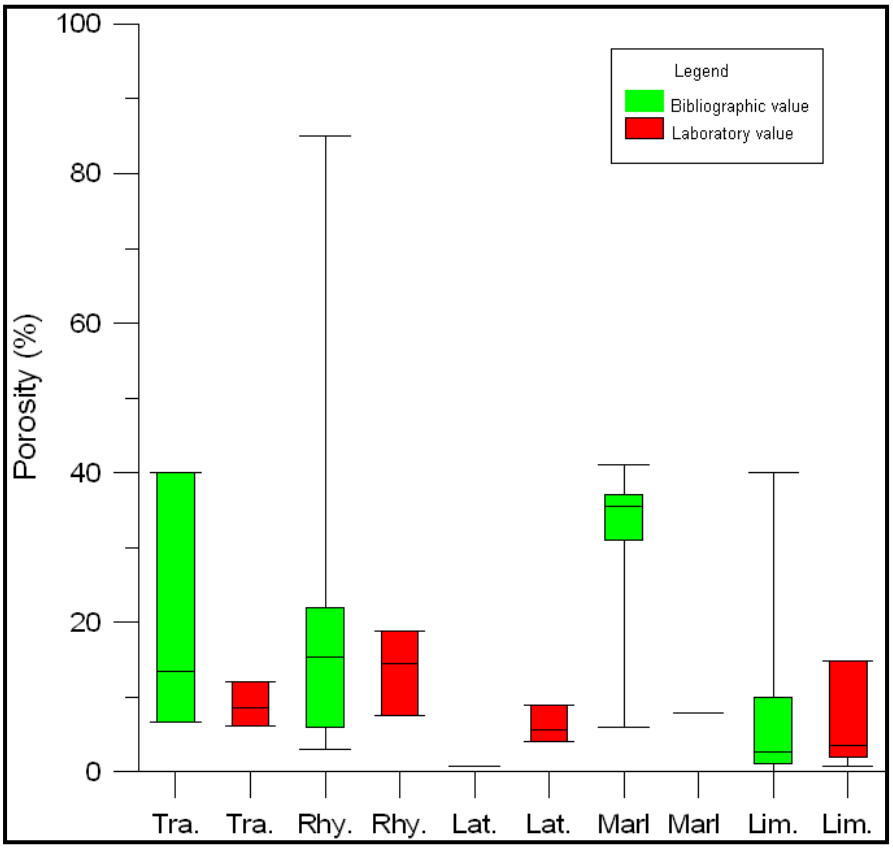

Figure 6.29 *Comparison between bibliographic values (green) and laboratory values (red) for porosity. Note: ""Tra." = Trachyte, "Rhy." = Rhyolite, "Lat." = Latite, Lim." = Limestone*

6.3.3 Thermal conductivity

The comparison of thermal conductivity was made both for values parallel (Figure 6.30) and perpendicular to the stratification (Figure 6.31). The graphs are very similar because the rocks considered in this work are mainly isotropic respect to thermal conductivity.

For effusive rocks (trachyte, rhyolite, latite) the values obtained in laboratory tests are lower than those found in bibliography, and usually the values determinate experimentally are half the bibliographic ones; probably this is due to the composition of rocks: for example the samples of rhyolite exhibits a very small crystal of quartz

(which is a mineral with high thermal conductivity value: it ranges from 6.5 to 13 (W $m^{-1}K^{-1}$) (Schön, 2004)).

For this reason the median values are different in particular for effusive rocks. Considering the parallel thermal conductivity the values (bibliographic and experimental, respectively) are: 3.25 (W $m^{-1}K^{-1}$) and 1.43 (W $m^{-1}K^{-1}$) for trachyte, 3.30 (W $m^{-1}K^{-1}$) and 1.51 (W $m^{-1}K^{-1}$) for rhyolite, 2.00 (W $m^{-1}K^{-1}$) and 1.7 (W $m^{-1}K^{-1}$) for latite, 1.65 (W $m^{-1}K^{-1}$) and 1.97 (W $m^{-1}K^{-1}$) for marl, 2.58 (W $m^{-1}K^{-1}$) and 2.82 (W $m^{-1}K^{-1}$) for limestone.

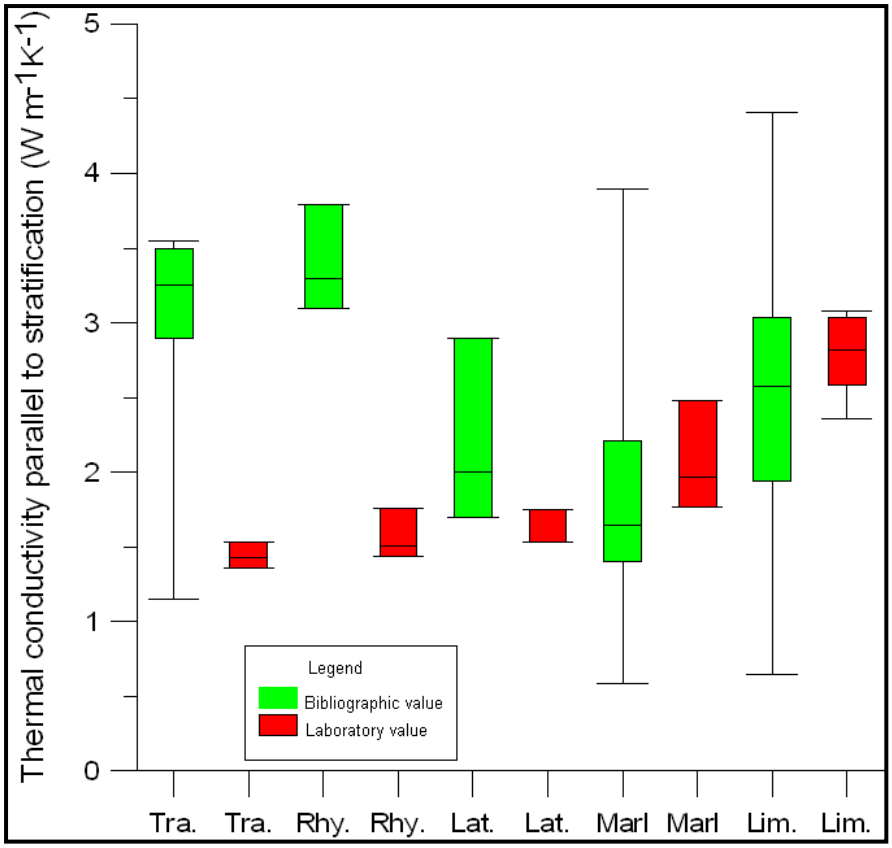

Figure 6.30 *Comparison between bibliographic values (green) and laboratory values (red) for parallel thermal conductivity Note: ""Tra." = Trachyte, "Rhy." = Rhyolite, "Lat." = Latite, Lim." = Limestone*

Considering the perpendicular thermal conductivity the values (bibliographic and experimental, respectively) are: 3.25 (W $m^{-1}K^{-1}$) and 1.45 (W $m^{-1}K^{-1}$) for trachyte, 3.30 (W $m^{-1}K^{-1}$) and 1.53 (W $m^{-1}K^{-1}$) for rhyolite, 2.00 (W $m^{-1}K^{-1}$) and 1.73 (W $m^{-1}K^{-1}$) for latite, 1.65 (W $m^{-1}K^{-1}$) and 1.99 (W $m^{-1}K^{-1}$) for marl, 2.58 (W $m^{-1}K^{-1}$) and 2.83 (W $m^{-1}K^{-1}$) for limestone.

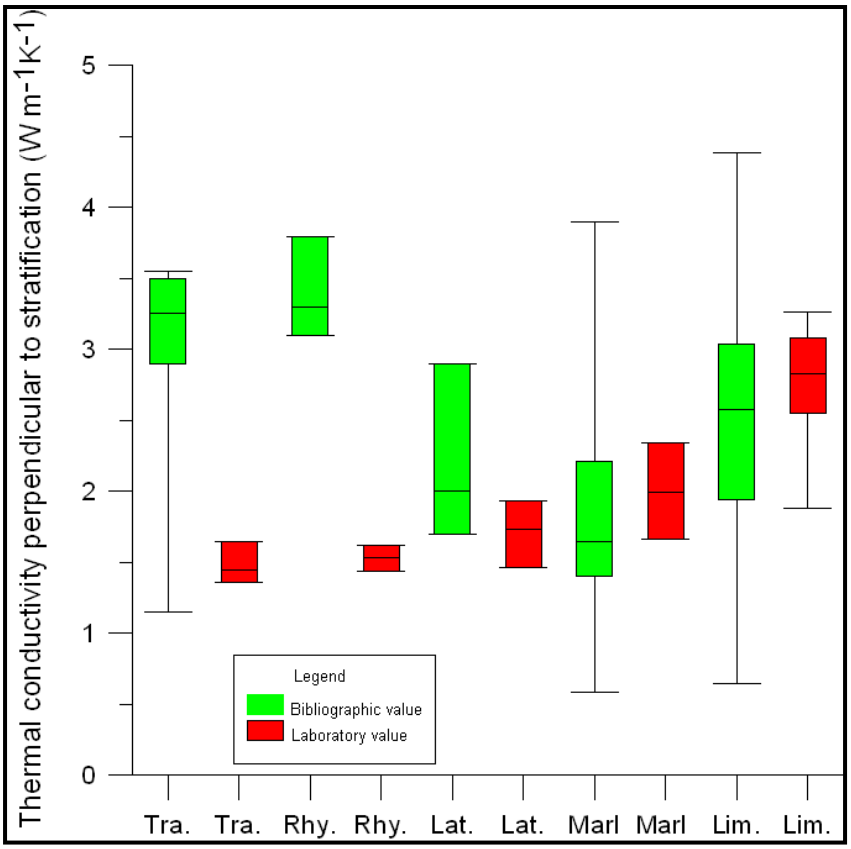

Figure 6.31 *Comparison between bibliographic values (green) and laboratory values (red) for perpendicular thermal conductivity Note: ""Tra." = Trachyte, "Rhy." = Rhyolite, "Lat." = Latite, Lim." = Limestone*

6.3.4 Volumetric heat capacity

The comparison for this parameters is shown in Figure 6.32. It is useful to remember that the values obtained in laboratory are calculated indirectly knowing the other parameters (Equation 6.1 was used in order to calculate the specific heat capacity which is then multiplied by porosity to obtain the volumetric heat capacity).

The median values (bibliographic and experimental, respectively) are similar: 2.10 (g cm^{-3}) and 1.93 (g cm^{-3}) for trachyte, 2.17 (g cm^{-3}) and 1.93 (g cm^{-3}) for rhyolite, 2.9 (g cm^{-3}) and 1.94 (g cm^{-3}) for latite, 2.20 (g cm^{-3}) and 1.96 (g cm^{-3}) for marl, 2.30 (g cm^{-3}) and 2.10 (g cm^{-3}) for limestone.

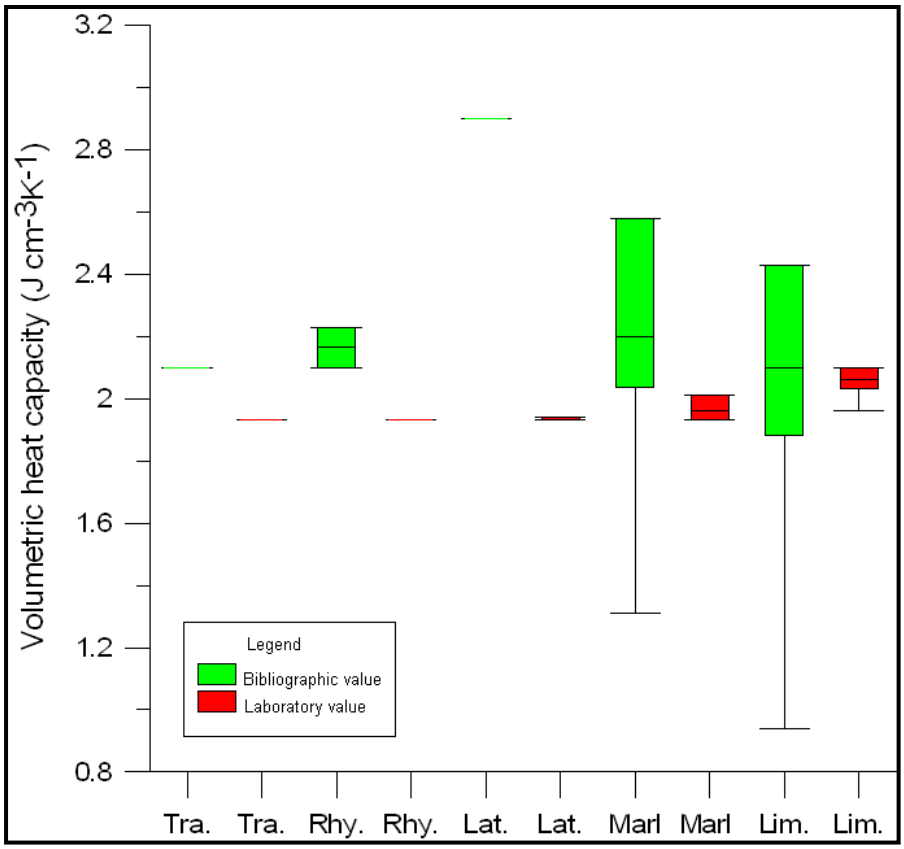

Figure 6.32 *Comparison between bibliographic values (green) and laboratory values (red) for perpendicular thermal conductivity Note: ""Tra." = Trachyte, "Rhy." = Rhyolite, "Lat." = Latite, Lim." = Limestone*

6.4 Precision and accuracy of the measures

Precision and accuracy are important parameters which define the quality of an instrument.

In the fields of science, engineering, industry, and statistics, the *precision* of a measurement system, related to reproducibility and repeatability, is the degree to which repeated measurements under unchanged conditions show the same results. Instead, the *accuracy* of a measurement system is the degree of closeness of measurements of a quantity to that quantity's actual (true) value (Taylor, 1997).

A quick test to determine the performance of the instrument was conducted using the data directly measured in laboratory. The results were compared with the precision and the accuracy declared by the manufacturer (1% for precision and 5% for the accuracy).

Before to proceed is useful recall (and integrated) the definitions given in Chapter 5 related to the measurement procedure.

"Acquisition" is defined as the single measure made by instruments: a series of acquisitions performed on the same point of the sample is called "set" or "set of acquisitions". The set in defined "complete" if all 8 "acquisitions" are considered,

"validated" if the first two acquisition of the set are discarded. Thermal properties are calculated using validated set.
Finally, for every sample are made 6 set of acquisitions: 3 perpendicular and 3 parallel with respect the stratification. The total of acquisition for a single sample are: 6 * 8= 48 acquisitions, of which only 6 * 6 = 36 are validated.
The total sets for all 21 samples are: 21 * 6 = 126 sets.

6.4.1 Precision

The precision define the agreement of two (or more) acquisitions obtained measuring the same quantity: usually it is specified with standard deviation, variance (Cremonini et al., 2009) or coefficient of variation (Abdì, 2010).
The variance and standard deviation (about thermal conductivity) are reported in Annex I and Annex II: they were calculated both for complete and validated set, respectively.
In this paragraph the attention is focused on the coefficient of variation (Cv), because probably the manufacturer gives the precision in this therm (but no formula which explained how the manufacturer calculates the precision are present in the operator manual). It is defined as the ratio of standard deviation and mean value of a specific set and if this result is multiplied by 100 it is expressed in percentage (Abdì, 2010):

$$Cv = \frac{\sigma}{\mu} * 100$$	6.3

Where σ is the standard deviation, μ the mean of a set of acquisition.
Always in Annex I and II are reported the coefficient of variation (expressed also as %) of all 6 sets for every sample.
In this paragraph are reported the results for a three selected samples: they are choose randomly but pay attention to their physical properties: in particular the sample choosen (34, Rosso Ammonitico; 46, marl; 36, rhyolite) have increasing values for porosity. This consideration is made because during the experiments was detected some acquisition problems for samples with high porosity due to the lack of contact with the surface of sensor and the aim of the works is also found if some relationship with porosity exist.
In Table 6.19, 6.20, 6.21 are reported are reported the values of the coefficient of variation (Cv) both for complete (marked with "8 acquisitions") and validate set (marked with "6 acquisitions").

Table 6.19 *Coefficient of variation (%) for validated (6 acquisitions) and completed (8 acquisitions) for sample 34 (Rosso Ammonitico formation). Porosity: 1.967%*

Sample/point	Cv for 6 acquisitions (%)	Cv for 8 acquisitions (%)
34_1	0.78	2.29
34_2	0.33	0.64
34_3	0.79	0.67
34_4	0.56	0.94
34_5	0.64	0.82
34_6	0.78	2.17

Table 6.20 *Coefficient of variation (%) for validated (6 acquisitions) and completed (8 acquisitions) for sample 46 (Marl). Porosity: 7.941%*

Sample/point	Cv for 6 acquisitions (%)	Cv for 8 acquisitions (%)
46_1	0.35	1.30
46_2	0.25	2.93
46_3	0.56	1.43
46_4	0.37	1.83
46_5	0.68	7.04
46_6	0.60	0.73

Table 6.21 *Coefficient of variation (%) for validated (6 acquisitions) and completed (8 acquisitions) for sample 36 (rhyolite). Porosity: 14.451%*

Sample/point	Cv for 6 acquisitions (%)	Cv for 8 acquisitions (%)
36_1	2.81	4.29
36_2	0.39	0.81
36_3	1.93	3.11
36_4	3.33	5.81
36_5	2.30	2.99
36_6	2.53	3.28

For sample 34 (Rosso Ammonitico formation) every of 6 “validated” sets have coefficient of precision lower than 1%, but considering “complete” sets (of same sample) 2 sets have value higher than 1%.

Also for sample 46 (marl) every of 6 “validated” sets have coefficient of precision lower than 1%, but considering “complete” sets (of same sample) 5 sets have value higher than 1% (for set number 46_5 in its equal to 7.04%).

For sample 36 (rhyolite) both “validated” and “complete” sets have 5 sets with values higher than 1% (The latter set has always value higher respect the first)

The information contained in these Table are used to generate three different plot (Figure 6.33, Figure 6.34, Figure 6.35). The comments just made reflect how showed by plots.

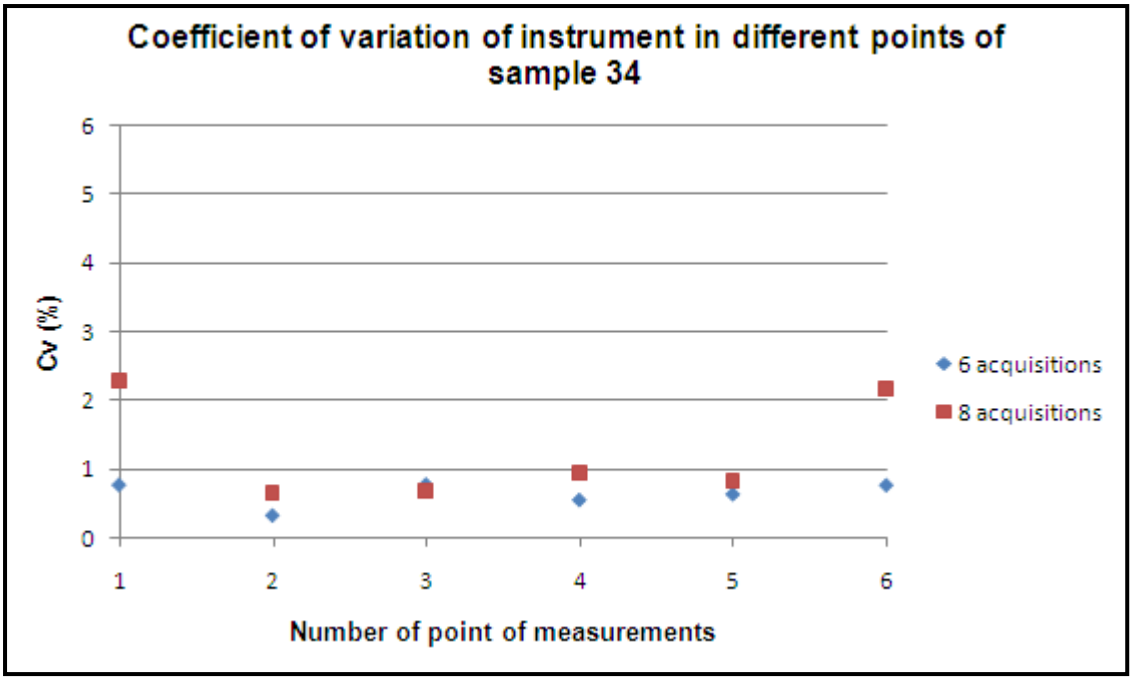

Figure 6.33 *Coefficient of variation (%) versus the 6 set of acquisitions (complete and validated) for sample 34*

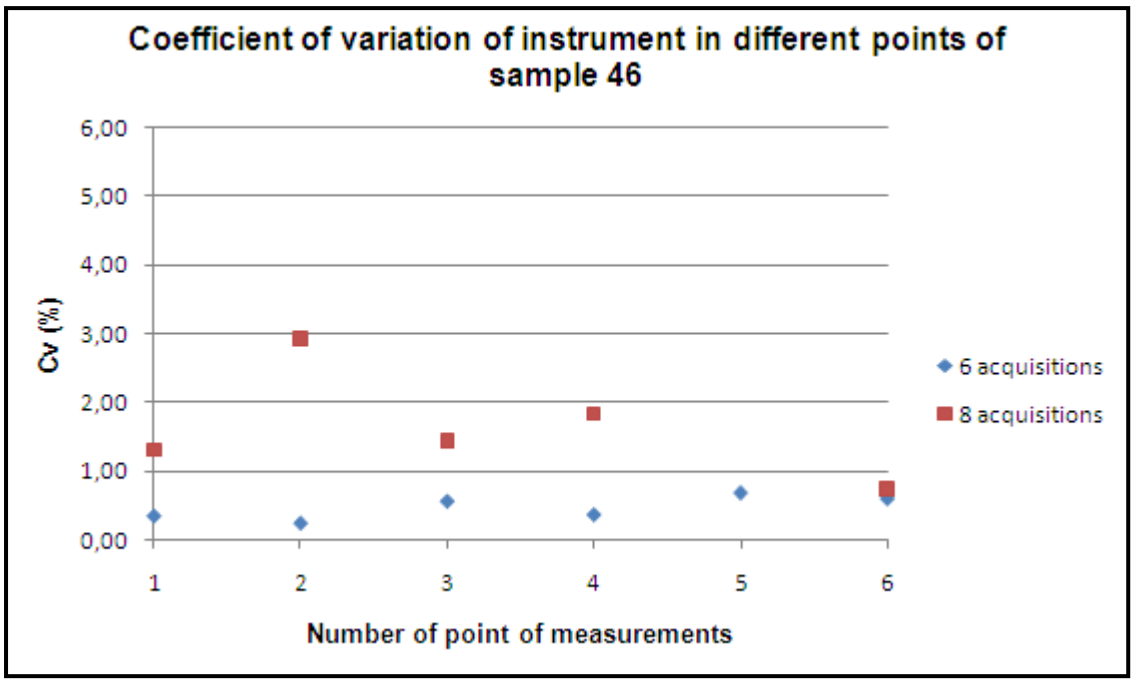

Figure 6.34 *Coefficient of variation (%) versus the 6 set of acquisitions (complete and validated) for sample 34*

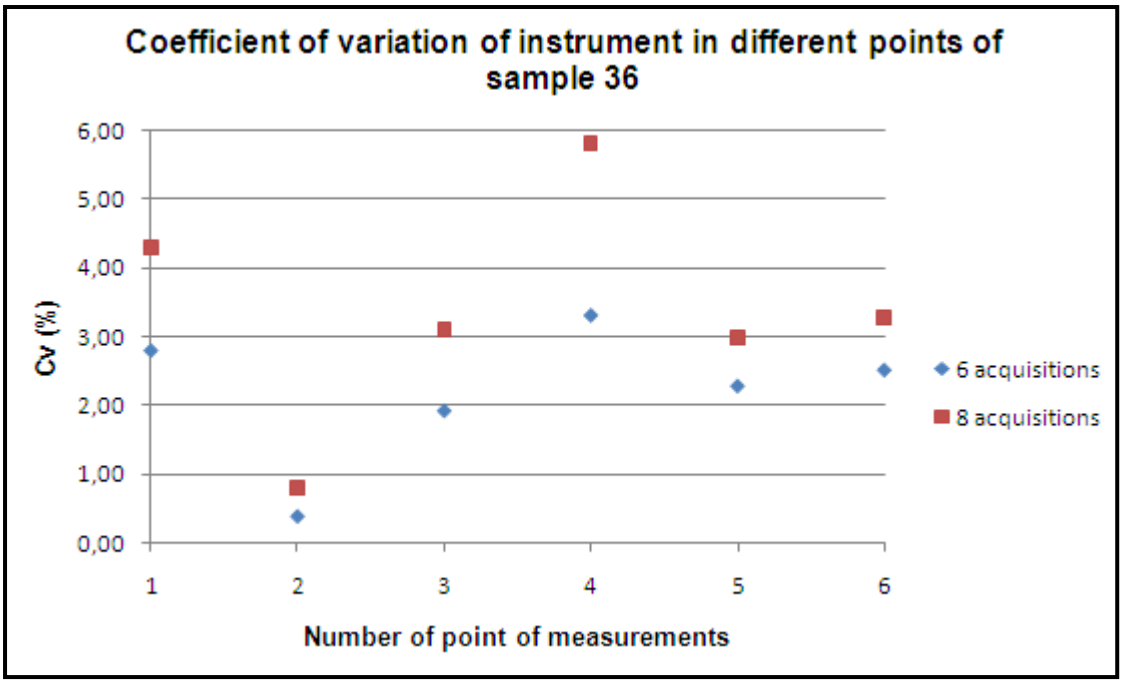

Figure 6.35 *Coefficient of variation (%) versus the 6 set of acquisitions (complete and validated) for sample 34*

For all samples has calculated how many validated and complete set have coefficient of variations <1% (Table 6.22, 6.23). The samples are grouped by lithology and in the second column is reported the value of experimental porosity for each lithology.

The 73.02% of validated sets have values of coefficient of precision lower than 1%, only 43.65% of complete sets respect this constrain. It is possible say which there is noticeable improvements in data precision when the first two acquisitions of every set are discarded.

The plot of Figure 6.36 explains a clear behavior of coefficient of precision vs porosity: the effusive rocks (trachyte, rhyolite, marl) which have a higher value of porosity respect to the sedimentary have a greater number of set where the coefficient of variation is not < 1%.

Table 6.22 *Number of validated sets of with coefficient of variation (%) lower than 1%*

Lithology	Porosity %	Number of samples	Sets for sample	Total sets for lithology	Number of set with Coefficient of variations < 1%	Ratio (%)
Trachyte	8.593	3	6	18	10/18	55.56
Rhyoilite	13.613	3	6	18	10/18	55.56
Latite	6.17	3	6	18	15/18	83.33
Marl	7.887	3	6	18	13/18	72.22
Limestone	6.615	9	6	54	44/54	81.48
TOTAL					92/126	73.02

Table 6.23 *Number of complete sets of with coefficient of variation (%) lower than 1%*

Lithology	Porosity %	Number of samples	Sets for sample	Total sets for lithology	Number of set with Coefficient of variations < 1%	Ratio (%)
Trachyte	8.593	3	6	18	6/18	33.33
Rhyoilite	13.613	3	6	18	6/18	33.33
Latite	6.17	3	6	18	10/18	55.56
Marl	7.887	3	6	18	5/18	27.78
Limestone	6.615	9	6	54	28/54	51.85
TOTAL					55/126	43.65

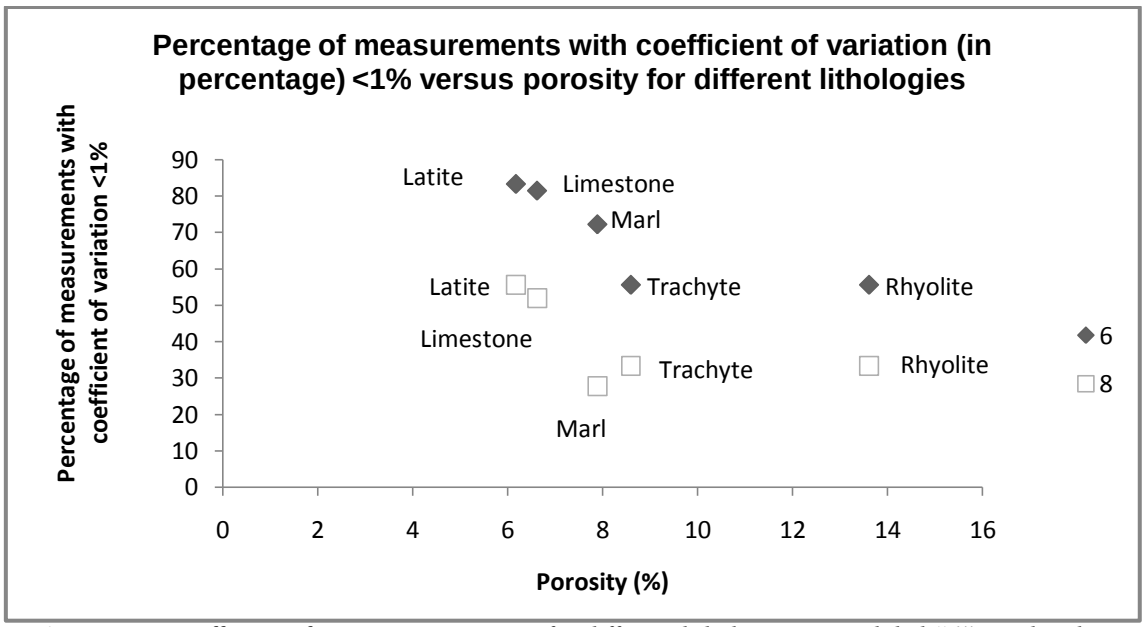

Figure 6.36 *Coefficient of variation vs porosity for different lithologies. Note: label "6" is related to validate sets, "8" to complete sets*

6.4.2 Accuracy

The accuracy (A) defines how near is a single acquisition respect the "real" value. The difference between the real value and the value of the acquisition is defined as "absolute accuracy". For a set of acquisitions, the accuracy is equal to the maximum difference between all acquisition of the set and the real value:

$$A = max \sum_i |x_i - x_0| \qquad 6.4$$

Where x_i is the single acquisition and x_0 the real value. For this work, the summation must be considered on a set (complete if i ranges from 1 to 8, validated if i ranges from 1 to 6).

The ratio between absolute accuracy and the real value is the "relative accuracy", which can be expressed in percentage (Cremonini et al., 2009):

$$A\% = \frac{A}{x_0} * 100 \qquad 6.5$$

In addition is reasonable assume that the average value of the set represents the correct value.

In Annex I and II are reported the accuracy for thermal conductivity measures (expressed also as %) of all 6 sets (validated and complete, respectively) for every sample.

In this paragraph are reported the results for a three selected samples: they are choose randomly but pay attention to their physical properties: in particular the sample choosen (34, Rosso Ammonitico; 46, marl; 36, rhyolite) have increasing values for porosity. This consideration is made because during the experiments was detected some acquisition problems for samples with high porosity due to the lack of contact with the surface of sensor and the aim of the works is also found if some relationship with porosity exist.

For sample 34 (Rosso Ammonitico formation) every of 6 "validated" sets have accuracy lower than 5%, considering "complete" sets (of same sample) 1 set have value higher than 5%.

Also for sample 46 (marl) every of 6 "validated" sets have coefficient of precision lower than 1%, but considering "complete" sets (of same sample) 2 sets have value higher than 5% (for set number 46_5 in its equal to 17.35%).

For sample 36 (rhyolite) every of 6 "validated" sets have accuracy lower than 5%, considering "complete" sets (of same sample) 3 sets have value higher than 5%.

The information contained in these Table are used to generate three different plot (Figure 6.37, Figure 6.38, Figure 6.39). The comments just made reflect how showed by plots.

Table 6.24 *Accuracy (%) for validated (6 acquisitions) and completed (8 acquisitions) for sample 34 (Rosso Ammonitico formation). Porosity: 1.967%*

Sample/point	Accuracy for 6 acquisitions (%)	Accuracy for 8 acquisitions (%)
34_1	1.23	4.95
34_2	0.60	1.00
34_3	1.16	1.17
34_4	0.66	1.45
34_5	0.91	1.34
34_6	1.10	5.05

Table 6.25 *Accuracy (%) for validated (6 acquisitions) and completed (8 acquisitions) for sample 46 (marl). Porosity: 7.941%*

Sample/point	Accuracy for 6 acquisitions (%)	Accuracy for 8 acquisitions (%)
46_1	0.41	3.11
46_2	0.46	7.17
46_3	1.03	2.78
46_4	0.56	4.38
46_5	1.23	17.35
46_6	1.02	1.30

Table 6.26 *Accuracy (%) for validated (6 acquisitions) and completed (8 acquisitions) for sample 36 (rhyolite). Porosity: 14.451%*

Sample/point	Accuracy for 6 acquisitions (%)	Accuracy for 8 acquisitions (%)
36_1	3.95	7.29
36_2	0.5	1.59
36_3	2.62	5.31
36_4	4.95	10.25
36_5	3.18	3.96
36_6	3.67	4.69

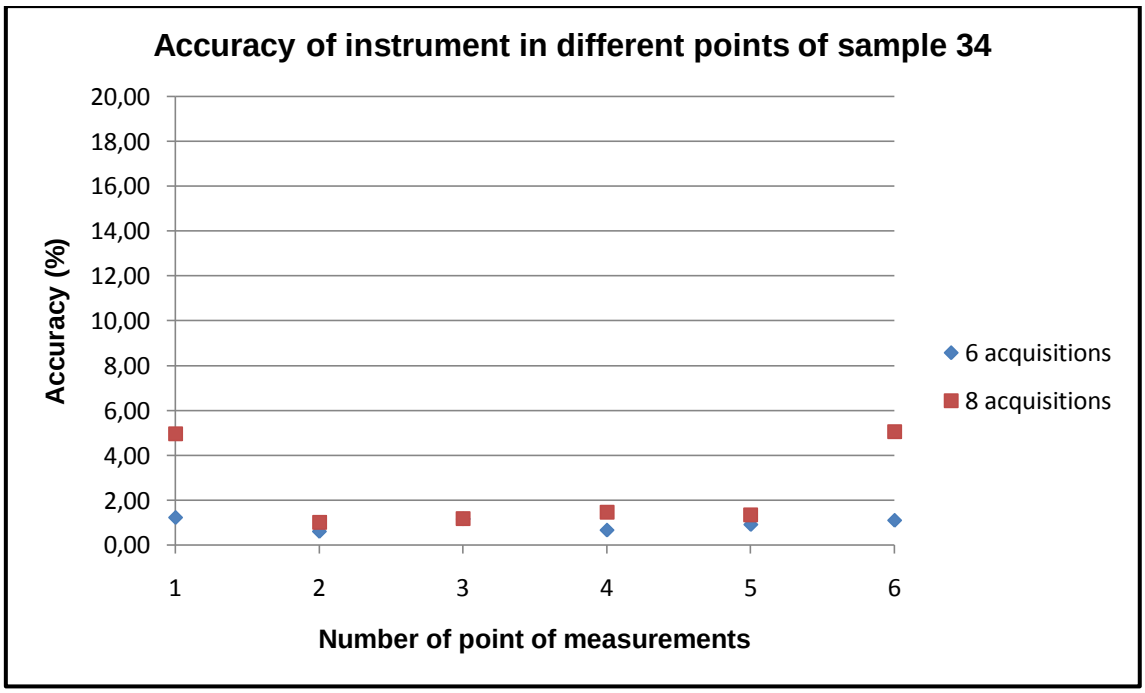

Figure 6.37 *Coefficient of variation (%) versus the 6 set of acquisitions (complete and validated) for sample 34*

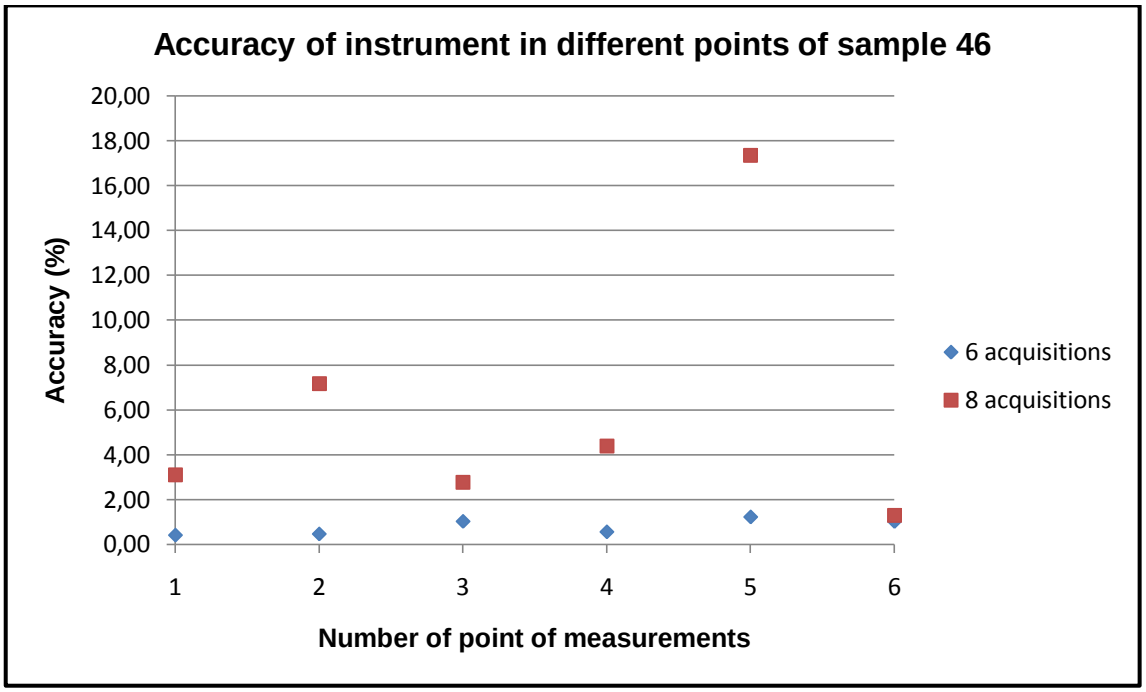

Figure 6.38 *Coefficient of variation (%) versus the 6 set of acquisitions (complete and validated) for sample 34*

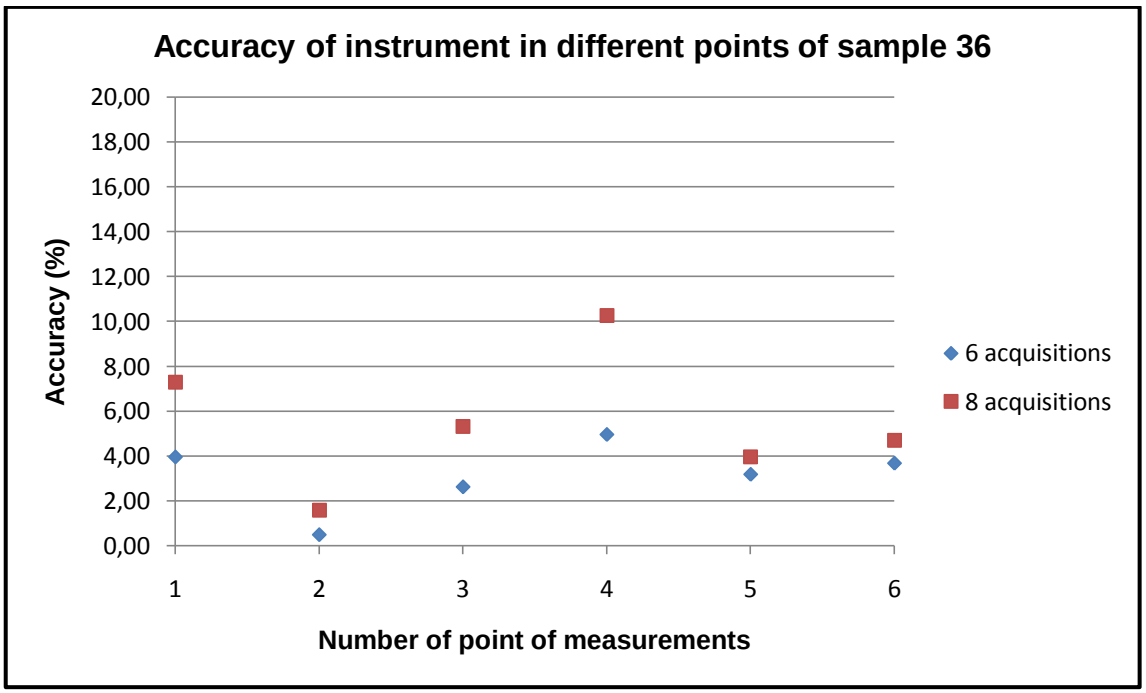

Figure 6.39 *Coefficient of variation (%) versus the 6 set of acquisitions (complete and validated) for sample 34*

For all samples has calculated how many validated and complete set have accuracy <5% (Table 6.27, 6.28). The samples are grouped by lithology and in the second column is reported the value of experimental porosity for each lithology.

The 100% of validated sets have accuracy lower than 5%, 76.98% of complete sets respect this constrain. It is possible say which there is noticeable improvements in data accuracy when the first two acquisitions of every set are discarded.
The plot of Figure 6.40 explains which accuracy in always verified when validates sets are used in the calculations. For complete sets exists a relation with porosity but it is not so significant probably because the range of 5% allow also at rocks with high value of porosity to fall within this range.

Table 6.27 *Number of validated sets of with accuracy (%) lower than 5%*

Lithology	Porosity %	Number of samples	Sets for sample	Total sets for lithology	Number of set with Coefficient of variations < 1%	Ratio (%)
Trachyte	8.593	3	6	18	18/18	100
Rhyoilite	13.613	3	6	18	18/18	100
Latite	6.17	3	6	18	18/18	100
Marl	7.887	3	6	18	18/18	100
Limestone	6.615	9	6	54	54/54	100
TOTAL					126/126	1000

Table 6.28 *Number of complete sets of with accuracy (%) lower than 5%*

Lithology	Porosity %	Number of samples	Sets for sample	Total sets for lithology	Number of set with Coefficient of variations < 1%	Ratio (%)
Trachyte	8.593	3	6	18	14/18	77.78
Rhyoilite	13.613	3	6	18	13/18	72.22
Latite	6.17	3	6	18	15/18	83.33
Marl	7.887	3	6	18	14/18	77.78
Limestone	6.615	9	6	54	41/54	75.93
TOTAL					97/126	76.98

In general it can be seen also for the accuracy there are considerable improvements when the first 2 acquisitions are discarded: the mean value of this parameter (averaged over all lithologies) pass from 77% to 100%.
The advice that may arise from these considerations are to discard (for rocks that have significant porosity values) a greater number of acquisitions: this practice could improve the accuracy (and especially) the precision of the data.

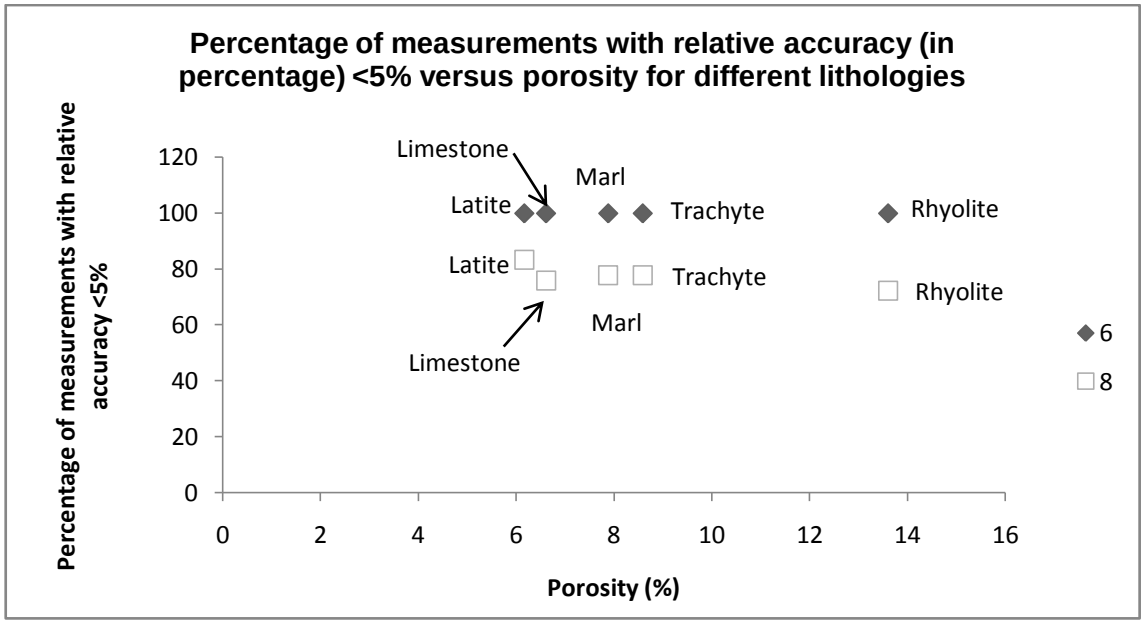

Figure 6.40 *Coefficient of variation vs porosity for different lithologies. Note: label "6" is related to validate sets, "8" to complete sets*

It is however evident that there are substantial benefits in using the data from validated by the set than complete.

This legitimizes the procedure used in the laboratory which has provided the standard deviation of the first two acquisitions for each set of measurements: this has allowed us to obtain values of thermal parameters generally more precise and more accurate.

7. Management of data through the use of a Geographical Information System (GIS)

A geographic information system (GIS) is a tool which allows to analyze, represent or query entities or events that occur on the territory.
For the users of this kind of software it is possible to explain events, plan strategies or designing territorial infrastructures.
In addition, the results obtained with a GIS are easy to understand and can be easily shared (www.comune.ra.it; www.esri.com).
There are many GIS software and mainly fall into two main groups, the open source (eg Grass GIS and Quantum GIS) and the proprietary ones (such as ArcGIS and Field-Map).
In this work the software ArcGIS (version 10) produced by ESRI was used. It includes a set of integrated applications (ArcMap, ArcCatalog, ArcToolbox) .
ESRI produces also a free software called ArcGIS Explorer able to perform simple analysis. As an example (Figure 7.1) it has been highlighted the boundary of the Euganean Hills.

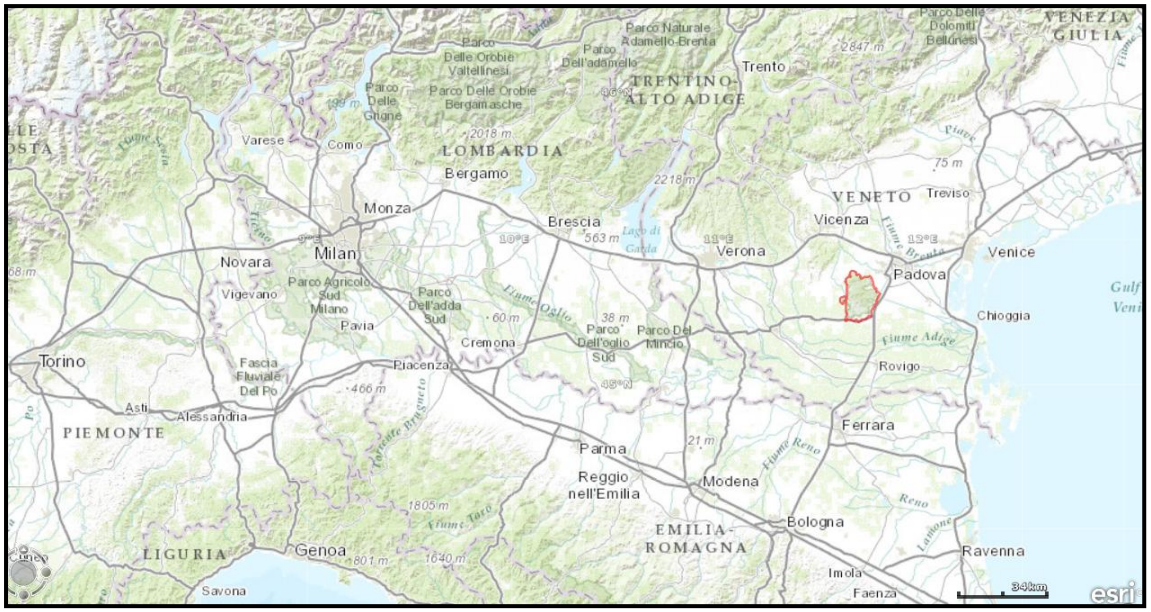

Figure 7.1 *Locating of the Euganean Hills (red line) with ArcGIS Explorer*

7.1 Geological Map of Euganean Hills

An important basis of the work is the Geological Map of the Euganean Hills. This map is available as shapefile, a document able to describe the geography of the area and to share geological information (Attribute Table) that can be accessed by the user. Using ArcGis is possible to know the extent and the surface distribution of each geological formation.

The map has been geo-referenced according to the geographic coordinates "Roma Montemario." At this information, the boundaries of “Parco Regionale dei Colli Eugani” (which includes all of the Euganean Hills) and the faults present in the zone are include. The result is reported in Figure 7.2

On the geological map are positioned 21 points in correspondence to the 21 outcrops where the samples were collected (Figure 7.3). This operations was made using the coordinates recorded during the phase of sampling and reported within the geological sheets (Chapter 3).

At every point are then associated the principal information about the sample: day of sampling, type of lithology and all the thermo-physical properties determinate in laboratory.

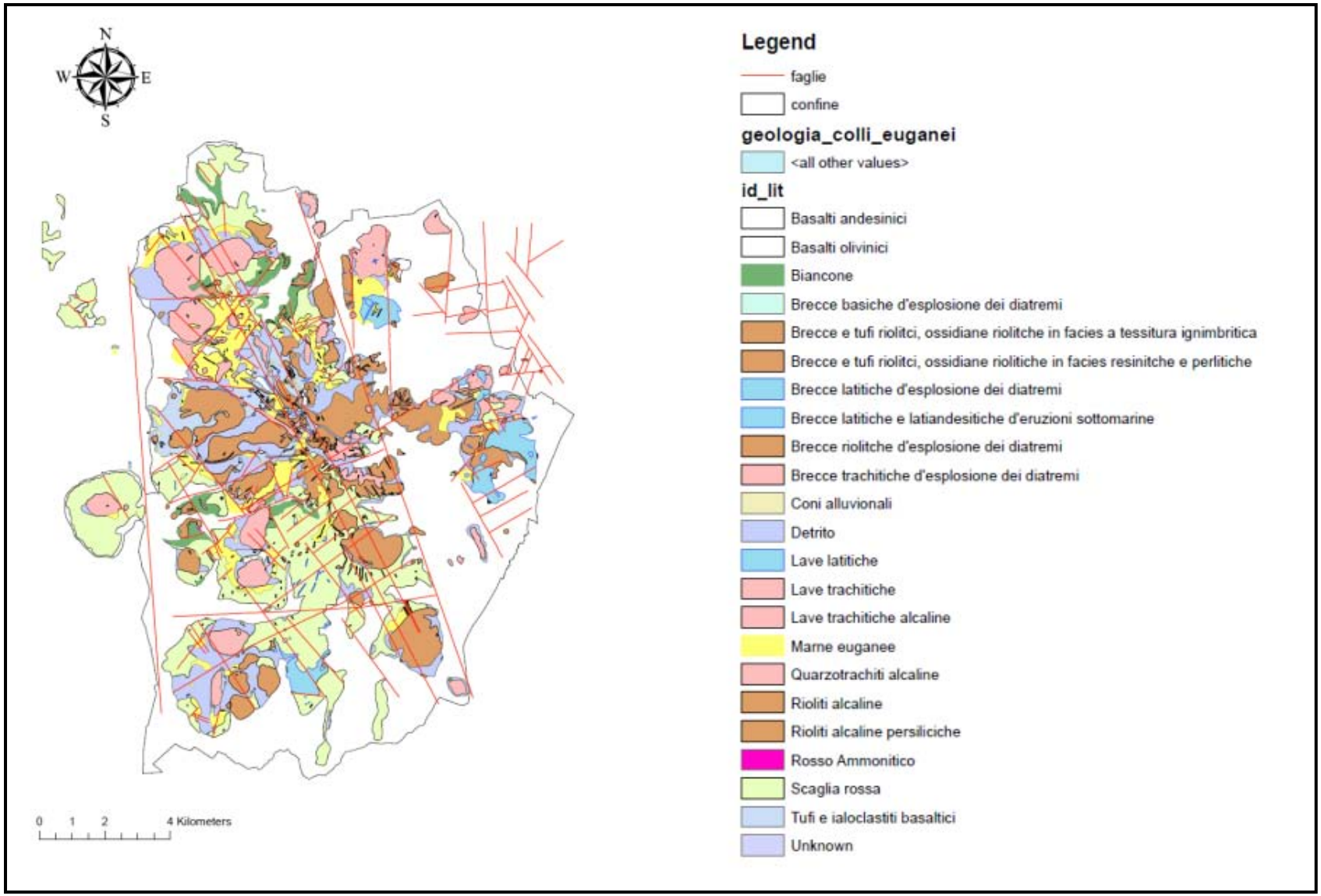

Figure 7.2 *Geological map of Euganean Hills*

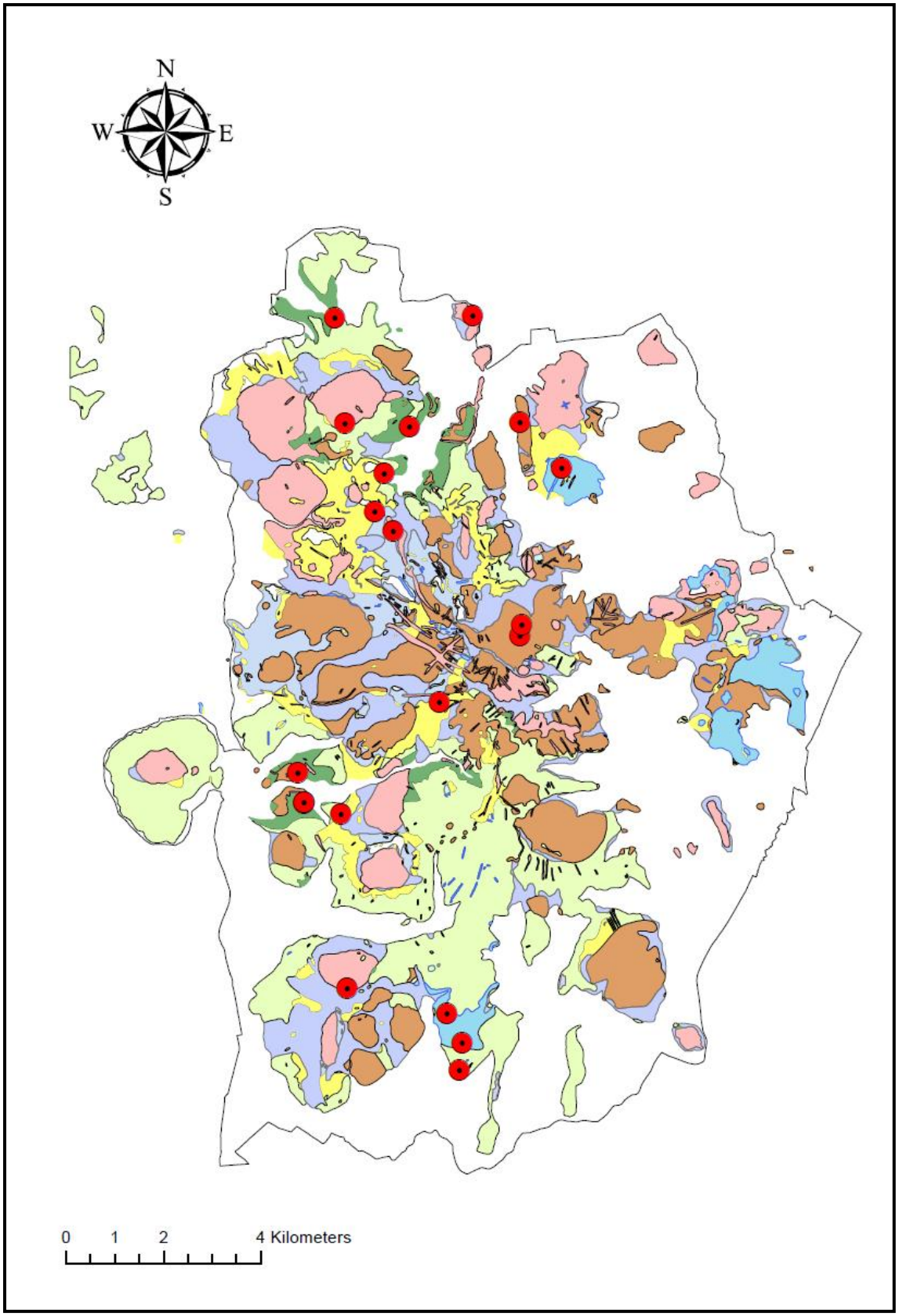

Figure 7.3 *Localization of sampling points*

7.2 Data Integration

The literature search and laboratory results presented in Chapter 6 are related to the main lithologies present in the Euganean Hills. In order to create thematic maps with different thermo-physical properties of the rocks in this area is necessary to associate the values for each lithology present in the geological map.

In particular, the data for the basalt, debris, alluvial cones and ialoclastiti are missing.

A literature search has completed the bibliographic data (in addition to the author cited in Chaper 6 are used data reported in Farouki, 1981; Castellaccio et al., 2012; Barry-Macaulay et al., 2013) while the laboratory results are integrated with values obtained from the low-enthalpy laboratory of University of Padua. These data came from samples collected near Euganean Hills (Verona and Trento area, north-east of Italy) with the aim to use data as close as possible to the actual.

In particular, for the debris are associated the values of gravel, for alluvial cones the values of sand.

Table 7.1 contains the average values obtained from the literature search for all lithologies present in the geological map.

The values are defined with the following symbols: density (ρ), porosity (η), thermal conductivity (λ) and volumetric heat capacity (ρ cp)

For sand and gravel density, thermal conductivity and volumetric heat capacity are considered in wet conditions and reported in bold numbers: in fact debris and alluvial cones are usually located near the rivers or in places where the ground water is few meters under the surface level.

The porosity is instead the same in dry or wet conditions: in the first case the pores are filled by air, in the second by water but the void volume does not change.

In Table 7.2 are reported the mean values obtained in laboratory test. The values of density and porosity for basalts, sand, gravel and ialoclastiti are the same of biliografic one because the database of the laboratory has not values of these two quantities for zones near Euganean Hills.

These two tables are than associated at the Attribute Table of the geological map; this operation is fundamental in order to create the thematic maps.

The thematic maps are not realized for thermal diffusivity: due to the scarcity of bibliographic values found in literature a comparison would not be significant.

Table 7.1 *Average bibliographic values for all lithologies present within the Euganean Hills*

Formations	Lithology	ρ (gcm^{-3})	η (%)	λ// ($Wm^{-1}K^{-1}$)	λ⊥ ($Wm^{-1}K^{-1}$)	ρ cp ($Jcm^{-3}K^{-1}$)
Basalti andesitici	Basalts	2,76	3,5	2,08	2,08	2,52
Basalti olivinici	Basalts	2,76	3,5	2,08	2,08	2,52
Biancone	Limestone	2,56	8,03	2,52	2,5	2,04
Brecce basiche d'esplosione dei diatremi	Basalts	2,76	3,5	2,08	2,08	2,52
Brecce e tufi riolitici, ossidiane riolitiche in facies a tessitura ignimbritica	Rhyolite	2,37	23,15	3,34	3,34	2,17
Brecce e tufi riolitici, ossidiane riolitiche in facies resinitiche e perlitiche	Rhyolite	2,37	23,15	3,34	3,34	2,17
Brecce latitiche d'esplosione dei diatremi	Latite	2,7	0,82	2,2	2,2	2,9
Brecce trachitiche d'esplosione dei diatremi	Trachyte	2,42	18,4	2,93	2,93	2,1
Coni alluvionali	Sand	**2,02**	41	**2,48**	**2,48**	**2**
Detrito	Gravel	**2,1**	31	**2,55**	**2,55**	**2,4**
Lave latitiche	Latite	2,7	0,82	2,2	2,2	2,9
Lave trachitiche alcaline	Trachyte	2,42	18,4	2,93	2,93	2,1
Marne euganee	Marl	2,37	31	1,84	1,84	2,09
Quarzotrachiti alcaline	Trachyte	2,42	18,4	2,93	2,93	2,1
Rioliti alcaline	Rhyolite	2,37	23,15	3,34	3,34	2,17
Rioliti alcaline persiliciche	Rhyolite	2,37	23,15	3,34	3,34	2,17
Rosso Ammonitico	Limestone	2,56	8,03	2,52	2,5	2,04
Scaglia Rossa	Limestone	2,56	8,03	2,52	2,5	2,04
Tufi e ialoclastiti basaltici	Ialoclastiti	2,85	12	1,8	1,8	2,52

Table *7.2 Average laboratory values for all lithologies present within the Euganean Hills*

Formations	Lithology	ρ (gcm^{-3})	η (%)	λ// ($Wm^{-1}K^{-1}$)	λ⊥ ($Wm^{-1}K^{-1}$)	ρ cp ($Jcm^{-3}K^{-1}$)
Basalti andesitici	Basalts	2,76	3,5	1,99	1,99	2,12
Basalti olivinici	Basalts	2,76	3,5	1,99	1,99	2,12
Biancone	Limestone	2,47	7,95	2,68	2,67	2,05
Brecce basiche d'esplosione dei diatremi	Basalts	2,76	3,5	1,99	1,99	2,12
Brecce e tufi riolitici, ossidiane riolitiche in facies a tessitura ignimbritica	Rhyolite	2,23	13,61	1,57	1,53	1,93
Brecce e tufi riolitici, ossidiane riolitiche in facies resinitiche e perlitiche	Rhyolite	2,23	13,61	1,57	1,53	1,93
Brecce latitiche d'esplosione dei diatremi	Latite	2,51	6,17	1,68	1,71	1,94
Brecce trachitiche d'esplosione dei diatremi	Trachyte	2,38	8,95	1,44	1,49	1,93
Coni alluvionali	Sand	**2,02**	41	**2,01**	**2,01**	**2,46**
Detrito	Gravel	**2,1**	31	**2,55**	**2,55**	**2,41**
Lave latitiche	Latite	2,51	6,17	1,68	1,71	1,94
Lave trachitiche alcaline	Trachyte	2,38	8,95	1,44	1,49	1,93
Marne euganee	Marl	2,43	7,89	2,07	2	1,97
Quarzotrachiti alcaline	Trachyte	2,38	8,95	1,44	1,49	1,93
Rioliti alcaline	Rhyolite	2,23	13,61	1,57	1,53	1,93
Rioliti alcaline persiliciche	Rhyolite	2,23	13,61	1,57	1,53	1,93
Rosso Ammonitico	Limestone	2,66	1,38	2,99	3,11	2,09
Scaglia Rossa	Limestone	2,42	10,51	2,59	2,44	2,02
Tufi e ialoclastiti basaltici	Ialoclastiti	2,85	12	1,48	1,48	2,19

7.3 Realization and discussion of thematic maps

In this paragraph are here reported and discussed the thematic maps. In Figure 7.4 is reported the areal distribution of density in Euganean Hills following the data obtained by literature search and laboratory test.

For this parameter there is a good agreement between bibliographic and laboratory values. In the map generated from the laboratory data are more present light green areas compared to that generated with the bibliographical data: this is due to the values of trachyte which has a mean value obtained from literature data equal to 2.42 (g/cm^3) which is slightly lower than that obtained from the experiments (2.38 g/cm^3). The difference is very small but enough to positioned the values into two different intervals.

Other rocks (for example rhyolite) present values with more difference between the bibliographic and laboratory data but both fall within the same range.

For porosity (Figure 7.5) the situation is similar but the agreement is less evident: there are important differences between the literature values for trachyte and rhyolite (18.4% and 23.15%, respectively) respect to laboratory values (8.95% and 13.61%, respectively).

In general physical parameters show a good correspondence between physical and laboratory value.

In Figure 7.6 and 7.7 are reported the areal distribution of thermal conductivity both for parallel and perpendicular with respect to the stratification. This two figures are almost identical, in fact in Chapter 6 was demonstrated which a part one sample all rocks have a very low values of anisotropy. The considerations are so valid for both figures. The map obtained with bibliographic data present show present higher values: this is true in particular for trachyte, rhyolite and latite; their values are about the double with respect to the laboratory values.

For this reason the first map indicate rhyolite as lithology with higher value (3,3 $W\ m^{-1}K^{-1}$) but the experimental results indicate limestone (and in particular the formation of Rosso Ammonitico) as the lithology with the highest value (the maximum is 3.11 $W\ m^{-1}K^{-1}$ measured parallel with respect to the stratification).

In Figure 7.8 is reported the thematic maps about volumetric heat capacity. Also in this case the bibliographic value are higher respect laboratory data. The main difference are related to latite (2,9 $Jcm^{-3}K^{-1}$ the bibliographic, 1.94 $Jcm^{-3}K^{-1}$ the laboratory value).

In general thermal properties are overestimate: in this case if a plant will be done following only bibliographic data most likely it will be underestimated, not being able to provide the theoretical performance.

In this contest limestone appear as the lithology with the best thermal property: it has in general high value of thermal conductivity and volumetric heat capacity.

Another advantage is the following: all bibliographic charts does not distinguish the different formations of limestone, instead after the experimental test each formation has its specific value.

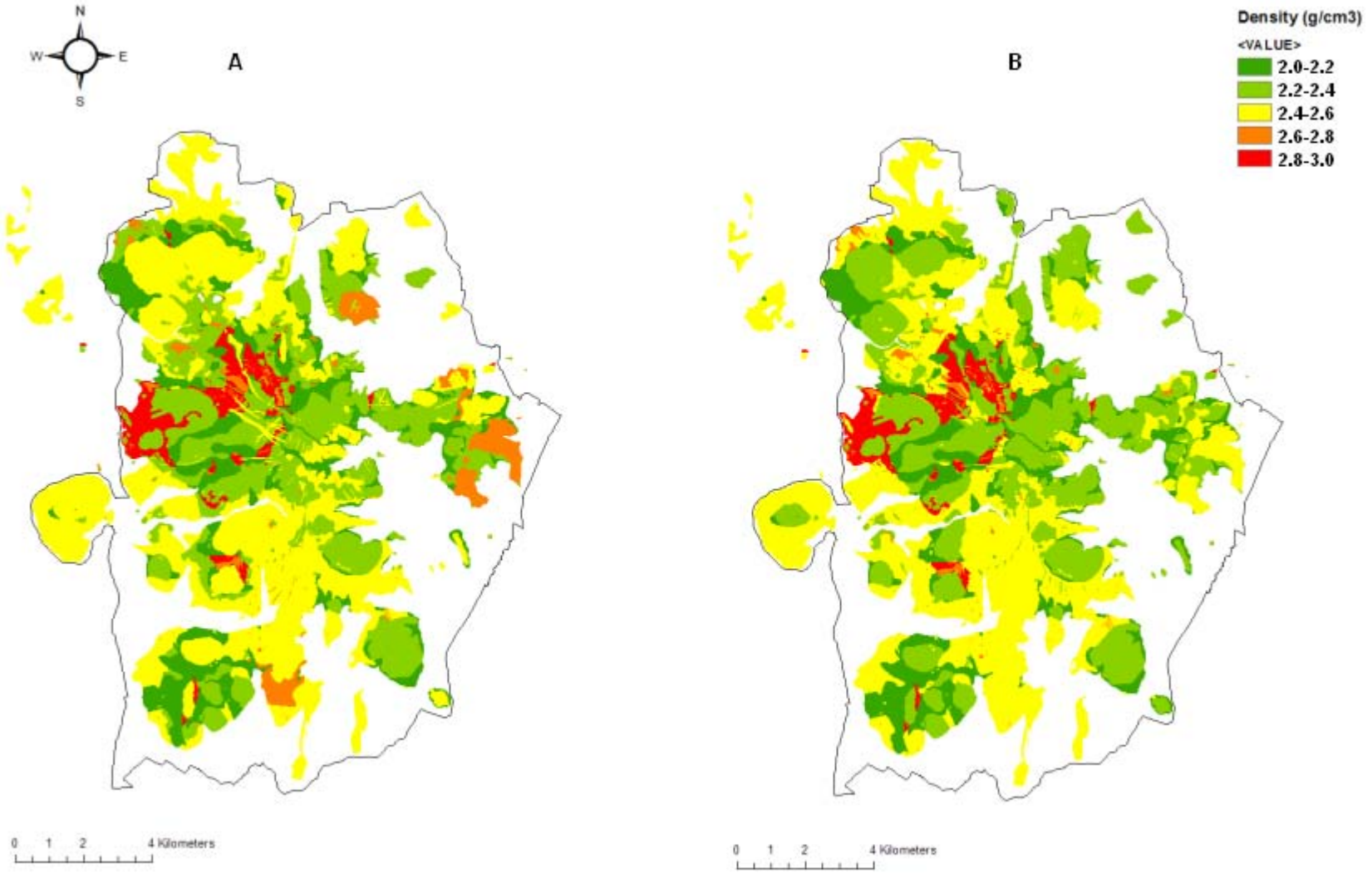

Figure 7.4 *Areal distribution of density: (A) using bibliographic data, (B) using experimental data*

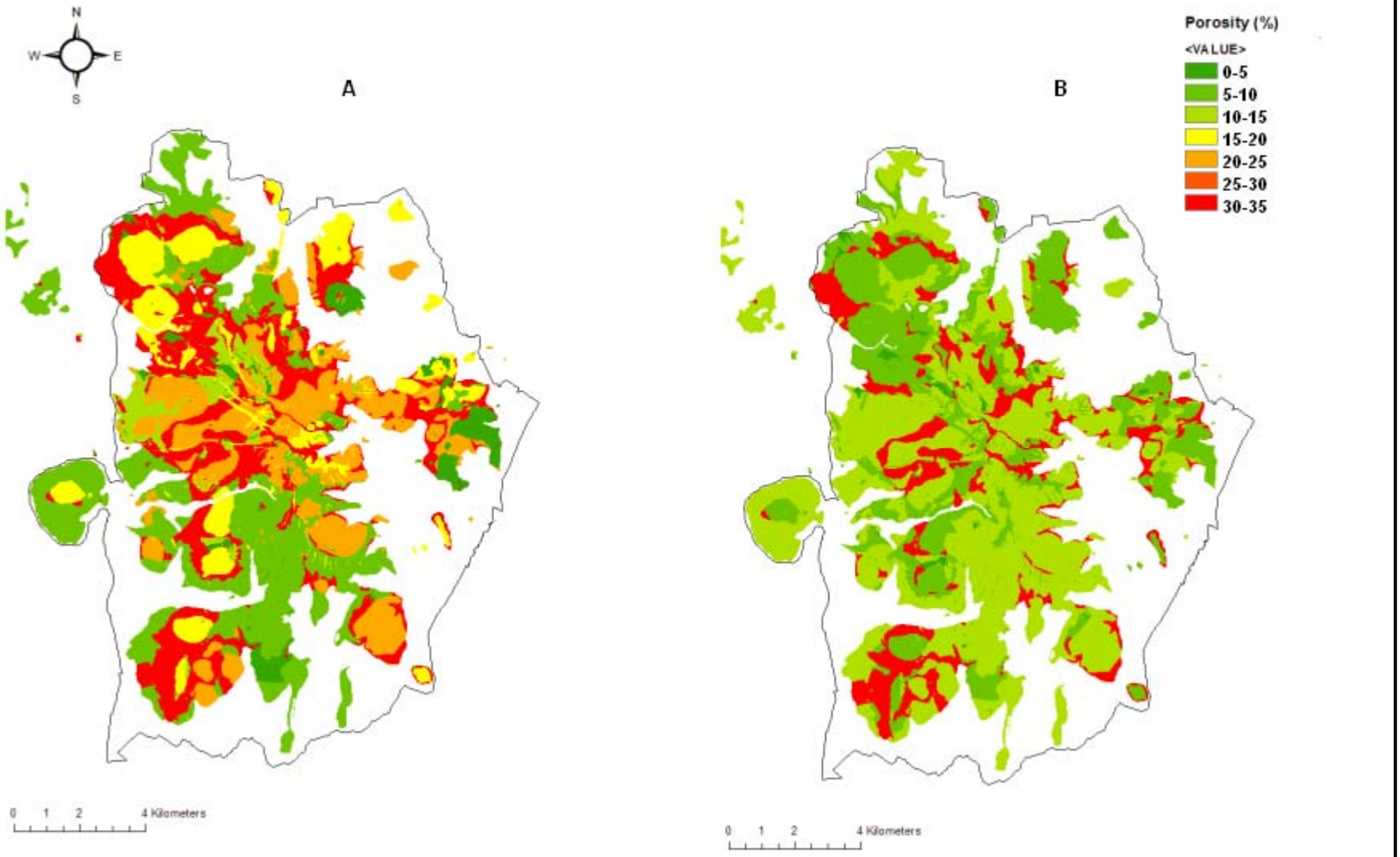

Figure 7.5 *Areal distribution of porosity: (A) using bibliographic data, (B) using experimental data*

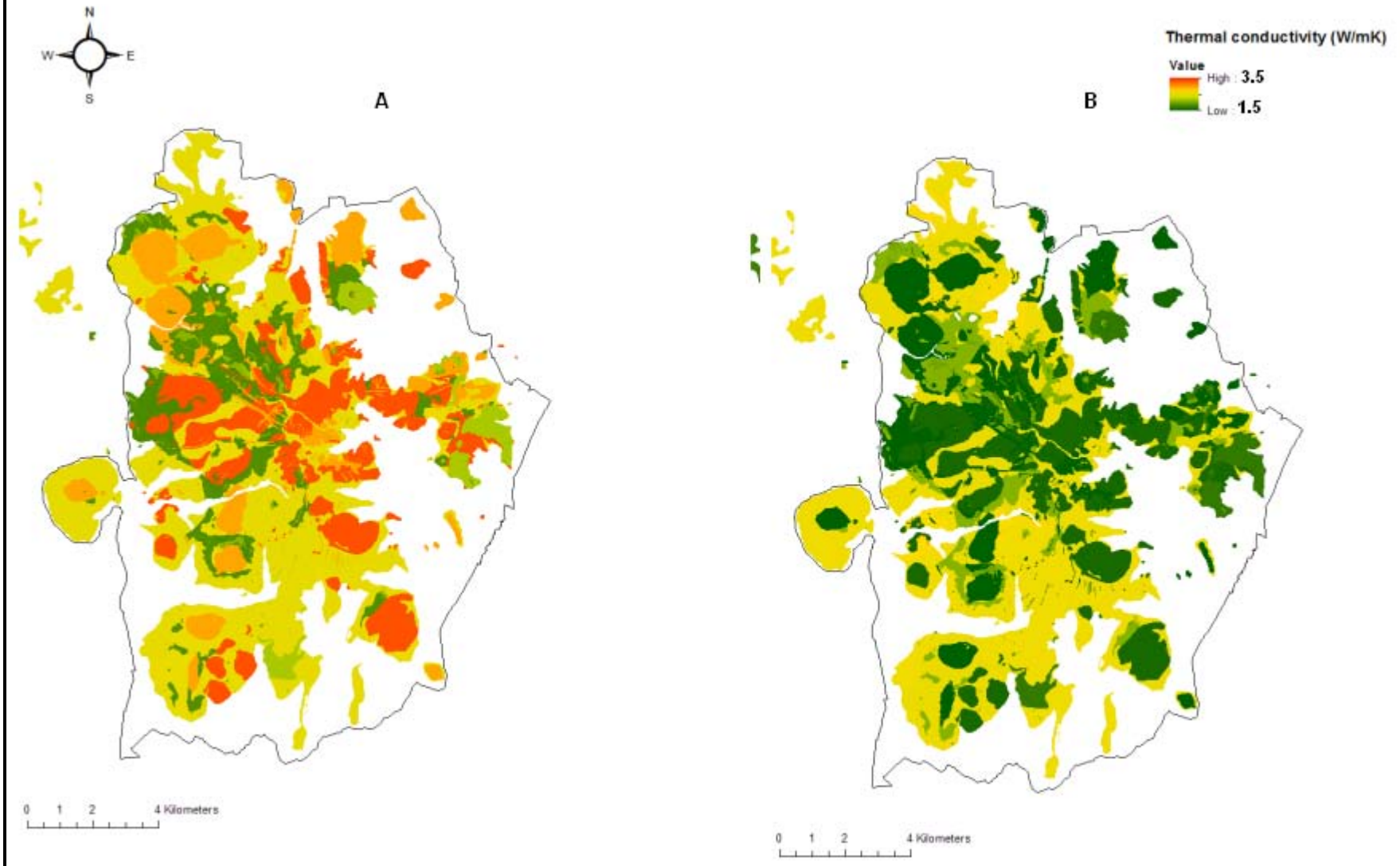

Figure 7.6 *Areal distribution of parallel thermal conductivity: (A) using bibliographic data, (B) using experimental data*

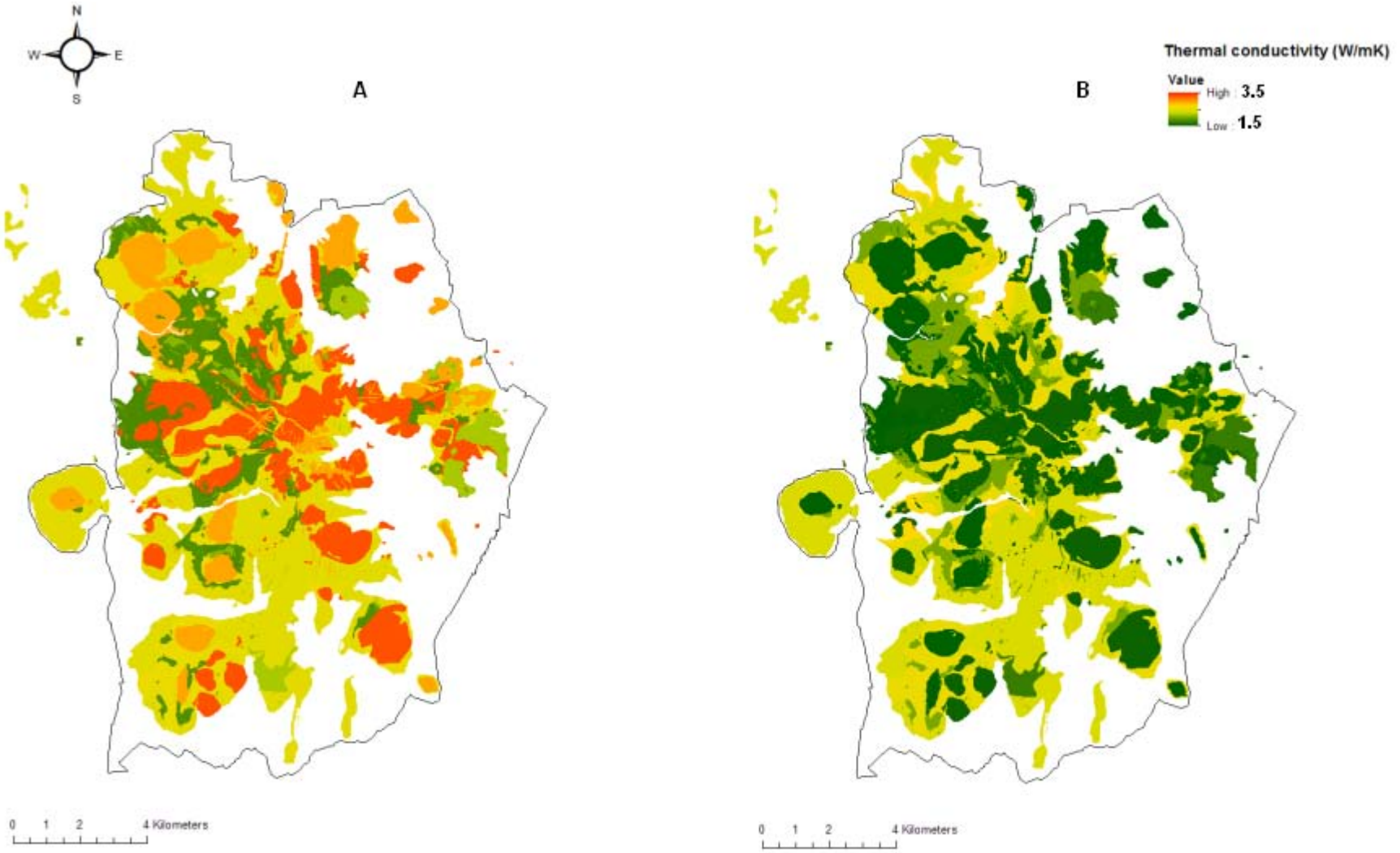

Figure 7.7 *Areal distribution of perpendicular thermal conductivity: (A) using bibliographic data, (B) using experimental data*

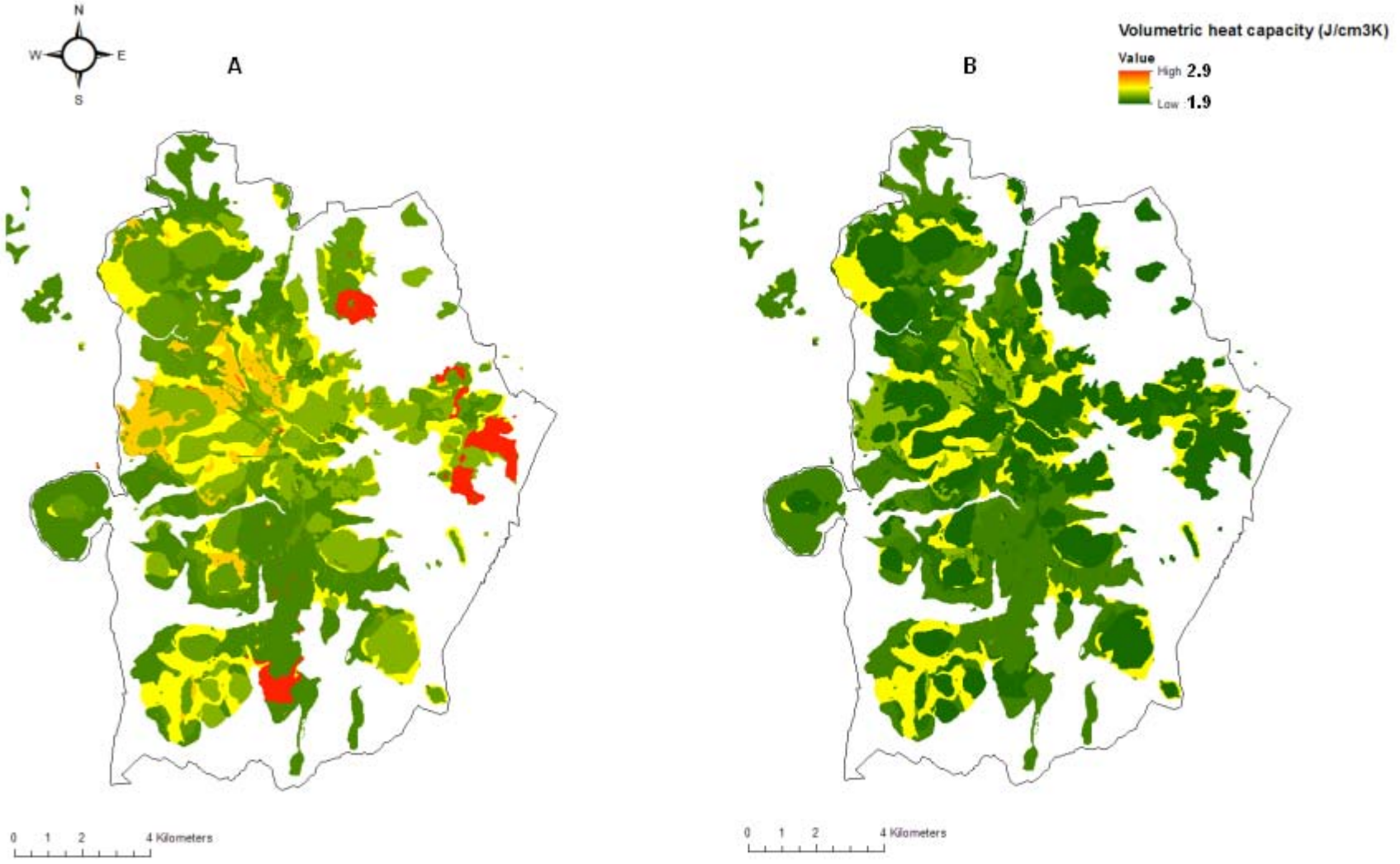

Figure 7.8 *Areal distribution of volumetric heat capacity: (A) using bibliographic data, (B) using experimental data*

Conclusions

The results of this work allowed to provide a first thermo-physical characterization of the main rocks present in the Euganean Hills.

The data obtained represent a reference point for future design related to thermal energy storage (TES) (in particular for borehole TES, BTES) or in the field of the Ground Source Heat Pump (GSHP) for the zone of Eugaenan Hills.

The values of main physical (density and porosity) and thermal properties (thermal conductivity, volumetric heat capacity) and are determinate both by literature search and by experimental data: density and porosity are obtained following the steps specified by the UNI EN 1936 while the instrument used for the determination of thermal properties is "Mathis TCi Thermal Property Analyzer" manufactured by C-Therm Technologies.

Physical parameters of the rocks have a good correspondence with literature values while for thermal properties some differences are revealed, in particular for effusive rocks (trachyte, rhyolite and latite).

The most significant difference is that related to the thermal conductivity of the effusive rocks. Laboratory data are lower (about 50%) compared to bibliographic values.

Probably this is due to the size of phenocrysts, which in the samples studied are often small. Their dimensions are important because they have significant values of thermal conductivity: for example quartz varies between 6.5 and 13 ($W\ m^{-1}K^{-1}$) (Schon, 2004), plagioclase has a value equal to 2.31($W\ m^{-1}K^{-1}$) (Schon, 2004), biotite ranges from 1.17 ($W\ m^{-1}K^{-1}$) (Schon, 2004) to 3.14 ($W\ m^{-1}K^{-1}$) (Clauser et al., 1995).

The lithology more adapt to thermal applications is limestone which has the highest value of thermal conductivity and volumetric heat capacity.

Within this lithology, the "Rosso Ammonitco" formation has the highest values of all thermal properties, thermal diffusivity included.

The study was also carried out to determine any anisotropy. A sample (number 47, Scaglia Rossa) presents a significant value ($\lambda//$) / ($\lambda\perp$) = 1.26). All effusive rocks presented values between 0.9 and 1.1, range usually adopted to define a slight anisotropy. For latter this is due to the genesis of these rocks and the random distribution of the crystals at the time of their formation does not allow the creation of preferential pathways.

A comparison of the thermal diffusivity measured by instrument was made with thermal diffusivity calculated with Equation 4.14: the comparison shows a good agreement.

A study was then conducted on the precision and accuracy about the acquisition of thermal parameters: the difference between using data which came from a complete set or a validated set are important. For this reason the procedure to discard the first two

acquisitions is correct in order to have more accurate and precise data about thermal properties.
The work is then continued on the use of a geographical information system (GIS): a first areal distribution of the thermo-physical properties was made in order to compare the bibliographic results with experimental ones.

Future research can be orientated for measure the thermal properties in wet conditions in order to create a database which could be used when groundwater is present.
A problem of difficult resolution is represented by the spatial variation of the properties of rocks: in the database created for GIS applications at every lithology is assigned its mean value.
In reality the properties of every lithology change along the three dimensions due to processes of genesis and weathering or different conditions of pressure or the presence of some stratification etc.
This leads to a problem of scale-dependence: for example, an anisotropy is not found at the magnitude of the sample may actually emerge on a larger scale.
The same issues emerge also when there is passage from outcrop scale to regional scale.
These problems can be resolved increasing the knowledge of the distribution of thermal properties in the three directions.
The knowledge of areal distribution of properties can be increased with in-situ measurements; in this case, given the high sensitivity of the instrument used for this work, could be more appropriate the use of portable equipment such as, for example, the ISOMET 2114 (www.appliedp.com).
The knowledge of variations of thermal properties in third dimension (depth) can increases collecting data from available wells and soundings.
If it is not possible (due to the costs) the results contained in this work can be used in specific models (some of them presented by Clauser, 2011) and if an idea of stratification are available, is possible estimates a global values that can be associated with a core of rock composed of different lithologies.
These assessments will then be confirmed in progress and possibly further validated by performing a thermal response test (TRT).

Annex I. Validate sets analysis

In this Annex are reported the results of calculations made on thermal conductivity for validated sets. For every rocks are made 6 set of acquisition, in the next formula the subscript "j" identify the single set (in particular "j" ranges from 1 to 6 if all sets are considered; ranges from1 to 3 for perpendicular sets made with respect the stratification and from 4 to 6 for sets parallel with respect the stratification).

The lines called "Measure 1,2,3,4,5,6" are the 6 acquisitions for a validated set, the index associated at different acquisition of same test will be indentify with subscript "i" in the next formulas.

The line mean value of single point is the arithmetic mean of the previous six acquisition, while SD relative to single point is the standard deviation.

In particular, mean (μ_j) is calculated for every "j" set as:

$\mu_j = \frac{1}{6} \sum_{i=1}^{6} x_i \qquad \left(\frac{W}{m\,K}\right)$	1

Where x_i is the value of the single acquisition within the same set. Standard deviation for single set (σ_j) is calculated as:

$\sigma_j = \sqrt{\frac{\sum_{i=1}^{6}(x_i - \mu_j)^2}{N-1}} \qquad \left(\frac{W}{m\,K}\right)$	2

Where N=6.

The Variance (VAR) relative to single set is calculated as the square of standard deviation:

$VAR_j = \sigma_j^2 \qquad \left(\frac{W}{m\,K}\right)^2$	3

The coefficient of variation (Cv) is calculated for every set "j" as:

$Cv_j = \frac{\sigma_j}{\mu_j} * 100$	4

The absolute accuracy for every "j" set is calculated as:

$A_j = max \sum_{i=i}^{6} \lvert x_i - \mu_j \rvert$	5

Where x_0 is the "true" value of the quantity measured. As indicated in Chapter 6, the true value are identify with the mean value μ_j calculated foe every set.

The Accuracy % is determinate for every "j" set as:

$A_j\% = \frac{A_j}{\mu_j} * 100$	6

The representative value of thermal conductivityfor single face (considering for example the face perpendicular with respect to the stratification, where "j" ranges from 1 to 3) is determined as:

$\mu_{face} = \frac{\sum_{j=1}^{3} x_j * p_j}{\sum_{i=1}^{3} p_j} \qquad \left(\frac{W}{m\,K}\right)$	7

Where:

$p_j = \left(\frac{1}{\sigma_j}\right)^2 \qquad \left(\frac{m\,K}{W}\right)^2$	8

(For the sets parallel to the stratification is used the same formula, but "j" ranges from 4 to 6)

The "SD relative to the face is calculate" (perpendicular to the stratification) is calculated in this way:

$\sigma_{face} = \frac{1}{\sqrt{\sum_{i=1}^{3} pj}} \qquad \left(\frac{W}{m\,K}\right)$	9

(For the sets parallel to the stratification is used the same formula, but "j" ranges from 4 to 6)

Factor of anisotropy is calculates as the ratio of representative value for single face parallel with respect to the stratification, (set number 4,5,6) and perpendicular with respect to the stratification (set number 1,2,3).

The "SD relative to the two faces" is calculated as:

$\sigma_{rock} = \frac{1}{\sqrt{\sum_{j=1}^{6} pj}} \qquad \left(\frac{W}{m\,K}\right)$	10

The different formulas are provided by: Bramanti 1997; Cremonini et al., 2009; Abdì, 2010; Ciroi, 2014

	THERMAL CONDUCTIVITY (λ)					
	Perpendicular			Parallel		
Sample / # set	1 / 1	1 / 2	1 / 3	1 / 4	1 / 5	1 / 6
Measure 1 ($Wm^{-1}K^{-1}$)	1.6165	1.6785	1.5488	1.4728	1.4977	1.5941
Measure 2 ($Wm^{-1}K^{-1}$)	1.6365	1.7058	1.5711	1.4820	1.5040	1.5804
Measure 3 ($Wm^{-1}K^{-1}$)	1.6388	1.7010	1.5813	1.4891	1.5075	1.5891
Measure 4 ($Wm^{-1}K^{-1}$)	1.6457	1.7127	1.5868	1.4846	1.4945	1.5975
Measure 5 ($Wm^{-1}K^{-1}$)	1.6462	1.7102	1.5777	1.4885	1.5070	1.6082
Measure 6 ($Wm^{-1}K^{-1}$)	1.6539	1.7109	1.5967	1.5097	1.5239	1.6137
Mean value for single point ($Wm^{-1}K^{-1}$)	1.6396	1.7032	1.5771	1.4878	1.5058	1.5972
SD relative to single point ($Wm^{-1}K^{-1}$)	0.0129	0.0128	0.0163	0.0122	0.0103	0.0123
Variance relative to single point $(Wm^{-1}K^{-1})^2$	0.000166	0.000164	0.000267	0.000150	0.000106	0.000151
Coefficient of variation %	0.785	0.751	1.037	0.823	0.683	0.769
Absolute accuracy ($Wm^{-1}K^{-1}$)	0.0231	0.0246	0.0283	0.0219	0.0182	0.0168
Accuracy %	1.41	1.45	1.79	1.47	1.21	1.05
Representative face value ($Wm^{-1}K^{-1}$)	1.6493			1.5271		
SD relative to face ($Wm^{-1}K^{-1}$)	0.0079			0.0066		
Factor of anisotropy	0.92591					
Weighted average of the two faces ($Wm^{-1}K^{-1}$)	1.5774					
SD relative to the two faces ($Wm^{-1}K^{-1}$)	0.0051					

	THERMAL CONDUCTIVITY λ					
	Perpendicular			Parallel		
Sample / # set	22B / 1	22B / 2	22B / 3	22B / 4	22B / 5	22B / 6
Measure 1 ($Wm^{-1}K^{-1}$)	1.2361	1.3515	1.3962	1.3685	1.4342	1.2010
Measure 2 ($Wm^{-1}K^{-1}$)	1.2499	1.3648	1.4107	1.3735	1.4336	1.2221
Measure 3 ($Wm^{-1}K^{-1}$)	1.2525	1.3687	1.4220	1.3958	1.4428	1.2144
Measure 4 ($Wm^{-1}K^{-1}$)	1.2667	1.3606	1.4267	1.4012	1.4535	1.2274
Measure 5 ($Wm^{-1}K^{-1}$)	1.2650	1.3670	1.4315	1.4067	1.4630	1.2377
Measure 6 ($Wm^{-1}K^{-1}$)	1.2823	1.3752	1.4356	1.3978	1.4607	1.2410
Mean value for single point ($Wm^{-1}K^{-1}$)	1.2588	1.3646	1.4205	1.3906	1.4480	1.2239
SD relative to single point ($Wm^{-1}K^{-1}$)	0.0160	0.0080	0.0147	0.0157	0.0130	0.0149
Variance relative to single point $(Wm^{-1}K^{-1})^2$	0.000257	0.000064	0.000215	0.000246	0.000168	0.000222
Coefficient of variation %	1.274	0.588	1.033	1.129	0.896	1.217
Absolute accuracy ($Wm^{-1}K^{-1}$)	0.0235	0.0131	0.0243	0.0221	0.0150	0.0229
Accuracy %	1.87	0.96	1.71	1.59	1.04	1.87
Representative face value ($Wm^{-1}K^{-1}$)	1.3583			1.3623		
SD relative to face ($Wm^{-1}K^{-1}$)	0.0064			0.0083		
Factor of anisotropy	1.0030					
Weighted average of the two faces ($Wm^{-1}K^{-1}$)	1.3598					
SD relative to the two faces ($Wm^{-1}K^{-1}$)	0.0051					

	THERMAL CONDUCTIVITY λ					
	Perpendicular			Parallel		
Sample / # set	44 / 1	44 / 2	44 / 3	44 / 4	44 / 5	44 / 6
Measure 1 ($Wm^{-1}K^{-1}$)	1.4725	1.4241	1.4331	1.3050	1.4236	1.4453
Measure 2 ($Wm^{-1}K^{-1}$)	1.4776	1.4263	1.4304	1.3249	1.4413	1.4459
Measure 3 ($Wm^{-1}K^{-1}$)	1.4895	1.4506	1.4423	1.3314	1.4384	1.4460
Measure 4 ($Wm^{-1}K^{-1}$)	1.4910	1.4260	1.4489	1.3431	1.4407	1.4558
Measure 5 ($Wm^{-1}K^{-1}$)	1.5044	1.4473	1.4566	1.3474	1.4446	1.4646
Measure 6 ($Wm^{-1}K^{-1}$)	1.5146	1.4622	1.4400	1.3558	1.4390	1.4618
Mean value for single point ($Wm^{-1}K^{-1}$)	1.4916	1.4394	1.4419	1.3346	1.4379	1.4532
SD relative to single point ($Wm^{-1}K^{-1}$)	0.0159	0.0161	0.0098	0.0182	0.0073	0.0087
Variance relative to single point $(Wm^{-1}K^{-1})^2$	0.000251	0.000258	0.000096	0.000333	0.000054	0.000076
Coefficient of variation %	1.063	1.117	0.679	1.367	0.510	0.599
Absolute accuracy ($Wm^{-1}K^{-1}$)	0.0230	0.0228	0.0147	0.0296	0.0143	0.0114
Accuracy %	1.54	1.58	1.02	2.22	1.00	0.78
Representative face value ($Wm^{-1}K^{-1}$)	1.4522			1.4348		
SD relative to face ($Wm^{-1}K^{-1}$)	0.0074			0.0054		
Factor of anisotropy	0.9881					
Weighted average of the two faces ($Wm^{-1}K^{-1}$)	1.4408					
SD relative to the two faces ($Wm^{-1}K^{-1}$)	0.0043					

	THERMAL CONDUCTIVITY λ					
	Perpendicular			Parallel		
Sample / # set	16 / 1	16 / 2	16 / 3	16 / 4	16 / 5	16 / 6
Measure 1 ($Wm^{-1}K^{-1}$)	1.7485	1.5816	1.6127	1.6832	1.7213	1.7892
Measure 2 ($Wm^{-1}K^{-1}$)	1.7639	1.5898	1.6210	1.6945	1.7357	1.7767
Measure 3 ($Wm^{-1}K^{-1}$)	1.7705	1.5853	1.6165	1.6922	1.7409	1.7755
Measure 4 ($Wm^{-1}K^{-1}$)	1.7699	1.5992	1.6215	1.7011	1.7436	1.7838
Measure 5 ($Wm^{-1}K^{-1}$)	1.7776	1.6006	1.6164	1.7201	1.7566	1.7924
Measure 6 ($Wm^{-1}K^{-1}$)	1.7997	1.6087	1.6238	1.7090	1.7413	1.7944
Mean value for single point ($Wm^{-1}K^{-1}$)	1.7717	1.5942	1.6186	1.7000	1.7399	1.7853
SD relative to single point ($Wm^{-1}K^{-1}$)	0.0169	0.0103	0.0041	0.0131	0.0115	0.0080
Variance relative to single point $(Wm^{-1}K^{-1})^2$	0.000284	0.000107	0.000017	0.000172	0.000132	0.000064
Coefficient of variation %	0.952	0.648	0.256	0.771	0.659	0.448
Absolute accuracy ($Wm^{-1}K^{-1}$)	0.0280	0.0145	0.0060	0.0201	0.0186	0.0098
Accuracy %	1.58	0.91	0.37	1.18	1.07	0.55
Representative face value ($Wm^{-1}K^{-1}$)	1.6230			1.7564		
SD relative to face ($Wm^{-1}K^{-1}$)	0.0038			0.0059		
Factor of anisotropy	1.0822					
Weighted average of the two faces ($Wm^{-1}K^{-1}$)	1.6617					
SD relative to the two faces ($Wm^{-1}K^{-1}$)	0.0032					

	THERMAL CONDUCTIVITY λ					
	Perpendicular			Parallel		
Sample / # set	36 / 1	36 / 2	36 / 3	36 / 4	36 / 5	36 / 6
Measure 1 ($Wm^{-1}K^{-1}$)	1.3805	1.4339	1.4036	1.3669	1.4313	1.3592
Measure 2 ($Wm^{-1}K^{-1}$)	1.4080	1.4461	1.4197	1.4002	1.4532	1.3842
Measure 3 ($Wm^{-1}K^{-1}$)	1.4262	1.4343	1.4296	1.4356	1.4649	1.4059
Measure 4 ($Wm^{-1}K^{-1}$)	1.4496	1.4460	1.4377	1.4570	1.4926	1.4250
Measure 5 ($Wm^{-1}K^{-1}$)	1.4696	1.4410	1.4662	1.4721	1.5153	1.4341
Measure 6 ($Wm^{-1}K^{-1}$)	1.4899	1.4447	1.4766	1.4965	1.5125	1.4580
Mean value for single point ($Wm^{-1}K^{-1}$)	1.4373	1.4410	1.4389	1.4381	1.4783	1.4111
SD relative to single point ($Wm^{-1}K^{-1}$)	0.0404	0.0057	0.0278	0.0478	0.0339	0.0357
Variance relative to single point $(Wm^{-1}K^{-1})^2$	0.001634	0.000032	0.000775	0.002288	0.001151	0.001273
Coefficient of variation %	2.813	0.394	1.934	3.326	2.295	2.528
Absolute accuracy ($Wm^{-1}K^{-1}$)	0.0568	0.0072	0.0377	0.0712	0.0470	0.0518
Accuracy %	3.95	0.50	2.62	4.95	3.18	3.67
Representative face value ($Wm^{-1}K^{-1}$)	1.4409			1.4446		
SD relative to face ($Wm^{-1}K^{-1}$)	0.0055			0.0219		
Factor of anisotropy	1.0026					
Weighted average of the two faces ($Wm^{-1}K^{-1}$)	1.4411					
SD relative to the two faces ($Wm^{-1}K^{-1}$)	0.0053					

	THERMAL CONDUCTIVITY λ					
	Perpendicular			Parallel		
Sample / # set	39 / 1	39 / 2	39 / 3	39 / 4	39 / 5	39 / 6
Measure 1 ($Wm^{-1}K^{-1}$)	1.5194	1.3827	1.5406	1.5119	1.5603	1.4027
Measure 2 ($Wm^{-1}K^{-1}$)	1.5256	1.3907	1.5584	1.5230	1.5660	1.4069
Measure 3 ($Wm^{-1}K^{-1}$)	1.5305	1.4125	1.5862	1.5333	1.5622	1.4006
Measure 4 ($Wm^{-1}K^{-1}$)	1.5453	1.4426	1.5936	1.5417	1.5730	1.3960
Measure 5 ($Wm^{-1}K^{-1}$)	1.5405	1.4370	1.6091	1.5370	1.5697	1.3948
Measure 6 ($Wm^{-1}K^{-1}$)	1.5415	1.4532	1.6096	1.5571	1.5685	1.3872
Mean value for single point ($Wm^{-1}K^{-1}$)	1.5338	1.4198	1.5829	1.5340	1.5666	1.3980
SD relative to single point ($Wm^{-1}K^{-1}$)	0.0102	0.0290	0.0280	0.0156	0.0048	0.0069
Variance relative to single point $(Wm^{-1}K^{-1})^2$	0.000104	0.000840	0.000783	0.000242	0.000023	0.000048
Coefficient of variation %	0.665	2.042	1.767	1.015	0.304	0.495
Absolute accuracy ($Wm^{-1}K^{-1}$)	0.0144	0.0371	0.0423	0.0231	0.0064	0.0108
Accuracy %	0.94	2.61	2.67	1.50	0.41	0.78
Representative face value ($Wm^{-1}K^{-1}$)	1.5278			1.5137		
SD relative to face ($Wm^{-1}K^{-1}$)	0.0091			0.0038		
Factor of anisotropy	0.9908					
Weighted average of the two faces ($Wm^{-1}K^{-1}$)	1.5158					
SD relative to the two faces ($Wm^{-1}K^{-1}$)	0.0035					

	THERMAL CONDUCTIVITY λ					
	Perpendicular			Parallel		
Sample / # set	18 / 1	18 / 2	18 / 3	18 / 4	18 / 5	18 / 6
Measure 1 ($Wm^{-1}K^{-1}$)	1.7523	1.9424	1.9451	1.6446	1.7589	1.8141
Measure 2 ($Wm^{-1}K^{-1}$)	1.7500	1.9484	1.9470	1.6465	1.7655	1.8360
Measure 3 ($Wm^{-1}K^{-1}$)	1.7497	1.9419	1.9491	1.6623	1.7633	1.8359
Measure 4 ($Wm^{-1}K^{-1}$)	1.7702	1.9522	1.9656	1.6597	1.7609	1.8575
Measure 5 ($Wm^{-1}K^{-1}$)	1.7874	1.9427	1.9679	1.6601	1.7699	1.8390
Measure 6 ($Wm^{-1}K^{-1}$)	1.7822	1.9569	1.9766	1.6622	1.7644	1.8568
Mean value for single point ($Wm^{-1}K^{-1}$)	1.7653	1.9474	1.9585	1.6559	1.7638	1.8399
SD relative to single point ($Wm^{-1}K^{-1}$)	0.0170	0.0062	0.0131	0.0081	0.0038	0.0161
Variance relative to single point $(Wm^{-1}K^{-1})^2$	0.000289	0.000038	0.000173	0.000066	0.000015	0.000258
Coefficient of variation %	0.962	0.317	0.671	0.489	0.216	0.874
Absolute accuracy ($Wm^{-1}K^{-1}$)	0.0221	0.0095	0.0180	0.0113	0.0061	0.0257
Accuracy %	1.25	0.49	0.92	0.68	0.34	1.40
Representative face value ($Wm^{-1}K^{-1}$)	1.9315			1.7485		
SD relative to face ($Wm^{-1}K^{-1}$)	0.0053			0.0034		
Factor of anisotropy	0.9052					
Weighted average of the two faces ($Wm^{-1}K^{-1}$)	1.8011					
SD relative to the two faces ($Wm^{-1}K^{-1}$)	0.0028					

	THERMAL CONDUCTIVITY λ					
	Perpendicular			Parallel		
Sample / # set	42 / 1	42 / 2	42 / 3	42 / 4	42 / 5	42 / 6
Measure 1 ($Wm^{-1}K^{-1}$)	1.3906	1.4182	1.4858	1.4288	1.5414	1.5147
Measure 2 ($Wm^{-1}K^{-1}$)	1.3828	1.4286	1.5022	1.4524	1.5405	1.5329
Measure 3 ($Wm^{-1}K^{-1}$)	1.3996	1.4509	1.4981	1.4512	1.5340	1.5330
Measure 4 ($Wm^{-1}K^{-1}$)	1.4171	1.4634	1.5116	1.4610	1.5467	1.5380
Measure 5 ($Wm^{-1}K^{-1}$)	1.4096	1.4676	1.5075	1.4717	1.5519	1.5172
Measure 6 ($Wm^{-1}K^{-1}$)	1.4065	1.4754	1.5151	1.4936	1.5606	1.5339
Mean value for single point ($Wm^{-1}K^{-1}$)	1.4011	1.4507	1.5034	1.4598	1.5458	1.5283
SD relative to single point ($Wm^{-1}K^{-1}$)	0.0127	0.0228	0.0106	0.0218	0.0094	0.0098
Variance relative to single point $(Wm^{-1}K^{-1})^2$	0.000161	0.000519	0.000112	0.000474	0.000089	0.000095
Coefficient of variation %	0.906	1.571	0.705	1.492	0.611	0.638
Absolute accuracy ($Wm^{-1}K^{-1}$)	0.0183	0.0325	0.0176	0.0338	0.0148	0.0135
Accuracy %	1.30	2.24	1.17	2.31	0.96	0.89
Representative face value ($Wm^{-1}K^{-1}$)	1.4601			1.5305		
SD relative to face ($Wm^{-1}K^{-1}$)	0.0077			0.0065		
Factor of anisotropy	1.0482					
Weighted average of the two faces ($Wm^{-1}K^{-1}$)	1.5011					
SD relative to the two faces ($Wm^{-1}K^{-1}$)	0.0049					

	THERMAL CONDUCTIVITY λ					
	Perpendicular			Parallel		
Sample / # set	43 / 1	43 / 2	43 / 3	43 / 4	43 / 5	43 / 6
Measure 1 ($Wm^{-1}K^{-1}$)	1.7534	1.6150	1.7315	1.6614	1.8163	1.7591
Measure 2 ($Wm^{-1}K^{-1}$)	1.7412	1.6010	1.7419	1.6793	1.8238	1.7648
Measure 3 ($Wm^{-1}K^{-1}$)	1.7401	1.6217	1.7355	1.6797	1.8538	1.7609
Measure 4 ($Wm^{-1}K^{-1}$)	1.7390	1.6249	1.7361	1.6770	1.8370	1.7691
Measure 5 ($Wm^{-1}K^{-1}$)	1.7407	1.6345	1.7391	1.6908	1.8628	1.7736
Measure 6 ($Wm^{-1}K^{-1}$)	1.7503	1.6340	1.7424	1.6872	1.8563	1.7781
Mean value for single point ($Wm^{-1}K^{-1}$)	1.7441	1.6218	1.7377	1.6792	1.8417	1.7676
SD relative to single point ($Wm^{-1}K^{-1}$)	0.0061	0.0126	0.0042	0.0102	0.0190	0.0074
Variance relative to single point $(Wm^{-1}K^{-1})^2$	0.000037	0.000160	0.000017	0.000104	0.000359	0.000055
Coefficient of variation %	0.349	0.780	0.240	0.606	1.029	0.419
Absolute accuracy ($Wm^{-1}K^{-1}$)	0.0093	0.0209	0.0063	0.0178	0.0254	0.0105
Accuracy %	0.53	1.29	0.36	1.06	1.38	0.60
Representative face value ($Wm^{-1}K^{-1}$)	1.7316			1.7465		
SD relative to face ($Wm^{-1}K^{-1}$)	0.0033			0.0057		
Factor of anisotropy	1.0086					
Weighted average of the two faces ($Wm^{-1}K^{-1}$)	1.7354					
SD relative to the two faces ($Wm^{-1}K^{-1}$)	0.0029					

	THERMAL CONDUCTIVITY λ					
	Perpendicular			Parallel		
Sample / # set	11 / 1	11 / 2	11 / 3	11 / 4	11 / 5	11 / 6
Measure 1 ($Wm^{-1}K^{-1}$)	1.8188	1.9635	2.0094	1.8341	1.8576	1.9833
Measure 2 ($Wm^{-1}K^{-1}$)	1.8440	1.9598	2.0129	1.8693	1.8723	1.9859
Measure 3 ($Wm^{-1}K^{-1}$)	1.8731	1.9560	2.0174	1.8823	1.8896	1.9833
Measure 4 ($Wm^{-1}K^{-1}$)	1.8762	1.9791	2.0257	1.9041	1.8789	1.9977
Measure 5 ($Wm^{-1}K^{-1}$)	1.8898	1.9690	2.0323	1.9135	1.8908	2.0055
Measure 6 ($Wm^{-1}K^{-1}$)	1.9134	1.9878	2.0354	1.9270	1.9193	1.9976
Mean value for single point ($Wm^{-1}K^{-1}$)	1.8692	1.9692	2.0222	1.8884	1.8848	1.9922
SD relative to single point ($Wm^{-1}K^{-1}$)	0.0335	0.0121	0.0106	0.0338	0.0209	0.0093
Variance relative to single point $(Wm^{-1}K^{-1})^2$	0.001124	0.000147	0.000113	0.001143	0.000437	0.000087
Coefficient of variation %	1.793	0.616	0.525	1.790	1.109	0.468
Absolute accuracy ($Wm^{-1}K^{-1}$)	0.0504	0.0186	0.0133	0.0543	0.0346	0.0133
Accuracy %	2.70	0.94	0.66	2.87	1.83	0.67
Representative face value ($Wm^{-1}K^{-1}$)	1.9922			1.9692		
SD relative to face ($Wm^{-1}K^{-1}$)	0.0078			0.0083		
Factor of anisotropy	0.9885					
Weighted average of the two faces ($Wm^{-1}K^{-1}$)	1.9814					
SD relative to the two faces ($Wm^{-1}K^{-1}$)	0.0057					

	THERMAL CONDUCTIVITY λ					
	Perpendicular			Parallel		
Sample / # set	24 / 1	24 / 2	24 / 3	24 / 4	24 / 5	24 / 6
Measure 1 ($Wm^{-1}K^{-1}$)	1.5454	1.6600	1.7086	1.6652	1.7531	1.7755
Measure 2 ($Wm^{-1}K^{-1}$)	1.5559	1.6616	1.6899	1.6682	1.7808	1.7668
Measure 3 ($Wm^{-1}K^{-1}$)	1.5657	1.6846	1.6967	1.6773	1.7871	1.7837
Measure 4 ($Wm^{-1}K^{-1}$)	1.5610	1.6843	1.7119	1.6921	1.7828	1.8016
Measure 5 ($Wm^{-1}K^{-1}$)	1.5783	1.6856	1.7166	1.7169	1.8126	1.8046
Measure 6 ($Wm^{-1}K^{-1}$)	1.5741	1.6879	1.7026	1.7344	1.8043	1.8046
Mean value for single point ($Wm^{-1}K^{-1}$)	1.5634	1.6773	1.7044	1.6923	1.7868	1.7895
SD relative to single point ($Wm^{-1}K^{-1}$)	0.0120	0.0129	0.0099	0.0280	0.0208	0.0164
Variance relative to single point $(Wm^{-1}K^{-1})^2$	0.000145	0.000166	0.000099	0.000783	0.000432	0.000269
Coefficient of variation %	0.771	0.768	0.584	1.654	1.164	0.917
Absolute accuracy ($Wm^{-1}K^{-1}$)	0.0180	0.0173	0.0145	0.0420	0.0337	0.0227
Accuracy %	1.15	1.03	0.85	2.48	1.89	1.27
Representative face value ($Wm^{-1}K^{-1}$)	1.6551			1.7716		
SD relative to face ($Wm^{-1}K^{-1}$)	0.0066			0.0117		
Factor of anisotropy	1.0704					
Weighted average of the two faces ($Wm^{-1}K^{-1}$)	1.6832					
SD relative to the two faces ($Wm^{-1}K^{-1}$)	0.0057					

	THERMAL CONDUCTIVITY λ					
	Perpendicular			Parallel		
Sample / # set	46 / 1	46 / 2	46 / 3	46 / 4	46 / 5	46 / 6
Measure 1 ($Wm^{-1}K^{-1}$)	2.3392	2.3043	2.4636	2.4879	2.4646	2.4262
Measure 2 ($Wm^{-1}K^{-1}$)	2.3542	2.3145	2.5053	2.4941	2.4416	2.4231
Measure 3 ($Wm^{-1}K^{-1}$)	2.3451	2.3149	2.4884	2.5025	2.4788	2.4416
Measure 4 ($Wm^{-1}K^{-1}$)	2.3584	2.3176	2.4954	2.5124	2.4811	2.4348
Measure 5 ($Wm^{-1}K^{-1}$)	2.3550	2.3204	2.4904	2.5071	2.4765	2.4635
Measure 6 ($Wm^{-1}K^{-1}$)	2.3405	2.3184	2.4921	2.5069	2.4887	2.4424
Mean value for single point ($Wm^{-1}K^{-1}$)	2.3487	2.3150	2.4892	2.5018	2.4719	2.4386
SD relative to single point ($Wm^{-1}K^{-1}$)	0.0082	0.0057	0.0139	0.0092	0.0168	0.0145
Variance relative to single point $(Wm^{-1}K^{-1})^2$	0.000067	0.000033	0.000192	0.000084	0.000282	0.000211
Coefficient of variation %	0.348	0.247	0.557	0.367	0.679	0.596
Absolute accuracy ($Wm^{-1}K^{-1}$)	0.0097	0.0108	0.0256	0.0140	0.0303	0.0249
Accuracy %	0.41	0.46	1.03	0.56	1.23	1.02
Representative face value ($Wm^{-1}K^{-1}$)	2.3428			2.4817		
SD relative to face ($Wm^{-1}K^{-1}$)	0.0044			0.0070		
Factor of anisotropy	1.0593					
Weighted average of the two faces ($Wm^{-1}K^{-1}$)	2.3823					
SD relative to the two faces ($Wm^{-1}K^{-1}$)	0.0038					

	THERMAL CONDUCTIVITY λ					
	Perpendicular			Parallel		
Sample / # set	3 / 1	3 / 2	3 / 3	3 / 4	3 / 5	3 / 6
Measure 1 ($Wm^{-1}K^{-1}$)	2.9036	2.6977	2.6637	2.5473	2.6245	2.3766
Measure 2 ($Wm^{-1}K^{-1}$)	2.9081	2.6857	2.6800	2.5629	2.6432	2.5017
Measure 3 ($Wm^{-1}K^{-1}$)	2.9183	2.7161	2.6868	2.5752	2.6579	2.4944
Measure 4 ($Wm^{-1}K^{-1}$)	2.9072	2.7091	2.6830	2.5828	2.6671	2.5177
Measure 5 ($Wm^{-1}K^{-1}$)	2.9114	2.7319	2.6790	2.5907	2.6766	2.5212
Measure 6 ($Wm^{-1}K^{-1}$)	2.9203	2.7364	2.6935	2.5682	2.6496	2.5251
Mean value for single point ($Wm^{-1}K^{-1}$)	2.9115	2.7128	2.6810	2.5712	2.6531	2.4894
SD relative to single point ($Wm^{-1}K^{-1}$)	0.0066	0.0196	0.0100	0.0154	0.0185	0.0565
Variance relative to single point $(Wm^{-1}K^{-1})^2$	0.000043	0.000383	0.000100	0.000236	0.000340	0.003198
Coefficient of variation %	0.226	0.721	0.372	0.598	0.695	2.271
Absolute accuracy ($Wm^{-1}K^{-1}$)	0.0088	0.0271	0.0173	0.0239	0.0286	0.1129
Accuracy %	0.30	1.00	0.64	0.93	1.08	4.53
Representative face value ($Wm^{-1}K^{-1}$)	2.8323			2.5999		
SD relative to face ($Wm^{-1}K^{-1}$)	0.0053			0.0116		
Factor of anisotropy	0.9180					
Weighted average of the two faces ($Wm^{-1}K^{-1}$)	2.7921					
SD relative to the two faces ($Wm^{-1}K^{-1}$)	0.0048					

	THERMAL CONDUCTIVITY λ					
	Perpendicular			Parallel		
Sample / # set	25 / 1	25 / 2	25 / 3	25 / 4	25 / 5	25 / 6
Measure 1 ($Wm^{-1}K^{-1}$)	2.5168	2.9350	2.5695	2.6543	2.9131	2.7363
Measure 2 ($Wm^{-1}K^{-1}$)	2.5248	2.9686	2.5537	2.6793	2.9275	2.7398
Measure 3 ($Wm^{-1}K^{-1}$)	2.5266	2.9883	2.5584	2.6745	2.8974	2.7432
Measure 4 ($Wm^{-1}K^{-1}$)	2.5266	2.9752	2.5584	2.7124	2.9142	2.7403
Measure 5 ($Wm^{-1}K^{-1}$)	2.5329	2.9797	2.5778	2.6994	2.9096	2.7359
Measure 6 ($Wm^{-1}K^{-1}$)	2.5603	3.0054	2.5763	2.6864	2.9189	2.7678
Mean value for single point ($Wm^{-1}K^{-1}$)	2.5313	2.9753	2.5657	2.6844	2.9134	2.7439
SD relative to single point ($Wm^{-1}K^{-1}$)	0.0151	0.0235	0.0102	0.0202	0.0100	0.0121
Variance relative to single point $(Wm^{-1}K^{-1})^2$	0.000228	0.000553	0.000105	0.000409	0.000100	0.000145
Coefficient of variation %	0.596	0.790	0.399	0.753	0.344	0.439
Absolute accuracy ($Wm^{-1}K^{-1}$)	0.0289	0.0404	0.0121	0.0301	0.0161	0.0240
Accuracy %	1.14	1.36	0.47	1.12	0.55	0.87
Representative face value ($Wm^{-1}K^{-1}$)	2.6032			2.8240		
SD relative to face ($Wm^{-1}K^{-1}$)	0.0080			0.0072		
Factor of anisotropy	1.0848					
Weighted average of the two faces ($Wm^{-1}K^{-1}$)	2.7248					
SD relative to the two faces ($Wm^{-1}K^{-1}$)	0.0053					

	THERMAL CONDUCTIVITY λ					
	Perpendicular			Parallel		
Sample / # set	47 / 1	47 / 2	47 / 3	47 / 4	47 / 5	47 / 6
Measure 1 ($Wm^{-1}K^{-1}$)	1.8445	1.8113	1.8890	2.2689	2.3751	2.4168
Measure 2 ($Wm^{-1}K^{-1}$)	1.8777	1.8281	1.8916	2.2719	2.3872	2.4105
Measure 3 ($Wm^{-1}K^{-1}$)	1.8682	1.8345	1.8936	2.2888	2.3682	2.3993
Measure 4 ($Wm^{-1}K^{-1}$)	1.8717	1.8545	1.8771	2.2935	2.4010	2.4139
Measure 5 ($Wm^{-1}K^{-1}$)	1.8887	1.8587	1.8951	2.2918	2.3864	2.4179
Measure 6 ($Wm^{-1}K^{-1}$)	1.8951	1.8616	1.8999	2.2997	2.4013	2.4347
Mean value for single point ($Wm^{-1}K^{-1}$)	1.8743	1.8414	1.8910	2.2858	2.3865	2.4155
SD relative to single point ($Wm^{-1}K^{-1}$)	0.0178	0.0200	0.0077	0.0125	0.0134	0.0115
Variance relative to single point $(Wm^{-1}K^{-1})^2$	0.000317	0.000402	0.000060	0.000156	0.000179	0.000133
Coefficient of variation %	0.949	1.088	0.410	0.546	0.561	0.477
Absolute accuracy ($Wm^{-1}K^{-1}$)	0.0298	0.0301	0.0140	0.0169	0.0183	0.0191
Accuracy %	1.59	1.64	0.74	0.74	0.77	0.79
Representative face value ($Wm^{-1}K^{-1}$)	1.8831			2.3645		
SD relative to face ($Wm^{-1}K^{-1}$)	0.0067			0.0072		
Factor of anisotropy	1.2556					
Weighted average of the two faces ($Wm^{-1}K^{-1}$)	2.1078					
SD relative to the two faces ($Wm^{-1}K^{-1}$)	0.0049					

Measure to confirm the anysotropy for 47	THERMAL CONDUCTIVITY λ					
	Perpendicular			Parallel		
Sample / # set	47 / 1	47 / 2	47 / 3	47 / 4	47 / 5	47 / 6
Measure 1 ($Wm^{-1}K^{-1}$)	1.8365	1.6233	1.7977	2.2363	2.1146	2.1650
Measure 2 ($Wm^{-1}K^{-1}$)	1.8291	1.6256	1.7991	2.2489	2.1139	2.1738
Measure 3 ($Wm^{-1}K^{-1}$)	1.8344	1.6535	1.8144	2.2494	2.1377	2.1851
Measure 4 ($Wm^{-1}K^{-1}$)	1.8501	1.6456	1.8268	2.2683	2.1493	2.1853
Measure 5 ($Wm^{-1}K^{-1}$)	1.8526	1.6454	1.8406	2.2864	2.1512	2.1888
Measure 6 ($Wm^{-1}K^{-1}$)	1.8802	1.6700	1.8179	2.2927	2.1498	2.1975
Mean value for single point ($Wm^{-1}K^{-1}$)	1.8472	1.6439	1.8161	2.2637	2.1361	2.1826
SD relative to single point ($Wm^{-1}K^{-1}$)	0.0186	0.0175	0.0164	0.0226	0.0176	0.0115
Variance relative to single point $(Wm^{-1}K^{-1})^2$	0.000347	0.000308	0.000270	0.000512	0.000310	0.000133
Coefficient of variation %	1.008	1.067	0.905	0.999	0.824	0.528
Absolute accuracy ($Wm^{-1}K^{-1}$)	0.0331	0.0261	0.0245	0.0291	0.0222	0.0176
Accuracy %	1.79	1.59	1.35	1.28	1.04	0.81
Representative face value ($Wm^{-1}K^{-1}$)	1.7683			2.1833		
SD relative to face ($Wm^{-1}K^{-1}$)	0.0101			0.0089		
Factor of anisotropy	1.2346					
Weighted average of the two faces ($Wm^{-1}K^{-1}$)	2.0023					
SD relative to the two faces ($Wm^{-1}K^{-1}$)	0.0067					

	THERMAL CONDUCTIVITY λ					
	Perpendicular			Parallel		
Sample / # set	6A / 1	6A / 2	6A / 3	6A / 4	6A / 5	6A / 6
Measure 1 ($Wm^{-1}K^{-1}$)	2.5915	2.3177	2.5144	2.4898	2.3629	2.5214
Measure 2 ($Wm^{-1}K^{-1}$)	2.6204	2.3437	2.5278	2.5524	2.3981	2.5218
Measure 3 ($Wm^{-1}K^{-1}$)	2.6440	2.4498	2.5418	2.5876	2.4050	2.5439
Measure 4 ($Wm^{-1}K^{-1}$)	2.6860	2.4526	2.5504	2.5926	2.4320	2.5587
Measure 5 ($Wm^{-1}K^{-1}$)	2.6904	2.4672	2.5641	2.6031	2.4423	2.5774
Measure 6 ($Wm^{-1}K^{-1}$)	2.7457	2.4571	2.5711	2.5956	2.4635	2.5803
Mean value for single point ($Wm^{-1}K^{-1}$)	2.6630	2.4147	2.5449	2.5702	2.4173	2.5506
SD relative to single point ($Wm^{-1}K^{-1}$)	0.0555	0.0658	0.0215	0.0431	0.0359	0.0261
Variance relative to single point $(Wm^{-1}K^{-1})^2$	0.003081	0.004335	0.000464	0.001861	0.001291	0.000680
Coefficient of variation %	2.084	2.727	0.846	1.679	1.486	1.022
Absolute accuracy ($Wm^{-1}K^{-1}$)	0.0827	0.0970	0.0305	0.0804	0.0544	0.0297
Accuracy %	3.10	4.02	1.20	3.13	2.25	1.17
Representative face value ($Wm^{-1}K^{-1}$)	2.5480			2.5173		
SD relative to face ($Wm^{-1}K^{-1}$)	0.0192			0.0190		
Factor of anisotropy	0.9879					
Weighted average of the two faces ($Wm^{-1}K^{-1}$)	2.5324					
SD relative to the two faces ($Wm^{-1}K^{-1}$)	0.0135					

	THERMAL CONDUCTIVITY λ					
	Perpendicular			Parallel		
Sample / # set	8 / 1	8 / 2	8 / 3	8 / 4	8 / 5	8 / 6
Measure 1 ($Wm^{-1}K^{-1}$)	2.8922	2.8719	2.8965	2.7955	2.7768	3.0212
Measure 2 ($Wm^{-1}K^{-1}$)	2.8855	2.8964	2.8924	2.7955	2.7719	3.0607
Measure 3 ($Wm^{-1}K^{-1}$)	2.9177	2.9100	2.9167	2.8141	2.8469	3.0336
Measure 4 ($Wm^{-1}K^{-1}$)	2.9312	2.9106	2.9123	2.7964	2.8621	3.0447
Measure 5 ($Wm^{-1}K^{-1}$)	2.9278	2.9052	2.9002	2.8065	2.8895	3.0359
Measure 6 ($Wm^{-1}K^{-1}$)	2.9663	2.8883	2.9025	2.8392	2.8932	3.0196
Mean value for single point ($Wm^{-1}K^{-1}$)	2.9201	2.8971	2.9034	2.8079	2.8401	3.0360
SD relative to single point ($Wm^{-1}K^{-1}$)	0.0293	0.0150	0.0093	0.0171	0.0538	0.0154
Variance relative to single point $(Wm^{-1}K^{-1})^2$	0.000860	0.000226	0.000087	0.000292	0.002890	0.000236
Coefficient of variation %	1.004	0.519	0.321	0.609	1.893	0.506
Absolute accuracy ($Wm^{-1}K^{-1}$)	0.0462	0.0252	0.0133	0.0314	0.0682	0.0248
Accuracy %	1.58	0.87	0.46	1.12	2.40	0.82
Representative face value ($Wm^{-1}K^{-1}$)	2.9029			2.9301		
SD relative to face ($Wm^{-1}K^{-1}$)	0.0076			0.0112		
Factor of anisotropy	1.0094					
Weighted average of the two faces ($Wm^{-1}K^{-1}$)	2.9116					
SD relative to the two faces ($Wm^{-1}K^{-1}$)	0.0063					

	THERMAL CONDUCTIVITY λ					
	Perpendicular			Parallel		
Sample / # set	27A / 1	27A / 2	27A / 3	27A / 4	27A / 5	27A / 6
Measure 1 ($Wm^{-1}K^{-1}$)	2.5112	2.5474	2.5653	2.4295	2.5258	2.5815
Measure 2 ($Wm^{-1}K^{-1}$)	2.5133	2.5332	2.5854	2.4685	2.5472	2.6023
Measure 3 ($Wm^{-1}K^{-1}$)	2.5372	2.5513	2.5891	2.4957	2.5614	2.6257
Measure 4 ($Wm^{-1}K^{-1}$)	2.5200	2.5431	2.5870	2.5079	2.5795	2.5954
Measure 5 ($Wm^{-1}K^{-1}$)	2.5370	2.5312	2.6024	2.5410	2.5746	2.6095
Measure 6 ($Wm^{-1}K^{-1}$)	2.5396	2.5372	2.5814	2.5383	2.5782	2.6061
Mean value for single point ($Wm^{-1}K^{-1}$)	2.5264	2.5406	2.5851	2.4968	2.5611	2.6034
SD relative to single point ($Wm^{-1}K^{-1}$)	0.0130	0.0080	0.0120	0.0427	0.0212	0.0148
Variance relative to single point $(Wm^{-1}K^{-1})^2$	0.000170	0.000064	0.000144	0.001826	0.000450	0.000218
Coefficient of variation %	0.515	0.315	0.465	1.711	0.828	0.567
Absolute accuracy ($Wm^{-1}K^{-1}$)	0.0152	0.0107	0.0198	0.0673	0.0353	0.0223
Accuracy %	0.60	0.42	0.76	2.70	1.38	0.86
Representative face value ($Wm^{-1}K^{-1}$)	2.5485			2.5827		
SD relative to face ($Wm^{-1}K^{-1}$)	0.0059			0.0117		
Factor of anisotropy	1.0134					
Weighted average of the two faces ($Wm^{-1}K^{-1}$)	2.5555					
SD relative to the two faces ($Wm^{-1}K^{-1}$)	0.0053					

	THERMAL CONDUCTIVITY λ					
	Perpendicular			Parallel		
Sample / # set	10B / 1	10B / 2	10B / 3	10B / 4	10B / 5	10B / 6
Measure 1 ($Wm^{-1}K^{-1}$)	3.2158	3.0688	3.3280	2.9198	3.0339	3.0959
Measure 2 ($Wm^{-1}K^{-1}$)	3.2422	3.0716	3.3512	2.9109	3.0609	3.0738
Measure 3 ($Wm^{-1}K^{-1}$)	3.2456	3.0854	3.3808	2.9179	3.0423	3.0685
Measure 4 ($Wm^{-1}K^{-1}$)	3.2263	3.0957	3.3583	2.9350	3.0564	3.0797
Measure 5 ($Wm^{-1}K^{-1}$)	3.2266	3.1789	3.3758	2.9530	3.0501	3.0762
Measure 6 ($Wm^{-1}K^{-1}$)	3.2248	3.1907	3.3804	2.9315	3.0478	3.0962
Mean value for single point ($Wm^{-1}K^{-1}$)	3.2302	3.1152	3.3624	2.9280	3.0486	3.0817
SD relative to single point ($Wm^{-1}K^{-1}$)	0.0114	0.0549	0.0208	0.0151	0.0097	0.0117
Variance relative to single point $(Wm^{-1}K^{-1})^2$	0.000130	0.003015	0.000433	0.000229	0.000094	0.000137
Coefficient of variation %	0.353	1.763	0.619	0.517	0.318	0.380
Absolute accuracy ($Wm^{-1}K^{-1}$)	0.0154	0.0755	0.0344	0.0250	0.0147	0.0145
Accuracy %	0.48	2.42	1.02	0.85	0.48	0.47
Representative face value ($Wm^{-1}K^{-1}$)	3.2560			3.0358		
SD relative to face ($Wm^{-1}K^{-1}$)	0.0098			0.0067		
Factor of anisotropy	0.9324					
Weighted average of the two faces ($Wm^{-1}K^{-1}$)	3.1057					
SD relative to the two faces ($Wm^{-1}K^{-1}$)	0.0055					

	THERMAL CONDUCTIVITY λ					
	Perpendicular			Parallel		
Sample / # set	34 / 1	34 / 2	34 / 3	34 / 4	34 / 5	34 / 6
Measure 1 ($Wm^{-1}K^{-1}$)	2.8000	3.0068	2.9566	2.8054	2.8851	2.8232
Measure 2 ($Wm^{-1}K^{-1}$)	2.8139	2.9890	2.9838	2.8123	2.9070	2.8338
Measure 3 ($Wm^{-1}K^{-1}$)	2.8293	3.0180	2.9873	2.8123	2.8973	2.8592
Measure 4 ($Wm^{-1}K^{-1}$)	2.8332	3.0081	2.9816	2.8356	2.9314	2.8647
Measure 5 ($Wm^{-1}K^{-1}$)	2.8647	3.0132	3.0250	2.8408	2.9186	2.8635
Measure 6 ($Wm^{-1}K^{-1}$)	2.8384	3.0078	3.0074	2.8379	2.9310	2.8834
Mean value for single point ($Wm^{-1}K^{-1}$)	2.8299	3.0071	2.9903	2.8241	2.9117	2.8546
SD relative to single point ($Wm^{-1}K^{-1}$)	0.0221	0.0098	0.0235	0.0157	0.0187	0.0221
Variance relative to single point $(Wm^{-1}K^{-1})^2$	0.000488	0.000097	0.000552	0.000247	0.000349	0.000490
Coefficient of variation %	0.780	0.328	0.786	0.556	0.641	0.775
Absolute accuracy ($Wm^{-1}K^{-1}$)	0.0347	0.0181	0.0347	0.0187	0.0266	0.0314
Accuracy %	1.23	0.60	1.16	0.66	0.91	1.10
Representative face value ($Wm^{-1}K^{-1}$)	2.9793			2.8591		
SD relative to face ($Wm^{-1}K^{-1}$)	0.0084			0.0106		
Factor of anisotropy	0.9596					
Weighted average of the two faces ($Wm^{-1}K^{-1}$)	2.9327					
SD relative to the two faces ($Wm^{-1}K^{-1}$)	0.0066					

	THERMAL CONDUCTIVITY λ					
	Perpendicular			Parallel		
Sample / # set	35 / 1	35 / 2	35 / 3	35 / 4	35 / 5	35 / 6
Measure 1 ($Wm^{-1}K^{-1}$)	2.9719	3.0981	3.1089	3.0089	3.1746	3.0650
Measure 2 ($Wm^{-1}K^{-1}$)	2.9901	3.0845	3.1185	3.0124	3.1633	3.0735
Measure 3 ($Wm^{-1}K^{-1}$)	3.0093	3.0935	3.1170	3.0355	3.1446	3.0742
Measure 4 ($Wm^{-1}K^{-1}$)	2.9997	3.1008	3.0913	3.0111	3.1861	3.0824
Measure 5 ($Wm^{-1}K^{-1}$)	2.9764	3.1105	3.0900	3.0288	3.1851	3.0710
Measure 6 ($Wm^{-1}K^{-1}$)	3.0010	3.0920	3.0820	3.0426	3.2006	3.0973
Mean value for single point ($Wm^{-1}K^{-1}$)	2.9914	3.0966	3.1013	3.0232	3.1757	3.0772
SD relative to single point ($Wm^{-1}K^{-1}$)	0.0148	0.0088	0.0155	0.0143	0.0197	0.0113
Variance relative to single point $(Wm^{-1}K^{-1})^2$	0.000218	0.000078	0.000240	0.000205	0.000388	0.000128
Coefficient of variation %	0.494	0.285	0.500	0.474	0.621	0.368
Absolute accuracy ($Wm^{-1}K^{-1}$)	0.0195	0.0139	0.0193	0.0194	0.0311	0.0201
Accuracy %	0.65	0.45	0.62	0.64	0.98	0.65
Representative face value ($Wm^{-1}K^{-1}$)	3.0751			3.0766		
SD relative to face ($Wm^{-1}K^{-1}$)	0.0068			0.0081		
Factor of anisotropy	1.0005					
Weighted average of the two faces ($Wm^{-1}K^{-1}$)	3.0757					
SD relative to the two faces ($Wm^{-1}K^{-1}$)	0.0052					

Annex II. Complete sets analysis

In this Annex are reported the results of calculations made on thermal conductivity for validated sets. For every rocks are here considered 8 set of acquisition which are used only for ste study related to accuracy and precision: all thermal properties are calculated using validated set (6 acquisition for set). In the next formula the subscript "j" identify the single set (in particular "j" ranges from 1 to 6 if all sets are considered; ranges from1 to 3 for perpendicular sets made with respect the stratification and from 4 to 6 for sets parallel with respect the stratification).
The lines called "First refused measure, second refused measure and Measure 1,2,3,4,5,6" are the 8 acquisitions for a complete set, the index associated at different acquisition of same test will be indentify with subscript "i" in the next formulas.
The line mean value of single point is the arithmetic mean of the previous six acquisition, while SD relative to single point is the standard deviation.
In particular, mean (μ_j) is calculated for every "j" set as:

$\mu_j = \frac{1}{8} \sum_{i=1}^{8} x_i \qquad \left(\frac{W}{m\,K}\right)$	1

Where x_i is the value of the single acquisition within the same set. Standard deviation for single set (σ_j) is calculated as:

$\sigma_j = \sqrt{\frac{\sum_{i=1}^{6}(x_i - \mu_j)^2}{N-1}} \qquad \left(\frac{W}{m\,K}\right)$	2

Where N=8.

The Variance (VAR) relative to single set is calculated as the square of standard deviation:

$VAR_j = \sigma_j^2 \qquad \left(\frac{W}{m\,K}\right)^2$	3

The coefficient of variation (Cv) is calculated for every set "j" as:

$Cv_j = \frac{\sigma_j}{\mu_j} * 100$	4

The absolute accuracy for every "j" set is calculated as:

$A_j = max \sum_{i=i}^{8} \lvert x_i - \mu_j \rvert$	5

Where x_0 is the "true" value of the quantity measured. As indicated in Chapter 6, the true value are identify with the mean value calculated foe every set μ_j.

The Accuracy % is determinate for every "j" set as:

$$A_j\% = \frac{A_j}{\mu_j} * 100 \qquad (6)$$

The different formulas are provided by: Bramanti 1997; Cremonini et al., 2009; Abdì, 2010; Ciroi, 2014

The representative value of thermal conductivity for single face are not calculated: the valid values are reported in Annex I.

	THERMAL CONDUCTIVITY (λ)					
	Perpendicular			Parallel		
Sample / # measure position	1 / 1	1 / 2	1 / 3	1 / 4	1 / 5	1 / 6
First refused measure	1.54	1.68	1.47	1.45	1.49	1.59
Second refused measure	1.61	1.69	1.53	1.45	1.49	1.59
Measure 1 ($Wm^{-1}K^{-1}$)	1.6165	1.68	1.55	1.47	1.50	1.59
Measure 2 ($Wm^{-1}K^{-1}$)	1.6365	1.71	1.57	1.48	1.50	1.58
Measure 3 ($Wm^{-1}K^{-1}$)	1.6388	1.70	1.58	1.49	1.51	1.59
Measure 4 ($Wm^{-1}K^{-1}$)	1.6457	1.71	1.59	1.48	1.49	1.60
Measure 5 ($Wm^{-1}K^{-1}$)	1.6462	1.71	1.58	1.49	1.51	1.61
Measure 6 ($Wm^{-1}K^{-1}$)	1.6539	1.71	1.60	1.51	1.52	1.61
Mean value for single point ($Wm^{-1}K^{-1}$)	1.6238	1.6984	1.5576	1.4789	1.5019	1.5955
SD relative to single point ($Wm^{-1}K^{-1}$)	0.04	0.01	0.04	0.02	0.01	0.01
Variance relative to single point $(Wm^{-1}K^{-1})^2$	0.001379	0.000200	0.001693	0.000383	0.000132	0.000118
Coefficient of variation %	2.29	0.83	2.64	1.32	0.76	0.68
Absolute accuracy ($Wm^{-1}K^{-1}$)	0.0850	0.0199	0.0852	0.0309	0.0220	0.0182
Accuracy %	5.24	1.17	5.47	2.09	1.46	1.14

	THERMAL CONDUCTIVITY (λ)					
	Perpendicular			Parallel		
Sample / # measure position	22B / 1	22B / 2	22B / 3	22B / 4	22B / 5	22B / 6
First refused measure	1.2196	1.3393	1.3893	1.3628	1.4204	1.1401
Second refused measure	1.2386	1.3432	1.3827	1.3633	1.4317	1.1886
Measure 1 ($Wm^{-1}K^{-1}$)	1.2361	1.3515	1.3962	1.3685	1.4342	1.2010
Measure 2 ($Wm^{-1}K^{-1}$)	1.2499	1.3648	1.4107	1.3735	1.4336	1.2221
Measure 3 ($Wm^{-1}K^{-1}$)	1.2525	1.3687	1.4220	1.3958	1.4428	1.2144
Measure 4 ($Wm^{-1}K^{-1}$)	1.2667	1.3606	1.4267	1.4012	1.4535	1.2274
Measure 5 ($Wm^{-1}K^{-1}$)	1.2650	1.3670	1.4315	1.4067	1.4630	1.2377
Measure 6 ($Wm^{-1}K^{-1}$)	1.2823	1.3752	1.4356	1.3978	1.4607	1.2410
Mean value for single point ($Wm^{-1}K^{-1}$)	1.2513	1.3588	1.4118	1.3837	1.4425	1.2090
SD relative to single point ($Wm^{-1}K^{-1}$)	0.0199	0.0128	0.0203	0.0184	0.0152	0.0330
Variance relative to single point $(Wm^{-1}K^{-1})^2$	0.000398	0.000165	0.000412	0.000338	0.000232	0.001088
Coefficient of variation %	1.593	0.945	1.438	1.329	1.057	2.728
Absolute accuracy ($Wm^{-1}K^{-1}$)	0.0317	0.0195	0.0292	0.0230	0.0221	0.0690
Accuracy %	2.53	1.44	2.07	1.66	1.53	5.70

	THERMAL CONDUCTIVITY (λ)					
	Perpendicular			Parallel		
Sample / # measure position	44 / 1	44 / 2	44 / 3	44 / 4	44 / 5	44 / 6
First refused measure	1.4458	1.3886	1.3846	1.2525	1.4106	1.4366
Second refused measure	1.4654	1.4002	1.4141	1.2926	1.4306	1.4469
Measure 1 ($Wm^{-1}K^{-1}$)	1.4725	1.4241	1.4331	1.3050	1.4236	1.4453
Measure 2 ($Wm^{-1}K^{-1}$)	1.4776	1.4263	1.4304	1.3249	1.4413	1.4459
Measure 3 ($Wm^{-1}K^{-1}$)	1.4895	1.4506	1.4423	1.3314	1.4384	1.4460
Measure 4 ($Wm^{-1}K^{-1}$)	1.4910	1.4260	1.4489	1.3431	1.4407	1.4558
Measure 5 ($Wm^{-1}K^{-1}$)	1.5044	1.4473	1.4566	1.3474	1.4446	1.4646
Measure 6 ($Wm^{-1}K^{-1}$)	1.5146	1.4622	1.4400	1.3558	1.4390	1.4618
Mean value for single point ($Wm^{-1}K^{-1}$)	1.4826	1.4282	1.4313	1.3191	1.4336	1.4504
SD relative to single point ($Wm^{-1}K^{-1}$)	0.0220	0.0251	0.0228	0.0343	0.0115	0.0095
Variance relative to single point $(Wm^{-1}K^{-1})^2$	0.000485	0.000628	0.000518	0.001179	0.000131	0.000090
Coefficient of variation %	1.486	1.755	1.591	2.603	0.800	0.654
Absolute accuracy ($Wm^{-1}K^{-1}$)	0.0368	0.0395	0.0467	0.0666	0.0230	0.0142
Accuracy %	2.48	2.77	3.26	5.05	1.60	0.98

	THERMAL CONDUCTIVITY (λ)					
	Perpendicular			Parallel		
Sample / # measure position	16 / 1	16 / 2	16 / 3	16 / 4	16 / 5	16 / 6
First refused measure	1.7507	1.4920	1.6051	1.6492	1.7318	1.7448
Second refused measure	1.7569	1.5818	1.6166	1.6704	1.7187	1.7560
Measure 1 ($Wm^{-1}K^{-1}$)	1.7485	1.5816	1.6127	1.6832	1.7213	1.7892
Measure 2 ($Wm^{-1}K^{-1}$)	1.7639	1.5898	1.6210	1.6945	1.7357	1.7767
Measure 3 ($Wm^{-1}K^{-1}$)	1.7705	1.5853	1.6165	1.6922	1.7409	1.7755
Measure 4 ($Wm^{-1}K^{-1}$)	1.7699	1.5992	1.6215	1.7011	1.7436	1.7838
Measure 5 ($Wm^{-1}K^{-1}$)	1.7776	1.6006	1.6164	1.7201	1.7566	1.7924
Measure 6 ($Wm^{-1}K^{-1}$)	1.7997	1.6087	1.6238	1.7090	1.7413	1.7944
Mean value for single point ($Wm^{-1}K^{-1}$)	1.7672	1.5799	1.6167	1.6900	1.7362	1.7766
SD relative to single point ($Wm^{-1}K^{-1}$)	0.0166	0.0368	0.0059	0.0224	0.0123	0.0178
Variance relative to single point $(Wm^{-1}K^{-1})^2$	0.000274	0.001354	0.000035	0.000502	0.000152	0.000316
Coefficient of variation %	0.937	2.329	0.365	1.325	0.710	1.000
Absolute accuracy ($Wm^{-1}K^{-1}$)	0.0325	0.0878	0.0116	0.0408	0.0204	0.0318
Accuracy %	1.84	5.56	0.72	2.41	1.17	1.79

	THERMAL CONDUCTIVITY (λ)					
	Perpendicular			Parallel		
Sample / # measure position	36 / 1	36 / 2	36 / 3	36 / 4	36 / 5	36 / 6
First refused measure	1.3084	1.4128	1.3439	1.2575	1.4027	1.3290
Second refused measure	1.3581	1.4264	1.3771	1.3232	1.4116	1.3463
Measure 1 ($Wm^{-1}K^{-1}$)	1.3805	1.4339	1.4036	1.3669	1.4313	1.3592
Measure 2 ($Wm^{-1}K^{-1}$)	1.4080	1.4461	1.4197	1.4002	1.4532	1.3842
Measure 3 ($Wm^{-1}K^{-1}$)	1.4262	1.4343	1.4296	1.4356	1.4649	1.4059
Measure 4 ($Wm^{-1}K^{-1}$)	1.4496	1.4460	1.4377	1.4570	1.4926	1.4250
Measure 5 ($Wm^{-1}K^{-1}$)	1.4696	1.4410	1.4662	1.4721	1.5153	1.4341
Measure 6 ($Wm^{-1}K^{-1}$)	1.4899	1.4447	1.4766	1.4965	1.5125	1.4580
Mean value for single point ($Wm^{-1}K^{-1}$)	1.4113	1.4357	1.4193	1.4011	1.4605	1.3927
SD relative to single point ($Wm^{-1}K^{-1}$)	0.0605	0.0116	0.0441	0.0814	0.0437	0.0457
Variance relative to single point $(Wm^{-1}K^{-1})^2$	0.003664	0.000134	0.001948	0.006619	0.001913	0.002085
Coefficient of variation %	4.289	0.807	3.110	5.806	2.995	3.279
Absolute accuracy ($Wm^{-1}K^{-1}$)	0.1029	0.0228	0.0754	0.1436	0.0578	0.0653
Accuracy %	7.29	1.59	5.31	10.25	3.96	4.69

	THERMAL CONDUCTIVITY (λ)					
	Perpendicular			Parallel		
Sample / # measure position	39 / 1	39 / 2	39 / 3	39 / 4	39 / 5	39 / 6
First refused measure	1.4473	1.3165	1.5052	1.4715	1.5535	1.3822
Second refused measure	1.4869	1.3486	1.5175	1.4909	1.5628	1.4019
Measure 1 ($Wm^{-1}K^{-1}$)	1.5194	1.3827	1.5406	1.5119	1.5603	1.4027
Measure 2 ($Wm^{-1}K^{-1}$)	1.5256	1.3907	1.5584	1.5230	1.5660	1.4069
Measure 3 ($Wm^{-1}K^{-1}$)	1.5305	1.4125	1.5862	1.5333	1.5622	1.4006
Measure 4 ($Wm^{-1}K^{-1}$)	1.5453	1.4426	1.5936	1.5417	1.5730	1.3960
Measure 5 ($Wm^{-1}K^{-1}$)	1.5405	1.4370	1.6091	1.5370	1.5697	1.3948
Measure 6 ($Wm^{-1}K^{-1}$)	1.5415	1.4532	1.6096	1.5571	1.5685	1.3872
Mean value for single point ($Wm^{-1}K^{-1}$)	1.5171	1.3980	1.5650	1.5208	1.5645	1.3965
SD relative to single point ($Wm^{-1}K^{-1}$)	0.0338	0.0480	0.0408	0.0282	0.0062	0.0083
Variance relative to single point $(Wm^{-1}K^{-1})^2$	0.001140	0.002303	0.001667	0.000797	0.000038	0.000070
Coefficient of variation %	2.226	3.433	2.609	1.856	0.393	0.598
Absolute accuracy ($Wm^{-1}K^{-1}$)	0.0698	0.0815	0.0598	0.0493	0.0110	0.0144
Accuracy %	4.60	5.83	3.82	3.24	0.71	1.03

	THERMAL CONDUCTIVITY (λ)					
	Perpendicular			Parallel		
Sample / # measure position	18 / 1	18 / 2	18 / 3	18 / 4	18 / 5	18 / 6
First refused measure	1.7201	1.9332	1.9014	1.6423	1.7522	1.7963
Second refused measure	1.7319	1.9172	1.9206	1.6483	1.7596	1.8250
Measure 1 ($Wm^{-1}K^{-1}$)	1.7523	1.9424	1.9451	1.6446	1.7589	1.8141
Measure 2 ($Wm^{-1}K^{-1}$)	1.7500	1.9484	1.9470	1.6465	1.7655	1.8360
Measure 3 ($Wm^{-1}K^{-1}$)	1.7497	1.9419	1.9491	1.6623	1.7633	1.8359
Measure 4 ($Wm^{-1}K^{-1}$)	1.7702	1.9522	1.9656	1.6597	1.7609	1.8575
Measure 5 ($Wm^{-1}K^{-1}$)	1.7874	1.9427	1.9679	1.6601	1.7699	1.8390
Measure 6 ($Wm^{-1}K^{-1}$)	1.7822	1.9569	1.9766	1.6622	1.7644	1.8568
Mean value for single point ($Wm^{-1}K^{-1}$)	1.7555	1.9419	1.9467	1.6532	1.7618	1.8326
SD relative to single point ($Wm^{-1}K^{-1}$)	0.0234	0.0123	0.0252	0.0086	0.0053	0.0207
Variance relative to single point $(Wm^{-1}K^{-1})^2$	0.000547	0.000152	0.000634	0.000073	0.000028	0.000427
Coefficient of variation %	1.333	0.634	1.293	0.518	0.299	1.127
Absolute accuracy ($Wm^{-1}K^{-1}$)	0.0354	0.0247	0.0453	0.0109	0.0097	0.0363
Accuracy %	2.01	1.27	2.33	0.66	0.55	1.98

	THERMAL CONDUCTIVITY (λ)					
	Perpendicular			Parallel		
Sample / # measure position	42 / 1	42 / 2	42 / 3	42 / 4	42 / 5	42 / 6
First refused measure	1.3441	1.3481	1.4756	1.3074	1.5283	1.5089
Second refused measure	1.3797	1.4117	1.4873	1.3922	1.5309	1.5195
Measure 1 ($Wm^{-1}K^{-1}$)	1.3906	1.4182	1.4858	1.4288	1.5414	1.5147
Measure 2 ($Wm^{-1}K^{-1}$)	1.3828	1.4286	1.5022	1.4524	1.5405	1.5329
Measure 3 ($Wm^{-1}K^{-1}$)	1.3996	1.4509	1.4981	1.4512	1.5340	1.5330
Measure 4 ($Wm^{-1}K^{-1}$)	1.4171	1.4634	1.5116	1.4610	1.5467	1.5380
Measure 5 ($Wm^{-1}K^{-1}$)	1.4096	1.4676	1.5075	1.4717	1.5519	1.5172
Measure 6 ($Wm^{-1}K^{-1}$)	1.4065	1.4754	1.5151	1.4936	1.5606	1.5339
Mean value for single point ($Wm^{-1}K^{-1}$)	1.3913	1.4330	1.4979	1.4323	1.5418	1.5248
SD relative to single point ($Wm^{-1}K^{-1}$)	0.0231	0.0416	0.0139	0.0587	0.0110	0.0109
Variance relative to single point $(Wm^{-1}K^{-1})^2$	0.000535	0.001733	0.000193	0.003447	0.000121	0.000118
Coefficient of variation %	1.662	2.905	0.928	4.099	0.713	0.714
Absolute accuracy ($Wm^{-1}K^{-1}$)	0.0472	0.0849	0.0223	0.1249	0.0189	0.0158
Accuracy %	3.39	5.92	1.49	8.72	1.22	1.04

	THERMAL CONDUCTIVITY (λ)					
	Perpendicular			Parallel		
Sample / # measure position	43 / 1	43 / 2	43 / 3	43 / 4	43 / 5	43 / 6
First refused measure	1.74	1.60	1.70	1.55	1.81	1.74
Second refused measure	1.74	1.61	1.71	1.63	1.81	1.75
Measure 1 ($Wm^{-1}K^{-1}$)	1.75	1.615	1.73	1.66	1.82	1.759
Measure 2 ($Wm^{-1}K^{-1}$)	1.74	1.60	1.74	1.68	1.82	1.76
Measure 3 ($Wm^{-1}K^{-1}$)	1.74	1.62	1.74	1.68	1.85	1.76
Measure 4 ($Wm^{-1}K^{-1}$)	1.74	1.62	1.74	1.68	1.84	1.77
Measure 5 ($Wm^{-1}K^{-1}$)	1.74	1.63	1.74	1.69	1.86	1.77
Measure 6 ($Wm^{-1}K^{-1}$)	1.75	1.63	1.74	1.69	1.86	1.78
Mean value for single point ($Wm^{-1}K^{-1}$)	1.7438	1.6173	1.7298	1.6567	1.8333	1.7615
SD relative to single point ($Wm^{-1}K^{-1}$)	0.01	0.01	0.02	0.05	0.02	0.01
Variance relative to single point $(Wm^{-1}K^{-1})^2$	0.00	0.00	0.00	0.00	0.00	0.00
Coefficient of variation %	0.30	0.87	0.90	2.85	1.22	0.77
Absolute accuracy ($Wm^{-1}K^{-1}$)	0.0096	0.0200	0.0301	0.1053	0.0295	0.0265
Accuracy %	0.55	1.24	1.74	6.35	1.61	1.50

	THERMAL CONDUCTIVITY (λ)					
	Perpendicular			Parallel		
Sample / # measure position	11 / 1	11 / 2	11 / 3	11 / 4	11 / 5	11 / 6
First refused measure	1.7802	1.9309	1.9902	1.7687	1.8243	1.4835
Second refused measure	1.8267	1.9464	1.9805	1.8155	1.8421	1.9512
Measure 1 ($Wm^{-1}K^{-1}$)	1.8188	1.9635	2.0094	1.8341	1.8576	1.9833
Measure 2 ($Wm^{-1}K^{-1}$)	1.8440	1.9598	2.0129	1.8693	1.8723	1.9859
Measure 3 ($Wm^{-1}K^{-1}$)	1.8731	1.9560	2.0174	1.8823	1.8896	1.9833
Measure 4 ($Wm^{-1}K^{-1}$)	1.8762	1.9791	2.0257	1.9041	1.8789	1.9977
Measure 5 ($Wm^{-1}K^{-1}$)	1.8898	1.9690	2.0323	1.9135	1.8908	2.0055
Measure 6 ($Wm^{-1}K^{-1}$)	1.9134	1.9878	2.0354	1.9270	1.9193	1.9976
Mean value for single point ($Wm^{-1}K^{-1}$)	1.8528	1.9616	2.0130	1.8643	1.8719	1.9235
SD relative to single point ($Wm^{-1}K^{-1}$)	0.0434	0.0180	0.0194	0.0544	0.0301	0.1785
Variance relative to single point $(Wm^{-1}K^{-1})^2$	0.001883	0.000323	0.000378	0.002959	0.000904	0.031871
Coefficient of variation %	2.342	0.916	0.966	2.918	1.606	9.281
Absolute accuracy ($Wm^{-1}K^{-1}$)	0.0725	0.0307	0.0325	0.0956	0.0476	0.4400
Accuracy %	3.92	1.56	1.61	5.13	2.54	22.87

	THERMAL CONDUCTIVITY (λ)					
	Perpendicular			Parallel		
Sample / # measure position	24 / 1	24 / 2	24 / 3	24 / 4	24 / 5	24 / 6
First refused measure	1.4879	1.6597	1.6897	1.6519	1.7411	1.8283
Second refused measure	1.5261	1.6661	1.7101	1.6673	1.7459	1.8369
Measure 1 ($Wm^{-1}K^{-1}$)	1.5454	1.6600	1.7086	1.6652	1.7531	1.7755
Measure 2 ($Wm^{-1}K^{-1}$)	1.5559	1.6616	1.6899	1.6682	1.7808	1.7668
Measure 3 ($Wm^{-1}K^{-1}$)	1.5657	1.6846	1.6967	1.6773	1.7871	1.7837
Measure 4 ($Wm^{-1}K^{-1}$)	1.5610	1.6843	1.7119	1.6921	1.7828	1.8016
Measure 5 ($Wm^{-1}K^{-1}$)	1.5783	1.6856	1.7166	1.7169	1.8126	1.8046
Measure 6 ($Wm^{-1}K^{-1}$)	1.5741	1.6879	1.7026	1.7344	1.8043	1.8046
Mean value for single point ($Wm^{-1}K^{-1}$)	1.5493	1.6737	1.7033	1.6842	1.7760	1.8003
SD relative to single point ($Wm^{-1}K^{-1}$)	0.0298	0.0129	0.0102	0.0284	0.0267	0.0244
Variance relative to single point $(Wm^{-1}K^{-1})^2$	0.000891	0.000166	0.000105	0.000806	0.000711	0.000597
Coefficient of variation %	1.926	0.770	0.600	1.686	1.502	1.357
Absolute accuracy ($Wm^{-1}K^{-1}$)	0.0614	0.0142	0.0135	0.0502	0.0366	0.0367
Accuracy %	3.97	0.85	0.79	2.98	2.06	2.04

	THERMAL CONDUCTIVITY (λ)					
	Perpendicular			Parallel		
Sample / # measure position	46 / 1	46 / 2	46 / 3	46 / 4	46 / 5	46 / 6
First refused measure	2.2641	2.1239	2.4031	2.3741	1.9911	2.4076
Second refused measure	2.3366	2.2899	2.4358	2.4784	2.4512	2.4153
Measure 1 ($Wm^{-1}K^{-1}$)	2.3392	2.3043	2.4636	2.4879	2.4646	2.4262
Measure 2 ($Wm^{-1}K^{-1}$)	2.3542	2.3145	2.5053	2.4941	2.4416	2.4231
Measure 3 ($Wm^{-1}K^{-1}$)	2.3451	2.3149	2.4884	2.5025	2.4788	2.4416
Measure 4 ($Wm^{-1}K^{-1}$)	2.3584	2.3176	2.4954	2.5124	2.4811	2.4348
Measure 5 ($Wm^{-1}K^{-1}$)	2.3550	2.3204	2.4904	2.5071	2.4765	2.4635
Measure 6 ($Wm^{-1}K^{-1}$)	2.3405	2.3184	2.4921	2.5069	2.4887	2.4424
Mean value for single point ($Wm^{-1}K^{-1}$)	2.3366	2.2880	2.4718	2.4829	2.4092	2.4318
SD relative to single point ($Wm^{-1}K^{-1}$)	0.0304	0.0670	0.0355	0.0454	0.1697	0.0177
Variance relative to single point $(Wm^{-1}K^{-1})^2$	0.000925	0.004495	0.001257	0.002062	0.028787	0.000313
Coefficient of variation %	1.302	2.930	1.434	1.829	7.042	0.727
Absolute accuracy ($Wm^{-1}K^{-1}$)	0.0726	0.1641	0.0687	0.1089	0.4180	0.0317
Accuracy %	3.11	7.17	2.78	4.38	17.35	1.30

	THERMAL CONDUCTIVITY (λ)					
	Perpendicular			Parallel		
Sample / # measure position	3 / 1	3 / 2	3 / 3	3 / 4	3 / 5	3 / 6
First refused measure	2.8927	2.6814	2.6496	2.4843	2.5494	2.1596
Second refused measure	2.8906	2.6752	2.6426	2.5321	2.6063	2.3351
Measure 1 ($Wm^{-1}K^{-1}$)	2.9036	2.6977	2.6637	2.5473	2.6245	2.3766
Measure 2 ($Wm^{-1}K^{-1}$)	2.9081	2.6857	2.6800	2.5629	2.6432	2.5017
Measure 3 ($Wm^{-1}K^{-1}$)	2.9183	2.7161	2.6868	2.5752	2.6579	2.4944
Measure 4 ($Wm^{-1}K^{-1}$)	2.9072	2.7091	2.6830	2.5828	2.6671	2.5177
Measure 5 ($Wm^{-1}K^{-1}$)	2.9114	2.7319	2.6790	2.5907	2.6766	2.5212
Measure 6 ($Wm^{-1}K^{-1}$)	2.9203	2.7364	2.6935	2.5682	2.6496	2.5251
Mean value for single point ($Wm^{-1}K^{-1}$)	2.9065	2.7042	2.6723	2.5555	2.6343	2.4289
SD relative to single point ($Wm^{-1}K^{-1}$)	0.0107	0.0231	0.0183	0.0344	0.0411	0.1305
Variance relative to single point $(Wm^{-1}K^{-1})^2$	0.0001	0.0005	0.0003	0.0012	0.0017	0.0170
Coefficient of variation %	0.3696	0.8529	0.6847	1.3455	1.5606	5.3747
Absolute accuracy ($Wm^{-1}K^{-1}$)	0.0159	0.0322	0.0296	0.0711	0.0850	0.2693
Accuracy %	0.55	1.19	1.11	2.78	3.22	11.09

	THERMAL CONDUCTIVITY (λ)					
	Perpendicular			Parallel		
Sample / # measure position	25 / 1	25 / 2	25 / 3	25 / 4	25 / 5	25 / 6
First refused measure	2.4995	2.8338	2.2165	2.3775	2.9025	2.6862
Second refused measure	2.4829	2.9148	2.4640	2.6050	2.9026	2.6986
Measure 1 ($Wm^{-1}K^{-1}$)	2.5168	2.9350	2.5695	2.6543	2.9131	2.7363
Measure 2 ($Wm^{-1}K^{-1}$)	2.5248	2.9686	2.5537	2.6793	2.9275	2.7398
Measure 3 ($Wm^{-1}K^{-1}$)	2.5266	2.9883	2.5584	2.6745	2.8974	2.7432
Measure 4 ($Wm^{-1}K^{-1}$)	2.5266	2.9752	2.5584	2.7124	2.9142	2.7403
Measure 5 ($Wm^{-1}K^{-1}$)	2.5329	2.9797	2.5778	2.6994	2.9096	2.7359
Measure 6 ($Wm^{-1}K^{-1}$)	2.5603	3.0054	2.5763	2.6864	2.9189	2.7678
Mean value for single point ($Wm^{-1}K^{-1}$)	2.5213	2.9501	2.5093	2.6361	2.9107	2.7310
SD relative to single point ($Wm^{-1}K^{-1}$)	0.02297	0.05524	0.12387	0.10948	0.00984	0.02613
Variance relative to single point $(Wm^{-1}K^{-1})^2$	0.000528	0.003051	0.015344	0.011985	0.000097	0.000683
Coefficient of variation %	0.911	1.872	4.936	4.153	0.338	0.957
Absolute accuracy ($Wm^{-1}K^{-1}$)	0.0390	0.1163	0.2929	0.2586	0.0168	0.0448
Accuracy %	1.55	3.94	11.67	9.81	0.58	1.64

	THERMAL CONDUCTIVITY (λ)					
	Perpendicular			Parallel		
Sample / # measure position	47 / 1	47 / 2	47 / 3	47 / 4	47 / 5	47 / 6
First refused measure	1.8228	1.7562	1.8735	2.1916	2.3270	2.4085
Second refused measure	1.8409	1.7989	1.8846	2.2527	2.3723	2.3976
Measure 1 ($Wm^{-1}K^{-1}$)	1.8445	1.8113	1.8890	2.2689	2.3751	2.4168
Measure 2 ($Wm^{-1}K^{-1}$)	1.8777	1.8281	1.8916	2.2719	2.3872	2.4105
Measure 3 ($Wm^{-1}K^{-1}$)	1.8682	1.8345	1.8936	2.2888	2.3682	2.3993
Measure 4 ($Wm^{-1}K^{-1}$)	1.8717	1.8545	1.8771	2.2935	2.4010	2.4139
Measure 5 ($Wm^{-1}K^{-1}$)	1.8887	1.8587	1.8951	2.2918	2.3864	2.4179
Measure 6 ($Wm^{-1}K^{-1}$)	1.8951	1.8616	1.8999	2.2997	2.4013	2.4347
Mean value for single point ($Wm^{-1}K^{-1}$)	1.8637	1.8255	1.8880	2.2699	2.3773	2.4124
SD relative to single point ($Wm^{-1}K^{-1}$)	0.0252	0.0359	0.0091	0.0353	0.0238	0.0117
Variance relative to single point $(Wm^{-1}K^{-1})^2$	0.000637	0.001292	0.000082	0.001244	0.000566	0.000137
Coefficient of variation %	1.354	1.969	0.480	1.554	1.001	0.485
Absolute accuracy ($Wm^{-1}K^{-1}$)	0.0409	0.0693	0.0145	0.0782	0.0503	0.0223
Accuracy %	2.20	3.80	0.77	3.45	2.12	0.92

	THERMAL CONDUCTIVITY (λ)					
	Perpendicular			Parallel		
Sample / # measure position	6A / 1	6A / 2	6A / 3	6A / 4	6A / 5	6A / 6
First refused measure	2.3861	2.1190	2.4903	2.3617	2.1267	2.4647
Second refused measure	2.5768	2.3142	2.4957	2.4241	2.2225	2.5013
Measure 1 ($Wm^{-1}K^{-1}$)	2.5915	2.3177	2.5144	2.4898	2.3629	2.5214
Measure 2 ($Wm^{-1}K^{-1}$)	2.6204	2.3437	2.5278	2.5524	2.3981	2.5218
Measure 3 ($Wm^{-1}K^{-1}$)	2.6440	2.4498	2.5418	2.5876	2.4050	2.5439
Measure 4 ($Wm^{-1}K^{-1}$)	2.6860	2.4526	2.5504	2.5926	2.4320	2.5587
Measure 5 ($Wm^{-1}K^{-1}$)	2.6904	2.4672	2.5641	2.6031	2.4423	2.5774
Measure 6 ($Wm^{-1}K^{-1}$)	2.7457	2.4571	2.5711	2.5956	2.4635	2.5803
Mean value for single point ($Wm^{-1}K^{-1}$)	2.6176	2.3652	2.5320	2.5259	2.3566	2.5337
SD relative to single point ($Wm^{-1}K^{-1}$)	0.1089	0.1193	0.0302	0.0913	0.1192	0.0395
Variance relative to single point $(Wm^{-1}K^{-1})^2$	0.011858	0.014229	0.000911	0.008343	0.014203	0.001560
Coefficient of variation %	4.160	5.043	1.192	3.616	5.057	1.559
Absolute accuracy ($Wm^{-1}K^{-1}$)	0.2315	0.2462	0.0416	0.1642	0.2300	0.0690
Accuracy %	8.84	10.41	1.64	6.50	9.76	2.72

	THERMAL CONDUCTIVITY (λ)					
	Perpendicular			Parallel		
Sample / # measure position	8 / 1	8 / 2	8 / 3	8 / 4	8 / 5	8 / 6
First refused measure	2.7698	2.7522	2.8337	2.6100	2.1422	3.0331
Second refused measure	2.8823	2.8438	2.8682	2.7474	2.7640	3.0192
Measure 1 ($Wm^{-1}K^{-1}$)	2.8922	2.8719	2.8965	2.7955	2.7768	3.0212
Measure 2 ($Wm^{-1}K^{-1}$)	2.8855	2.8964	2.8924	2.7955	2.7719	3.0607
Measure 3 ($Wm^{-1}K^{-1}$)	2.9177	2.9100	2.9167	2.8141	2.8469	3.0336
Measure 4 ($Wm^{-1}K^{-1}$)	2.9312	2.9106	2.9123	2.7964	2.8621	3.0447
Measure 5 ($Wm^{-1}K^{-1}$)	2.9278	2.9052	2.9002	2.8065	2.8895	3.0359
Measure 6 ($Wm^{-1}K^{-1}$)	2.9663	2.8883	2.9025	2.8392	2.8932	3.0196
Mean value for single point ($Wm^{-1}K^{-1}$)	2.8966	2.8723	2.8903	2.7756	2.7433	3.0335
SD relative to single point ($Wm^{-1}K^{-1}$)	0.0584	0.0535	0.0272	0.0717	0.2485	0.0142
Variance relative to single point $(Wm^{-1}K^{-1})^2$	0.003415	0.002863	0.000737	0.005134	0.061776	0.000203
Coefficient of variation %	2.017	1.863	0.940	2.582	9.060	0.469
Absolute accuracy ($Wm^{-1}K^{-1}$)	0.1268	0.1201	0.0566	0.1656	0.6012	0.0272
Accuracy %	4.38	4.18	1.96	5.97	21.91	0.90

	THERMAL CONDUCTIVITY (λ)					
	Perpendicular			Parallel		
Sample / # measure position	27A / 1	27A / 2	27A / 3	27A / 4	27A / 5	27A / 6
First refused measure	2.4735	2.5427	2.5578	2.1693	2.5509	2.5858
Second refused measure	2.5027	2.5279	2.5538	2.2581	2.5640	2.5878
Measure 1 ($Wm^{-1}K^{-1}$)	2.5112	2.5474	2.5653	2.4295	2.5258	2.5815
Measure 2 ($Wm^{-1}K^{-1}$)	2.5133	2.5332	2.5854	2.4685	2.5472	2.6023
Measure 3 ($Wm^{-1}K^{-1}$)	2.5372	2.5513	2.5891	2.4957	2.5614	2.6257
Measure 4 ($Wm^{-1}K^{-1}$)	2.5200	2.5431	2.5870	2.5079	2.5795	2.5954
Measure 5 ($Wm^{-1}K^{-1}$)	2.5370	2.5312	2.6024	2.5410	2.5746	2.6095
Measure 6 ($Wm^{-1}K^{-1}$)	2.5396	2.5372	2.5814	2.5383	2.5782	2.6061
Mean value for single point ($Wm^{-1}K^{-1}$)	2.5168	2.5393	2.5778	2.4260	2.5602	2.5993
SD relative to single point ($Wm^{-1}K^{-1}$)	0.0223	0.0082	0.0170	0.1380	0.0183	0.0147
Variance relative to single point $(Wm^{-1}K^{-1})^2$	0.000496	0.000067	0.000288	0.019042	0.000336	0.000215
Coefficient of variation %	0.885	0.323	0.659	5.688	0.716	0.564
Absolute accuracy ($Wm^{-1}K^{-1}$)	0.0433	0.0120	0.0246	0.2567	0.0344	0.0265
Accuracy %	1.72	0.47	0.95	10.58	1.34	1.02

	THERMAL CONDUCTIVITY (λ)					
	Perpendicular			Parallel		
Sample / # measure position	10B / 1	10B / 2	10B / 3	10B / 4	10B / 5	10B / 6
First refused measure	3.1899	3.0502	3.2914	2.8757	2.6137	3.0708
Second refused measure	3.2094	3.0878	3.3369	2.9094	3.0515	3.0629
Measure 1 ($Wm^{-1}K^{-1}$)	3.2158	3.0688	3.3280	2.9198	3.0339	3.0959
Measure 2 ($Wm^{-1}K^{-1}$)	3.2422	3.0716	3.3512	2.9109	3.0609	3.0738
Measure 3 ($Wm^{-1}K^{-1}$)	3.2456	3.0854	3.3808	2.9179	3.0423	3.0685
Measure 4 ($Wm^{-1}K^{-1}$)	3.2263	3.0957	3.3583	2.9350	3.0564	3.0797
Measure 5 ($Wm^{-1}K^{-1}$)	3.2266	3.1789	3.3758	2.9530	3.0501	3.0762
Measure 6 ($Wm^{-1}K^{-1}$)	3.2248	3.1907	3.3804	2.9315	3.0478	3.0962
Mean value for single point ($Wm^{-1}K^{-1}$)	3.2226	3.1036	3.3503	2.9192	2.9946	3.0780
SD relative to single point ($Wm^{-1}K^{-1}$)	0.0179	0.0521	0.0309	0.0227	0.1541	0.0122
Variance relative to single point $(Wm^{-1}K^{-1})^2$	0.000319	0.002713	0.000957	0.000514	0.023756	0.000150
Coefficient of variation %	0.555	1.678	0.924	0.776	5.147	0.397
Absolute accuracy ($Wm^{-1}K^{-1}$)	0.0326	0.0871	0.0590	0.0434	0.3809	0.0182
Accuracy %	1.01	2.81	1.76	1.49	12.72	0.59

	THERMAL CONDUCTIVITY (λ)					
	Perpendicular			Parallel		
Sample / # measure position	34 / 1	34 / 2	34 / 3	34 / 4	34 / 5	34 / 6
First refused measure	2.6612	2.9719	2.9940	2.7794	2.8637	2.6875
Second refused measure	2.7586	2.9677	2.9972	2.7709	2.8874	2.8285
Measure 1 ($Wm^{-1}K^{-1}$)	2.8000	3.0068	2.9566	2.8054	2.8851	2.8232
Measure 2 ($Wm^{-1}K^{-1}$)	2.8139	2.9890	2.9838	2.8123	2.9070	2.8338
Measure 3 ($Wm^{-1}K^{-1}$)	2.8293	3.0180	2.9873	2.8123	2.8973	2.8592
Measure 4 ($Wm^{-1}K^{-1}$)	2.8332	3.0081	2.9816	2.8356	2.9314	2.8647
Measure 5 ($Wm^{-1}K^{-1}$)	2.8647	3.0132	3.0250	2.8408	2.9186	2.8635
Measure 6 ($Wm^{-1}K^{-1}$)	2.8384	3.0078	3.0074	2.8379	2.9310	2.8834
Mean value for single point ($Wm^{-1}K^{-1}$)	2.7999	2.9978	2.9916	2.8118	2.9027	2.8305
SD relative to single point ($Wm^{-1}K^{-1}$)	0.0641	0.0192	0.0200	0.0263	0.0239	0.0614
Variance relative to single point $(Wm^{-1}K^{-1})^2$	0.004112	0.000370	0.000401	0.000693	0.000570	0.003770
Coefficient of variation %	2.290	0.641	0.670	0.936	0.822	2.169
Absolute accuracy ($Wm^{-1}K^{-1}$)	0.1387	0.0301	0.0350	0.0409	0.0390	0.1430
Accuracy %	4.95	1.00	1.17	1.45	1.34	5.05

	THERMAL CONDUCTIVITY (λ)					
	Perpendicular			Parallel		
Sample / # measure position	35 / 1	35 / 2	35 / 3	35 / 4	35 / 5	35 / 6
First refused measure	2.9705	3.1075	3.1321	3.0245	3.1273	2.7253
Second refused measure	2.9808	3.0801	3.0803	3.0069	3.1372	3.0454
Measure 1 ($Wm^{-1}K^{-1}$)	2.9719	3.0981	3.1089	3.0089	3.1746	3.0650
Measure 2 ($Wm^{-1}K^{-1}$)	2.9901	3.0845	3.1185	3.0124	3.1633	3.0735
Measure 3 ($Wm^{-1}K^{-1}$)	3.0093	3.0935	3.1170	3.0355	3.1446	3.0742
Measure 4 ($Wm^{-1}K^{-1}$)	2.9997	3.1008	3.0913	3.0111	3.1861	3.0824
Measure 5 ($Wm^{-1}K^{-1}$)	2.9764	3.1105	3.0900	3.0288	3.1851	3.0710
Measure 6 ($Wm^{-1}K^{-1}$)	3.0010	3.0920	3.0820	3.0426	3.2006	3.0973
Mean value for single point ($Wm^{-1}K^{-1}$)	2.9875	3.0959	3.1025	3.0213	3.1648	3.0293
SD relative to single point ($Wm^{-1}K^{-1}$)	0.0147	0.0105	0.0192	0.0135	0.0262	0.1237
Variance relative to single point $(Wm^{-1}K^{-1})^2$	0.000216	0.000111	0.000368	0.000181	0.000689	0.015298
Coefficient of variation %	0.492	0.340	0.619	0.445	0.829	4.083
Absolute accuracy ($Wm^{-1}K^{-1}$)	0.0219	0.0158	0.0296	0.0213	0.0375	0.3039
Accuracy %	0.73	0.51	0.95	0.70	1.19	10.03

Bibliography

Abdi, H. (2010). Coefficient of variation. Encyclopedia of Research Design. SAGE Publications, Inc., Thousand Oaks, CA, 169-171.

Alishaev, M. G., Abdulagatov, I. M., & Abdulagatova, Z. Z. (2012). Effective thermal conductivity of fluid-saturated rocks: Experiment and modeling.Engineering Geology, 135, 24-39.

Andolfsson T. (2013). Analyses of thermal conductivity from mineral composition and analyses by use of Thermal Conductivity Scanner: A study of thermal properties in Scanian rock types, Master's thesis, Department of Geology, Lund University.

Arent, D. J., Wise, A., & Gelman, R. (2011). The status and prospects of renewable energy for combating global warming. Energy Economics, 33(4), 584-593.

Astolfi, G. F. Colombara. 2003. La geologia dei Colli Euganei. Edizioni Canova, Treviso.

Aurighi M., Vittadello A. (1999). Testimonianze geologiche dei Colli Euganei. Provincia di Padova, collana Studi sul territorio: l'ambiente ed il paesaggio n. 8

Bagdassarov, N. S., & Dingwell, D. B. (1992). A rheological investigation of vesicular rhyolite. Journal of volcanology and geothermal research, 50(3), 307-322.

Bailey, D.K. (1964). Crustal warping. A possible tectonic control of alcaline magmatism. Journal of Geophysical Research **69**, 1103-1114.

Bailey, D.K. (1974). Continental rifting and alkaline magmatism. In: Sorensen, H. (ed.) The alkaline rock, regional distribution and tectonic relations. London: Wiley & Sons, 148-159.

Barbieri, M., Turi, B., De Pieri, R., De Vecchi, G.P., Piccirillo, E.M. & Gregnanin, A. (1978). Oxygen and stronzium isotope variations in the igneous rocks the Euganeam Hills Venetian Tertiary Province, Northern Italy. In: Robinson, B.W. (ed.) Stable isotopes in the Earth Sciences. Wellington, DSIR Bulletin, 139-148.

Bargar K.E., Beeson, M. H. (1985). Hydrothermal alteration in research drill hole Y-3, Lower Geyser Basin, Yellowstone National Park, Wyoming: US Geological Survey Professional Paper 1054-C.

Barry-Macaulay, D., Bouazza, A., Singh, R. M., Wang, B., & Ranjith, P. G. (2013). Thermal conductivity of soils and rocks from the Melbourne (Australia) region. Engineering Geology, 164, 131-138.

Bartoli O., Meli S., Sassi R., Magaraci D. (2013). Amphiboles and clinopyroxenes from Euganean (NE Italy) cumulus enclaves: evidence of subduction-related melts below Adriamicroplate. Rend. Fis. Acc. Lincei, 24, 151–161.

Bateman R., Park A., Harris A. (2011). MTPS sensor to determine thermal conductivity of geological samples. CTAS2011 Conference © Guelph Ontario, Canada.

Borinaga-Treviño R., Pascual-Muñoz P.,Castro-Fresno D., Del Coz-Díaz JJ. Study of different grouting materials used in vertical geothermal closed-loop heat exchangers, Applied Thermal Engineering (2012), doi: 10.1016/j.applthermaleng.2012.05.029.

Borsi, S., Ferrara, G., & Piccoli, G. (1969). Determinazione col metodo K/Ar dell'età delle eruzioni euganee.

Bramanti, M. (1997). Calcolo delle probabilità e statistica: teoria ed esercizi. Progetto Leonardo.

Buntebarth G. (1980) Geothermie: Eine Einführung in die allgemeine und angewandte Wärmelehre des Erdkörpers. Berlin ua Springer.

C-Therm Technologies: TCi Operator Manual

Cabeza L. F. (2012). Reference Module in Earth Systems and Environmental Sciences, from Comprehensive Renewable Energy Volume 3. 211-253.

Capedri, S., Venturelli, G., & Grandi, R. (2000). Euganean trachytes: discrimination of quarried sites by petrographic and chemical parameters and by magnetic susceptibility and its bearing on the provenance of stones of ancient artefacts. Journal of Cultural Heritage, 1(4), 341-364.

Cashman, K., Rust, A., Wright, H., & Roberge, J. (2003). Permeability of porour rhyolite. In EGS-AGU-EUG Joint Assembly (Vol. 1, p. 7543).

Castellaccio E., Zorzin R (2012). Acque calde e geotermia della provincia di Verona. Aspetti geologici e applicazioni. Memorie del Museo Civico di Storia Naturale di Verona - 2. Serie. Sezione Scienze della Terra, 8.

Cha, J., Seo, J., & Kim, S. (2012). Building materials thermal conductivity measurement and correlation with heat flow meter, laser flash analysis and TCi.Journal of thermal analysis and calorimetry, 109(1), 295-300.

Cermak, V., Kresl, M., Kucerová, L., Safanda, J., Frasheri, A., Kapedani, N., ... & Cano, D. (1996). Heat flow in Albania. Geothermics, 25(1), 91-102.

Chekonin E., Parshin A., Pissarenko D., Popov Y., Romushkevich R., Safonov S., Spasennykh M., Chertenkov M:V:, Stenin V.P. (2012) When rocks get hot: thermal properties of reservoirs rocks. Schlumberger.

Clauser, C., & Huenges, E. (1995). Thermal conductivity of rocks and minerals.AGU reference shelf, 3, 105-126.

Clauser, C. (2006). Geothermal Energy, In: K. Heinloth (ed), Landolt-Börnstein, Group VIII: Advanced Materials and Technologies, Vol. 3: Energy Technologies, Subvol. C: Renewable Energies, Springer Verlag, Heidelberg-Berlin, 493-604.

Clauser, C. (2011). Thermal storage and transport properties of rocks, I: Heat capacity and latent heat. Encyclopedia of Solid Earth Geophysics, 1423-1431.

Clauser, C. (2011). Thermal storage and transport properties of rocks, ii: thermal conductivity and diffusivity. In Encyclopedia of Solid Earth Geophysics(pp. 1431-1448). Springer Netherlands.

Conedera, C., Dal Passo, G., Piccoli, G. & Travaglia-Saccardi, P. (1969). Studio fotogeologico del Veneto centro-occidentale fra il Lago di Garda ed il fiume Brenta. Memorie degli Istituti di Geologia e Mineralogia dell'Università di Padova 28, 121-272.

Cremonini, C., & Zanuttini, R. (2009). Metrologia e gestione della strumentazione per il settore legno-arredo. Lampi di stampa.

De Carli M., Roncato N., Zarrella A., Zecchin R. (2007) "Energia dal terreno", AICARR Convegno Energie rinnovabili: tecniche e potenzialità.

De Vecchi, G.P. & Sedea, R. (1974). Sui basalti Eocenici dei Colli Euganei. Memorie degli Istituti di Geologia e Mineralogia dell'Università di Padova **31**, 3-26.

De Vecchi, G.P., Gregagnin, A. & Piccirillo E.M. (1976). Aspetti del vulcanismo terziario veneto. Memorie degli Istituti di Geologia e Mineralogia dell'Università di Padova **30**, 3-32.

De Vallejo, L. I. G. (2004). Geoingegneria. Pearson Italia Spa.

Di Sipio, E., Galgaro, A., Destro, E., Teza, G., Chiesa, S., Giaretta, A., & Manzella, A. (2014). Subsurface thermal conductivity assessment in Calabria (southern Italy): a regional case study. Environmental Earth Sciences, 1-19.

Dincer, I., & Rosen, M. A. (2001). Energetic, environmental and economic aspects of thermal energy storage systems for cooling capacity. Applied Thermal Engineering, 21(11), 1105-1117.

Dincer, I. (2002). Thermal energy storage systems as a key technology in energy conservation. International journal of energy research, 26(7), 567-588.

Farouki, O. T. (1981). Thermal properties of soils (No. CRREL-MONO-81-1). COLD REGIONS RESEARCH AND ENGINEERING LAB HANOVER NH.

Froldi, P. (2013). Impianti geotermici. Maggioli Editore.

Galgaro (2008). Sistemi di geoscambio termico. Convegno di Udine **Ordine** regionale dei Geologi FVG.

Galgaro A., Busoni S., Destro E. Geoscambio nella provincia di Treviso.

Gong G. (2005) Physical Properties of Alpine Rocks: A Laboratory Investigation, Faculty of Science, Department of Mineralogy, University of Geneva.

Grunert S., Szilagyi J. (2010) Petrophysikalische eingenschaften einer auswahl von baugesteinen aus Deutschland und ihr Bezug zur Petrographie dieser Gesteine. Journal of Central European Geology 56/1, 39-82.

Hamdhan, I. N., & Clarke, B. G. (2010). Determination of thermal conductivity of coarse and fine sand soils. In Proceedings of World Geothermal Congress.

Hartmann, A., Pechnig, R., & Clauser, C. (2008). Petrophysical analysis of regional-scale thermal properties for improved simulations of geothermal installations and basin-scale heat and fluid flow. International Journal of Earth Sciences, 97(2), 421-433.

Hegger, M. (2009). Construire: atlas des matériaux. PPUR Presses polytechniques.

Hendriks, M., Snijders, A., & Boido, N. (2008, May). Underground thermal energy storage for efficient heating and cooling of buildings. In 1st International Conference on Industrialised, Integrated, Intelligent Construction, Loughborough (pp. 315-324).

Herrera de Figueiredo E.R. (2006). Condutividade térmica de rocas: uma aplicação para granitos ornamentais. Programa de pòs-graduação o em geodinamica e geofisica. Universidade federal do Rio grande do norte.

Holston, I., & King Jr, D. T. (1989). Depositional Facies, Porosity Loss, and Cementation in the Upper Cretaceous Mooreville and Demopolis Chalks, Central Alabama.

Homand, F., Duffaut, P., Berest, P., Billaux, D., Boulon, M., Cornet, F., ... & Souley, M. (2000). Manuel de mécanique des roches(Tome 1, Fondements).

Iqbal, M., McCullough, M., Harris, A., & Eichhorn, S. H. (2012). Thermal conductivity of polyurethane composites containing nanometer-and micrometer-sized silver particles. Journal of thermal analysis and calorimetry, 108(3), 933-938.

Kodešová, R., Vlasáková, M., Fér, M., Teplá, D., Jakšík, O., Neuberger, P., & Adamovský, R. (2013). Thermal Properties of Representative Soils of the Czech Republic. Soil and Water Research, 8(4), 141-150.

Krishnaiah, S., D. N. Singh, and G. N. Jadhav. "A methodology for determining thermal properties of rocks." International journal of rock mechanics and mining sciences 41.5 (2004): 877-882.

Kuvandykova, D., & Bateman, R. (2013). Conductivity of Asphalt. Thermal Conductivity 31/Thermal Expansion 19, 98.

Lau, L. C., Lee, K. T., & Mohamed, A. R. (2012). Global warming mitigation and renewable energy policy development from the Kyoto Protocol to the Copenhagen Accord-A comment. Renewable and Sustainable Energy Reviews, 16(7), 5280-5284.

Lee, Y., & Deming, D. (1998). Evaluation of thermal conductivity temperature corrections applied in terrestrial heat flow studies. Journal of Geophysical Research: Solid Earth (1978–2012), 103(B2), 2447-2454.

Lee, Y. (1999). Thermal state of the Arkoma Basin and the Anadarko Basin, Oklahoma (Doctoral dissertation).

Lee, Y., Deming, D. (1999). Heat flow and thermal history of the Anadarko Basin and the western Oklahoma Platform. Tectonophysics, 313(4), 399-410.

Liebethat C. (2012) Erdwärmesonden – bedeutende Untergrundparameter und thermische Auswirkungen auf Porengrundwasserleiter. Masterstudium Erdwissenschaften. Institut für Erdwissenschaften.

Marinelli, G. (1975). Magma evolution in Italy. In: Squyres, C.H. (ed.) Geology of Italy. Tripoli, Petroleum Exploration Society Libya, 165-219.

Maritan, L., Mazzoli, C., Sassi, R., Speranza, F., Zanco, A., & Zanovello, P. (2013). Trachyte from the Roman aqueducts of Padua and Este (north-east Italy): a provenance study based on petrography, chemistry and magnetic susceptibility. European Journal of Mineralogy, 25(3), 415-427.

Mathis, N. (2000). Transient thermal conductivity measurements: comparison of destructive and nondestructive techniques. High Temperatures High Pressures(UK), 32(3), 321-327.

Mazzoldi, P., Nigro, M., & Voci, C. (2007). Elementi di fisica: Meccanica e termodinamica. EdiSES.

Mikulić, D., & Milovanović, B. (11). TCi System for Non-Destructive Determination of Thermal Properties of Materials. In 10th European Conference on Non Destructive.

Milovanovic, B., Banjad, P. I., & Gabrijel, I. (2011, September). Measuring thermal properties of hydrating cement pastes. In 31st Cement and Concrete Science Conference, Novel Developments and Innovation in Cementitious Materials, Imperial College London, United Kingdom.

Moiseyenko U.I., Sokolova L.S., Istomin V.E.(1972) Electric and thermal properties of rocks. National Aeronautics and Space Administration.

Nordell, B. (2000). Large-scale thermal energy storage. WinterCities' 2000, Luleå, Sweden, February, 14.

Nordell, B., Grein, M., & Kharseh, M. (2007). Large-scale utilisation of renewable energy requires energy storage. International confernce for renewable energies and sustainable development (ICRESD_07), Université Abou Bakr BELKAID— TLEMCEN, Algeria, May, 21-24.

Nordell, B. (2012). Underground Thermal Energy Storage (UTES). Luleå University of Technology, 16.

Oró, E., Miró, L., Farid, M.M., Martin, V., Cabeza, L.F., Energy management and CO_2 mitigation using phase change materials (PCM) for thermal energy storage (TES) in cold storage and transport, International Journal of Refrigeration (2014).

Pasquale, V., Gola, G., Chiozzi, P., & Verdoya, M. (2011). Thermophysical properties of the Po Basin rocks. Geophysical Journal International, 186(1), 69-81.

Pereira E.S. (2008). Determinação das propriedades térmicas das rochas do embasemento adjacente à bacia do recôncavo. Curso de graduação em geofìsica. Universidade federal da Bahia.

Personenkreises Oberflächennahe Geothermie (2008). Sachstandsbericht für einen bundeseinheitlichen Produktkatalog zur wirtschaftlichen Anwendung oberflächennaher geothermischer Daten.

Piccoli, G. (1966). Studio geologico del vulcanismo paleogenico veneto. Società Cooperativa Tipografica.

Piccoli, G., Sedea, R., Bellati, R., Di Lallo, E., Medizza, F., Girardi, A., ... & Norinelli, A. Dal Pra'A (1981) Note illustrative della carta geologica dei Colli Euganei alla scala 1: 25000. Mem Sci Geol, 34, 523-566.

Popov, Y. A., Pevzner, S. L., Pimenov, V. P., & Romushkevich, R. A. (1999). New geothermal data from the Kola superdeep well SG-3. Tectonophysics,306(3), 345-366.

Popov, Y., Romushkevich, R., Bayuk, I., Korobkov, D., Mayr, S., Burkhardt, H., & Wilhelm, H. (2004). Physical properties of rocks from the upper part of the Yaxcopoil-1 drill hole, Chicxulub crater. Meteoritics & Planetary Science, 39(6), 799-812.

Primavari P. (2008). I materiali lapidei della Sardegna. Sardegna ricerche.

Ray, L., Förster, H. J., Schilling, F. R., & Förster, A. (2006). Thermal diffusivity of felsic to mafic granulites at elevated temperatures. Earth and Planetary Science Letters, 251(3), 241-253.

Ross D.C. (1970). Pegmatitic trachyandesite plugs and associated volcanic rocks in the Saline Range-Inyo Mountains region, California. US Geological Survey Professional Paper 614-D

Rubin, A. (2013). L'accumulo dell'energia termica: stato dell'arte e studio di sistemi e soluzioni per la media temperatura.

Rubino, S. (2011). Abitare il futuro… dopo Copenhagen. Giornate internazionali di studio alla ricerca di un nuovo modello di città. FOLIO, 19.

Sanna U., Atzeni C. (2009). Il manuale tematico della pietra. Tipografia del genio civile.

Sassi R., Mazzoli C., Spiess R., Cester T. (2004) Towards a Better Understanding of the

Fibrolite Problem: the Effect of Reaction Overstepping and Surface Energy Anisotropy. Journal of Petrology, 45 (7), 1467-1479

Schiavinato, G. (1950). La provincia magmatica del Veneto sud-occidentale. Società Cooperativa Tipografica.

Schön, J. H. (2004). Physical Properties of Rocks: Fundamentals and Principles of Petrophysics, ser. Handbook of Geophysical Exploration: Seismic Exploration, K. Helbig and S. Treitel, Eds. Amsterdam, The Netherlands: Elsevier, 18.

Sedea, R., Di Lallo, E. (1973). I camini vulcanici d'esplosione dei Colli Euganei. Bollettino della Societa Geologica Italiana, 92(4), 783-800.

Slifka, A. J. (2000). Thermal-conductivity apparatus for steady-state, comparative measurement of ceramic coatings. Journal of Research of the National Institute of Standards and Technology, 105(4), 591-605.

Taylor, J. (1997). Introduction to error analysis, the study of uncertainties in physical measurements (Vol. 1).

Türkdönmez, O., & Bozcu, M. (2012). The geological, petrographical and engineering properties of rhyolitic tuffs (Çan Stone) in Çan-Etili area (Çanakkale), NW Turkey: their usage as building and covering stones. Open Journal of Geology, 2, 25.

Ufficio geologico cantonale (1982). Costanti fisiche di alcuni tipi di rocce (densità, porosità, capacità termica massica (calore specifico) capacità termica volumica, conduttività termica) rapporto interno 006.

UNI EN 1936:2001. Metodi di prova per pietre naturali - Determinazione delle masse volumiche reale e apparente e della porosità totale e aperta.

Verein Deutscher Ingenieure (2010). Thermische Nutzung des Untergrunds.

Verrone A. (2009). Sistemi per la climatizzazione mediante pompe di calore geotermiche e pali energetici.

Waples, D. W., & Waples, J. S. (2004). A review and evaluation of specific heat capacities of rocks, minerals, and subsurface fluids. Part 1: Minerals and nonporous rocks. Natural resources research, 13(2), 97-122.

Waples, D. W., & Waples, J. S. (2004). A review and evaluation of specific heat capacities of rocks, minerals, and subsurface fluids. Part 2: fluids and porous rocks. Natural resources research, 13(2), 123-130.

Wood, W. W., & Fernandez, L. A. (1988). Volcanic rocks. The Geology of North America, 2, 353-365.

Xu, J., Wang, R. Z., & Li, Y. (2013). A review of available technologies for seasonal thermal energy storage. Solar Energy.

Zharikov A.V., Vitovtova V.M., Gurbanov A.G. (2009) Transport properties of rocks from the elbrus volcanic center (experimental data). Informational Bulletin of the Annual Seminar of Experimental Mineralogy, Petrology and Geochemistry

Websites:

geoportale.regione.emilia-romagna.it
www.appliedp.com
www.bgs.ac.uk
www.britannica.com
www.cavepietra.it
www.ctherm.com
www.astro.unipd.it/ciroi/spfis1/
www.comune.ra.it
www.esri.com
www.gemmarum.it
www.isprambiente.it
www.lgrb.uni-freiburg.de
www.sardatrachiti.com
www.sardegnaricerche.it
www.struers.com
www.unina2.it

Acknowledgements - Ringraziamenti

Desidero ringraziare il Prof. Raffaele Sassi per avermi dato la possibilità di sviluppare un lavoro di tesi in un ambito molto interessante ed innovativo (quale l'immagazzinamento di energia termica nelle rocce) le cui applicazioni possono condurre ad importanti benefici ambientali. Lo ringrazio inoltre per tutto il tempo che mi ha dedicato nei vari incontri, venendo incontro alle mie necessità, e ai consigli forniti.
Contestualmente ringrazio il Prof. Antonio Galgaro per aver fornito importanti indicazioni e consigli, indirizzando con la sua esperienza le ricerche più opportune da effettuare.
Ringrazio la Dott.ssa Eloisa Di Sipio per avermi seguito durante le varie fasi del lavoro, per avermi insegnato ad usare la strumentazione di laboratorio e per aver risolto i numerosi dubbi incontrati durante il percorso.
Un grazie lo rivolgo anche al personale dei vari laboratori del Dipartimento di Geoscienze dell'Università di Padova ed in particolare al Sig. Leonardo Tauro del "Laboratorio sezioni sottili e sezioni lucide", al Dott. Lorenzo Raccagni del "Laboratorio di minerografia e giacimenti minerari", al Dott. Aurelio Giaretta del "Laboratorio di analisi chimiche".

A questo punto desidero ringraziare mia mamma Gabriella e mio papà Francesco per avermi quotidianamente supportato in questi anni di studio con ogni strumento a loro disposizione. Grazie perché senza di voi tutto ciò non sarebbe stato possibile.
Grazie anche a mia sorella Paola e a mio cognato Enrico per la loro preziosa e allegra vicinanza che spesso è servita per "spezzare" qualche periodo di studio intenso. Grazie di cuore.
Grazie alla mia ragazza Tiziana per ogni consiglio, per l'ascolto, le parole e le attenzioni che mi riserva sempre. La ringrazio per avermi sempre incitato in questi anni di studio ma (ancora di più) per farmi sentire, giorno dopo giorno, sempre più fortunato di stare con lei.
Grazie anche ai suoi genitori Loretta e Verano e a suo fratello Cristian per l'appoggio e l'interesse dimostrato nei confronti degli argomenti trattati durante i miei studi (tesi compresa) e in generale delle mie passioni.
Esprimo inoltre gratitudine ai miei zii Antonia con Antonio, Giovanni, Marisa con Alessandro e Maurizio con Daniela. Grazie alle mie cugine Enrica e Claudia con le rispettive famiglie, Elisa con Davide, Anna, Alessia e Martina con Yarin e ai miei cugini Valerio con Mariù ed Alberto.

Grazie anche a zia Rosetta (anche per aver pronosticato la mia laurea in tempi non sospetti…circa vent'anni fa!). Un grazie sentito anche a Laura e al marito Francesco.
Grazie infine a tutti gli amici nuovi e vecchi. Grazie ai miei ex compagni delle superiori Simone ed Enrico con Alice, grazie ai miei compagni di corso Gian e Martino per ogni momento di studio (ma anche di svago!) che ha caratterizzato e accumunato il nostro percorso universitario. Grazie per questi anni insieme.

Un pensiero speciale va a mia zia Loredana, a mia zia Teresa, ai nonni Carmela, Mario e Orfelia che se ne sono andati durante questi anni di Università.
Grazie per tutto quello che mi avete dato, il vostro ricordo rimarrà sempre con me.